Doctoral Program in Neuroscience

Biophysical and pharmacological characterization of novel TRPM8 channel modulators

Doctoral thesis presented by

Khalid Oudaha

Director of the thesis

Dr. Félix Viana de la Iglesia

Co-director of the thesis

Dr. Salvador Sala Pla

Miguel Hernández University of Elche

- 2024 -

UNIVERSITAS Miguel Hernández

This Doctoral Thesis, entitled "**Biophysical and pharmacological characterization of novel TRPM8 channel modulators**", is submitted under the format of **conventional thesis with the following quality indicator**:

- "**The ion channel TRPM8 is a direct target of the immunosuppressant rapamycin in primary sensory neurons**" José Miguel Arcas, Khalid Oudaha, Alejandro González, Jorge Fernández -Trillo, Francisco Andrés Peralta, Julia Castro -Marsal, Seyma Poyraz, Francisco Taberner, Salvador Sala, Elvira de la Peña, Ana Gomis, Félix Viana. British journal of pharmacology**.** DOI: 10.1111/bph.16402

Dr. *"**Félix Viana De la Iglésia**"*, director, and Dr. *"**Salvador Sala Pla**"*, co-director of the doctoral thesis entitled **"Biophysical and pharmacological characterization of novel TRPM8 channel modulators"**.

REPORT:

That *"**Khalid Oudaha**"* has performed, under our supervision, the work entitled "**Biophysical and pharmacological characterization of novel TRPM8 channel modulators"** pursuant to the terms and conditions established in the Research Plan and following the Code of Good Practices of the Miguel Hernández University of Elche, successfully meeting the objectives planned for its public defence as a doctoral thesis.

In witness whereof I/we sign for all pertinent purposes, in San Juan de Alicante on 22 May 2024.

Thesis director	Thesis co-director
Dr. *"**Félix Viana De la Iglésia**"*	**Dr**. *"**Salvador Sala Pla**"*

Dra." ***Cruz Morenilla Palao***", Coordinator of the Doctoral Program in Neurosciences

REPORTS:

That *"**Khalid Oudaha**"* has performed, under the supervision of our Doctoral Program, the work entitled **"Biophysical and pharmacological characterization of novel TRPM8 channel modulators"** pursuant to the terms and conditions established in the Research Plan and following the Code of Good Practices of the Miguel Hernández University of Elche, successfully meeting the objectives planned for its public defence as a doctoral thesis.

In witness whereof I sign for all pertinent purposes, in San Juan de Alicante on 22 May 2024.

Prof. (Dra.) *"**Cruz Morenilla Palao**"*
Coordinator of the Doctoral Program in Neuroscience

Acknowledgments

A thanks memory from my heart bottom to all the teachers and professors who believed in me and supported me since my first steps in the primary school up to the master's degree (17 years).

The previous 4 years as PhD student have been full of special emotions and great experiences, which shaped who I'm today.

At first, I extend my sincerest thanks to my dear thesis Director, Dr Félix Viana , for allowing me to carry out this work under his guidance. It seems obvious to me that without you, I would not have been able to complete the entirety of this project. Thank you for trusting me and accepting me as a student. I am grateful for benefiting from your immense expertise, intellectual rigor, dynamism, and undeniable efficiency throughout this work, qualities that I will never forget. I appreciate you instilled in me the scientific rigor, perseverance, and for respecting my independent nature. I believe I have matured significantly over these years, and I can confidently say that you played a significant role in that. Finally, I thank you for always trusting me with experiments and managing my time.

I extend warm thanks to my dear thesis co-director, Dr Salvador sala, for his unwavering attention to my work, his insightful advice, and his attentive ear, all of which were crucial for the successful completion of this thesis. I am also grateful for the substantial time you dedicated to me, your pedagogical and scientific qualities, and your friendliness. I have learned a great deal alongside you, and I express my gratitude for all of it. I have thoroughly enjoyed working with you.

I would like to also to thank my dear tutor, Dr Ana Gomis, for her help since the first day when I applied to the PhD position, you were the first Spanish person I got in touch with, the first one who helped me with paperwork and the first one welcoming in the lab when I arrived. Thank you for your unconditional support, advice, and trust.

Thanks to all of you for spending so much time correcting all my oral presentations, annual reports and, of course, this manuscript. It has been a real pleasure working with you over these past years, and I appreciate the time you dedicated to me during my early days as a "research apprentice." I express my attachment and profound gratitude.

Many thanks to the special people that offered me further scientific input and technical help: Elvira de la Peña, Francisco for always motivating me with good words after every lab meeting, Francisco Taberner (Paco) for making me learn skin nerve and for your wise advice and guidance, Eva Quintero Mireille Tora, Maria Remedios Torres and Clara Serrano . But Special thanks goes to Eva Quintero

and Ana Mireille for showing me all technical skills needed since the first day at the lab. I would also like to warmly thank both Bibian Garcia and Marina Carratala for all their help when dealing with Spanish paperwork.

Enormous thanks for my dear lab mates for always helping me solving technical problems or answering any scientific question because of you I have learned many thinks as researcher, also what I did like the most is that we evolved to become good friends with such a bunch of great memories. Many thanks extended to Dr. and Professor Jorge Fernandez Trillo. I will always remember your support in difficult moment as well as our interesting philosophical, cultural and scientific discussions, to Dr Alejandro Gonzalez for teaching me calcium imaging and for always giving me wise advices regarding research field, to Dr Aida Marcoti for sharing with me all what I need based on your experience , to Dr Katharina Gers-Barlag for your special smiles full of positivity you will be always remembered as my first germen friend, Dr. Ana Gomez for our friendly discussion and your unconditional support , to Manuela De Las Casas for your funny character full of energy and peace, Dr. Francisco Peralta for you nice advices and the practice of different languages, Seyma Poyraz for your peaceful character and calm personality during your internship stay in the lab.

Warm and eternal thanks for the closer friend to me who evolved to be my Spanish brother, Pablo Hernandez Ortego, you have been lab mate and flat mate our friendship started from the first day as we share passion towards football, I would like to thank you for being always here helping me with everything I will never forget your support during hard times as well for sharing the good vibes, your marked my life in gold, remember that you have now a family in Marrakech.

Special and profound thanks to two special Moroccan scientists legends from Bordeaux University Dr Abdelhamid Benazzouz and his wife Rabia Bouali-Benazzouz, you become both members of my family, without you would have been difficult to make it that far away, you were my first inspiration to push hard and try to become a good scientists and make both of you proud, you really deserve my eternal respect and love.

To all my Moroccan community friends, Dr Otmane Bouchata a brother with whom many positivity and inspiration was built thanks for the support with many things glad you form part of my lie cercle, Abderazak so unique friend with whom we look like chiral molecules and we were laughing and smiling when no hopes were giving, I'm proud of you brother too, Oussama you are my old standing friend thanks for always believing in me , TAHA in one word a friend ´´discovery`` thanks for all the moment we shared together you are special to me.

A special and warm thanks to my two Egyptian friends Amer and Salim for being supportive and for good moments we shared together during our thesis adventures.

To all my international friends, Chiara Nappi, ESPE, Sergio, Dani, Alberto, Salma, Lucia, Khalil, Enrico Juan, Diego. Also, to special other INA football colleagues with whom I have been sharing my passion to football you have been amazing and special during my stay in Alicante.

I would like to also extend my thanks to my aunt Samira which supported me all the way financially and with paper works every time need she like my second mother, also many thanks to my two awesome cousins Abdelghani, Abdullatif who supported me psychically and for always believing on me, I hope you would be proud by the time I graduate.

Everything I said before would not have been possible without the eternal support of my small family, My lovely mother, my great father, my supportive brother and my wonderful sister. Without you I wouldn't be able to reach this special moment in my life, I made it this far for you only you because you deserve at least a special gift in this life for your patience and good hearts. This graduation is for all of you, but especially for my unique mother who believed in my dreams, objectives and who supported me when there was any hope.

This work would not have been possible without the financial support of the three-year GRISOLIA fellowship 2019/089, offered by the GENERALITAT VALENCIANA.

GENERALITAT VALENCIANA
Conselleria d'Innovació, Universitats, Ciència i Societat Digital

Index

Abbreviations **1**
Abstract **3**
Resumen **5**
1. Introduction: **7**
1.1 Nervous system hierarchy and somatosensory system: 9
1.1.1 Nervous system 9
1.1.2 Somatosensory system and sensory transduction 11
1.1.2.1 Somatosensory system 11
1.1.2.2 Sensory transduction 12
1.2 TRP channels and thermosensation 15
1.2.1 Transient receptors potential (TRPs) family 15
1.2.2 Thermo-TRPs 18
1.3 TRPM8 20
1.3.1 TRPM8 identification and expression profile 20
1.3.2 Structural and biophysical properties 21
1.3.2.1 TRPM8 structure 21
1.3.2.2 Biophysical properties 26
1.3.3 TRPM8: pharmacology and modulation 28
1.3.3.1 TRPM8 agonists 29
1.3.3.2 TRPM8 antagonists 31
1.3.4 TRPM8 modulation 34
1.3.4.1 Calcium ions: desensitization/activation of TRPM8 channel 34
1.3.4.2 pH modulation 34
1.3.4.3 PI(4,5)P2 : activate/ desensitize TRPM8 channel 35
1.3.4.4 G-protein coupled receptors (GPCRs) modulate TRPM8 channel 35
1.3.4.5 Post-translational modifications modulate TRPM8 channel 36
1.3.4.6 Other modulatory mechanisms of TRPM8 37
1.3.5 TRPM8: (Patho)physiological implications 37
1.3.5.1 TRPM8 physiology 38
1.3.5.2 TRPM8 pathophysiology 47
1.4 Agonists: Rapamycin and Agonist-109-HCl, Agonist-145 51
1.4.1 The immunosuppressant macrolide rapamycin 51
1.4.2 Novel TRPM8 agonists : G-RGM-145 and G-RGM-109 53
2. Objectives: **54**
3. Materials and Methods: **57**
3.1 Animals 59
3.2 Mammalian HEK293 cell lines: Culture and transfection 59
3.3 Single point mutagenesis 61
3.4 Primary sensory neurons culture: Dorsal root ganglia (DRG) 62

3.5 Fluorescence calcium imaging 63
3.6 Electrophysiological patch clamp recordings in HEK293 cells 64
3.7 Perfusion and temperature control systems 67
3.8 Isolated saphenous skin nerve preparation 67
3.9 Data Analysis 69
3.9.1 Calcium imaging 69
3.9.2 Electrophysiological recordings 70
3.9.2.1 Whole-cell patch-clamp electrophysiological recordings in Transfected HEK293 cells 70
3.9.2.2 TRPM8 Temperature threshold calculated from voltage ramp patch clamp experiment 73
3.9.2.3 Electrophysiological Analysis of DRG voltage and current clamp recordings 74
3.9.3 Analysis of rapamycin effects on wild type TRPM8 gating kinetics 75
3.9.4 Software and statistics 79
3.10 Chemicals 79
4. Results 82
4.1 The immunosuppressant macrolide Rapamycin activates cold-sensitive TRPM8 channels 84
4.1.1 Rapamycin activates heterologously expressed mouse TRPM8 channel 84
4.1.2 Rapamycin activates TRPM8 channels currents 86
4.1.3 Rapamycin induces typical biophysical effect on TRPM8 gating 88
4.1.3.1 Rapamycin shiftes voltage dependance towards more negative potentials 88
4.1.4 Rapamycin behaves as a TRPM8 type 1 agonist (or Menthol-like) 89
4.1.5 Rapamycin activates inward currents and elicites action potential firing in cold thermoreceptors 93
4.1.6 Rapamycin activates cutaneous cold thermoreceptors in mice 95
4.1.7 Rapamycin action on TRPM8 channels is independent from a key Menthol- and WS-12-binding residue 98
4.1.7.1 Rapamycin activates the menthol-insensitive mutant Y745H and potentiates cold-evoked responses 98
4.1.7.2 Rapamycin activation hypersensitivity following segment 4 (S4) mutations at I846 residue 105
4.1.7.3 TRP domain mutations Y1005A and R1008A decrease TRPM8 sensitivity to rapamycin 130
4.2 The segment 4 TRPM8 mutants I846A and I846T are constitutively active at rest, and alter the AMTB blockade efficacy 145
4.3 The segment 4 TRPM8 mutants I846A and I846T show an altered channel trafficking 152
4.4 Agonist G-RGM-145 is a novel activator of the cold sensor TRPM8 156
4.4.1 G-RGM-145 activated TRPM8-expressing DRG sensory neurons and potentiated their cold responses 156
4.4.2 TRPM8 is the exclusive transducer mediating G-RGM-145 responses within DRG sensory neurons 159
4.4.3 G-RGM-145 activates heterologously expressed mouse TRPM8 channel 160
4.4.4 G-RGM-145 activation of TRPM8 is mediated through the menthol- and WS-12 binding site 162
4.5 Agonist G-RGM-109 is a novel activator of the cold sensor mouse TRPM8 169

4.5.1 G-RGM-109 activates TRPM8-espressing DRG sensory neurons and potentiates their cold responses 169
4.5.2 TRPM8 mediates G-RGM-109 responses in mouse DRG sensory neurons 172
4.5.3 G-RGM-109 activates heterologously-expressed mouse TRPM8 channels 173
4.5.4 G-RGM-109 activation is mediated through menthol- and WS-12 binding site 175
5. Discussion 181
5.1 The immunosuppressant macrolide rapamycin is a novel TRPM8 Agonist 183
5.1.1 Pharmacological and biophysical characteristics of rapamycin agonism on TRPM8 183
5.1.2 Therapeutical implications of RAP effects on TRPM8 185
5.1.3 Segment 4 residue I846 mutation induces a constitutively active TRPM8 channel 188
5.1.4 Some I846 mutations cause alteration in channel trafficking 190
5.1.5 Isoleucine at position 846 plays a pivotal role in the modulation of both RAP and WS-12 sensitivity 191
5.2 G-RGM-145 and G-RGM-109 are two novel TRPM8 agonists 194
5.2.1 TRPM8 channels in mouse DRG neurons are activated by G-RGM-145 and G-RGM-109 194
5.2.2 G-RGM-145 and G-RGM-109 HCl act through the menthol binding site 195
5.2.3 Novel TRPM8 Agonists : From basic characterization to the clinical trial 196
6. Conclusions: 199
7. Conclusiones 202
8. Bibliography 205
9. Annex: 240

Abbreviations

AITC	Allyl isothiocyanate
AMTB	,[N-(3-aminopropyl)-2-{[(3-methylphenyl)methyl]oxy}N(2thienylmethyl)benzamide]
AP	Action potential
AR	Adrenoreceptor
ASIC	Acid-sensing ion channel
ATP	Adenosine triphosphate
B2R	Bradykinin receptor
BAC	Bacterial Artificial Chromosome
BAT	Brown adipose tissue
BCTC	[N-(4-tert-butylphenyl)-4(3-chloropyridin-2-yl)piperazine-1-carboxamide]
CCI	Chronic constriction injury
CFA	Complete freud ajuvant
CHO	Chinese hamster ovary cell
CLT	Clotrimazole
CNS	Central nervous system
CTPC	[(2R)-4-(3-chloro-2-pyridinyl)-2 methylN[4(trifluoromethyl)phenyl]1piperazinecarboxamide]
DED	Dry eye disease
DHT	Dihydrotestosterone
DMEM	Dulbecco's Modified Eagle Medium
DMSO	Dimethyl sulfoxide
DNA	Deoxyribonucleic Acid
DRG	Dorsal root ganglia
DTR	Diphtheria toxin
EC_{50}	Half maximal effective concentration
EGTA	Ethyleneglycol- bis(β-aminoethyl)-N,N,N′,N′-tetraacetic Acid
EM	Electron microscopy
ER	Endoplasmic reticulum
EYFP	Enhanced yellow fluorescent protein
FBS	Fetal bovine serum
FDA	United States Food and Drug Administration
Fura-2 AM	Fura-2 acetoxymethyl ester group
GA	Golgi apparatus
GFP	Green fluorescent protein
GPCR	G protein-coupled receptors
GTP	Guanosine triphosphate
H1R	Histamine receptor
HBSS	Hank's Balanced Salt Solution
HCN	Hyperpolarization-activated cyclic nucleotide-gated
HEK293	Human Embryonic Kidney 293 cell line
HEPES	4-(2-hydroxyethyl)-1-piperazineethanesulfonic acid
IC_{50}	Half maximal inhibitory concentration
IF	Intensely fluorescent
IP3	Inositol-1,4,5-trisphosphate
KCl	Potassium chloride
KCS	Keratoconjunctivitis Sicca

LBS	ligand binding sites
LPL	lysophospholipids
MEM	Minimum Essential Medium
MHR	Melastatin homology regions
PBMC	[1- phenylethyl-4-(benzyloxy)-3-methoxybenzyl(2-aminoethyl)carbamate]
PBS	Phosphate buffered saline
PCR	Polymerase Chain Reaction
PEI	Polyethylenimene
PIP_2	Phosphatidylinositol 4,5-bisphosphate
PKA	Protein kinase A
PLC	Phospholipase C
PMBC	[1- phenylethyl-4-(benzyloxy)-3-methoxybenzyl(2-aminoethyl)carbamate]
PNS	Peripheral nervous system
PSA	Prostate specific antigen
PSN	Peripheral sensory neurons
PUFA	Polyunsaturated fatty acids
RAP	Rapamycin
RE	endoplasmic reticulum
RNA	Ribonucleic acid
ROI	Regions of interest
RQ00203078	4-[[[3-Chloro-5-(trifluoromethyl)-2-pyridinyl][[4-(trifluoromethoxy)phenyl]methyl]amino]sulfonyl]benzoic acid
SNS	Somatosensory nervous system
TG	Trigeminal ganglia
TM	Transmembrane domain
mTOR	Mammalian target of rapamycin
TRP	Transient receptor potential
TRPA	Transient receptor potential ankyrin
TRPC	Transient receptor potential canonical
TRPM	Transient receptor potential melastatin
TRPML	Transient receptor potential mucolipin
TRPP	Transient receptor potential polycystin
TRPV	Transient receptor potential vanilloid
TTX	Tetrodotoxin
VAMP7	Vesicle-associated membrane protein 7
VSLD	Voltage sensing like domains

Abstract

The transient receptor melastatin 8 (TRPM8), is a polymodal nonselective cation channel activated by cold (≤ 28 ˚C) and ligands (menthol, WS-12 and icilin). TRPM8 channel is expressed within a subpopulation of peripheral sensory neurons, where it functions as the prime physiological sensor of environmental cold. Moreover, TRPM8 is implicated in many other physiological functions such as warm perception, basal tear production, thermoregulation and energy balance. In counterpart, dysregulation of this channel is responsible for the emergence of different pathologies including dry eye disease, cold allodynia and migraine. Interestingly, either the activation of TRPM8 using agonists (for example cold, menthol, cryosim3) or blockade of the channel by antagonists (for example AMTB or BCTC) had analgesic, antipruritic, anti-inflammatory or antitumoral effects. The dual role of TRPM8 in physiological and pathological conditions highlights the need for the identification of novel TRPM8 modulators. Alongside, understanding the mechanism of the action of different modulators on TRPM8 may help to better understand both channel function and contribute to the development of more selective and potent modulators.

In this thesis, TRPM8 channel modulation by three novel agonists, as well as their mechanisms of action on TRPM8 have been studied. First, I show that mouse TRPM8 is a pharmacological target of the natural macrolide rapamycin (Sirolimus), previously known as an mTOR inhibitor. Rapamycin has been widely used in the clinic as an immunosuppressant, to prevent organ rejection during organ transplant. Moreover, more recently, the topical application of rapamycin either on the skin or in the eye has shown promising results in improving dermatitis and dry eye disease, respectively. Therefore, by combining calcium imaging and patch-clamp experiments, I demonstrate that rapamycin activates heterologously expressed mouse TRPM8 channels and sensitizes their response to cold stimuli. More specifically, rapamycin activates TRPM8 channels by inducing a leftward shift of the voltage of activation activation ($V_{1/2}$) towards more negative potentials. I demonstrate that the effect of rapamycin on the TRPM8 channel is independent from the known menthol and its derivative WS-12 binding sites, and that TRP domain residues are essential for TRPM8 activation, whether induced by rapamycin or other known agonists such as cold or WS-12. In mouse DRG cultured neurons, I found, using patch-clamp recordings, that rapamycin not only elicited inward currents but also potentiated the inward current evoked by cold stimulus. Furthermore, rapamycin triggered action potential firing in TRPM8-expressing cold sensory DRG neurons. Next, following skin nerve experiments, I found that rapamycin elicits action potential firing in cold free endings innervating mouse skin by shifting the threshold towards warmer temperatures.

Secondly, I characterized the agonistic effects of two newly synthetized molecules, G-RGM-145 y G-RGM-109 on TRPM8. I demonstrated, by calcium imaging, that both agonists activate heterologously expresed mouse TRPM8 channels and potentiate cold-evoked responses. Furthermore, I found that both agonists, G-RGM-145 y G-RGM-109, share a similar mechanism of action as menthol, acting through

the same biding site, Y745, located in transmembrane segment 1. In DRG cultured neurons, following calcium imagine experiments, I demonstrated that both, G-RGM-145 y G-RGM-109, selectively activate TRPM8-epressing cold sensory neurons and sensitize their cold response. Furthermore, these responses were fully abolished upon the application of TRPM8 antagonists.

In summary, these results identify TRPM8 as a molecular target of the immunosuppressant molecule rapamycin and the novel synthetic molecules G-RGM-145 y G-RGM-109, which contributes to the expansion of the arsenal of drugs targeting TRPM8.

Resumen

El receptor transitorio de melastatina 8 (TRPM8) es un canal catiónico no selectivo, polimodal, activado por el frío (≤28 °C) y ligandos (mentol, WS-12 e icilin). El canal TRPM8 se expresa en una subpoblación de neuronas sensoriales periféricas, donde funciona como el principal sensor fisiológico del frío ambiental. Además, el canal TRPM8 está implicado en muchas otras funciones fisiológicas, como la percepción del calor, el lagrimeo, la termorregulación y el equilibrio energético, entre otras. Por otro lado, la desregulación de este canal participa en el desarrollo de diferentes patologías, como la enfermedad del ojo seco, la alodinia por frío o la migraña. Curiosamente, tanto la activación de TRPM8 mediante agonistas (por ejemplo, frío, mentol, cryosim3) como el bloqueo del canal con antagonistas (por ejemplo, AMTB o BCTC) tienen efectos analgésicos, antipruríticos, antiinflamatorios o antitumorales. El doble papel de TRPM8, tanto en condiciones fisiológicas como patológicas, enfatiza la necesidad de identificar nuevos moduladores de TRPM8. Además, comprender el mecanismo de acción de diferentes moduladores en TRPM8 podría ayudar a comprender mejor tanto la función del canal como a diseñar moduladores más efectivos.

A lo largo de esta tesis, se ha estudiado la modulación del canal TRPM8 por diferentes agonistas novedosos, así como sus mecanismos de acción. En primer lugar, demostré que el TRPM8 de ratón es una diana farmacológica del macrólido natural rapamicina (sirolimus), conocido anteriormente como inhibidor de la quinasa mTOR. La rapamicina se ha utilizado ampliamente en la clínica como agente inmunosupresor para prevenir el rechazo de órganos durante su trasplante. Además, la aplicación tópica de rapamicina en la piel o en el ojo ha mostrado resultados prometedores en la mejora de la dermatitis o la enfermedad del ojo seco, respectivamente.

Mediante experimentos de imagen de calcio y de fijación de voltaje (“patch-clamp”), demuestro que la rapamicina activa el canal TRPM8 expresado heterólogamente y sensibiliza su respuesta al frío. La rapamicina activa el canal TRPM8 induciendo un desplazamiento hacia potenciales negativos de su voltaje de activación. También demuestro que el efecto de la rapamicina sobreel canal TRPM8 es independiente de los sitios de unión al mentol y al derivado WS-12, y que los residuos del dominio TRP son esenciales para la activación del TRPM8 tanto por la rapamicina como por otros agonistas conocidos (frío o WS-12). En las neuronas cultivadas de ganglios raquídeos de ratones, descubrí, mediante experimentos de patch-clamp, que la rapamicina induce una corriente de entrada, así como la potenciación robusta de dicha corriente evocada por el frío, y provoca la generación de potenciales de acción en las neuronas sensoriales del frío que expresan TRPM8. A continuación, mediante experimentos en una preparación *in vitro* de los nervios de la piel (“skin nerve preparation”), descubrí que la rapamicina provoca la generación de potenciales de acción en las terminaciones libres de frío que inervan la piel del ratón al desplazar el umbral hacia temperaturas más cálidas.

En segundo lugar, colaboré en la caracterización del efecto agonista de dos moléculas recién sintetizadas llamadas G-RGM-145 y G-RGM-109. Demostré, mediante imagen de calcio que ambos agonistas

activan el canal TRPM8 de ratón expresado heterologamente y potencian sus respuestas al frío. Además, descubrí que ambos agonistas (G-RGM-145 y G-RGM-109) comparten el mecanismo de acción similar al del mentol, actuando a través del mismo sitio de unión Y745 (ubicado en el segmento 1). En neuronas cultivadas de ganglios raquídeos, mediante experimentos de imagen de calcio, demostré que tanto G-RGM-145 como G-RGM-109 activan selectivamente las neuronas sensoriales del frío que expresan TRPM8 y sensibilizan su respuesta al frío, mientras que estas respuestas se anularon por completo después de la aplicación de antagonistas de TRPM8.

Finalmente, estos resultados indican que el canal TRPM8 es una diana molecular tanto de la molécula inmunosupresora rapamicina como de las nuevas moléculas sintéticas (G-RGM-145 y G-RGM-109), lo que contribuye a ampliar el arsenal de fármacos dirigidos contraTRPM8.

1. Introduction:

1.1 Nervous system hierarchy and somatosensory system:

1.1.1 Nervous system

The nervous system serves as the central command center, regulating the functions and behaviours of the entire body. Comprised of specific units known as "neurons" and other non-neuronal cells, it is a complex network. Neurons, specialized cells that form intricate connections through synapses, create well-organized networks. Despite their structural and functional diversity, neurons share essential properties such as excitability and the capacity to transmit a variety of internal and external information through electrical discharges.

Neurons have distinct roles: some are specialized to process and integrate environmental cues in a specific manner, while others focus on generating output responses based on perceptual context. Another group, interneurons, can modulate both afferent sensory inputs and efferent outputs. Together, these neuron types contribute to maintaining physiological homeostasis, facilitating homogeneous bidirectional interactions between the body and its internal/external environments, and generating protective behaviours.

In vertebrates, the nervous system is typically divided into two parts: the central nervous system (CNS), encompassing the brain and spinal cord, acts as the center for integration and the elaboration of appropriate responses to changes in the surrounding environment. The peripheral nervous system (PNS) consists of the dorsal root ganglia (DRG), trigeminal ganglia (TG), peripheral and cranial nerves innervating the skin, sense organs and viscera. Equipped with specific nerve endings, the PNS transduces, discriminates, and conveys a wide range of environmental cues to the CNS (Purves, 2004; Kandel, 2013).

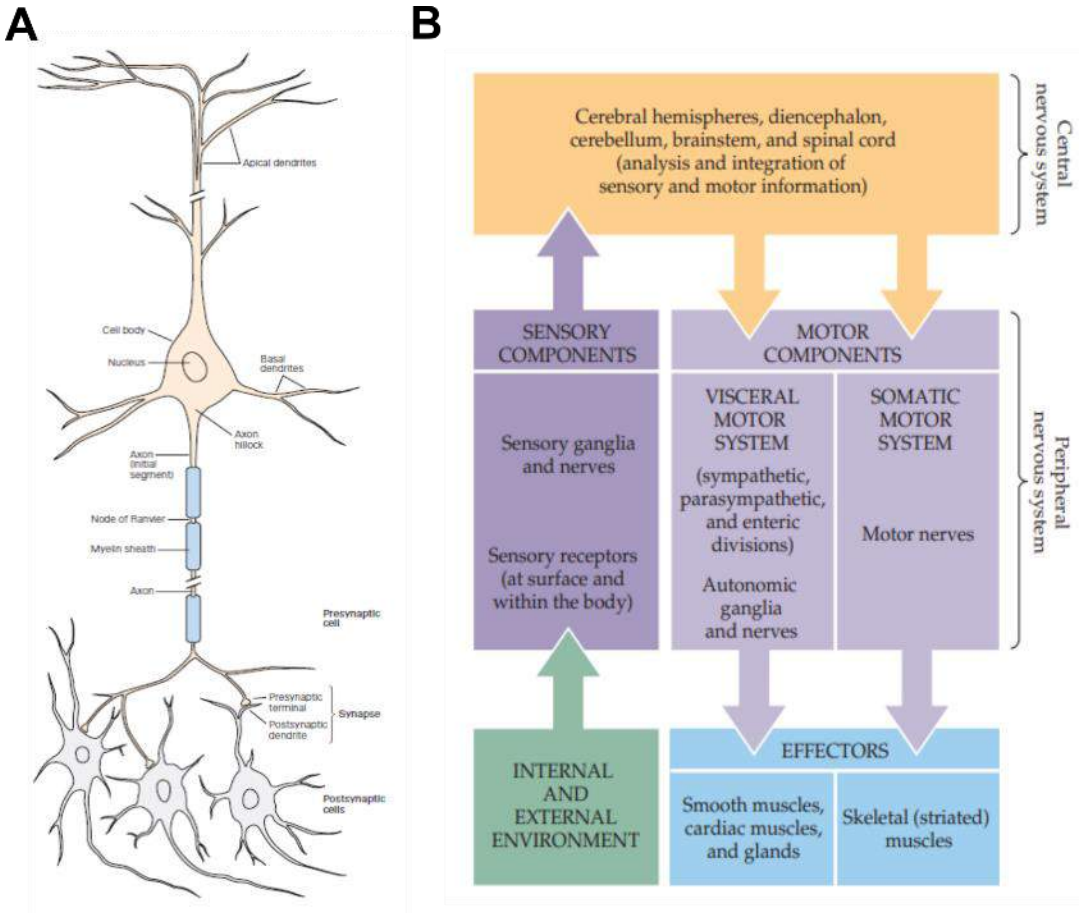

Figure 1.A., Schematic showing the structure of a neuron which is the functional unit of the nervous system. B., Diagram of the nervous system formed by the major peripheral and central components and their functional relations, arrows indicated the sense of the information flow from or towards the CNS. All the implicated structures contribute to maintaining the well-functioning and coordination of the body. Modified from Kandel 5th edition (2013) and Purves (2004) respectively.

1.1.2 Somatosensory system and sensory transduction

1.1.2.1 Somatosensory system

The somatosensory nervous system (SNS) serves as a crucial link between our body (including the skin surface, muscles, and visceral organs) and the environment, enabling us to process stimuli of various types, such as mechanical, thermal, and chemical. While the ancient Greek philosopher Aristotle initially defined five senses by associating sense organs with their functions (eyes for vision, ears for hearing, skin for touch, tongue for taste, and nose for smell), the modern functional characterization of the SNS, thanks to the work of the British physiologist Charles Sherrington, introduced three additional concepts. Sherrington' outlined three primary functions of the somatosensory system. The first is proprioception, involving sensory information gathered from muscles, tendons, and joints, providing us with conscious awareness of our body's posture, position, and movements. Second is exteroception, which includes information related to sensing touch, thermal cues (cold and heat), and nociception (pain). Finally, interoception involves cues received from internal organs (viscera) and the regulation of autonomic functions (Sherrington, 1906).

The somatosensory system comprises specialized peripheral sensory neurons (PSN), structurally identified as pseudo-unipolar, which innervate various parts of our body. Their soma is located within the dorsal root ganglia and trigeminal ganglia (Kandel, 2013; Krames, 2014). The axon of these neurons divides into two branches. The first afferent branch innervates the skin, muscles, joints, blood vessels, and internal organs through highly specialized nerve terminal endings. The second branch projects to sensory spinal cord lamina or to brainstem nuclei. The PSN neurons serve as the initial relay in the somatosensory system, connecting through a first synapse to the second-order sensory neuron in the spinal cord or the trigeminal sensory nucleus located in the hindbrain. This arrangement ensures a continuous somatosensory flow to the higher sensory areas of the brain.

The sensory nerve endings of the peripheral sensory neurons (PSN) are equipped with highly specialized transducers, or receptors, selectively activated by specific types of stimulus energy (e.g., baroreceptors for blood pressure). This activation generates an electrical signal known as the receptor potential in the nerve terminals. As multiple receptor potentials summate, they reach a certain voltage threshold, leading to the generation of action potentials (AP) in the trigger zone of the axon. Additionally, each stimulus is encoded in terms of its intensity and duration.

The resulting action potentials maintain their characteristics, including frequency and duration, as they travel along the axon. They are then transmitted to the postsynaptic sensory neurons and eventually relayed to specific areas of the brain where the stimulus-dependent sensation process takes place. The somatosensory system facilitates the perception of various sensation modalities due to the diverse

segregation of transducers within the nerve terminals. Each type of sensory nerve modality expresses specific transducers that recognizes different types of stimulus energy (Kandel, 2013).

Nerve terminals, based on their morphology, present either as free endings or encapsulated structures, forming intricate sensory configurations. Additionally, the functional classification of peripheral sensory neuron (PSN) endings depends on the nature of the stimulus that triggers their activation. This categorization encompasses thermoreceptors, responsive to temperature (cold or heat); mechanoreceptors, activated by mechanical forces (such as touch, stroking, stretch, and vibrations); and nociceptors, responsible for detecting potentially damaging or painful stimuli across various modalities.

Moreover, building on the foundational work of Erlanger and Gasser in 1937, different types of sensory fibers have been described, taking into account factors like conduction velocity, diameter, and degree of myelination (Erlanger & Gasser, 1937; Manzano et al., 2008; Kandel, 2013). This classification results in three categories of somatosensory fibers:

- **Aβ fibres:** are thickly myelinated fibres, with large diameter 5-12 µm, and high conduction velocity 30-70 m/s. In general, they convey innocuous mechanical stimuli (discriminative touch, pressure).
- **Aδ fibres:** are thinly myelinated fibres, with diameter 1-5 µm, and an intermediate conduction velocity 5-30 m/s. They convey stimuli of different modalities: mechanical, thermal, and painful sensations.
- **C fibres:** are unmyelinated fibres, with diameter 0.1-1.3 µm, and low conduction velocity 0.6-2 m/s, they are considered as free ending fibres and convey thermal, mechanical, and painful stimuli.

1.1.2.2 Sensory transduction

The sensory transduction phenomenon occurs selectively, giving rise to diverse somatosensory modalities in sensory terminals. This process involves the specific and selective conversion of a particular physical or chemical stimulus energy into electrical energy by transducers that recognize one or more types of stimuli. For the past decades, many studies have been conducted to uncover the nature of these somatosensory transducers, which enable each nerve terminal to sense a specific somatosensory modality.

The journey began with the discovery of the mammalian heat-sensitive TRPV1 ion channel (Caterina et al., 1997) and the mechanosensitive OSM-9 channel in *C. elegans* (Colbert et al., 1997), both considered the first somatosensory transducers identified molecularly. Subsequently, numerous somatosensory transducers were identified, including subtypes of acid-sensing ion channels (ASICs)

implicated in mechano-transduction. Further investigations led to the identification of the transient receptor potential ion channel family (TRPs), which was found to cover a wide range of stimuli in the thermal somatosensation spectrum (Lumpkin & Bautista, 2005; Lumpkin & Caterina, 2007).

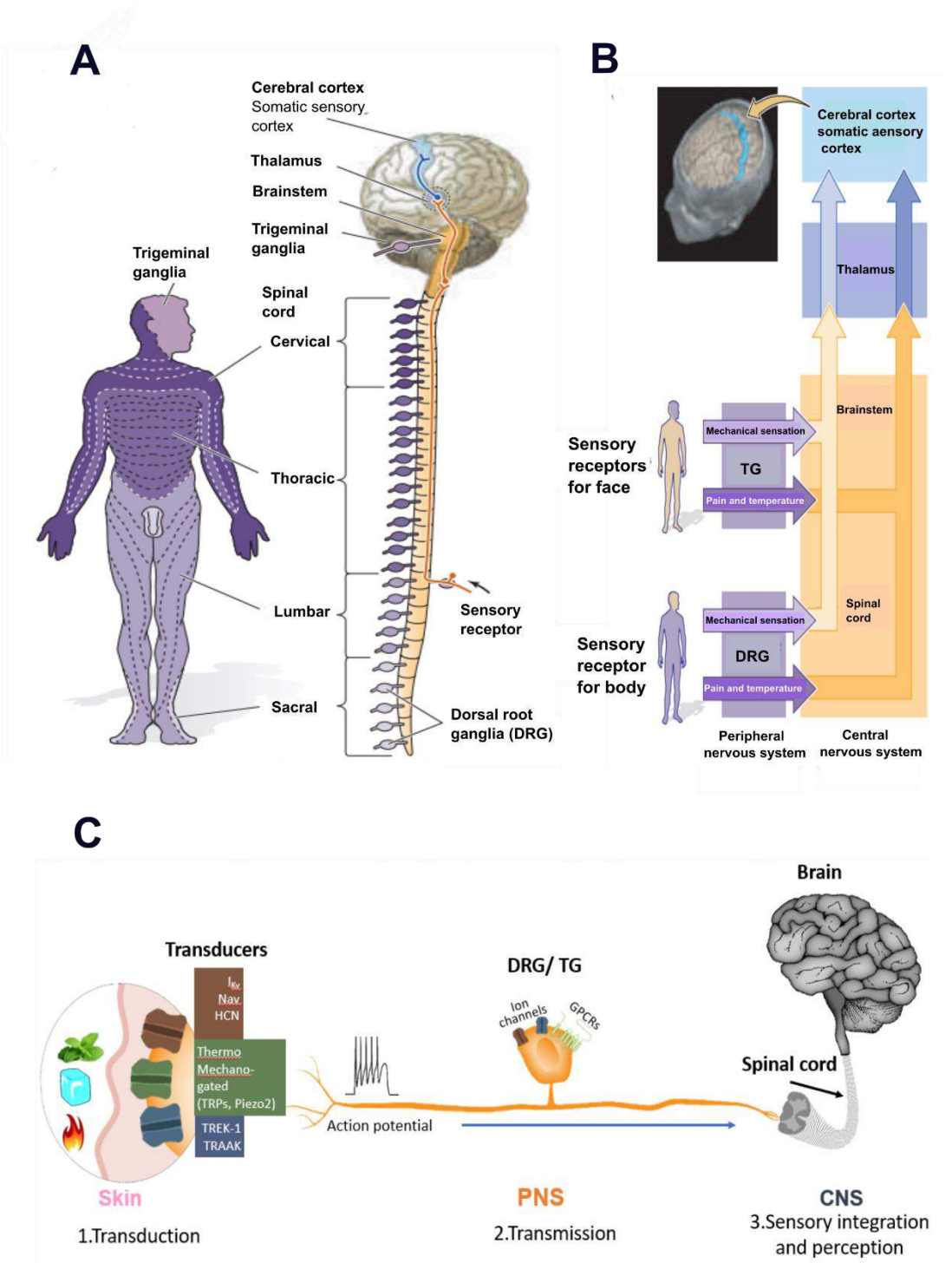

Figure 2. Anatomical and functional organization of somatosensory system. A. the somatosensorial afferents collected at the body surface are relayed through the DRG to the central nervous system. **B**. Diagram showing the pathway of somatosensory information collected by the sensory receptors at the periphery. It is initially relayed to the thalamus and then projected to the somatosensory cortex. **C.** Simplified schematic of the steps of the somatosensory function, including 1. transduction by the specific transducers at the skin, 2 transmissions mediated by the peripheral sensory neurons, and 3 finally, the integration and perception of the sensory percept at higher brain areas. A) and B) were modified from Purves (2004).

1.2 TRP channels and thermosensation

1.2.1 Transient receptors potential (TRPs) family

In 1969, Cosens and Manning published a seminal paper on the visual system of the fruit fly *Drosophila melanogaster*. Their study focused on a mutant fly exhibiting impaired visual responses to light illumination, characterized by a transient receptor potential recorded through an electro-retinogram, as opposed to the sustained receptor potential observed in the wild type (Cosens & Manning, 1969). This mutant was consequently named transient receptor potential (TRP). It took nearly two decades before Montell and Rubin identified the trp gene in 1989. Notably, introducing the trp gene into the mutant fly successfully restored the lacking phenotype, providing strong evidence for its role in phototransduction (Montell & Rubin, 1989). Subsequent research confirmed that the TRP photosensitive effect was mediated through calcium ion (Ca^{2+}) cell permeation (Hardie & Minke, 1992).

TRP channels receptors are expressed across various species, including fungi (e.g., yeast), invertebrates (such as fruit flies), and mammals, including primates (Denis & Cyert, 2002; H. Li, 2017; Nilius & Owsianik, 2011; Talavera et al., 2020).

Mammalian TRP ion channels, encoded by approximately 30 genes, are classified into six subgroups based on the homology of their transmembrane domains. This classification does not consider their endogenous ligands, functions, or selectivity due to their disparate nature. The TRP family members are grouped into two categories: Group 1, with high similarity to *Drosophila* TRP, including TRPM (melastatin), TRPV (vanilloid), TRPC (canonical), and TRPA (ankyrin); and Group 2, comprising TRPP (polycystin) and TRPML (mucolipin) (Clapham, 2009; H. Li, 2017).

All TRP channel subunits consist of six transmembrane domains (S1-S6), with the N-terminal (amino) and C-terminal (carboxy) regions located intracellularly. Cryo-EM studies have reported that subunits assemble into homo- or hetero-tetramers, forming a central pore between the S5-S6 helices, and a selectivity filter located in the upper side of the pore (S5-S6) (Dixon et al., 2022). Additionally, ligand/voltage-sensing domains are situated in S1-S4, similar to other voltage-gated potassium channels (Clapham, 2009).

TRP subfamily	Characteristics	Members	Expression
TRPC (Canonical)	- Homology close to first discovered Drosophila TRP. - TRPC proteins form heterotetramers.	Seven subtypes: **TRPC1-C7**	-Different cell types: -Brain, kidney, olfactory tract and sperm (Samanta et al., 2018).
TRPA (Ankyrin)	- Called ANKTM1: due to several N-terminal ankyrin repeats. - Thermo-sensible (Cold/heat) (Vangeel & Voets, 2019a). - Mechanotransduction (Story et al., 2003). - Pain (Viana, 2016).	-**TRPA1**: only member in mammals. - Drosophila: four members. -C-elegans: two members.	-Sensory neurons : - DRG, TG and nodose ganglia (Nagata et al., 2005).
TRPV (Vanilloid)	-Name referred to the activator agonist vanillin. -Thermotransduction, osmosensation and mechanosensation.(Lumpkin & Caterina, 2007).	-Six subtypes: **TRPV1-V6** (TRPV1-V4, are heat sensitive).	-Keratinocytes/ epithelial cells. -Sensory neurons. -Brain (hypothalamic). -Bladder (reflex).
TRPM (Melastatin)	-Name based on melastatin gene discovered, as the first TRPM1 (Duncan et al., 1998). -Thermotransduction.	-Eight subtypes: **TRPM1-M8**	-Widely distributed in the organism (Ordás et al., 2021).
TRPML (Mucolipin)	-Name related to MCOlN (Mucolipina) protein indispensable for the well-functioning of the channel (Sun, 2000).	-Three subtypes: **TRPML1-ML3**	-Expressed mainly in the membrane of lysosomes (Samanta et al., 2018).

TRPP (Polycystin)	-Name was related to its first discovered channel TRPP1(PKD1), its mutation is causing Polycystic Kidney Disease (Mochizuki et al., 1996). -Large loop between S1 and S2.	- Three subtypes: **TRPP1-TRPP3**	-Kidney.

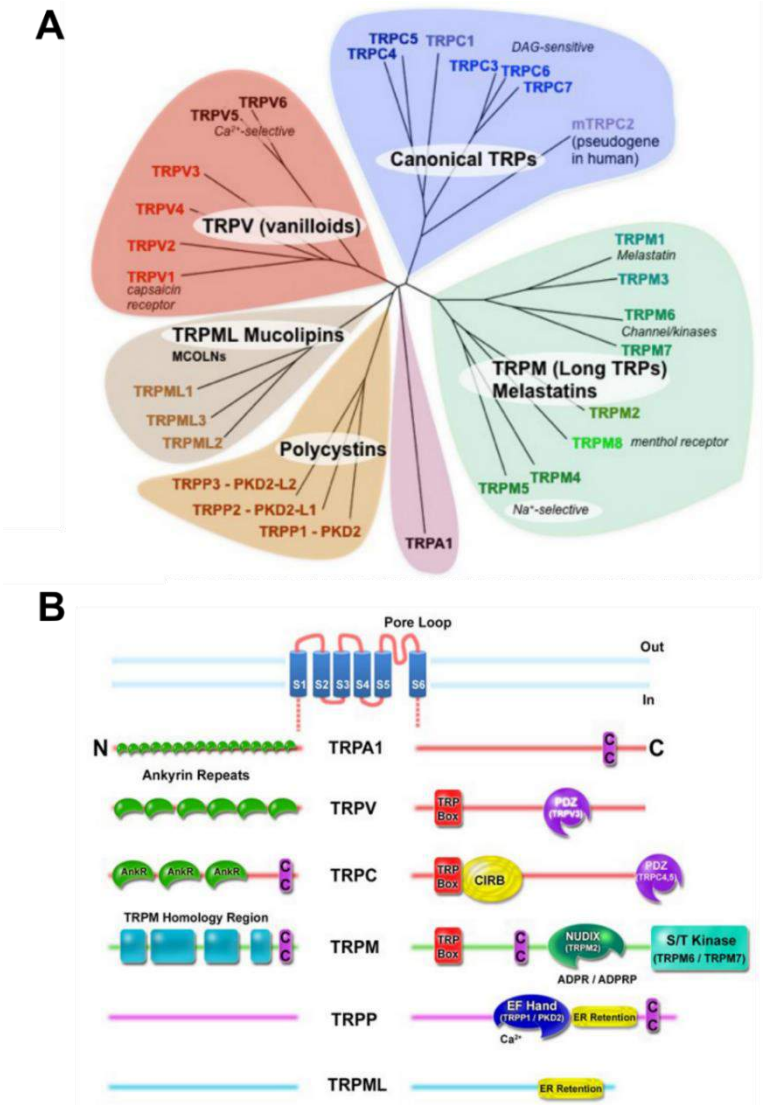

Figure 3. TRP channel superfamily. A., Phylogenetic tree of human TRP ion channel family subgroup, each subgroup is designed by a different color and were clustered based on their homology. **B.,** Schematic representation of general structure and specific protein specification within each subgroup. Starting from upper side which show the six transmembrane domains (S1-S2) common with TRPs family, the ionic pore formed by S5-S6 and both carboxy and n terminal located intracellularly. By Going down comes the detailed protein structure related to each of TRP channel family subgroup. Modified from Doerner and Clapham (2018) (Doerner, J. F. and D. E. Clapham., 2018).

TRPs are characterized as non-selective cation channels that facilitate the passage of Ca^{2+} and Na^{+} ions through the pore, displaying variable permeability ratios ranging between 0.1 and 20 (PCa/PNa) (Vangeel & Voets, 2019b). The entry of Ca^{2+} through TRPs into the cytosol is a pivotal factor in determining changes in intracellular calcium concentration. While calcium ions generally maintain a lower concentration in the cytosol compared to the extracellular compartment, a giving increase of the intracellular [Ca^{2+}] initiates a myriad of intracellular signalling cascades that govern various biological and physiological pathways crucial for cell adaptation, survival, and apoptosis programming (Berridge, 2017).

Among the diverse subtypes of TRP ion channels, some cover a broad range of the thermal sensing spectrum, responding to stimuli from noxious cold to noxious heat. These specific subtypes are referred to as thermo-TRPs.

1.2.2 Thermo-TRPs

Thermosensation is initiated at thermosensitive, poorly myelinated Aδ and unmyelinated C-fibers in the skin (Lumpkin & Caterina, 2007). These thermal cues are primarily sensed by members of the transient receptor potential (TRP) family, covering the entire thermal spectrum (Ramsey et al., 2006). In the late 1990s, the identification of the mammalian TRPV1 channel, the first cloned TRP channel, marked a significant development. This channel is activated by capsaicin (the pungent ingredient in chili peppers) and responds to noxious heat (≥ 43 ºC). In addition, the authors suggested that endogenous protons may potentiate TRPV1 activation under tissue damage, leading to pain sensation(Caterina et al., 1997).

Subsequent research established the involvement of other TRPV subtypes in heat sensing. These include TRPV2, activated by noxious heat (≥ 50 ºC) within sensory neurons (Caterina et al., 1999), and TRPV3/TRPV4, responding to moderate heat (≥ 27 ºC) (Güler et al., 2002; Smith et al., 2002).

Members of the TRPM family were also found to be involved in thermal transduction. TRPM2 is activated by warm temperatures (≥ 35 ºC) (Togashi et al., 2006), TRPM3 is activated by noxious temperatures (≥ 40 ºC) and is implicated in heat-evoking hyperalgesia (Vriens et al., 2011), and TRPM5 has been shown to be heat-sensitive (15-35 ºC) (Talavera et al., 2005). More recently, it has been demonstrated that the heat inhibition of TRPM8 is crucial for warm temperatures (22-42 ºC) perception in mice (Paricio-Montesinos et al., 2020).

For cold temperature sensing, the transient receptor potential melastatin 8 (TRPM8) has been identified as the crucial sensor for innocuous cold (≤27 ºC) in the peripheral nervous system (PNS) (McKemy et al., 2002). TRPA1, on the other hand, has been a subject of debate regarding its role in noxious cold sensation (≤18 ºC), with conflicting results. Some studies support its function as a noxious cold sensor, while others fail to reproduce these results, excluding its role in cold transduction (reviewed by (Viana,

2016)). TRPA1 has also been described as a heat-sensing (≥35 ºC) receptor, rather than a cold sensor, in some invertebrate species (fruit fly, mosquito) (K. Kang et al., 2012; Kwon et al., 2008). This reported thermal sensing divergence among species has been conserved in humans, confirming the U-shaped thermosensitivity profile (cold-heat transducer) of the TRPA1 receptor (Moparthi et al., 2016), and in mice (Vandewauw et al., 2018).

The canonical family member TRPC5 has been proposed to sense cold (27-35 ºC) in peripheral sensory neurons (PSN) (Zimmermann et al., 2011), although ongoing debates persist. Recently, TRPC5 has been identified as a cold sensor in healthy teeth (Bernal et al., 2021).

Considering the gating of these thermal-TRPs channels by temperature, which is similar to many other chemical and biochemical reactions, in 2012, Thomas Voets proposed a set of biophysical and functional criteria to distinguish a real Thermo-TRPs channel label (Voets, 2012). These criteria are:

First: Steep temperature dependence

Based on the calculation of the value Q_{10} : Q_{10} is defined as the relative current response amplitude when the temperature increases by 10 ºC (calculated as $Q_{10} = I_{T+10}/I_T$). For a channel to be considered thermo TRP sensitive Q_{10} should be greater or equal to 5, and bigger is Q_{10} more sensitive is the channel.

Second: Expression in sensory neurons or other peripheral cells

Genuine Thermo-TRPs channels are expected to be expressed in tissues exposed to significant temperature variations. This includes sensory nerve endings, keratinocytes (skin cells), and the oral mucosa.

Third: Thermo-TRPs channels should exhibit temperature dependence over some (patho)physiological conditions and show thermosensitivity *in vivo* evidence.

Based on these three criteria, only six TRP channels meet the requirements and could be considered as thermos-TRPs: counting as heat transducers: TRPV1, TRPM2, TRPM3, TRPM5 and TRPA1 while for cooling transducers: TRPM8 and TRPA1.

Thermo-TRPs channels are essential for the temperature transduction process within the peripheral nervous system. Furthermore they are also involved in thermoregulation and contribute to thermal hypersensitivity in pain condition (Laing & Dhaka, 2016).

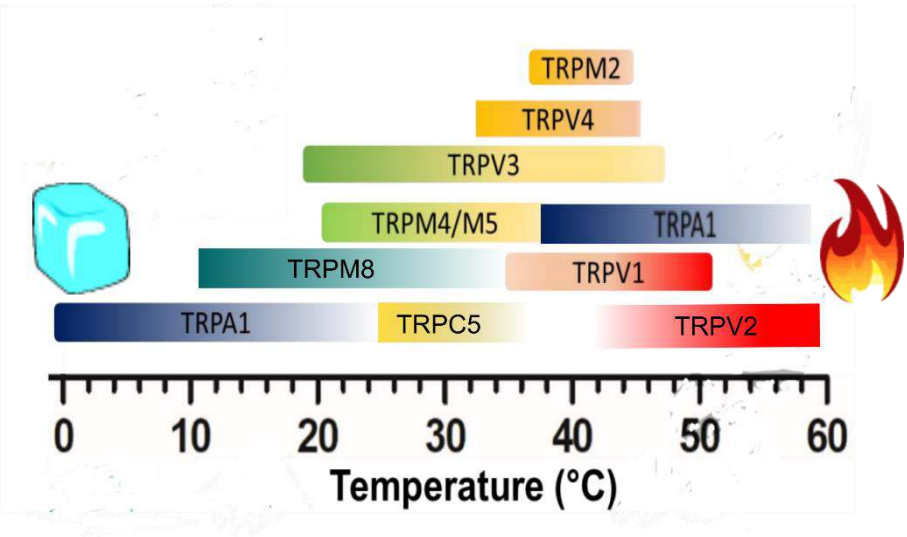

Figure 4. Thermo-TRPs ion channel family covering the whole thermal sensing spectrum. Modified from (Castillo et al., 2018).

1.3 TRPM8

Transient Receptor Melastatin 8 (TRPM8) is a polymodal, nonselective cation channel activated by cold (<28 ºC), cooling compounds and voltage (McKemy et al., 2002; Peier et al., 2002; González-Muñiz et al., 2019). Recognized as a crucial sensor for mild cold in the body, TRPM8 is also involved in various physiological functions, including warm perception (Paricio-Montesinos et al., 2020), thermoregulation, energy balance (Reimúndez et al., 2018), and sexual behavior (Mohandass et al., 2020). Dysfunctions or dysregulations of this ion channel have been associated with several pathologies, including different types of cancer (Tsavaler et al., 2001; Oh et al., 2018), migraine (González-Muñiz et al., 2019), dry eye disease (J. M. Yang et al., 2017a, 2018), and cold pain (Xing et al., 2007; Knowlton et al., 2013). Currently, due to its multiple physiological roles, TRPM8 is being screened by the drug industry as a significant therapeutic target for TRPM8-dependent diseases. Consequently, there is an intense effort underway to develop selective and potent TRPM8 modulators.

1.3.1 TRPM8 identification and expression profile

Initially identified and cloned in 2001 through the analysis of a cDNA genome library of prostate cancer samples by Tsavaler and collaborators, TRPM8 is widely expressed in various human organs (Tsavaler et al., 2001). It emerged as a newly upregulated gene showing significant homology with TRP family members and was originally named trp-p8 before being renamed in a new nomenclature as TRPM8 (Montell et al., 2002).

Through two distinct experimental approaches by different research groups, TRPM8 was cloned and characterized in a subset of trigeminal sensory neurons (10-15%), where it was shown to play a role in

mediating responses to cold and cooling compounds. These studies confirmed that heterologously transfected cells with the isolated gene exhibited cold responsiveness (McKemy et al., 2002; Peier et al., 2002).

Expression of TRPM8 was also identified in rodent dorsal root ganglia (DRG) (McKemy et al., 2002; Stein et al., 2004; Dhaka et al., 2008), cornea (Parra et al., 2010), and taste papillae (Abe et al., 2005). Cumulatively, the peripheral nervous system (PNS) expression patterns suggested the role of TRPM8 as the primary cold transducer in the peripheral sensory system. Additionally, TRPM8 was found in various other organs, including the skin, brain, bladder, testis, thymus, macrophage immune cells, nasal mucosa, and colon (reviewed by Liu et al., 2020).

1.3.2 Structural and biophysical properties

1.3.2.1 TRPM8 structure

The TRPM8 protein is encoded by the *TRPM8* gene located into region 2q37.1 of the chromosome 2, it contains 102,124 bases enclosing 25 exons. The transcription of the *TRPM8* gene codes for a protein consisting of 1,104 amino acids. TRPM8 is an homotetrameric channel, a characteristic feature of TRP family members. Each of the four subunits contains six transmembrane domains (S1-S6), similar to voltage-gated potassium (K_v) channels. Both the Carboxy (C-) and Amino(N-) termini are located intracellularly within the cytoplasm, and the putative pore loop is formed between transmembrane segments S5 and S6. The TRPM8 subunits tetramerize into a functional channel (see figure 5) (Dragoni et al., 2006; Stewart et al., 2010).

The mechanisms of TRPM8 activation are complex and still not fully understood. Mutagenesis studies made possible to explore the structural and functional features of ion channel activation and regulation. The S4 segment and S4-S5 linker region found to act as the voltage sensor of the channel since neutralizing the positive charges within this regions provoked alteration of both voltage and thermal sensitivity highlighting the strong link between voltage and temperature sensing (Voets et al., 2007a; Stewart et al., 2010; Almaraz et al., 2014). Moreover, the TRPM8 channel has the shortest C- terminal with 120 amino acids compare to all TRPM subfamily members (Tsuruda et al., 2006). The C-terminal contains a highly conserved sequence called TRP domain (residues 990-1025 recognized as essential for the activation and regulation by phosphatidylinositol 4,5-bisphosphate (PIP_2). The PIP_2 acts through three charged residues (K998, R998 and R1008), and is implicated in coupling channel opening to agonist-binding (Bandell et al., 2006). Furthermore, this carboxy terminal has a coiled-coil domain comprising 50 residues with a high number of hydrophobic amino acids. These hydrophobic residues are crucial for the tetramerization of TRPM8 channels and the expression of functional channels at the plasma membrane. The deletion of the TRPM8 C-terminus generated a non-functional channel due to

the failure of tetramer expression, which was attributed to the lack of self-assembly of TRPM8 monomers. In addition, the mutation of the hydrophobic amino acids within the coiled-coil residues lead to a non-functional channel due to the disruption of the self-assembly capacity. It was also found that TRPM8 protein mutants lacking the C-terminal were trapped in the endoplasmic reticulum (ER) (Tsuruda et al., 2006).

In contrast, other studies found that TRPM8 mutants could tetramerize and localize at the membrane after C-terminal deletion. However these mutants result into inactive channels, leading to the conclusion that the carboxy terminal is essential for channel function (Phelps & Gaudet, 2007).

The N-terminal of the TRPM8 channel consists of approximately 693 amino acid residues, and includes four regions with sequence similarity among members of the TRPM family, collectively named Melastatin homology regions (MHR) (Fleig & Penner, 2004; Phelps & Gaudet, 2007). Following the work of Phelps and Gaudet in 2007, the MHR sequence was identified as comprising 116-amino acids, they found that deletion of the first 39 residues (Δ39) still preserved the wild type TRPM8 activity, while two mutants with deletions of 86 (Δ86) or 116 (Δ116) residues, which are considered as regions of high similarity, generated an insensitive ion channel to either cold or menthol. These mutants also exhibited altered trafficking towards the membrane due to retention in the endoplasmic reticulum (ER) and/or Golgi apparatus (GA).

Subsequently, Pertusa and collaborators (2014) explored the role of the N-terminal region in TRPM8 agonist sensitivity and maturation. They found that the deletion of the first 39 amino acids, residues dispensable for the normal TRPM8 channel function, caused a phenotype showing an enhancement in responses to both cold and menthol agonists. They also emphasized the relevance of the residues 40-60 in the biogenesis of TRPM8. In addition, by performing a single targeted mutation (S27P) they were able to mimic the cold and menthol hypersensitivity seen in the mutant TRPM8 (Δ39) phenotype.

The cytosolic N-terminal tail was also reported to enclose five putative PKA phosphorylation sites (Ser9, Thr17, Thr32, Ser121 and Ser-367). Among these, residues Ser9 and Thr17 were identified as crucial for the inhibitory effect of the Gi-protein coupled α2A adrenoreceptor (α2A-AR) on TRPM8 through PKA cascades. Thus, S9D and T17D mutations supress the α2A-AR inhibitory effect, suggesting that these two PKA phosphorylation sites are important for TRPM8 physiological modulation (Bavencoffe et al., 2010; Pertusa et al., 2014).

Nowadays, the structural and functional study of proteins has been revolutionized by the use of novel technique called single-particle cryo-electron microscopy (Cryo-EM) rather than mutagenesis methods or protein crystallography. The Cryo-EM technique was the ground-breaking discovery by Jacques Dubochet, Joachim Frank and Richard Henderson which received the Nobel Prize in Chemistry in 2017. This technique was used to image biological samples from a structural biology perspective. Interestingly, this sophisticated technique allowed scientists to study TRPM8 structural changes in both

ligand-free and ligand-binding states, providing detailed 3D structural-dynamic information. The structural characteristics obtained by Cryo-EM align with previous descriptions in the literature reporting the homotetrameric assembly, with six transmembrane domains S1-S6, the C- and N-termini located intracellularly, and the formation of the pore between transmembrane segments S5-S6.

Cryo-EM structural dynamics of TRPM8 started firstly in avian species *Ficedula albicollis* (FaTRPM8) and *Parus major* (PmTRPM8) which share 81% and 91% of sequence identity respectively to mouse TRPM8 (mTRPM8). Then, comparing these two avian TRPM8 (FaTRPM8 and PmTRPM8) channels with other mammalian TRPM proteins they spotted several structural differences. In the ligand free state, bird TRPM8 channels showed that the S4-S5 linker formed a straight helix with S5, and the pore helixes was resolved in low resolution (~4 Å) and that both the selectivity filter as well as the outer pore loop are invisible because of their dynamics. However, during calcium (Ca^{2+})-icilin-PIP_2 bound configuration, the S4-S5 linker and S5 helices formed a canonical conformation, followed by structural rearrangement of all transmembrane domains (S1-S4 voltage sensor, S5-S6 pore helix and TRP helix), while both the selectivity filter and outer pore loop became more visible (Yin et al., 2018; Diver et al., 2019).

Recently, Zhao and collaborators succeeded to resolve for the first time the mammalian mouse TRPM8 channel (mTRPM8) structure using Cryo-EM in both free-ligand and in the presence of either Ca^{2+} and icilin in closed state, at a resolution. The mouse TRPM8 channel has 82% and 94% sequence identity with FaTRPM8 and human TRPM8 respectively. Structural analysis confirmed the resemblance of the previously described tetrameric structure assembly of TRPM8 channel. The authors described the cations conduction mechanism through the pore that enclosed a long outer loop ranging from Val915 to Pro952 forming a vestibule at the entrance of channel pore. This vestibule was found to contain several negatively charged residues at the inner surface aiming to facilitate the cations access to the pore. Moreover, the selectivity filter, defined by residues Phe912-Gly913 and Gln914, where the backbone carbonyls of Phe912-Gly913 and the side chain of Gln914 formed the ion conduction pathway with an atom-to-atom diameter between Phe912 and Gly913 of 9 Å favouring the passage of hydrated cations during ion conduction. In addition, they also described the interactions between the voltage sensing like domains S1-S4 (VSLD) and the pore following three ways, first was through S4 that form a hydrophobic packing with S5, second considering that VSLD is covalently linked to the pore by S4–S5 linker with an ability to perform about 150º smooth turn at the residue Met863, and finally TRP helix which found to link the pore domain to VSLD through tightly hydrophobic interaction with S4-S5 linker, and mentioning its capacity to perform 120º turn at residue Val986.

Thereafter, the authors disclosed the structural basis of both $Ca^{2+}$and icilin coupling with channel and the mechanism of calcium potentiating icilin activation. Their observation supported the hypothesis that one calcium ion binds at the loop formed by the side chains of amino acids residues Glu782, Glu785,

Asn799 and Asp802 from S2 and S3 of VSLD within 3 Å atom-to-atom interaction. Moreover, they observed that icilin interacted with Phe839 side chain and created an hydrogen bond with Arg842 within (S4) VSLD. Interestingly, they have disclosed the mechanism of calcium potentiation that arises from the coordination through Asp802, which stabilized icilin through anion interaction and help into setting a fix orientation of Arg842 side chain. Finally, they concluded that the TRPM8 closed conformation was similar either in the ligand-free or ligand-binding configurations (C. Zhao et al., 2022).

Interestingly, later in the year of 2022 a breaking news achievement in the field came to reality. Until then, scientists lacked the TRPM8 channel structure in the open conformation, which could help towards a better understanding of either cold or cooling agents sensing underlying mechanisms. This knowledge may serve for better therapeutic design of molecules targeting this channel. However, Yin and collaborators were able to perform cryo-EM on mouse TRPM8 channel (MmTRPM8) in different states (Closed, Intermediate and Open). The open state was achieved by combining the application of PIP_2 ligand with type I agonist cryosim (C3) and type II agonist AITC. They observed that during gating the pore undergoes numerous non-canonical changes and that progressively decreases in size (pore radii) (Fig. 5E), and that the short selectivity filter progressively shaped to a canonical conduction pathway. In addition, the surface charges of the pore became more electronegative allowing the installation of the pore gradient selectivity favouring the passage of cations (Fig. 5E). Then, the pore-forming helix S6 undergoes helical rotation/ translation modifications into S6 gate position and dynamics based on the mechanism including the amino acids gate residues Met978 and Val979 that formed a hydrophobic seal of 5.8 Å, which were retracted away from the pore. The Val979 appeared into ion pathway permeating of wide conduction passage of 9.1 Å in diameter favouring a smooth flow of hydrates cations. Finally, they also described the different binding pockets of the PIP_2 (S4b, TRP domain and PreS1), Type I agonist (C3) positioned between S1 (interacting at residues Y745) and S4b (interaction with Arg842 and His845), type II agonist AITC positioned at loop enclosing S3 (at residues Trp798) and the S4-S5 linker (at residues Gln861, where its mutation supresses completely AITC activation) (Yin et al., 2022).

Finally, Palchevskyi and collaborators published, in the year 2022, an interesting study in which they have described for the first time the human TRPM8 (hsTRPM8) channel structure in closed state, based on cryo-EM technique at a very high resolution of 2.7 Å. Their results confirmed 3D homotetrameric arrangements, in line with previously described TRPM8 structures (Yin et al., 2018; Diver et al., 2019; Yin et al., 2022; C. Zhao et al., 2022). The HsTRPM8 pore formed by S5, PH and S6 includes two gates, the lower gate composed of hydrophobic side chains of M978 and F979 responsible of closing the pore and the upper gate that is formed by flexible selectivity filter and pore loop (914-951). Remarkably, the human conformation of the pore in closed state was different from the recently published mouse TRPM8, while was similar to avian structures (PmTRPM8 apo, PmTRPM8-antagonists and FaTRPM8 apo states) (Palchevskyi et al., 2022).

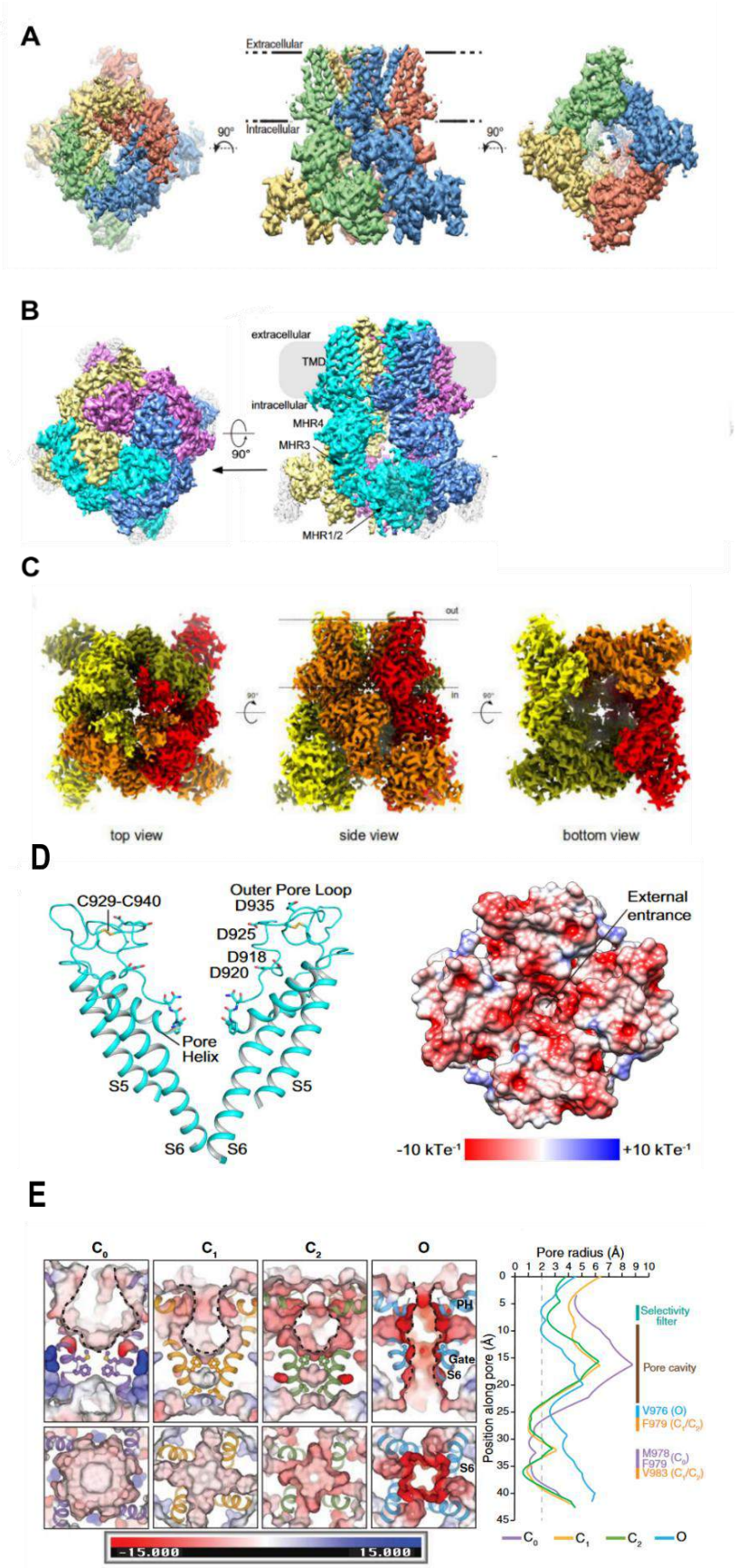

Figure 5. TRPM8 Homotetrameric structure obtained by Cryo-EM in different species and conduction pore of MmTRPM8 ligand free. (In Cryo-EM each color identifies one subunit). **A.,** Avian TRPM8 (Yin et al., 2018). **B.,** Mice TRPM8 (Zhao et al., 2022), **C.,** Human TRPM8 (Palchevskyi et al., 2022). **D**., Pore S5-S6 helix (left) and Top view of surface electrostatic potential at the external entrance (right). **E**., Electrostatic potential of the pore surface (left) (Zhao et al., 2022), and pore radii along central axis (right) in C0, C1, C2 and O states (Yin et al., 2022).

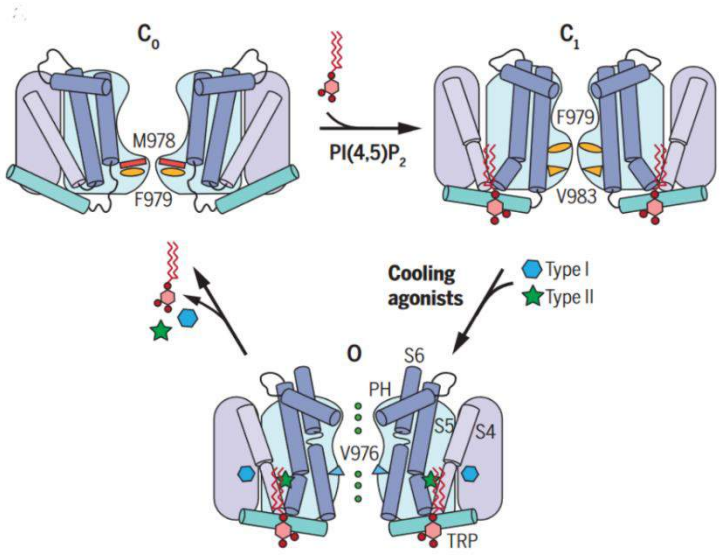

Figure 6. Schematic showing mice TRPM8 activation that was mediated by combining type-1 and type-2 agonists in the presence of PIP2. TRPM8 gating was undergoing several conformational rearrangements either at the pore or lower gate position. Extracted from Yin et al., 2022.

1.3.2.2 Biophysical properties

TRPM8 is a channel activated by various stimuli, including cooling temperatures (<28 ºC), ligands (Menthol, Tacrolimus, and Icilin), osmolality, and voltage (McKemy et al., 2002; Peier et al., 2002; Voets et al., 2004; Kühn et al., 2013; Quallo et al., 2015; Arcas et al., 2019). One notable biophysical characteristic of the TRPM8 channel is its steep temperature sensitivity, represented by Q_{10} values ranging from 24 to 40. The TRPM8 cold sensitivity is membrane-delimited process, as demonstrated by the preservation of cold sensitivity in cell-free membrane patches and artificial bilayer configurations. The intrinsic nature of the cold sensitivity is supported by several studies showing that it persists in the absence of extracellular Ca^{2+} and Mg^{2+} ions (Brauchi et al., 2004; Voets et al., 2004; Zakharian et al., 2010).

The voltage-dependent gating property of TRPM8 is evident in the current-voltage relationship curve (I-V), which displays strong outward current rectification with membrane depolarization. This rectification property was explored by Voets et al. (2004) using a tail current protocol, revealing that the channel activates upon depolarization up to +120 mV and closes at negative potentials. The resulting I-V curve obtained upon depolarization had a linear shape, suggesting an ohmic feature in the opening of TRPM8. Voets et al. (2004) concluded that the rectification feature is voltage-dependent, with the channel closing at negative voltages rather than being an intrinsic property of the pore (Voets et al., 2004).

Interestingly, subsequent research by the same group (Voets et al., 2007a) identified voltage sensor structures underlying the voltage gating of TRPM8. Charge neutralizing mutations at residues in the S4 (R842A) and S4-S5 linker (K856A) significantly altered voltage gating but did not fully suppress it. These mutations also disrupted temperature and menthol sensitivity. Later studies linked voltage sensitivity to electrostatic interactions between charged residues in the S4 (R842) and S3 (D802) transmembrane domains. Reversing charges through double mutations at these positions (R842D+D802R or R842E+D802R) restored voltage dependency suppressed by S4 mutations (R842D or R842E) (Kühn et al., 2013).

Additionally, the nonselective cation channel TRPM8 exhibits a characteristic reversal potential (Erev), typically around 0 mV. Erev represents the point where the current-voltage curve intersects the voltage axis, indicating no net current flow. This reversal is influenced by the permeability of different cations (Na^+, K^+, Ca^{2+}, and Cs^+). The channel shows low discrimination between monovalent cations Na^+, K^+, and Cs^+ (P_K/P_{Na} = 1.1, P_{Cs}/P_K = 1.2) and exhibits maximum permeability for divalent calcium ions Ca^{2+} (P_{Ca}/P_{Na} = 3.2) (McKemy et al., 2002).

In 2004, Voets and colleagues investigated the impact of cooling on TRPM8 voltage dependency using a voltage steps protocol ranging from -120 mV to +160 mV. They observed that at 37 ºC, the outward current at depolarized potentials had a midpoint voltage ($V_{1/2}$) of +200 mV. Lowering the temperature to 15 ºC induced a significant negative shift in $V_{1/2}$ of about 150 mV. Moreover, they demonstrated that the cooling agent menthol (30 µM) induced a more pronounced negative shift of $V_{1/2}$ compared to cooling down to 5 ºC. Consequently, they concluded that cold is a less potent agonist than menthol, and agonists exert their effect by shifting the voltage dependence toward more negative potentials (Voets et al., 2004).

Subsequent work by Mälkiä and colleagues showed that agonists and antagonists exerted an opposite, bidirectional shift in the voltage dependence of TRPM8 activation (Mälkiä et al., 2007). They found that different TRPM8 antagonists (BCTC, SKF96365, and 1,10-phenanthroline) had a similar effect, shifting the voltage dependence towards more positive potentials. Additionally, they demonstrated that BCTC induced a shift in the temperature-response threshold towards colder values, both in TRPM8-expressing trigeminal neurons (Madrid et al., 2006) and in a heterologous HEK293 expression system. Remarkably, simultaneous application of both BCTC (antagonist) and menthol (agonist) resulted in the cancellation of the expected temperature threshold shifts, maintaining the same threshold as in control conditions in TRPM8-expressing HEK293 cells. This suggests that both types of modulators converge into a common molecular process (Mälkiä et al., 2007).

In 2016, Janssens and colleagues investigated TRPM8 gating using two different agonists, menthol and AITC, through a series of whole-cell recording experiments. Employing a voltage steps protocol ranging from -140 to +220 mV, they identified two TRPM8 agonist types: type 1 (menthol-like) and

type 2 (AITC-like). Both menthol and AITC shifted the voltage activation curve towards more negative potentials. The kinetic analysis revealed that AITC (3 mM) accelerated the activation kinetics upon depolarization to +120 mV, while the current relaxation upon repolarization at -80 mV remained similar to control conditions. Conversely, menthol slowed both the activation gating kinetics and the current relaxation upon repolarization (deactivation tail). Thus, based on these distinct actions of these two agonists on channel kinetics, they proposed the current classification of TRPM8 agonists into Type 1 agonists or menthol-like, which stabilize the channel in an open state conformation by preventing it from closing, and Type 2 agonists or AITC-like, which induce an acceleration of voltage-dependent channel activation and deactivation, meaning that they destabilize the channel in the closed conformation (Janssens et al., 2016).

1.3.3 TRPM8: pharmacology and modulation

The TRPM8 ion channel is not only known for its sensitivity to voltage and temperature but is also recognized as an ionotropic receptor due to its responsiveness to specific pharmacological ligands. Given its crucial role in various (patho)physiological conditions, such as neuropathic pain, irritable bowel syndrome, chronic cough, hypertension, and its widespread involvement in the progression of different cancer types (skin cancer, lung cancer, bladder and colon cancer, etc.), TRPM8 has emerged as a significant target in drug discovery. Modulators of TRPM8 have been suggested as an effective therapeutic strategy for pain relief and the management of visceral inflammation (Moran & Szallasi, 2018). Additionally, the activation of meningeal TRPM8 afferents by exogenous agonists has been proposed to alleviate headaches and migraines (Dussor & Cao, 2016), and subsequently found to mediate a dimorphic fast recovery from mechanical hypersensitivity in chronic migraine mouse model (Alarcón-Alarcón et al., 2022).

Multiple pharmacological studies are characterizing endogenous modulators and exploring new natural or synthetic compounds, including both agonists and antagonists. Crucially, these modulators need to meet specific criteria, such as specificity towards the receptor, high efficacy to avoid the use of high doses, and selectivity to minimize side effects associated with cross-pharmacology with other receptors, either within the same family or different receptor families. These considerations aim to ensure the validity of clinical applications(Fleig & Penner, 2004; Palchevskyi et al., 2022).

The TRPM8 receptor can be targeted by either agonists or antagonists, and both the channel function and its biophysical properties can also be influenced by other types of modulators, including pH, calcium ions, post-transcriptional modifications, and co-factors. These factors might impact the TRPM8 ion channel trafficking process, as well as its physical and chemical sensitivity.

1.3.3.1 TRPM8 agonists

Textbooks define an agonist as a molecule capable of binding and functionally activating a specific target, typically a metabotropic and/or ionotropic receptor (protein). The complex formed between the agonist and its target is qualified as specific, reversible, and dose-dependent. However, the TRPM8 receptor, known as the canonical target for cold stimulus, is not only activated by cold but also responds to various endogenous (e.g., testosterone), natural (e.g., menthol), or synthetic ligands (e.g., icilin).

Menthol, also referred to as mint camphor, is an organic cyclic alcohol monoterpene and serves as the first natural TRPM8 agonist to be characterized. Extracted from plants of the *Mentha genus*, menthol has been used since ancient times in traditional medicine for treating infections (antifungal and antibacterial), pain (analgesic), and itch (antipruritic) (Oz et al., 2017). Its strong flavoring properties have led to its incorporation in various industries, including pharmaceuticals, cosmetics, pesticides, chewing gum, candies, toothpaste, shampoos, and soaps (Kamatou et al., 2013). Classical neurophysiological studies demonstrated that menthol activates cold thermoreceptors (Hensel & Zotterman, 1951; Schäfer et al., 1986; Reid et al., 2002; Viana et al., 2002).

Upon the cloning of TRPM8, it was revealed that cold sensory neurons express the channel, and TRPM8 serves as the primary mediator of their sensitivity to cold and agonists such as menthol and icilin (McKemy et al., 2002; Madrid et al., 2006). Several studies have reported that menthol activates the TRPM8 channel with an EC_{50} ranging from 3.6 to 66.7 µM (McKemy et al., 2002; Behrendt et al., 2004; Bödding et al., 2007; Y. Wang, 2017).

Over the years, mutagenesis screening studies have contributed to understanding the crucial residues implicated in menthol's action mechanism of action on TRPM8. For instance, a single targeted mutation at tyrosine amino acid position 745 (Y745), located at the transmembrane segment 1 (based on the recent TRPM8 Cryo-EM characterization) (Yin et al., 2018, 2022), completely suppressed sensitivity to menthol while preserving the normal response to cold and voltage (Bandell et al., 2006; L. Xu et al., 2020). Mutating other residues, such as arginine residue R842 (R842A), tyrosine amino acid at position Y1005 (Y1005A), and arginine R1008 (R1008A), produced a strong alteration of menthol sensitivity as well (Plaza-Cayón et al., 2022).

Beyond its primary interaction with TRPM8, menthol can also activate other TRP channels, including the heat-sensitive TRPV3, with an EC_{50} within the millimolar range (0.5-2 mM). At lower concentrations (micromolar range), menthol activates the TRPA1 channel, while at higher concentrations (millimolar range), it inhibits the TRPA1 channel. Interestingly, menthol also regulates ion channels outside the TRP channel family, including voltage-gated sodium (Na^+) and calcium channels (Ca^{2+}), potassium (K^+) channels, as well as $GABA_A$ and glycine receptors (Oz et al., 2017).

In summary, while studies confirm the cross-pharmacology of menthol and its lack of specificity toward TRPM8, numerous menthol derivatives, synthetic compounds, and natural products have been generated and characterized in the hopes of developing more potent, selective, and specific TRPM8 agonists.

Several menthol derivatives were studied in HEK293 cell lines and neuronal cultures, revealing their activation of TRPM8 channels with EC_{50} values in the nanomolar to low micromolar ranges. These derivatives include carboxamide agents such as WS-12 (EC_{50}=193 nM), CPS-113 (EC_{50}=1.2 µM), CPS-369 (EC_{50}=3.6 µM), and carboxylic acid WS-30 (EC_{50}=1.2 µM). Another menthol-unrelated molecule, phosphine oxide WS-148, was found to activate the channel with an EC_{50} of 4.1 nM. Among the tested agonists, WS-12 emerged as the most potent and selective TRPM8 agonist, exhibiting no cross-pharmacology towards other thermos-TRP ion channels (TRPA1, TRPV1, TRPV3, and TRPV4) (Bödding et al., 2007; Ma et al., 2008). Additionally, other menthol derivatives, including WS-3 (EC_{50}=3.7 µM), Frescolat-MAG (EC_{50}=4.8 µM), Frescolat-ML (EC_{50}=3.3 µM), PMD38 (EC_{50}=31 µM), and cooling agent 10 (EC_{50}=6 µM), demonstrated clear agonism towards TRPM8 (Behrendt et al., 2004).

Next, several synthetic cooling compounds with variable potencies were characterized such as the super cooling agent icilin (AG-3-5), which was reported to behave as a TRPM8 agonist (McKemy et al., 2002). Icilin gated TRPM8 channel with an elevated efficacy and potency compared to menthol, and this activation required the simultaneous presence of the calcium ions in the cytosolic compartment. Moreover, icilin binding to residues (N799, D802 and G805) that linked the transmembrane domain 2 and 3, were revealed using rat-avian chimeras since the chicken TRPM8 was validated as icilin-insensitive, however icilin-binding sites were distinct from menthol action mechanism (Chuang et al., 2004). Furthermore, the intracellular pH was found to modulate responses to icilin and cold but not to menthol, since decreasing the bath pH (more acid) suppressed the TRPM8 channel sensitivity to both icilin and cold, while maintained response to menthol (Andersson et al., 2004). In spite of acting through different mechanisms, both menthol and icilin shared non-specificity towards TRPM8, as they both found to modulate TRPA1 (Story et al., 2003). In addition, icilin was classified as a type 1 agonist regarding the effects on TRPM8 gating kinetics, which were similar to menthol (Janssens et al., 2016). Cryosim-3 (C3), a water-soluble synthesized molecule, used for the treatment of dry eye disease, behaved as potent and selective TRPM8 channel agonist compared to menthol, without activating any other TRP channel members (TRPV1 and TRPA1)(J. M. Yang et al., 2018) with an EC_{50} within lower micromolar range (J. M. Yang et al., 2017a; Yin et al., 2022). The residues involved in C3 action mechanism included the transmembrane domains S1 (Y745) and voltage sensor S4 (R842 and H845) as well as gating kinetics effects, were similar to results obtained with menthol, therefore cryosim-3 was considered as type 1 agonist (Yin et al., 2022).

AITC (or mustard oil), is a compound extracted from *Brassica* plants, describer in earlier work as a specific TRPA1 agonist, and mainly used in experimental studies to trigger nocifencive behaviour reactions (Bautista et al., 2006). Later, it was shown that AITC also activated another nocisensor channel: TRPV1 (Everaerts et al., 2011). Recently, AITC was found to activate recombinant and native TRPM8 channels, at millimolar concentrations, in a direct and reversible manner (Janssens et al., 2016). The AITC or type 2 agonist binding sites were defined between the critical residue tryptophane at the position 798 (W798) located at transmembrane segment 3 (S3) and glycine at the position 861 (Q861) located at intersection between transmembrane domain 4 and 5 (S4-S5), mutation of one of these residues abolished AITC activation (Yin et al., 2022).

The broad concept of drug reprofiling, which consists in the search of novel targets of an already commercialized drug, is considered an efficient drug screening strategy, offering great efficiency, less costs and reduced risks. Praziquantel, an anthelminthic drug, was shown to act as a partial agonist of mammalian and avian TRPM8 channel with an EC_{50}= 25 µM. In addition, Praziquantel action mechanism, similar to menthol acting, through the crucial residue Y745 (Babes et al., 2017). In 2019, our lab has discovered a new TRPM8 agonist, the immunosuppressant macrolide tacrolimus, which is a clinically approved drug used largely in the treatment of organ rejection during organ transplant. Tacrolimus activated TRPM8 in different species, with an approximative EC_{50} = 14.1 µM. The binding sites of tacrolimus were distinct from ilicin and menthol action mechanism. Whereas, the study also revealed that tacrolimus presented a crossed pharmacology within TRP family showing an activation of nocisensor TRPA1, but not TRPV1 (Arcas et al., 2019).

Many additional synthetized menthol derivatives TRPM8 agonists were reported in two comprehensive reviews (González-Muñiz et al., 2019; Izquierdo et al., 2021). Finally, other natural agonists compounds that activated the TRPM8 channel at millimolar range such as linalool (EC_{50}=6.7 mM), geraniol (EC_{50}=5.6 mM), hydroxycitronellal (EC_{50}=19.6 mM), eucalyptol (EC_{50}=7.7 mM) (Behrendt et al., 2004) and camphor (EC_{50}=4.48 mM) (Selescu et al., 2013) and borneol (showed a high selectivity to TRPM8) (G.-L. Chen et al., 2016).

1.3.3.2 TRPM8 antagonists

An antagonist is a substance that binds to a receptor without triggering any biological effects, thereby preventing or blocking the activation of the receptor by an agonist. Like agonists, effective blocker compounds for receptors should meet three key criteria: specificity, reversibility, and a dose-dependent response. Since the cloning of TRPM8, numerous TRPM8 blockers have been reported in the literature, with several recent reviews summarizing this body of work. In this discussion, I will highlight some of the better-characterized antagonists.

In the early literature, most reported TRPM8 antagonists lacked selectivity for TRPM8 and showed cross-modulation primarily with TRPV1 and TRPA1. Up to now, only three selective TRPM8 compounds have reached clinical trials: PF-05105679 (IC_{50} = 181nM), AMG-333 (IC_{50} = 13 nM), and Cannabidivarin (IC_{50} = 0.9 µM). However, efforts must be intensified to develop novel selective antagonists, as emphasized in a recent review (González-Muñiz et al., 2019).

BCTC [N-(4-tert-butylphenyl)-4(3-chloropyridin-2-yl)piperazine-1-carboxamide] was identified as a TRPM8 antagonist, antagonizing the response of TRPM8 to menthol in a dose-dependent manner with IC_{50} = 0.8 µM (Behrendt et al., 2004). Subsequent research supported the higher potency and selectivity of BCTC blockade effects, with a similar IC_{50}=0.475 µM (Madrid et al., 2006) and IC_{50}=0.54 µM (Mälkiä et al., 2007) on cold-activated responses in the TRPM8 channel. The lack of specificity towards TRPM8 in initial studies identifying BCTC, thio-BCTC, and capsazepine as potent TRPV1 blockers was noted. Thio-BCTC and capsazepine were also reported as inhibitors of TRPM8 with respective IC_{50} values of 3.5 µM and 18 µM (Behrendt et al., 2004). Additionally, other TRPV1 antagonists were found to behave as TRPM8 blockers, such as phenanthroline (IC_{50}=180 µM), CTPC, a related piperazinyl urea [(2R)-4-(3-chloro-2-pyridinyl)-2 methylN[4(trifluoromethyl)phenyl]1piperazinecarboxamide] (IC_{50}=131 nM), and the urea derivative SB-452533 (IC_{50}=571 nM) (Weil et al., 2005). Furthermore, ethanol, a previously reported TRPV1 agonist, known to potentiate responses to chemicals activating TRPV1, was found to inhibit menthol-evoking TRPM8 activation at different concentrations: 0.5%, 2%, and 3% (Weil et al., 2005).

SKF96365 is a non-specific blocker of several calcium permeable channels, including receptor-operated and voltage gated channels, TRP channels and potassium channels (Reid et al., 2002; Singh et al., 2010). In later studies, SKF96365 was found to reduce cold-activated currents by about 70% in dorsal root ganglia sensory neurons (Reid et al., 2002), as well as blockade of the cold evoked response of TRPM8 expressed in HEK293 line with an IC_{50}= 1 µM (Mälkiä et al., 2007). Furthermore, a study aimed at identifying the action mechanism of different TRPM8 antagonists revealed that the mutation of the menthol binding site Y745 (Y745H) supressed completely the blockade mediated by SKF96365, but did not affect the inhibition by other antagonists such as BCTC, capsazepine and clotrimazole. Thus, menthol binding site Y745 is critical for SKF96365 antagonism effect (Malkia et al., 2009).

AMTB,[N-(3-aminopropyl)-2-{[(3-methylphenyl)methyl]oxy}N(2thienylmethyl)benzamide] hydrochloride salt was characterized as a TRPM8 blocker, the application of AMTB inhibited icilin-evoked TRPM8 channel activation in HEK293 cells with IC_{50} = 6.23 µM In contrast, AMTB showed no modulation of other TRP channels including TRPV1 and TRPV4 (Lashinger et al., 2008). Additionally, it was also described as an inhibitor of voltage-gated sodium channels with an IC_{50} ranging between 4.83-5.38 µM (Yapa et al., 2018).

Clotrimazole (CLT) is a clinically approved antimycotic drug, used for the topical treatment of yeast infection within the skin, mouth and vagina. Nevertheless, many side effects were reported such as irritation and burning pain. However, the enigma surrounding the molecular targets responsible for the side effects was solved after showing that clotrimazole activated heterologous expression of nocisensors TRPV1 and TRPA1, as well as CLT stimulated a subset of capsaicin-sensitive and mustard oil-sensitive trigeminal sensory neurons, and evoked nocifensive behaviours following intraplanar injection in mice (Meseguer et al., 2008). The same study reported that CLT blocked cold and menthol activation of recombinant and native TRPM8 with an IC_{50} = 200 nM. One year later, a study identified a clotrimazole structurally related compound called econazole, which found to exert a more potent TRPM8 antagonism compared to clotrimazole, with an IC_{50}=420 nM. Moreover, like clotrimazole the inhibitory effect of econazole was decreased in the menthol insensitive Y745H mutant channel (Malkia et al., 2009).

PBMC [1- phenylethyl-4-(benzyloxy)-3-methoxybenzyl(2-aminoethyl)carbamate] identified as a novel potent and highly selective TRPM8 antagonist, without any effects on other TRP channels such as TRPV1 and TRPA1. In electrophysiological experiments, PMBC showed an IC_{50}= 0.6 nM at + 80 mV, and IC_{50}=0.4 nM at -80 mV. Later, it was shown that PBMC improved some TRPM8-pathological related-responses (Knowlton et al., 2011).

RQ-00203078, is 2-pyridyl-benzensulfonamide derivative, designated as compound 36, based on a structure-activity study. It was identified *in vitro* as robust antagonist of heterologousely expressed either human TRPM8 (IC_{50}=8.3 nM) or rat TRPM8 (IC_{50}=5.8 nM) in HEK293 cell line. Interestingly, the compound was shown to be orally active: it diminished significantly icilin-induced wet dog shakes in a dose dependent manner after oral treatment in rats. However, compound 36 was found to lack selectivity as it induces inhibition on other TRP channels (TRPA1, TRPV1 and TRPV4) at micromolar range (Ohmi et al., 2014).

Numerous new TRPM8 antagonists have been identified, including compounds derived from Chinese Medicine, such as sesamin (extracted from the *sesame* plant). Sesamin inhibits the TRPM8 channel with an IC50 of 9.79 µM, but it has also been reported to modulate other TRP channels. Notably, sesamin exhibits antitumoral activity (Sui et al., 2020). Kissei Pharmaceutical Co. has identified a novel compound named KPR-5714, which demonstrates a potent and selective TRPM8 antagonist effect with an IC_{50} of 25.3 nM, along with a favorable pharmacokinetic profile (Nakanishi et al., 2020). AMG-333, another potent and selective TRPM8 antagonist (IC_{50}=13 nM), progressed to phase one of human clinical trials as a potential treatment for migraine (Horne et al., 2018). RaQualia Pharma Inc. synthesized an imidazolinone derivative called RQ-00434739, exhibiting a potent inhibitory effect on TRPM8 with an IC_{50} of 14 nM. This compound also demonstrated significant behavioral effects related to TRPM8 channel involvement, such as cold allodynia. Importantly, RQ-0043739 did not affect body temperature, which could be a significant advantage for future clinical treatments (Aizawa et al., 2019;

Izquierdo et al., 2021). To date, only three compounds have reached the clinical phase, including AMG-333 (IC_{50}=13 nM), PF-05105679 (IC_{50}=181 nM), and Cannabidivarin (IC_{50}=0.9 µM) (reviewed by (González-Muñiz et al., 2019)). However, both AMG-333 and PF-05105679 were discontinued from clinical trials due to numerous reported side effects (reviewed by (Izquierdo et al., 2021))..

1.3.4 TRPM8 modulation

TRPM8 channel's function and biophysical characteristics are influenced by various mechanisms beyond agonists and antagonists. These include calcium ions, pH levels, the second messenger inositol phosphate PIP2, posttranscriptional modifications, receptors coupled to G proteins, and endogenous agonists (e.g., testosterone, phospholipids).

1.3.4.1 Calcium ions: desensitization/activation of TRPM8 channel

Calcium ions serve as crucial signaling molecules in various cellular processes, playing a pivotal role in regulating ion channels, including members of the TRP ion channel family. The TRPM8 channel, in particular, exhibits substantial permeability to calcium (P_{Ca}^{2+}/P_{Na}^{+}~3) (Diver et al., 2019). Calcium ions have been identified as inducers of desensitization in TRPM8 signals activated by cold or cooling compounds. Cryo-EM studies have revealed that calcium ions are situated within the transmembrane domain S2, S3, and the S2/S3 linker, interacting with several negatively charged residues (Glu773, Gln776, Asn790, Asp793, and Tyr784) (Diver et al., 2019). Mutation of these residues has been shown to reduce desensitization. The inhibition of TRPM8 by calcium is attributed to a shift in the voltage dependence of TRPM8 activation towards positive potentials (Mahieu et al., 2010).

Moreover, the involvement of phosphatidylinositol 4,5-bisphosphate (PIP2) in the Ca^{2+}-dependent desensitization process has been reported. Calcium entry through TRPM8 activates Ca^{2+}-dependent phospholipase C, leading to a decrease in PIP_2 levels and, consequently, channel desensitization (Rohács et al., 2005). Other cations, such as Mg^{2+} and Br^{2+}, have been found to induce a similar effect on the TRPM8 channel (Mahieu et al., 2010). Additionally, calcium ions play a critical role in TRPM8 activation by icilin. To achieve maximum efficacy in the icilin activation of the TRPM8 channel, an increase in cytosolic calcium ion concentration is required, classifying the TRPM8 channel as a coincidence detector (Chuang et al., 2004)..

1.3.4.2 pH modulation

TRPM8 agonists, including menthol, icilin, and cold, elicit responses at physiological pH (7.3). However, a switch to an acidic pH (6) completely eliminates sensitivity to icilin and cold, although menthol sensitivity remains unaffected (Andersson et al., 2004). Notably, the acidic pH induces a shift in the threshold for cold activation towards lower temperatures (Andersson et al., 2004), aligning with

a recent study that demonstrated the inhibition of TRPM8 currents by the proton H^+ resulting from a shift in voltage dependence towards positive potentials (Mahieu et al., 2010).

1.3.4.3 PI(4,5)P2 : activate/ desensitize TRPM8 channel

Various ion channels are directly regulated by the plasma membrane phospholipid phosphatidylinositol 4,5 bisphosphate [PI(4,5)P_2], including voltage-gated potassium channels (K_v), inward rectifying potassium channels (Kir), voltage-gated calcium channels (Ca_v2.1 and Ca_v2.2), two-pore potassium channels K2P (TASK1, TASK3, and TREK1), and various TRP channels (reviewed by (Suh & Hille, 2008)). PI(4,5)P_2's importance for TRPM8 activity has been highlighted in different studies (Rohács et al., 2005; Zakharian et al., 2010). In patch-clamp recordings in the inside-out configuration, a rundown phenomenon was observed, characterized by a decrease in TRPM8 channel activity. This decrease resulted from the loss of cytoplasmic modulators maintaining PI(4,5)P_2 equilibrium and increased depletion of PI(4,5)P_2 by active membrane-associated lipid phosphatase (Ca^{2+}-sensitive PLCδ1) in the excised plasma membrane. Rundown was reversed by applying dic8PI(4,5)P_2, a soluble PI(4,5)P_2 analogue (Rohács et al., 2005), or phosphatase inhibitors like FVPP (Liu & Qin, 2005). PI(4,5)P_2 scavengers and increased lipid phosphatase activity accelerated rundown, while PI(4,5)P_2-interacting mutations involving positive residues (K995, R998, and R1008) in the TRP domain reduced sensitivity to PI(4,5)P_2 and menthol (Rohács et al., 2005). These results collectively support the conclusion that the TRP domain acts as a PI(4,5)P_2-interacting domain.

Furthermore, PI(4,5)P_2 is proposed to mediate TRPM8 channel activation through the interaction of the TRP domain with PI(4,5)P_2, leading to channel opening and subsequent Ca^{2+} influx. This activation triggers calcium-sensitive phospholipase C (PLCδ1), inducing PI(4,5)P_2 hydrolysis and causing TRPM8 channel desensitization (Rohács et al., 2005).

1.3.4.4 G-protein coupled receptors (GPCRs) modulate TRPM8 channel

Numerous G protein-coupled receptors (GPCRs) play a crucial role in modulating inflammatory and neuropathic pain. Inflammatory mediators such as bradykinin, ATP, prostaglandin, and histamine regulate GPCRs (Rohács et al., 2005; Zhang et al., 2012; Zhang, 2019; L. Liu et al., 2019). The majority of GPCRs activated by these inflammatory mediators are coupled to the Gαq heterotrimeric G-proteins (Rohacs, 2016). In both, dorsal root ganglia (DRG) neurons and heterologous systems, the activation of Gαq-coupled GPCRs indirectly inhibits TRPM8 channel activity. For example, receptors like bradykinin (B2R) or histamine (H1R) receptors activate an intracellular cascade involving the activation of phospholipase C (PLCβ), leading to the hydrolysis of PI(4,5)P_2 (Liu et al., 2019).

Contrastingly, other studies report the direct inhibition of the TRPM8 channel by Gαq independently of downstream signaling. In this scenario, Gαq binds at both N-terminus positive arginine residues

(R364, R368, and R470) and the two C-terminus fragments, N7 (F245 and E398) and N8 (R451 and N606). Mutations in these effector binding sites result in increased sensitivity to TRPM8 agonists, suggesting a decrease in inhibition due to disrupted binding of the activated Gαq (Zhang et al., 2012; Zhang, 2019). Interestingly, the inhibition of TRPM8 channels by Gαq-coupled receptor activation is suggested to contribute to thermal hyperalgesia in inflammation (Zhang et al., 2012).

1.3.4.5 Post-translational modifications modulate TRPM8 channel

Receptors, including ion channels, carrier proteins, and G protein-coupled receptors, undergo continuous expression and renewal in the plasma membrane through the cellular processes of endocytosis and exocytosis (Stillwell, 2016). The TRPM8 protein undergoes post-translational modifications within the endoplasmic reticulum (ER)-Golgi apparatus axis before its integration into the plasma membrane. N-glycosylation, a relevant but not essential process for multimerization, transport, and compartmentalization of TRPM8 within the lipid microenvironment called "Lipid raft," involves attaching saccharide N-glycan moieties to an asparagine residue (N934) in the extracellular loop S5-S6 linker (Erler et al., 2006; Morenilla-Palao et al., 2009; Stanley et al., 2022). Mutation of the N-glycosylated residue N934Q (unglycosylated TRPM8 mutant) significantly affected the biophysical and functional properties of the mutant TRPM8 channel compared to the wild type. Specifically, the unglycosylated mutant exhibited decreased sensitivity to agonists (cold and menthol) and a shift in the activation threshold toward colder temperatures (Pertusa et al., 2012).

The mature TRPM8 ion channel resides within the plasma membrane lipid raft through the fusion of exocytosis vesicles with the plasma membrane, mediated by vesicle-associated membrane protein 7 (VAMP7) (Ghosh et al., 2016). Lipid rafts, in both native and heterologous expression systems, are enriched with cholesterol and sphingolipids. This lipid microenvironment facilitates channel activation and the assembly of intracellular signaling cascades. Interestingly, the disruption of lipid raft composition increased the response of TRPM8 to agonist activation (Morenilla-Palao et al., 2009).

Phosphorylation by kinase activity represents another form of post-translational modulation of the TRPM8 channel (Rivera et al., 2021). Studies have suggested that TRPM8 channel activity is regulated by different kinases (Premkumar et al., 2005; Bavencoffe et al., 2010; Manolache et al., 2020). Four serine residues within the N-terminal, including S26, S29, S541, and S542, are identified as specific constitutively phosphorylated sites. Inhibition of kinase activity with staurosporine enhanced the channel response to different TRPM8 agonists in both heterologous expression systems and sensory neurons, indicating that the phosphorylation mechanism acts as a molecular brake on channel activity (Rivera et al., 2021). The study also revealed that the mutation at residue S29A alone was sufficient to render the TRPM8 channel hypersensitive to agonists. Additionally, the unphosphorylated TRPM8

channel exhibited changes in biophysical properties compared to the wild type, showing a marked shift in voltage dependence toward negative potentials.

1.3.4.6 Other modulatory mechanisms of TRPM8

Various lipid molecules have been identified as modulators of TRPM8 channel activity. Arachidonic acid, for instance, was found to induce channel inhibition through an indirect mechanism involving the phospholipase A2 signaling cascade (Bavencoffe et al., 2011). Polyunsaturated fatty acids (PUFAs) and lysophospholipids (LPLs), both products of phospholipase A2 activation, have distinct effects on TRPM8 modulation. LPLs positively regulate TRPM8 by shifting the threshold toward body temperature, while PUFAs like arachidonic acid inhibit TRPM8 activation by various agonists (Andersson et al., 2007). These findings underscore the crucial role of lipids in modulating TRPM8 channel activity.

PIRT, a membrane protein widely expressed in peripheral sensory neurons, has been identified as a regulator of TRPM8 channels through direct interaction within the TRPM8 S1-S4 domain (Tang et al., 2013; Hilton et al., 2018). PIRT-regulated TRPM8 channels exhibit a species-dependent role, where human PIRT decreases human TRPM8 conductance, while mouse PIRT increases mouse TRPM8 conductance (Hilton et al., 2018).

Notably, testosterone, a male steroid hormone, has been recognized as the first endogenous TRPM8 agonist (Asuthkar et al., 2015; Mohandass et al., 2020). It activates the channel in a potent and selective manner, with an EC_{50} within the picomolar range. Moreover, other steroids, such as dihydrotestosterone (DHT) (EC_{50}=23.5 nM), progesterone (EC_{50}=0.49 µM), and 17β-estradiol (EC_{50}=1.2 µM), were found to activate the TRPM8 channel with less potency compared to testosterone (Mohandass et al., 2020). Behavioural experiments in humans demonstrated that acute skin application of testosterone induces a cooling sensation (Asuthkar et al., 2015). Additionally, in mice, testosterone was found to regulate dimorphic sex and social behaviours (Mohandass et al., 2020).

1.3.5 TRPM8: (Patho)physiological implications

The widespread expression of the TRPM8 ion channel across various tissues and organs underscores its potential relevance in numerous physiological functions. Numerous studies involving transgenic mice lacking TRPM8 provide substantial evidence supporting the contribution of TRPM8 to a variety of physiological processes. Conversely, the dysregulation of this channel has been implicated in the development of TRPM8-dependent diseases, positioning the channel as a promising target for the development of therapeutic interventions.

1.3.5.1 TRPM8 physiology

1.3.5.1.1 Cold sensing

The initial physiological function ascribed to the TRPM8 ion channel was the transduction of cold temperatures. Early studies attributed cold sensing in cultured primary sensory neurons to the activation of the TRPM8 channel (McKemy et al., 2002; Peier et al., 2002). Subsequent *ex-vivo* experiments conducted at the level of peripheral sensory nerve terminals further supported this finding (Madrid et al., 2006). In 2007, three independent studies employing TRPM8-deficient mice provided robust confirmation of the central role of the TRPM8 channel in cold perception by thermoreceptors, both in *vitro* and in *vivo*. The TRPM8-deficient mice exhibited an absence of detectable levels of TRPM8 mRNA or proteins, coupled with a reduction in neurons responding to cold and menthol compared to wild-type mice. *In vivo* behavioural tests, including the two-temperature choice assay and the thermotaxis assay of temperature gradient, consistently demonstrated that TRPM8-deficient mice exhibited reduced avoidance of cold temperatures. These mice spent more time in cold zones compared to their wild-type counterparts. Additionally, TRPM8-deficient mice displayed a marked deficiency in icilin-induced wet dog shakes or jumping and reduced nocifensive behaviours in response to acetone, an unpleasant cold stimulus (Bautista et al., 2007; Colburn et al., 2007; Dhaka et al., 2007).

Despite the evident deficit in cold sensing in TRPM8 knockout (KO) mice, all three studies reported the existence of a significant percentage of responses remaining to noxious cold temperatures within neuronal cultures: 18% (Bautista et al., 2007), 45% (Dhaka et al., 2007), and 60% (Colburn et al., 2007). Consistent with these *in vitro* findings, behavioural tests in TRPM8 mutant mice revealed avoidance of surfaces below 10 °C (Bautista et al., 2007). Furthermore, Dhaka et al.(2007) observed similar nocifensive behaviour latencies in both wild-type and TRPM8-deficient mice when placed on a cold plate (-1°C). Colburn et al.'s study (2007) reported delayed responses to noxious cold in TRPM8-deficient mice, suggesting the involvement of other TRPM8-independent molecular or cellular mechanisms in noxious cold detection.

Previous studies showed using genetic TRPM8-knock out mice, demonstrated by the remaining partial noxious cold avoidance, which could be due to an residual presence of TRPM8-expressing neurons. This limitation drove neuroscientist to develop new strategy that consisted into a selective ablation of the TRPM8-expressing neuronal population. The first study was reported by Mishra and collaborators (Mishra et al., 2011), using a genetic tool based on BAC transgenic mice called $TRPV1^{DTR}$. These transgenic mice express diphtheria toxin (DTR) receptor within the lineage of TRPV1-expressing sensory neurons, and upon diphtheria toxin injection selectively deleted TRPV1-expressing neurons. However, giving that TRPV1 was characterized as a common marker of both all nociceptors, and TRPM8-expressing neurons at embryonic stage, which disappeared after birth. The $TRPV1^{DTR}$ mice

line showed a complete lack of TRPM8 expressing neurons, and interestingly, this result was corroborated with behavioural responses since TRPV1^{DTR} mice showed both a complete suppression of icilin evoked wet dog shakes and a complete insensitivity during cold plate (-5˚C) test. Furthermore, to examine the relevance of selective ablation of TRPM8-expressing neurons, McKemy's lab conducted a behavioural study, where they have generated a BAC transgenic mouse line called TRPM8^{DTR} (ablated mice) characterized by the expression of DTR receptor gene fused with the gene coding for GFP (Fluorescent green protein) and driven by the TRPM8 promoter. They found that, like embryonic deletion of TRPM8 (TRPM8$^{-/-}$), the ablated TRPM8 neurons transgenic mice were insensitive to innocuous cold during acetone test, as well as they presented an impairment of icilin evoked shivering or wet dog shakes. In contrast , the ablated mice showed no avoidance to noxious cold since they showed more activity at 5 ˚C surface and they failed to distinguish between cold and preferable warm temperatures surfaces, compared to either wild type or TRPM8$^{-/-}$ knockout mice that showed a strong noxious cold avoidance and warm surface preference (but largely distinct from wild type). Thus, these new results support the findings described previously, highlighting TRPM8 as the prime transducer of cool to noxious cold temperatures. Noteworthy, both heat or mechanical sensitivity in ablated and TRPM8$^{-/-}$ mice were not different from wild type, which strongly support that TRPM8 is solely implicated in cold transduction. Interestingly, they also found that in ablated and TRPM8$^{-/-}$ mice, both showed a marked attenuation of cold pain associated with inflammation and nerve injury, and both genotypes showed an abolished cold evoked analgesia after nerve injury (Knowlton et al., 2013).

Taken together, these results confirmed the crucial role of TRPM8 in thermosensation of innocuous to noxious cold temperatures, although the genetic suppression of TRPM8 did not dampen the noxious cold aversion behaviour, which may suggest the existence of another noxious cold transducer that contributed to avoidance behaviour in the absence of TRPM8.

Several studies have looked at the mechanisms underlying TRPM8-independent noxious cold transduction. An early study suggested the implication of a voltage gated potassium (K^+) channels and the closure of background K^+ channels during cooling, leading to increased excitability of cold sensory neurons resulting their depolarization and firing (Viana et al., 2002). Another study revealed the importance of TASK-3 leak potassium channels in the setting of the cold threshold in TRPM8 expressing neurons, where the pharmacological blockade of this channel or TASK-3 KO mice produced cold hypersensitivity (Morenilla-Palao et al., 2014). Moreover, the two pore domain K^+ channels (TREK1, TREK2 and TRAAK) were characterized as temperature sensitive either in heterologous expression system and in sensory neurons, since the channels were hyperactive at physiological temperature (37 ˚C) while they inactivate at 24 ˚C (Maingret et al., 2000; D. Kang et al., 2005). Besides, other voltage gated potassium channels such as $Kv_{1.1}$ and $Kv_{1.2}$ had been also related to control of cold sensitivity (Madrid et al., 2009; González et al., 2017). Furthermore, the TTX-resistant voltage gated sodium channel $Na_v1.8$ was found to modulate noxious cold transduction at low temperatures, where

$Na_v1.8$-null mice showed a marked reduction of noxious cold responses (Zimmermann et al., 2007).Thus, neither the potassium nor sodium channels were attributed to directly behave as noxious cold sensor.

Several studies support the role of TRPA1 in the transduction of noxious cold, but this evidence is still debated (Story et al., 2003; Kwan & Corey, 2009). Numerous studies support the fact that TRPA1 expressed either in sensory neurons or in heterologous expression systems, is activated by cold with lower temperature threshold compared to TRPM8 channels (Story et al., 2003; Karashima et al., 2009). In contrast, other laboratories failed to confirm TRPA1 as a direct cold nociceptor in both sensory neuronal cultures and heterologous system (Jordt et al., 2004) ,or argued that the activation is an indirect effect of an elevated intracellular calcium (Zurborg et al., 2007). Furthermore, TRPA1 thermosensitivity in many species including rodents, primates and invertebrates showed a clear thermal species-dependent divergence extending from cool to heat temperatures (Kwon et al., 2008; K. Kang et al., 2012). More interestingly, the human TRPA1 channel showed a U-shape thermosensitivity showing both cold and warm sensitivity, which suggested an evolutionary conservation of TRPA1 thermal sensitivity (Moparthi et al., 2016).

In 2019 a fascinating report suggested the role of peripheral glutamate receptors in noxious cold sensing (Gong et al., 2019). Using a genetic screen, they found the GLR-3 (Kainate-type glutamate receptor homolog) acting as a noxious cold receptor in *C-elegans* that was responsible for cold avoidance behaviours. The GLR-3 recombinant expression in mammalian cells generated cold sensitivity in the noxious range below 20 ˚C. Interestingly, the GLR-3 was found to function as a metabotropic receptor coupled to Gi-protein rather than as an ion channel. Additionally, the GLR-3 homolog glutamate receptor GluK2 from different species (fish, mouse, and human) was found to act as a cold receptor *in vitro*. In DRG neurons the GluK2 receptor played a clear role in noxious cold (10 ˚C) response but not cool (22 ˚C). Thus, this study highlighted an evolutionary conservation of glutamate receptors as noxious cold receptors, which could explain the residual responses to noxious cold observed after genetic deletion of TRPM8 ($TRPM8^{-/-}$ mice) (discussed previously).

Cold sensitivity is found to vary across species and also depending on the animal habitat (Matos-Cruz et al., 2017; S. Yang et al., 2020). The mammalian hibernators, such as ground squirrel (*Ictidomys tridecemlineatus*) and hamster (*Mesocricetus auratus*), withstand prolonged exposure to cold and extreme hypothermia, whereby adaptation at the molecular level. This adaptation includes a marked decrease of TRPM8 channel cold sensitivity compared to mice (no hibernating mammal), The interesting decrease in sensitivity to cold in squirrel was related to molecular changes implicating six amino acids residues within squirrel TRPM8 channel, but the replacement of those six residues with their homologue residues from rat TRPM8 (H726Y, A762S, P819S, A927S, H946Y and S947N) conferred to squirrel TRPM8 robust cold sensitivity (Matos-Cruz et al., 2017). Those six

transmembrane domains were not conserved between squirrel and hamster, while the transposition of rat TRPM8 transmembrane core induced an increase of Hamster TRPM8.cold sensitivity.

Moreover, the cold activation of TRPM8 was found to correlate with habitat temperature as well. A relevant study found that eTRPM8 elephant (L*oxodonta africana*) from Sahel desert showed a higher cold activation current compared to Antarctic penguin (*Aptenodytes forsteri*) TRPM8 that demonstrated a lower cold current activation. The molecular mechanism underlying such habitat-dependent cold sensitivity included the pore domain residue at position 919, however mutating this residue either in African elephant (V919Y) or emperor penguin (Y919V) reversed their cold sensitivity (S. Yang et al., 2020).

In conclusion, different studies suggest that cold transduction depends mostly, but not exclusively, on TRPM8. Other sensory mechanisms also participate, which make cold sensing the result of the convergence of different actors.

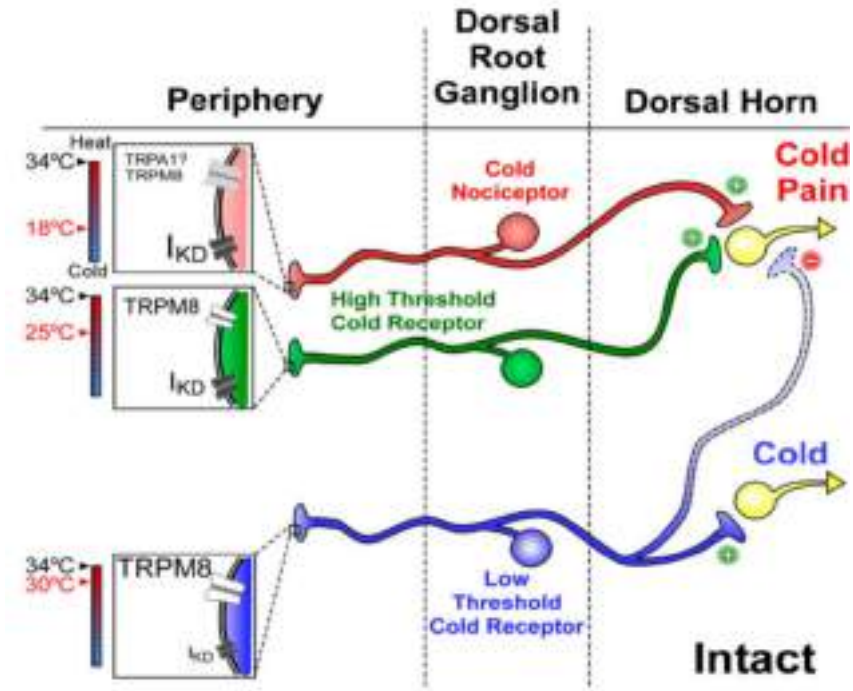

Figure 7. Hypothetical model of innocuous cold and cold pain sensing mechanisms of the peripheral sensory neurons. The model integrating other non-TRPM8 dependent cold sensing mechanism represented within the left squares. The relative density of each cold transducer is represented by the size of the labelling, and the temperature sensing by each neuronal cluster was represented by red colour at thermometer scale. The perception of either cool or cold pain was determined by the positive (+) and negative (-) modulation mechanism occurring at central nervous system. Figure was taken from (Gonzalez et al., 2017)

1.3.5.1.2 Warm perception

Numerous studies have investigated the involvement of TRP channel family members, such as TRPV3, TRPV4, TRPV1, and TRPM2, in the transduction of warm temperatures (H. Xu et al., 2002; Moqrich et al., 2005; Tan & McNaughton, 2016). Recently, a compelling study shed light on the central role of TRPM8 in warm temperature perception. Utilizing a combination of behavioural tests and skin-nerve recordings, the authors revealed that warm perception relies on the simultaneous functioning of two distinct populations of polymodal C-fibers.

In this intricate process, warm temperatures activate the first pathway, expressing warm-sensing TRP channels (TRPM2, TRPV1, and TRPM3), while concurrently inhibiting the ongoing activity of cool-driving TRPM8-expressing C-fibers. Furthermore, the study demonstrated that neither the deletion of TRPM2 nor TRPV1, nor the use of triple knockout mice (TRPV1, TRPA1, and TRPM3), fully eliminated warm perception. However, pharmacological silencing of TRPM8 using the PBMC antagonist or the use of TRPM8-null mice resulted in a complete loss of the ability to sense warmth (Paricio-Montesinos et al., 2020). Thus, TRPM8-expressing C-fibers play a crucial role in sensing warm temperatures, operating through a mechanism involving the reduction of ongoing activity in cutaneous cold thermoreceptors.

1.3.5.1.3 Eye neurobiology

The eye-ball is a complex organ responsible for vision in animals, including humans. It detects light and converts it into electrochemical impulses that the brain (occipital cortex) interprets as visual images. Key components include the cornea (transparent front part), iris (coloured part regulating light), pupil (adjustable opening), lens (focuses light), retina (light-sensitive layer with photoreceptor cells), optic nerve (transmits signals to the brain), sclera (tough outer layer), and choroid (provides blood supply). Together, these elements enable the eye to perceive and process visual information (Purves, 2004).

The cornea, a transparent and avascular tissue situated in front of the lens within the eyeball, facilitates the entry of light rays into the eye (Purves, 2004). The cornea is composed of cellular components, including epithelial cells, keratocytes, and endothelial cells, as well as acellular components such as collagen and glycosaminoglycans (Sridhar, 2018). Its physiological relevance lies in its dual role as a structural and infectious barrier for the eye. Additionally, the clarity of the cornea is crucial for proper vision (DelMonte & Kim, 2011). The cornea is a densily innervated structure. Corneal sensory nerves originate from the trigeminal ganglion. Neurons innervating the cornea are categorized based on axon myelination degree into thinly myelinated (type-Aδ, 30% in mouse) or unmyelinated (type-C, 70% in mouse). Additionally, corneal nerves exhibit heterogeneity based on conveyed stimuli, with 20% being mechanonociceptors responsive to noxious mechanical stimuli, 70% polymodal nociceptors excited by

extreme temperatures, irritant chemicals, and inflammatory mediators, and 10% cold-sensitive terminals (Belmonte et al., 2004).

Cold fibres in the cornea exhibit irregular spontaneous activity at rest, enhanced by moderate cooling and ceasing following warming (Gallar et al., 1993; Belmonte et al., 1997, 2004). Several studies have identified TRPM8 channels as the primary cold sensors of cool-driven ongoing activity in corneal cold fibres (Parra et al., 2010; Quallo et al., 2015). Furthermore, these studies revealed that corneal TRPM8 channels contribute to the regulation of other eye physiological functions, including the control of basal tearing and eye blinking. Notably, TRPM8 agonists such as cold, menthol (at low concentrations), borneol, Cryosim-3, and tacrolimus enhance corneal cold cell activity, tear production, and eye blinks in wild-type animals. However, in TRPM8 knockout mice or in the presence of a TRPM8 blocker, there is a decrease in both ongoing and cold-induced corneal fibre activity, as well as basal tearing (Parra et al., 2010; Robbins et al., 2012; G.-L. Chen et al., 2016; J. M. Yang et al., 2017a; Arcas et al., 2019). Collectively, these studies support the conclusion that TRPM8-expressing corneal fibres play a crucial role in the control of tear production and eye blinks. Interestingly, some studies reported nocifensive behaviors following the application of higher concentrations of agonists such as menthol (50 mM) or tacrolimus (12 mM), but not cryosim-3 or borneol, suggesting the involvement of other TRPM8-independent nocisensor targets (Robbins et al., 2012; G.-L. Chen et al., 2016; J. M. Yang et al., 2017a; Arcas et al., 2019).

Moreover, the application of hyperosmotic solutions or the drying of the ocular surface increases the ongoing activity of corneal cold fibres, leading to elevated tear production (Hirata & Meng, 2010; Quallo et al., 2015). Quallo and collaborators demonstrated that an increase in osmolality activates TRPM8-expressing sensory neurons in dorsal root ganglia (DRG), trigeminal ganglia (TG), and cold fibre terminals innervating the cornea, with this response being absent in TRPM8$^{-/-}$ mice (Quallo et al., 2015). Additionally, hyperosmotic solutions were found to enhance the spontaneous electrical activity of TRPM8-expressing corneal nerve terminals, while hypo-osmotic solutions reduced their firing activity. Furthermore, topical application of the TRPM8 antagonist BCTC resulted in a significant reduction in basal blinking frequency compared to non-treated mice, and a similar effect was observed when comparing TRPM8 knockout mice with wild type. Altogether, these findings suggest that TRPM8 serves as a direct osmosensor and a crucial regulator for eye blinking, contributing to maintaining the wetness of the eye surface.

In summary, trigeminal TRPM8-expressing sensory fibres innervating the cornea play a vital role in maintaining a stable and homogeneous humidity in the ocular environment by controlling both tear production and eye blinks.

1.3.5.1.4 Body temperature and energy balance

Thermoregulation is a fundamental body homeostatic function in both poikilothermic and homeothermic animals, used in adaptation to continuous fluctuations in environmental temperature, that help preserving a constant internal environment. In poikilothermic animals or cold blooded, body temperature depends directly on the external temperature. They are characterized by the absence of any physiological processes to generate heat and regulate their internal temperature (Kearney et al., 2009). Although, cold blooded animals can use some specific homeostatic behaviours that lead to adequate their body temperature properly for the execution of specific functions (Kiefer et al., 2006). In contrast, homeothermic animals or warm blooded take advantage of specific physiological processes for heat control-balance, that are governed by the central nervous system, in order to stabilize their internal body temperature (Señarís et al., 2018). Moreover, homeothermic animals exhibit a basal level of thermogenesis with the eventual capacity to increase it under demand. Noteworthy, in conditions where the basal thermogenesis turned insufficient to keep a stable body temperature the body activate heat-saving physiological mechanisms such as vasoconstriction and piloerection (Señarís et al., 2018). In addition, for example when exposed to cold environment, the organism adapts immediately and executes an increase of the heat production through shivering thermogenesis, which is generated by skeletal muscles contractions in order to produce metabolic energy following ATP hydrolysis (independently of exercise). Then, if the is cold condition is sustained over weeks, our organism will adopt a non-shivering adaptative thermogenesis of brown adipose tissue (BAT).

The detection of ambient temperatures variations is mediated by thermosensitive transient receptor potential (TRPs) ion channels expressed in the peripheral sensory nerve terminals innervating the skin (Señarís et al., 2018; Buijs & McNaughton, 2020). TRPM8-expressing peripheral sensory nerve endings innervating the skin are responsible for cold-environmental transduction, although not the solely mechanism (Buijs & McNaughton, 2020). TRPM8 expression is also found within brain thermoregulatory circuit (Ordás et al., 2021). In addition, several studies linked TRPM8 channel activity to thermoregulation, where TRPM8 agonist application induced an increase of body temperature (hyperthermia), oxygen consumption, muscle shivering, and tail vasoconstriction in wild type mice. All these physiological changes are considered as heat-gain responses (Tajino et al., 2007). In contrast, administration of a TRPM8 antagonist provoked a decrease in either body temperature (hypothermia), or shivering and non-shivering thermogenesis in wild type mice, but no such effect was observed in TRPM8-deficient mice (Almeida et al., 2012). More recently, an interesting study provided further evidence about the important role of TRPM8 in thermoregulation, where they showed that TRPM8-deficient mice housed at cold temperatures (17 ˚C) exhibited a diminished body temperature of about 0.7 ˚C. Moreover, TRPM8-deficient mice experienced an increase in tail heat loss, indicating that TRPM8 participates in the autonomic control of tail vessel muscle tone (Reimúndez et al., 2018). In addition, the same study highlighted the implication of TRPM8 in energetic metabolism control, since

they found that TRPM8 deficient mice raised at mild cold temperatures (21˚C) developed late onset obesity compared to wild type animals, which was accompanied with glucose and lipid metabolism dysfunctions. In the same line, another study showed that TRPM8 knockout mice raised at room temperature (22 ˚C) developed obesity, glucose intolerance and showed a decrease in icilin-induced energy expenditure compared to wild type animals, whereas no differences were found when housed at thermoneutrality (30 ˚C) (Liskiewicz et al., 2023). In contrast, other studies found that TRPM8 deletion had no effect on body gain weight, and did not find a reduction of body temperature compared to wild type (McCoy et al., 2013; Carvalho et al., 2021). Furthermore, the genetic deletion or pharmacological inhibition of TRPM8 had no effect on cold-evoked shivering or body temperature, which ruled out the direct implication of TRPM8 in thermoregulation and energy balance, while suggesting the participation of the heat activated TRPV1 channel as another thermoregulatory effector (Feketa et al., 2013).

1.3.5.1.5 Analgesia mediated by TRPM8 activation

Early psychophysical studies suggested the beneficial use of cool stimulation to evoke pain analgesia (Bini et al., 1984), further supported by several clinical trials highlighting the efficacy of cool application on the alleviation of back pain, and postoperative pain (Sauls, 1999). Additionally, menthol, a substance that mimics cool sensation, was widely used empirically in Western and Chinese medicine for the relief of pain and itch (Göbel et al., 1994; Green & McAuliffe, 2000; Davies et al., 2002). Later, a series of studies succeeded in uncovering the mechanism of analgesia produced by both cool or menthol applications, using different animal models of neuropathic and inflammatory pain. These studies reported the central role of TRPM8-expressing peripheral sensory fibres in the observed cold-evoked analgesia (Proudfoot et al., 2006; Dhaka et al., 2007; Knowlton et al., 2013; Liu et al., 2013). Proudfoot and collaborators showed, using a rat model of chronic constriction injury (CCI) of the sciatic nerve, that immersion of the paw at cool temperatures (20 to 16 ˚C) for 5 min evoked a significant mechanical analgesia. Furthermore, they also found that either topical application or intrathecal injection of TRPM8 agonist icilin induced a striking thermal and mechanical analgesia. In contrast these beneficial effects were absent after the specific TRPM8 knock down (using TRPM8 antisense oligonucleotide) (Proudfoot et al., 2006). Similar results were obtained by Knowlton and collaborators confirming the requirement of TRPM8 for cooling-induced mechanical analgesia. This effect was observed in wild type mice but abolished in mice lacking the expression of TRPM8 channel, or after the ablation of TRPM8-expressing neurons (Knowlton et al., 2013). Furthermore, in a mice model of acute pain induced by paw injection of formalin (2%), wild type mice showed nociceptive reactions when placed on a plate at room temperature (24 ˚C), whereas those nocifensive behaviours were markedly reduced at cold temperature (17 ˚C) plate. Finally, cold-evoked analgesia was absent in TRPM8-deficent mice (Dhaka et al., 2007). Thus, all the mentioned studies support the requirement of TRPM8 signalling in cool-induced pain relief.

Besides, the Peppermint (menthol) found to decreased efficiently noxious heat, irritant chemicals (Capsaicin, acrolein, acetic acid) and inflammation (induced by complete Freund´s adjuvant) evoked pain behaviours, nevertheless the effect was abolished either in TRPM8-knock out or following inhibition by a selective TRPM8 agonist (AMG2850) (B. Liu et al., 2013). In the same study, systemic or topical application of menthol doubled the withdrawal latencies in the hot plate test (52 ˚C or 55 ˚C). Moreover, the menthol derivative WS-12 (more selective than menthol) mimicked menthol-induced acute inflammatory pain reduction.

Clinical studies demonstrated that cooling also induces itch relief (Fruhstorfer et al., 1986). A recent study showed that both cool- and menthol-induced itch relief required TRPM8 signalling (Palkar et al., 2018). Interestingly, the topical application of pruritogens (Histamine, Cqx and compound 40/48) on the wild type mice hind paw induced itch behaviours (licking, lifts and biting) at preferred temperature 30 ˚C plate, while placed on a cold plate set at temperatures below 20˚C abolished strikingly itch response. Nonetheless, cooling -induced (20 ˚C) antipruritic effect was lost in TRPM8 null mice.

Several studies have tried to dissect the mechanism through which the TRPM8-expressing sensory neurons induced pain and itch relief, but is still unclear up to now. Some results suggest a centrally-mediated inhibitory effect, implicating a neuronal circuitry resembling those of the gate control theory (Melzack & Wall, 1965), where the primary afferents releasing glutamate neurotransmitter target the group II/III metabotropic glutamate leading to the inhibition of spinal nociceptive inputs (Proudfoot et al., 2006). While, other findings suggested that TRPM8 agonists (Menthol and WS-12) induced analgesia through the activation of endogenous opioid-dependent pathways (B. Liu et al., 2013).

Nowadays, several preclinical studies aimed at dissecting the central circuits underlying the analgesic effect of TRPM8 agonists in chronic pain and itch. The manipulation of those circuits represent an efficacious therapeutical treatments of chronic pain and itch in human (Ständer et al., 2017; S. Wang et al., 2017).

1.3.5.1.6 Other physiological roles of TRPM8

The broad distribution of the TRPM8 channel across various tissues and organs, including the bladder, prostate, testis, gastric fundus, and gastrointestinal system, suggests its involvement, either fully or partially, in numerous physiological functions (McKemy, 2007; Y. Liu et al., 2020b). Recent evidence highlights the necessity of TRPM8 channel signaling for proper sexual and social behaviours (Mohandass et al., 2020). Additionally, the expression of the TRPM8 channel in retinal ganglion cells projecting to the suprachiasmatic nucleus of the hypothalamus, the pacemaker for the circadian cycle, indicates its contribution to regulating both central and peripheral clocks and influencing circadian regulation of body temperature (Reimúndez et al., 2023).

1.3.5.2 TRPM8 pathophysiology

The TRPM8 channel has been associated with the pathophysiology of various diseases, including tumours, migraines, dry eye disease, and cold hypersensitivity, as comprehensively reviewed by Pertusa et al. (Pertusa et al., 2023). The strength of evidence linking TRPM8 to specific pathologies varies, with some conditions having robust supporting evidence, while in others, the association is more circumstantial and is based on the channel's expression in particular tissues. Nevertheless, due to the significant implication of TRPM8 in numerous pathologies, it has emerged as a key target for potential treatments of prevalent diseases.

1.3.5.2.1 Malign Tumours

The expression of TRPM8 in different tumours suggest a potential role of the channel in cancer physiology. Early work identified TRPM8 ion channel in the human prostate, and the expression was found upregulated in prostate cancer (Tsavaler et al., 2001), as well as in many other tumours (Q. Li et al., 2009; Kijpornyongpan et al., 2014). Interestingly, in the prostate cancer the expression of TRPM8 was found positively correlated with the tumour aggressiveness, (Tsavaler et al., 2001). Furthermore, TRPM8 has been linked to many other life threatening tumours such as melanoma, breast cancer and pancreatic cancer (Y. Liu et al., 2020b). All those studies supported the TRPM8 relevance in cancer cell biology.

Subsequently, an interesting study reported that the activation of TRPM8 expressed in prostate cancerous cells by the PSA (prostate specific antigen), an endogenous agonist, provoked a drastically decrease of cell migration suggesting a potential role of TRPM8 in cancer progression (Gkika et al., 2010). Moreover, in line with previous finding the expression of TRPM8 was also correlated with pancreatic cancer progression, and suggested that TRPM8 channel overexpression in pancreatic cancers induced an increase of intracellular calcium signalling, which suggested to play a role in cell proliferation and metastasis (Du et al., 2018). Next, a recent study also confirmed an upregulation of TRPM8 channel in colon primary tumours, in contrast they found that either TRPM8-deficient mice or pharmacological blocking of the channel (using WS-12 induced desensitization) were associated with robust reduction of tumour growth. The observed reduction resulted from the inhibition of the oncogene Wnt/B-catenin signalling pathway involved in regulating cell cycle, suggesting again the central role of TRPM8 channel in cancer progression (Pagano et al., 2023). In melanoma, TRPM8 expressed in plasma membrane was suggested to regulate the equilibrium of calcium (Ca^{2+}) in cytosol, which is considered as relevant secondary messenger responsible for the control of both cell proliferation and differentiation processes. In addition, either TRPM8 channel activation or blockade elicited a dysregulation of calcium balance leading to melanoma cells death (Kijpornyongpan et al., 2014; Y. Liu et al., 2020b). Clinical

studies showed that the overexpression of the TRPM8 channel in cancerous cell was correlated negatively with life survival in patients (Du et al., 2018; Pagano et al., 2023).

Taken together, TRPM8 can be considered as biomarker for diagnosis, progress assessment and treatment of different life-threatening cancers. Nevertheless, TRPM8 has been also linked to the side effect following chemotherapy drug treatment for example with oxaliplatin that leads to a marked cold allodynia in distinct species, which may suggest the use of TRPM8 antagonist alongside oxaliplatin to alleviate this symptom. Therefore, understanding more TRPM8 role in cancer etiology and progression will support considering TRPM8 channel potential as a drug target in oncology (reviewed by (Z. Liu et al., 2016)).

1.3.5.2.2 Migraine

Migraine is the second most debilitating disease worldwide, and the second most common chronic neurological disorder affecting approximately 12 % of the general population. It is defined as a primary and unilateral headache, characterized by sporadic attacks of moderate to strong severity that are lasting for 4-72 h. Other clinical symptoms include phono or photophobia, nausea, and vomiting. This sensorial disease seriously affects the quality of life and major economic costs (Benemei & Dussor, 2019; Villar-Martinez & Goadsby, 2022; Spekker et al., 2023). Sometimes, migraine is associated with an aura phenomenon, which includes visual, sensory and speech symptoms occurring before or during a migraine attack (Shankar Kikkeri & Nagalli, 2023). Migraine has a strong genetic component, and numerous genome-wide association studies in different cohorts consistently link TRPM8 ion channel with migraine, although TRPM8 gene reported of being differentially distributed across the earth based on latitude (Key et al., 2018).

TRPM8 is expressed in trigeminal small to medium-sized sensory neurons (McKemy et al., 2002; Kayama et al., 2018). The TRPM8-expressing fibres densely innervate the dura matter, but is regulated during development, since in adult mice either the density or number of fibre expressing TRPM8 drastically decreased, raising speculation about the contribution of this channel to migraines (Dussor & Cao, 2016).

Clinical studies have shown that environmental cold activation of TRPM8 could trigger headache or migraine (Prince et al., 2004), and about 50 % of the patients suffering from migraine presented cold allodynia (Burstein et al., 2000). Moreover, an interesting preclinical study conducted in a rat model of headache, showed that the application of icilin in dural fibres induced cutaneous facial and hind paw mechanical allodynia. In contrasts, the oral pretreatment with a TRPM8 antagonist (AMG116), sumatriptan or nitric oxide synthase inhibitor prevented markedly the reduction of facial and hind paw withdrawal threshold (decreased mechanical allodynia) caused by icilin dural application (Burgos-Vega et al., 2016).

Subsequently, another interesting study showed that both the simultaneous activation of TRPM8 channel based on facial application of icilin with an ongoing meningeal inflammation elicited by inflammatory soup provoked heat analgesia in wild type mice, although the effect was absent in TRPM8-null mice (Kayama et al., 2018). Noteworthy, the meningeal inflammation was found to upregulate TRPM8 transcripts level, increasing the number of trigeminal neurons co-expressing both TRPM8 and TRPV1. Besides, a clinical study showed that topical menthol application alleviated migraine symptoms such as pain, nausea, vomiting , phonophobia and photophobia (Borhani Haghighi et al., 2010). Recently, a preclinical study found that endogenous testosterone TRPM8 activation reverse mechanical hypersensitivity in mouse model of migraine (Alarcón-Alarcón et al., 2022).

Taken together, these studies implicateTRPM8 in the pathophysiology of migraine. However, a better understanding of the specific role of TRPM8 in migraine is needed, for the purpose of using better TRPM8 modulatory strategies for migraine treatment.

1.3.5.2.3 Dry eye disease

Wetness is crucial for preserving the integrity of the ocular surface, which is mediated through both continuous tear secretion by the lachrymal glandes and the basal blinking. The dysregulation of these two physiological processes leads to the eye dryness. Dry eye disease (DyD) is an ophthalmological disease affecting about 5-30% of the population, and represents a true economic burden (Yang et al., 2017). DyD is manifested with several symptoms including redness, tearing, irritation, grittiness, soreness and dryness of the ocular surface. The eye surface, especially the cornea, is densely innervated with TRPM8-expressing cold trigeminal neurons (Parra et al., 2010). This innervation decreases with aging, resulting in a drastic decrease in tear production and high incidence of DyD in old people (Alcalde et al., 2018). Moreover, several studies suggested the implication of TRPM8 in sensing the dryness of the ocular surface. The TRPM8 channel is activated by either evaporative cooling or an increase in osmolality that lead to tear secretion and eye blinking (Belmonte et al., 2015; Quallo et al., 2015).

Interestingly, preclinical studies have suggested that TRPM8 agonists such as menthol, borneol and tacrolimus could be potential treatments for dry eye disease. The application of these agonists to the eye surface in experimental settings has shown promising results, including increased basal tear secretion and eye blinks. However, some agonists induced side effects such as irritation and burning pain (G.-L. Chen et al., 2016; J. M. Yang et al., 2018; Arcas et al., 2019).

In a study by Yang and collaborators (2017) a novel water-soluble TRPM8 agonist called cryosim3 (C3) demonstrated effectiveness in treating dry eye disease. The application of the drug on eyelids of the patients with DED for 2 weeks (4 times/day) resulted in increased tear secretion, which improved their dry eye discomfort (J. M. Yang et al., 2017a). Notably, both Borneol and C3 TRPM8 agonists

were characterized as most likely safe drugs that could be used for the treatment of dry eye disease without side effects (J. M. Yang et al., 2018). Thus, selective TRPM8 agonists can be considered as a novel effective therapeutic approach in the treatment of dry eye disease.

1.3.5.2.4 Cold pain

The cold spectrum ranges from innocuous cold temperatures (28 ˚C to 18 ˚C), responsible for the chilling sensation, to noxious cold temperatures (≤ 15 ˚C), which induce a painful sensation such as aching, burning and pricking (Davis, 1998). However, in pathological conditions the normally innocuous cold stimuli are perceived as painful (cold allodynia), while the normally painful noxious cold stimuli are exacerbated, evoking an exaggerated pain sensation (cold hyperalgesia).

In inflammatory and neuropathic conditions caused by damage to peripheral sensory neurons, there is an increased sensitivity to cold, a condition called cold allodynia. This is often associated with enhanced TRPM8 channel expression and/or function within nociceptors (Colburn et al., 2007; Dhaka et al., 2007; Xing et al., 2007; Proudfoot et al., 2006).

In a study by Xing and collaborators (2007) using a rat model of chronic nerve constriction (CCI), they found that in vivo innocuous cold stimulation, elicited by the application of acetone to the plantar surface of the hind paw, resulted in marked cold allodynia in CCI rats compared with sham-operated rats. Moreover, they also found that cool induced allodynia in CCI rats was attenuated after the use of unspecific TRPM8 antagonists such as capsazepine. Also, they have also observed in vitro, an upregulation of TRPM8 expression in the L5 dorsal root ganglia (DRG) neurons of the CCI rats. Both calcium imaging and patch clamp experiments performed in CCI DRG sensory neurons showed a hypersensitivity to both menthol and innocuous cold compared to sham-operated rats (Xing et al., 2007). Similar results were obtained by Colburn and collaborators (2007), showing that TRPM8 was required for acetone induced cold allodynia in both neuropathic (CCI) and inflammatory (CFA injection) mouse models (Colburn et al., 2007).

However, while the previous studies collectively highlighted the crucial role of TRPM8 ion channel in cold allodynia induced after neuropathic injury and inflammation, other works reported the contribution of the misregulation of other ion channels, such as the noxious cold sensor (TRPA1), voltage gated sodium ($Na_v1.8$) and different potassium channels in cold hypersensitivity (TREK1,TRAAK, $K_v1.1$ and HCN1), rather than TRPM8 (Descoeur et al., 2011; González et al., 2017).

Cold hypersensitivity was described as the hallmark of oxaliplatin-induced neuropathy, where oxaliplatin exacerbates cold perception by promoting hyperexcitability in peripheral cold sensory neurons. This involves a drastic decrease in the expression of several potassium channels (TREK1 and TRAAK) and an enhancement in the expression of the pro-excitability channels such as HCNs. Moreover, all this changes contributed to shape the response to cold by shifting the temperature

threshold to warmer values, although the cold hypersensitivity was abolished after either genetic deletion or pharmacological blocking of those potassium channels (Descoeur et al., 2011). Furthermore, they also found that the expression level of the noxious cold sensor TRPA1 was slightly increased in oxaliplatin cells compared to control, but TRPM8 did not appear to be affected. Besides, in the same line, another interesting study showed that in CCI mice model, the excitability break currents I_{kD} generated by voltage gated potassium channels (Kv1.1 and Kv1.2) was markedly decreased in CCI cold sensory neurons compared to sham. Meanwhile, the TRPM8 channel current density (I_{TRPM8}) measured in CCI cold sensory neurons were indistinguishable from the one measured from neurons in sham animals, suggesting that CCI induced cold allodynia was not TRPM8-dependent (González et al., 2017).

In summary, based on the previous results, we could suggest that the cold sensitivity is mostly shaped by a functional counterbalance between the crucial innocuous cold sensor TRPM8 ion channel and the noxious cold sensor TRPA1. Both channels are essential for cold transduction, together with other types of ion channels that play a role in shaping the excitability by shifting the temperature threshold towards warmer temperatures.

1.4 Agonists: Rapamycin and Agonist-109-HCl, Agonist-145

1.4.1 The immunosuppressant macrolide rapamycin

Macrolide immunosuppressants are a family of natural molecules with macrolide-like structure and showing immunosuppressive activity, both in vivo and in vitro. Rapamycin, commercially named ``Sirolimus´´, was isolated from bacteria *Streptomyces hygrsocopicus* in the soil of easter island (1972) and directed primary as an antibiotic (antifungal) agent (Sehgal et al., 1975). Thereafter, it was characterized as a potent immunosuppressant compound (Dumont & Su, 1995). Following this discovery, nowadays rapamycin is extensively used in the clinic as a potent immunosuppressant to prevent organ rejection during solid organ transplants. Moreover, rapamycin and its derivatives were found to be effective in the treatment of several diseases (Ballou & Lin, 2008). In 2011, Everolimus (a rapamycin derivative) was approved by the American Food and Drug Administration (FDA) as antitumor drug for the treatment of numerous cancers. Over the last decades, rapamycin has been found to extend lifespan in different species, ranging from primitive microorganism (yeasts) to higher evolved organisms such as invertebrates (flies) and mammals (mice). Additionally, it has been observed to delay age-related dysfunctions. Therefore, rapamycin has attracted increasing attention in aging biology field (Alvers et al., 2009; Cox & Mattison, 2009; Wilkinson et al., 2012).

Within the intracellular environment, rapamycin binds to the immunophilin FKB12 and forms an active complex rapamycin-FKB12, which binds with high affinity to the mTOR receptor (the mammalian target of rapamycin). The complex rapamycin-FKB12 induces a block of mTOR-complex1 (mTORC1),

and as consequence abolishes its downstream signalling (Heitman et al., 1991; Ballou & Lin, 2008). The mammalian target of rapamycin (mTOR) receptor is considered a signal integrator that transduces numerous intracellular signals such as growth factors, nutrients, energy and oxygen levels. These signals are necessary to control vital cellular processes like mRNA transcription, proteins, lipids, nucleotides energy balance and autophagy essential for the cell growth and proliferation (Sabatini, 2017).

Recently, rapamycin therapeutical efficiency has been extended and repositioned for the treatment of other diseases such as dry eye disease, lacrymal gland inflammation, dermatitis, and psoriasis. In a study by Linares-Alba et al. (2016) liposomes containing Sirolimus (rapamycin) contributed to a significant improvement of dry eye disease in spontaneous KCS (Keratoconjunctivitis Sicca)-dog model whereby enhancing the basal lacrimal production and tear secretion as well as the anti-inflammatory activity (Linares-Alba et al., 2016). Furthermore, another study demonstrated that daily topical rapamycin treatment for 12 weeks in a mouse model of Sjögren's syndrome, characterized by autoimmune-mediated inflammation of the lacrimal gland, suppressed lacrimal gland inflammation and increased tear secretion (Shah et al., 2017). Taken together, both studies highlight rapamycin as a promising candidate for the treatment of dry eye disease.

Interestingly, another study suggested that the topical rapamycin application induced a significative therapeutic potential in the treatment of skin diseases such as psoriasis and dermatitis by reducing inflammation and increasing autophagy activity at the skin (Kim et al., 2021).

In 2019, our lab reported that tacrolimus, a different immunosuppressant macrolide, had agonistic effects on TRPM8 channels (Arcas et al., 2019). In this study, it was found that tacrolimus activated TRPM8 recombinant from distinct species. Moreover, tacrolimus activated the peripheral sensory neurons but was absent in TRPM8 knock out mice or after the use of TRPM8 antagonist. Furthermore, it was observed that tacrolimus activated both cutaneous and corneal thermoreceptors. Interestingly, similarly to tacrolimus, it was found that the application of rapamycin into the eye triggered eye blinking and tearing. Taken together, those results drove our attention to explore first whether the TRPM8 agonism is common within all the macrolides family members, including rapamycin, and if so, whether the previously described therapeutical effect of rapamycin application, either in the eye for the treatment of dry eye disease, or in the skin for the treatment of dermatitis, were mediated through TRPM8 signaling.

Rapamycin (Sirolimus)

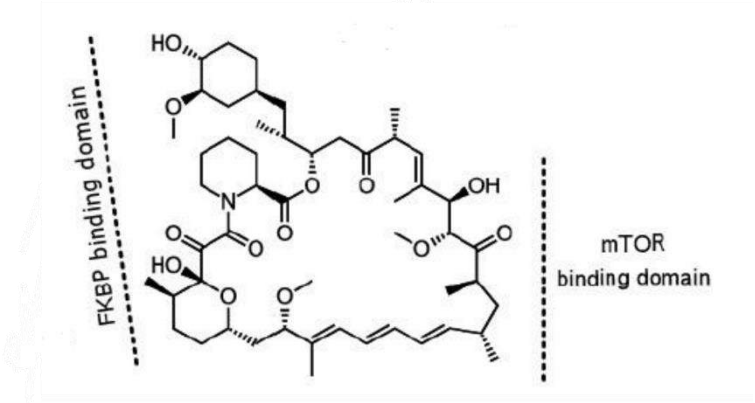

1.4.2 Novel TRPM8 agonists : G-RGM-145 and G-RGM-109

The chemical reactions for the synthesis of both novel tested agonists consisted basically in multicomponent UGI reactions using the menthoyl1-carboxylate. Note that the G-RGM-145 agonist is a mixture of L and D configurations at the phenylglycine alpha-carbon. Besides, G-RGM-109 resulted from a reaction of the N-benzylpiperidin-4-one and the above indicated carboxylic acid, and was assayed as the corresponding hydrochloride salt. The EC_{50} parameters were provided by our lab of origin at Institute of medical chemistry (Madrid).

G-RGM-145 (EC_{50}=1.76 µM)

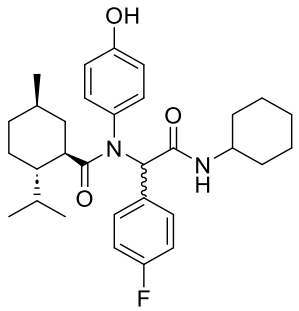

N-[(4-hydroxyphenyl)-N-(2-isopropyl-5-methylcyclohexane-1-carbonyl)-L,D-Phg(4-F)-NH-cyclohexyl

G-RGM-109 (EC_{50}=2.5 µM)

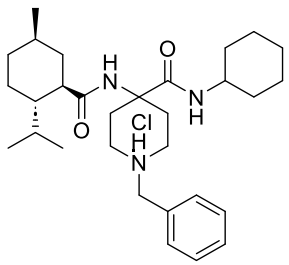

1-Benzyl-4-[(1*R*,2*S*,5*R*)-2-isopropyl-5-methylcyclohexane-1-carboxamido)piperidine-4-(*N*-cyclohexyl)carboxamide hydrochloride

2. Objectives:

- To investigate the agonistic effect of the immunosuppressant macrolide rapamycin on the mouse TRPM8 ion channel, as well as identify potential binding sites for rapamycin on the channel.

- To validate the efficacy of new TRPM8 agonists, namely G-RGM-145 and G-RGM-109-HCl (Ag109-HCl), and explore their mechanisms of action on the TRPM8 ion channel.

3. Materials and Methods:

3.1 Animals

Adult mice (1-4 months) from both sexes were used for DRG sensory neurons cultures. They were kept in a barrier facility under 12/12-hour light/dark cycle. The genotype of each mouse was determined using PCR. The experimental procedures followed the norms of the Spanish Royal Decree 1201/2005 and the European Community Council directive 2010/63/EU, which regulate the manipulation of animals in research.

I used one transgenic mice line called TRPM8^{BAC}-EYFP that was generated in our laboratory following the work of Morenilla-Palao in 2014, using a Bacterial Artificial Chromosome (BAC) transgenesis aiming to genetically label TRPM8-expressing neurons (Morenilla-Palao et al., 2014). This actual modified chromosome BAC containing the EYFP coding sequence under the control of regulatory components from the mouse TRPM8, thus EYFP proteins expression occurred selectively into endogenous TRPM8-expressing neurons. This transgenic line facilitated the identification of TRPM8 expressing cells.

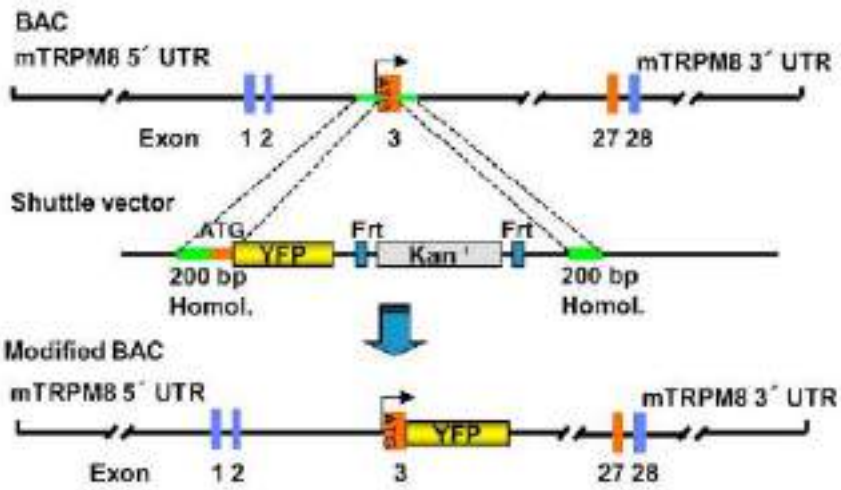

Figure 8. Genetic strategy used to obtain BAC that control EYFP expression under TRPM8 gene promotor control in TRPM8-YFP mice. Taken from Morenilla-Palao et al. (2014)

3.2 Mammalian HEK293 cell lines: Culture and transfection

Human embryonic kidney 293 cells (HEK293) were used as a heterologous system, and it was considered as a powerful tool to conduct our study on the isolated protein of interest, enabling us to investigate its functional and modulatory properties. It was in 1973 when HEK293 cells were extracted from human kidney of an aborted embryo, since that time it has been widely used in basic research of biology regarding their potential growth and natural tendency for transfection (Graham et al., 1977).

HEK293 cells were maintained in Dulbecco's Modified Eagle Medium (DMEM)+Glutamax, (Thermo Fisher Scientific) supplemented with 10% FBS and 1% penicillin/streptomycin, incubated at 37°C in a 5% CO2 atmosphere. The number of cell passages was tracked, limiting the number up to 30 therefore a new batch of cell was unfreezing and put to work with low passing number. The integrity of cells was controlled once a month checking for mycoplasma infection.

To deliver the foreign nucleic acids into the cells, I used a transient transfection strategy (Kim & Eberwine, 2010). I used two transfection methods, the first was lipofection that consisted of the use of lipidic vesicles to deliver nucleic acids that merge with cell membrane. After I introduced the mammalian cDNA vectors that encode the expression of different proteins of interest, these expression vectors facilitate the expression of the inserted sequences without getting into the genome of the host cells. The protocol steps used were the following: HEK293 cells were plated in 24-well dishes at 2 $x10^5$ cells/well and transiently transfected with Lipofectamine 2000 (Thermo Fisher Scientific). Cells were co-transfected with two plasmids simultaneously fixing the total amount of cDNA at 2 µg (1.5 µg of TRPM8 channel plasmid and 0.5 µg of Cl-GFP plasmid). For the transfection, 2 µl of Lipofectamine 2000 was mixed with the cDNA in 100µl of OptiMem (Thermo Fisher Scientific), a reduced serum media, incubated for 20 minutes then added to the well. 4-6 hours later the medium was replaced with a fresh complete medium. The second method used was polyethylenimene PEI 25K transfection (polysciences #23966-1) considered as stable cationic polymer (Boussif et al.,1995). Based on electrostatic properties the DNA negatively charged is condensed into the polymer forming a complex PEI-DNA, thereafter it bonded to anionic charges of the cell membrane. Then, the complex was internalized by the host cells through the process of endocytosis, next the nucleic acid was released into cytoplasm. The PEI 25K stock of 500 mL was prepared as follows: dissolving 161.5 mg linear PEI 25 K (Polysciences# 23966-1) in 200 mL of boiling milliQ water (using a microwave), adjusted pH =7. The volume of the solution was then adjusted to 500 mL by adding additional water, followed by stirring to ensure homogeneity. The final solution was filtered and divided into aliquots in 15 mL falcon tubes. These aliquots were subsequently stored at -20 ºC for future use. In a similar manner to the lipofectamine method, HEK293 cells were co-transfected with two plasmids. The process began with the preparation of mix 1, which contained: fluorescent Cl-EYFP (100 ng) plasmid mixed with mouse TRPM8 channel plasmid (600 ng) in PBS1X and the final volume was V_f = 10 µL, then the mix 2 was prepared containing: PEI 25K(3.5 µL) mixed with PBS 1X (4.5 µL) giving a final volume V_f=8 µL. Next, I mixed both mixes 1 and 2 (final volume = 18 µL) and incubate for 5 min. Finally drops of the final mix (18 µL) were added to the cells in one of a 24-well plate (preserving the same medium of the cells). Both strategies worked similarly well, but I did focus during most of my transfection work on the PEI method rather than lipofection method, because it is less expensive.

Calcium imaging and electrophysiological recordings in vitro were performed 24 hours after transfection, in the early morning preceding the experiments, the cells were trypsinized (0.25% trypsin-EGTA) and reseeded at lower density in 12-mm-diameter (glass coverslips previously treated with Poly-L-lysine 0.01%(sigma)) for 1-2 hours of incubation before the experiments.

Plasmid	Vector	plasmid	vector
mTRPM8	pcDNA5	mTRPM8-I846T	pcDNA5
mTRPM8-Y745H	pcDNA5	mTRPM8-I846D	pcDNA5
mTRPM8-I846A	pcDNA5	mTRPM8-Y1005A	pcDNA5
mTRPM8-I846V	pcDNA5	mTRPM8-R1008A	pcDNA5
Cl-GFP / Cl-EYFP	pcDNA		

Table 1. Series of the transiently transfected plasmids into HEK293 cells line. All the TRPM8 coding sequences were from mice (m, mouse).Cl.GFP: Clover green fluorescent protein; Cl-EYFP: Clover enhanced yellow fluorescent protein.

3.3 Single point mutagenesis

We have used the expression vectors mouse (m) wildtype (WT) TRPM8. A range of mutants mTRPM8 (R1008A, Y1005A, R842, I846A, I846T, I846D and Y745H) that were obtained by site-directed mutagenesis from this WT construct as described previously (Malkia et al., 2009). Point mutations were confirmed by sequencing of the plasmids and posterior analysis with Lasergene software (DNASTAR). The mutant mTRPM8-Y745H is considered as a menthol insensitive and previously generated and characterized in our laboratory (Malkia et al., 2009). Below are attached the primers used to generate our mutants.

Mutant I846A **ATT** original sequence (coding for I, Ile)
mM8 I846A (For): 5´- GCTCATCCAC**GCT**TTCACCGTC-3´
mM8 I846A (REV): 5´-GACGGTGAA**AGC**GTGGATGAGC-3´
primers with incorporated mutation (Code for A, Ala)

Mutant I846V **ATT** original sequence (coding for I, Ile)
mM8 I846V (FW): 5´- GCTCATCCAC**GTT**TTCACCGTC-3´
mM8 I846V (REV): 5´-GACGGTGAA**AAC**GTGGATGAGC-3´
primers with incorporated mutation (Code for V, Val)

Mutant I846T **ATT** original sequence (Coding for I, Ile)
mM8 I846T (For): 5´- GCTCATCCAC**ACT**TTCACCGTC-3´
mM8 I846T (REV): 5´-GACGGTGAA**AGT**GTGGATGAGC-3´
primers with incorporated mutation (Code for T, The)

Mutant I846D **ATT** original sequence (Coding for I, Ile)
mM8 I846D FW: 5´- GCTCATCCAC**GAT**TTCACCGTC-3´
mM8 I846D REV: 5´-GACGGTGAA**ATC**GTGGATGAGC-3´
primers with incorporated mutation (Code for D, Asp)

Mutant Y1005A **TAC** original sequence (Coding for Y, Tyr)
mM8 Y1005A FW: 5´- CTTCCTGGTGCAGGAG**GCC**TGCAACCGCCTAAAC-3'
mM8 Y1005A REV: 5´- GTTTAGGCGGTTGCA**GGC**CTCCTGCACCAGGAAG-3´
primers with incorporated mutation (Code for A, Ala)

Mutant R1008A **CGC** original sequence (coding for R, Arg)
mM8 R1008A FW: 5´- GCAGGAGTACTGCAAC**GCC**CTAAACATCCCCTTC-3'
mM8 R1008A REV: 5´- GAAGGGGATGTTTAG**GGC**GTTGCAGTACTCCTGC-3´
primers with incorporated mutation (Code for A, Ala)

Mutant R842A **AGG** original sequence (Coding for R, Arg)
mM8 R842A FW: 5´- CACGCTA**GCG**CTCATCCAC-3´
mM8 R842A REV: 5´- GTGGATGAG**CGC**TAGCGTG-3´
primers with incorporated mutation (Code for A, Ala)

3.4 Primary sensory neurons culture: Dorsal root ganglia (DRG)

I have used DRG sensory neurons since they are widely used as a model of peripheral sensory system in primary culture. They are located within the spinal ganglia that is in the intervertebral foramen along the spinal column (Malin et al., 2007). DRGs were extracted from adult mice, then used enzymatic digestion combined with mechanical dissociation resulting in cell suspension of sensory neurons and other non-neuronal cells. The cells mix was plated on a Poly-L-lysine pre-treated glass coverslip (6mm of diameter). Under light transmission microscopy DRG neurons can be easily identified due to their oval or rounded soma shape. Within a few hours, these neurons initiate the development of new axons and dendrites. Most of the studies related to the mechanisms of the sensory transduction always considered the soma of peripheral sensory neurons as model because of the limitation into conveying investigations of these molecular mechanisms in the sensory terminal endings due to their small size (< 1µm) as well as due to the consensus of the ion channels expression in the membrane of the terminal ending and soma (Heppelmann et al., 2001). Nevertheless, we assumed the fact that these conditions of

applying our techniques to the soma of DRG neurons make the experimental environment rather different than the in vivo conditions where stimuli interacted with the sensory nerve terminals.

To prepare my own DRG culture these are the protocol steps I was following:

Adult mice of either sex (1-4months) were sacrificed using cervical dislocation strategy. The vertebral column was located, and then the spinal cord was isolated and DRGs were pulled out using stereo microscope. After that, DRGs were maintained in ice cold Hank's Balanced Salt Solution (HBSS) during the process of the separation, thereafter a step of cleaning of DRGs from spinal nerfs and roots. After that DRGs were incubated with collagenase type XI (1800U/ml, Sigma) and dispase II (5U/ml, GIBCO) for 40-45 min in Ca^{2+} and Mg^{2+} free HBSS at 37 ºC in 5% CO2 atmosphere. Furthermore, DRG cells were mechanically dissociated manually using a 1 ml pipette. The cells suspension was pipetted up and down 15-20 times to achieve dissociation. Subsequently, the suspension was filtered using a 70 µm nylon cell strainer (Falcon) to remove any remaining debris or clumps. The neurons suspension was centrifuged at 1250 rpm for 5 minutes, and the pellet was resuspended in Minimum Essential Medium (MEM) supplemented with 10% FBS, 1% MEM-vit (Thermo Fisher scientific) and 1% penicillin/streptomycin. Finally, DRG neurons were plated, using the same medium (without growth factor), on Poly-L-lysin 0.01% (Sigma) pre-treated glass coverslips (Thermos Scientific). Calcium imaging and electrophysiological recordings were performed after 12-24 hours in culture.

3.5 Fluorescence calcium imaging

Ratiometric calcium imaging is a technique using specific calcium indicators to reflect the change of the intracellular calcium concentration inside de cells. During our calcium in vitro experiments I used the fluorescent indicator fura-2 AM (Invitrogen™F1221), a membrane permeable fluorophore. After its penetration into the cell an esterase enzyme cuts the acetoxymethyl ester group (AM) from the fura-2 core body resulting in the stabilization of the fluorophore inside the cytoplasm of the cells. The main property of fura-2 fluorophore is being able to change between two spectrum peaks of excitation depending on the binding to calcium. The wavelength excitation peak of fura-2 unbound configuration is 362 nm, that switch upon binding to calcium to 335 nm, on the other hand, the emission spectrum of the either configuration is slightly constant with a maximum emission at 510 nm. During my experiments Fura-2 was excited using two excitation wavelengths: 340 nm and 380 nm. The emitted light resulting from these excitation wavelengths was then used to calculate the ratio (F340/F380), which is directly proportional to the intracellular calcium concentration (Grynkiewicz et al., 1985; Moore et al., 1990). DRG neurons or HEK293 cells line were incubated in control solution containing 5 µM Fura-2 AM and 0.02% Pluronic acid (Thermo Fisher Scientific) for 45-60 min at 37 °C and CO_2. Fluorescence measurements were obtained from an inverted microscope (Leica Microsystems) fitted with an Imago-QE Sensicam camera (PCO). Fura-2 was excited at 340 and 380 nm (excitation time 60 ms) with an LED-based system (Lambda OBC, Sutter Instruments). Mean fluorescence intensity ratios

(F340/F380) were displayed online with Metafluor software every 3s. The standard bath solution contained the following (in mM): 140 NaCl, 3 KCl, 2.4 CaCl2, 1.3 MgCl2, 10 HEPES, 10 glucose, and was adjusted to a pH of 7.4 with NaOH 5 M (Osmolarity 290 mOsm/kg). Calcium imaging was performed at a basal temperature of 33 ± 1°C. Before starting the acquisition of fura-2 fluorescence signal following specific protocols of drug applications, then images of the microscopic field were obtained with transmitted light, under 460 nm excitation wavelength that facilitate the identification of fluorescent green cells.

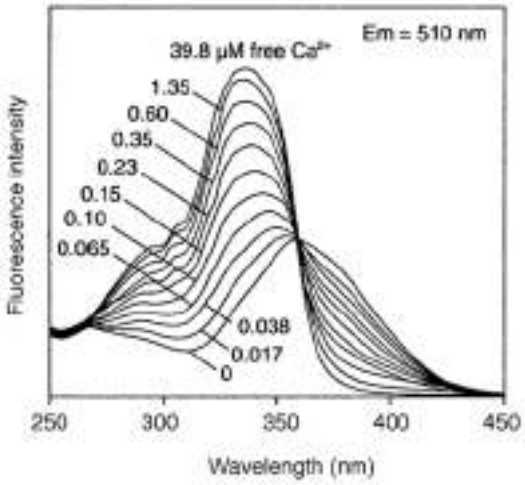

Figure 9. Excitation spectra of the Fura-2 molecule in solution at different calcium concentrations ranging from 0 to 39,8 µM. Fura-2AM product (Invitrogen™ REF. F1221).

3.6 Electrophysiological patch clamp recordings in HEK293 cells

Patch clamp is known as a critical tool to study ion channels in excitable and non-excitable cells, this technique was early developed by Neher and Sakmann in 1970 to perform high resolution electrophysiological recordings of cell-attached membrane patches and whole cell recordings (Neher & Sakmann, 1976; Neher et al., 1978; Hamill et al., 1981). During my work I used whole-cell patch clamp recordings to perform currents measurement, a glass micropipette (borosilicate glass patch-pipettes, Sutter Instruments) with a resistance between 3-7 MΩ were used. The pipettes were filled (2/3) with a solution similar to the ionic conditions of the cytosol, which contained the following (in mM): 135 CsCl, 3 KCl, 1 EGTA, 2 $MgCl_2$, 10 HEPES, 5 Na_2-ATP and 0.1 Na_2-GTP glucose and was adjusted to a pH of 7.4 with CsOH 2 M (osmolarity 282 mOsm/kg). The micropipette was connected to an Axopatch 200B patch clamp amplifier (Molecular devices). Once the cell membrane is into contact with the pipette, a seal of high resistance was formed (> 1GΩ) right after applying gentle negative pressure resulted the precursor configuration called cell-attached configuration, breaking into the membrane patch at the tip of the pipette by the application of suction pulse through the patch pipette was how we

get into whole cell recording configuration of our interest. Thereafter, upon having access to the cytoplasm of the cell where I saw large capacitative currents during the square current pulses since the membrane behaves as capacitator in parallel with a resistor. Then, I proceed to the compensation of the capacitative transients using manual setting of the whole-cell capacitance and series resistance, and the transient was minimized after adjusting the amplifier. Thus, we get an estimated whole cell capacitance reflecting indirectly the plasma membrane area, which I used later to normalize the currents amplitude to the area of the membrane presented as current density (pA/pF).

The current was digitized with a Digidata 1322A AD converter (Molecular Devices). Stimulus delivery and data acquisition were performed using pCLAMP9 software (Molecular devices). The voltage clamp (VC) recording was performed in HEK293 cells, the amplifier gain was set at x0.5, the acquisition rate was set to 10 kHz, and the signal was filtered at 2 kHz (low pass 4 pole Bessel filter). During the whole cell configuration, the holding potential was -60 mV in voltage ramp protocols, or -80 mV in voltage steps protocols. The recording temperature was between 32 and 34℃ or between 22 and 24℃ according to the type of the protocol (specified later in the text). The intracellular solution used for heterologously transfected HEK293 cells expressing TRPM8 ion channel recordings was based on caesium as major cation instead of potassium known of being the major cation in the cytosol, the main reason of using caesium was to block potassium currents flowing through endogenous K^+ channel expressed in HEK293. In DRG neurons, voltage clamp (VC) recordings were performed alongside with current clamp recordings (CC). During voltage clamp the amplifier gain was set at x1, the acquisition rate was set at 10 kHz, the signal was filtered at 2 kHz (low pass 4 pole Bessel filter), after entering to the whole-cell configuration the neurons were voltage clamped at holding potential of -60 mV. Moreover, in current clamp (CC) recordings, the membrane voltage was recorded, amplifier gained x0.5, the signal was filtered at 10 kHz and the sampling rate was 50 kHz. During CC recordings neurons that were firing action potentials at rest were injected with a small DC current to set the membrane potential at a value around -55 mV. Finally, ligands were applied in the flowing bath solution.

Extracellular solutions			
Control solution		**Ca^{2+} Free solution**	
Compound	**Concentration (mM)**	**Compound**	**Concentration (mM)**
NaCl	140	NaCl	144.8
KCl	3	KCl	3
$CaCl_2$	2.4	$MgCl_2$	1.3
$MgCl_2$	1.3	Glucose	10
Glucose	10	HEPS	10
HEPS	10	EGTA	1
PH=7.4 adjusted using NaOH Osmolarity=290-300 mOsm/			

Intracellular solutions			
TRPM8 channels		**Neurons**	
Compound	**Concentration (mM)**	**Compound**	**Concentration (mM)**
CsCl	135	K-gluconate	115
$MgCl_2$	2	KCl	25
HEPES	10	NaCl	9
EGTA	1	$MgCl_2$	1
Na2-ATP	5	EGTA	0.2
Na-GTP	0.5	HEPES	10
		K_2-ATP	3
		Na-GTP	1
pH=7.4 set using CsOH Osmolarity= 282 mOsm/L		pH=7.4 adjusted with NaOH Osmolarity= 294 mOsm/L	

3.7 Perfusion and temperature control systems

The coverslips containing the cultured cells were placed inside the microscope chamber. (2 × 1.5 cm). By using six separated lines irrigating continuously the chamber based on the gravity fed system with an extracellular solution pre-warmed (except when it is indicated) to 33 ºC ± 1 through a perfusion manifold (Warmer Instruments) that offer a quick solution switch (perfusion flow 1-1,2 ml/min). The solution input tube was placed just above the cells, and the solution temperature was controlled with a Peltier device (Cool Solution, Cork, Ireland) positioned right before the input tube, and controlled using a feedback device.

The coverslips containing the cultured cells were placed inside the microscope chamber. In parallel with the recordings, the bath temperature was continuously registered with an IT-18 T-thermocouple connected to a Physitemp BAT-12 micro-probe thermometer (Physitemp Instruments) and digitized by an Axon Digidata 1322A converter running pCLAMP9 software (Molecular Devices).

3.8 Isolated saphenous skin nerve preparation

The skin is considered as one of densely innervated sensory organs with primary sensory afferents. In vitro cutaneous sensory fibers skin recordings started in the late 1950s for the first time conveyed in several mammal's species. Skin nerve is a sophisticated ex-vivo extracellular recording, which consisted on recording from the cutaneous primary sensory afferents covering different sensory modalities (temperature, pressure etc.), including nociceptors (Bessou et al., 1971). Recordings were performed also in isolated mouse skin –saphenous nerve preparation (Roza et al., 2006; Zimmermann et al., 2009).

I used wild type mice (C57BL/6J) from either sex, that were sacrificed by cervical dislocation, then the hairy skin from the either hind paw was extracted along with intact saphenous nerve, ensuring that it was cleaned and set free from any attaching tissue and blood vessels. The skin preparation was then positioned in a specific recording chamber, as described in literature (Zimmermann et al., 2009; Arcas et al., 2019). The skin was continuously perfused with oxygenated external solution (95% Oxygen / 5% CO_2) that contains (in mM): 108 NaCl, 26 NaHCO3, 9.5 Na-gluconate, 7.5 sucrose, 5.5 glucose, 3.5 KCl, 1.7 NaH_2PO_4-$2H_2O$, 1.5 $CaCl_2$-$2H_2O$ and 0.7 $MgSO_4$-$7H_2O$, set to pH=7.4. The flow rate was about 4 ml/min. The chamber temperature was set and maintained at ~35 ºC by a SC-20 heater/cooler system controlled by a CL-100 bipolar temperature controller (Warner Instruments) as used in our previous work (Arcas et al., 2019).

Once the skin-saphenous was isolated, the skin flap was fixed gently in a perfused bath chamber, thereafter the saphenous nerve was passed through a hole to the adjacent recording chamber containing mineral oil, then the perineurium (which is a protective membrane surrounding the nerve) was pulled back using Dumont #5SF forceps. As a result, the fibres automatically got loose, and a small bundle of fibers was subsequently placed on a gold recording electrode connected to high gain AC differential amplifier (Model DAM 80; World Precision Instruments). Both chambers were grounded with reference electrodes. Spike 2 software was used for recording and analysis, and the signal was collected, amplified, and digitized at 25 kHz (CED Micro3-1401; Cambridge Electronic Design) and saved in the hard drive for off-line analysis.

The methodology used to search the cold spots was by carefully passing a small Eppendorf of frozen external solution along the dermis side of the skin. Once in the spot the cold-receptor fiber started firing immediately and stopped right after displacing the cold probe from the site. After that the receptive field was isolated using a thermoplastic ring, where the circular area was 5.5 mm of diameter, which represented to the exchange area. The cold ramps were delivered by cooling the administered solution, that is going through a Peltier system, cooling from baseline temperature of 35 ±1ºC down to~10 ºC in about 100 s, adapted to deliver a small and controlled volume inside the ring in the delimited skin area. After the application of the cooling ramp, some silent cold receptors at baseline temperature 35 ± 1ºC, started firing action potentials or the cold receptors showing ongoing activity increase their action potential upon cooling. In addition to test the effect of our drug on cold fibres, Rapamycin (30 µM) was applied at the basal temperature. A response was considered valid only if there were at least 20 spikes observed during the 2-minute application period prior to the second cold ramp. In addition, to evaluate rapamycin potentiation effect on cold sensitivity, a second cold ramp was applied in the presence of Rapamycin. The threshold temperature was considered as the temperature at which the first action potential firing occurred. Additionally, the temperature at which the maximum frequency of action potential firing was observed was also determined and recorded.

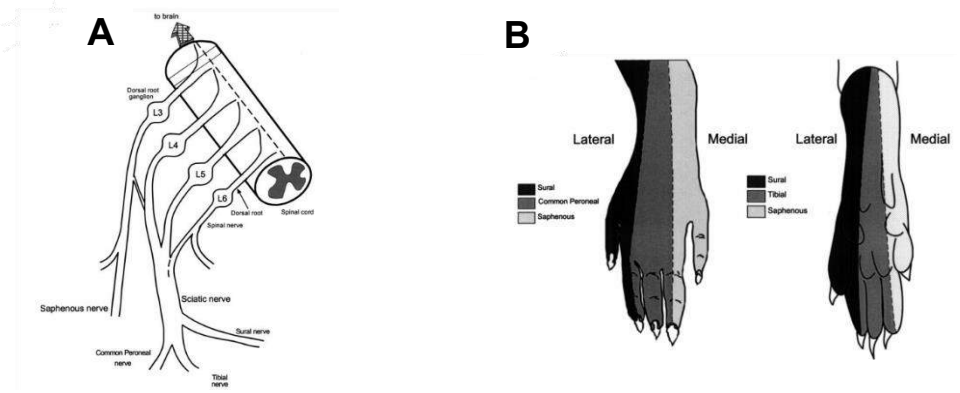

Figure 10.Schematic showing saphenous nerve origin down to their peripheral innervation. A, Diagram of both saphenous and sciatic nerves from dorsal root origin to their terminal innervations. Not distinct origin of saphenous nerve (L3,DRG) compared to sciatic nerve (L4,5 and 6 DRGs **B**, Saphenous nerve innervation

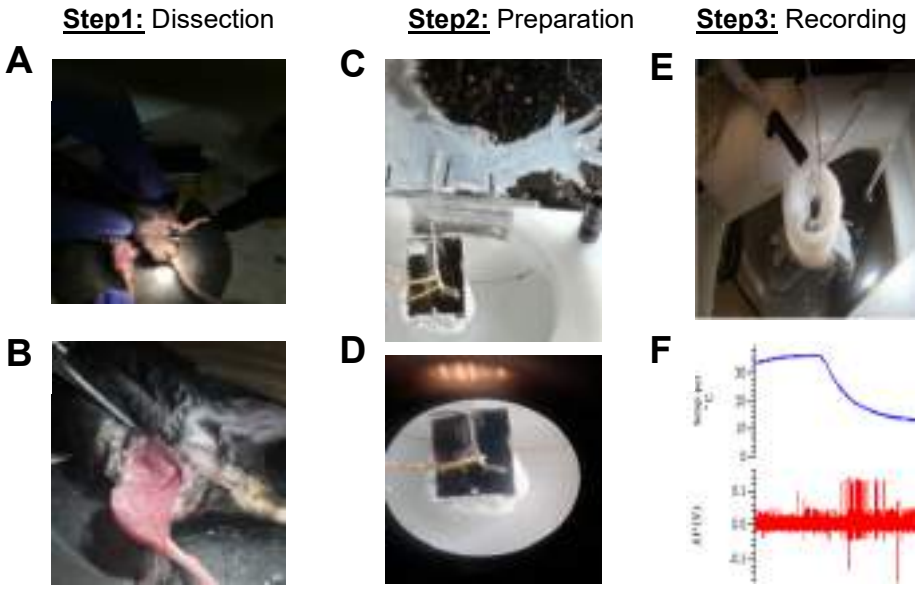

Figure 11.The skin nerve preparation steps: Step1 A, Mouse skin incision**,** Saphenous nerve tracking. **Step2 C,** Skin nerve preparation set up on recording chamber**,** Saphenous nerve fibers set on gold electrode recording. **Step3 E,** Isolation of the receptive filed and perfusion of solutions. **F,** Spike 2 recording of cold activated action potentials.

3.9 Data Analysis

3.9.1 Calcium imaging

All the cells were tracked with specific regions of interest (ROIs), then the single Fura 2 ratio fluorescence (F340/F380) of each ROI was downloaded, and the single cell fluorescence were studied individually and represented as amplitude of fluorescence (ΔFura2) response by using MATLAB scripts, and all the responses were re-checked manually to avoid the inclusion of false negatives or positives. After the sequential application of agonists, various parameters were extracted from the recordings. This included the determination of the amplitude of the responses as well as the temperature threshold required to elicit a response. The amplitude is determined by subtracting the peak of maximum fluorescence observed during the agonist's application time $(F340/F380)_{peak}$ and the mean baseline level of fura2 ratio$(F340/F380)_{baseline}$ 30s before the agonists (cold and drugs) application**:**

$$\textbf{Amplitude} = \Delta\ \textbf{Fura2} = (F340/F380)_{peak} - (F340/F380)_{baseline}$$

Only cells with ΔFura2 ≥ 0.05 were considered as positive responses. As a control of the viability of the excitable DRG neurons, KCl 30 mM was applied at the end of each protocol. Regarding HEK293 cells line, the cholinergic agonist carbachol (CCh) at 30 µM was used to test their viability.

The inclusion criteria of the positive cells in the analysis were based on the response to the specific agonists of our channel of interest applied during the protocols. Likewise, if they responded or not to KCl in case of neurons, or carbachol in HEK293 cell line experiments. In addition, the cells that did not respond to any of the stimulus were excluded from the analysis.

Note: when comparing wild type TRPM8 channel response to agonists to different mutants groups, I used the single wild type group obtained by averaging coverslips coming from different days.

3.9.2 Electrophysiological recordings

3.9.2.1 Whole-cell patch-clamp electrophysiological recordings in Transfected HEK293 cells

Both recording protocols were performed in HEK293 cells expressing mouse TRPM8 (wild type or mutants).

3.9.2.1.1 Voltage Ramp protocol:

The patched cells were continuously perfused with control solution at bath temperature of 33 ºC ± 1 to maintain our channel in the closed state. The protocol consisted into application of a voltage ramp going from a resting potential of -60 mV down to -100mV where the patched cells were maintained for 100 ms, then depolarized up to +150 mV for a duration of 800ms (in some recordings ramps go up only to +100 mV), with a frequency of 0.33 Hz. At the end of the protocol the membrane potential gets back to the initial resting potential. The holding potential was - 60 mV.

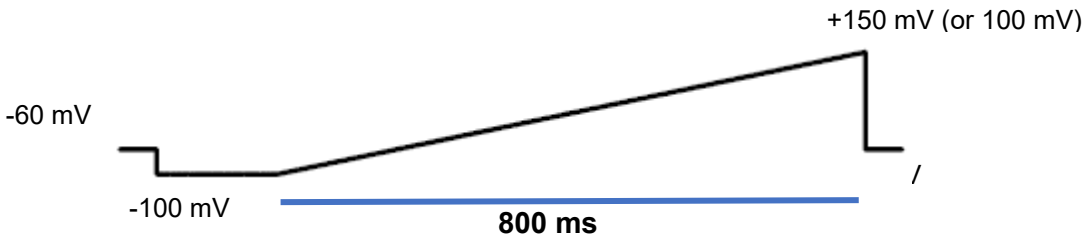

Figure 12. Example of the voltage ramp applied during patch clamp recording.

Based on this voltage ramp currents resulting from different TRPM8 agonists applications were extracted at specific voltages, -100 mV and +100 mV. These voltages produced inward and outward currents, respectively. The results were analysed using Clampfit (Axon, Molecular Devices LLC; 2014). The value of the maximum peak current activation (**$I_{max\ peak}$**) resulting from each agonist activation were extracted and divided by the capacitance previously obtained during the patch seal from each cell, therefore the current values were converted to current density (pA/pF).

$$\textbf{Current density (pA / pF)} = \mathbf{I_{max\ peak}\ (pA)} / \textbf{Capacitance (pF)}$$

Since the agonists are exhibiting a shift in voltage dependence of TRPM8 activation, the current-voltage (I-V) relationship obtained from repetitive voltage ramps, as described above, were fitted to a modified Boltzmann equation that includes a linear conductance multiplied by a Boltzmann factor, to quantify the shift in the voltage of half maximal activation ($V_{1/2}$), which is a biophysical parameter characterizing the activation effect of specific voltage-gated channel modulators.

$$\mathbf{I = (V - Vr) \cdot (G_{max} + (G_{min} - G_{max}) / (1 + \exp((V - V_{1/2}) / dx)))}$$

Where:

Vr: Reversal potential (mV).

V: Potential at a given protocol pulse (mV).

$V_{1/2}$: Voltage of half maximal activation (mV).

G_{max}: Maximal conductance (nS).

G_{min}: Minimal conductance (nS).

dx: Slope factor (mV).

3.9.2.1.2 **Voltage steps protocol**

HEK293-expressing TRPM8 cold receptors were perfused with control solution at room temperature (24 ºC ± 1), in order to set a basal activation level of the TRPM8 channels. The protocol involved the application of voltage steps ranging from -80 mV up to + 240 mV with ΔV = 40 mV, and a duration of 50 ms for each step. The holding membrane potential was -80 mV. This protocol is performed in a control condition where the patched cell was perfused with control solution, then started the application of different drugs including rapamycin as well as the canonical agonists (menthol and WS-12) consecutively, separated by a period of wash out.

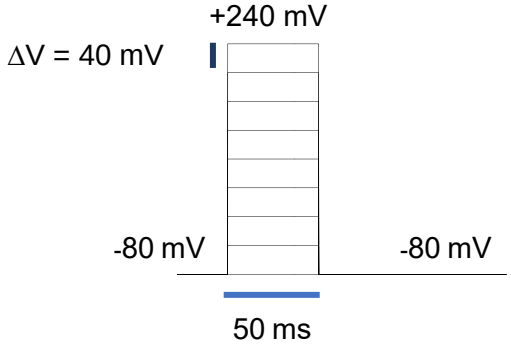

Figure 13 Example of the voltage. Steps protocol applied during patch clamp recording.

The Conductance-Voltage relationship (G-V) were derived from the current-voltage relationship (I-V) rather than the standard method using the tail currents only to keep the same methodology used in our previous characterized tacrolimus work (Arcas et al., 2019), and preserve the tail currents data for further channel kinetics analysis. The conductance (G) was calculated by dividing the evoked current by the driving force as the following:

$$G = I / (V_m - V_{rev})$$

Where:

I: Evoked current (pA).

V_m: Test potential (mV).

V_{rev}: Reversal potential of the currents (mV).

Following different voltage pulse protocol, the conductance was calculated and normalized to the maximum conductance (G_{max}). The G_{max} was considered as the conductance obtained with WS-12 10 µM at a voltage step of + 240 mV within each wild typeTRPM8 cell. While I used RAP 30 µM at +240 mV as G_{max} for the segment 4 mutants (I846T, I846V and I846D) due to their hypersensitivity to RAP. Then, the G/G_{max}-voltage relationship was fitted to a Boltzmann equation:

$$G/G_{max} = A2 + (A1 - A2) / (1 + \exp((V_m - V_{1/2}) / dx))$$

Where:

A2: Maximal normalized conductance.

A1: Minimal normalized conductance.

V_m: Test potential (mV)

$V_{1/2}$: Voltage of half maximal activation (mV).

dx: Slope factor (mV).

All the fittings were performed using the methods available in the origin 8.0 software.

3.9.2.2 TRPM8 Temperature threshold calculated from voltage ramp patch clamp experiment

During the voltage ramp protocol (-100 mV to +150 mV, 800 ms) applied in HEK293 cells, expressing either wild type TRPM8 or mutants, I wanted to check whether different mutations utilized in this study affect the temperature threshold of TRPM8 activation. The cold threshold activation was determined as the temperature value preceding the outward current increase during cooling (blue dot, note the change of the temperature threshold following mutations). The wild type TRPM8 temperature threshold was around 28 ˚C.

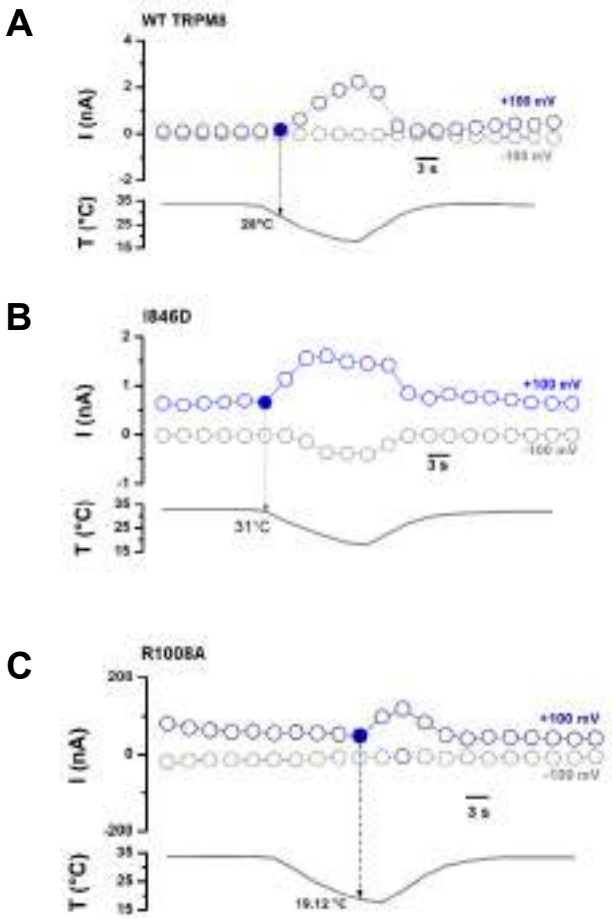

Figure 14. Cold threshold of wild type TRPM8 compared to mutants (I846D and R1008A). A, Current time course of HEK293 cell expressing WT TRPM8 in response to a cold ramp. Note the temperature threshold at 28˚C. **B,** Current time course of HEK293 cell expressing I846D mutant in response to cold ramp. Note the temperature threshold at 31˚C (shifted toward warmer temperature). **C,** Current time course of HEK293 cell expressing R1008A mutant in response to cold ramp. Note the temperature threshold at 19.12˚C (shifted toward colder temperature).

3.9.2.3 Electrophysiological Analysis of DRG voltage and current clamp recordings

Voltage clamp:

The results were presented as current density amplitude I (pA/pF). First the current amplitude (ΔI) was calculated by the difference between the value of peak maximal current (I_{max}) and the basal current (I_{basal}), which was the point before the current increase.

Current amplitude: $\Delta I = I_{max} - I_{basal}$.

The current density was calculated by dividing the current amplitude (ΔI) by the capacitance (C) that directly registered from the amplifier:

Current density: $I\ (pA/pF) = \Delta I\ (pA) / C\ (pF)$

Current clamp:

The results were presented as firing frequency (Hz).

- Firing frequency for cold was taken as the number of action potential spikes divided by the time between the first and the last spike (Δt) during the cooling ramp. The firing frequency in control conditions was calculated during the 60 s prior to rapamycin application.
- Rapamycin-evoked firing was calculated counting the number of spikes during rapamycin application until the start of the second cold ramp divided by the time between the first and the last spike.
- Finally, the frequency of dual application of cold and RAP was calculated similarly in the cold condition (note that spikes tended to inactivate).

Firing frequency (Hz) = Number of Spikes / Δt (s)

Electrophysiological Analysis of the skin nerve action potential recordings:

The results were presented as the following:

- Validate fibres cold sensitivity: presented as number of action potentials in 60 s (# AP / 60 s). To validate the cold sensitivity of our cold fibres recorded, I calculated the number of actions potentials 60 s before the initiation of the 1st cooling ramp and compared it to the number of action potentials generated 60 s right after the initiation of 1st cooling.
- The firing frequency in 5 s (# AP / 5 s). I used the maximum peak frequency (max peak frequency) evoked by each stimulus during the application time (During 1st cold application time; rapamycin 2 min before the second cold ramps; and during the 2nd cooling in the presence of rapamycin).

- Temperature threshold (T. Threshold (˚C)): was considered as the temperature at which the first action potential is generated upon stimulus application. Note that rapamycin sensitive neurons start firing at basal temperature.
- Temperature at peak frequency (T. at peak frequency (˚C)): was the temperature at which the highest frequency is reached during stimulus application.

3.9.3 Analysis of rapamycin effects on wild type TRPM8 gating kinetics

The mechanisms of TRPM8 gating by chemical agonists was described by Janssens and collaborators where they defined two agonists categories including the type-1 agonists or menthol-like group which acted by inducing a stabilization of the open channel and slowing the closing of the channel, while type-2 agonists or AITC-like group acts by destabilizing the closed state and force the channel to close faster (Janssens et al., 2016). I fitted the raw data of currents obtained from a voltage step protocol (-80 mV to +120 mV, 50 ms) at room temperature (24 ˚C) to exponential equations. This allowed me to determine the time constants during the activation step from -80 mV up to +120 mV and the deactivation during the current relaxation period at -80 mV. I performed this analysis both in control conditions and in the presence of TRPM8 agonists.

-In the activation phase (following a depolarizing pulse from -80 mV up to 120 mV), the normalized current recorded in control condition was fitted to a monoexponential equation of activation to obtain the activation time constant (**τ**) used for comparaison. The fitting equation used was :

$$\textbf{(A)}\ Y = (1 - \exp(-t/\tau_a))$$

Where:

t: time from the beginning of the pulse (ms).

τ_a **:** Activation Time constant in control condition (ms).

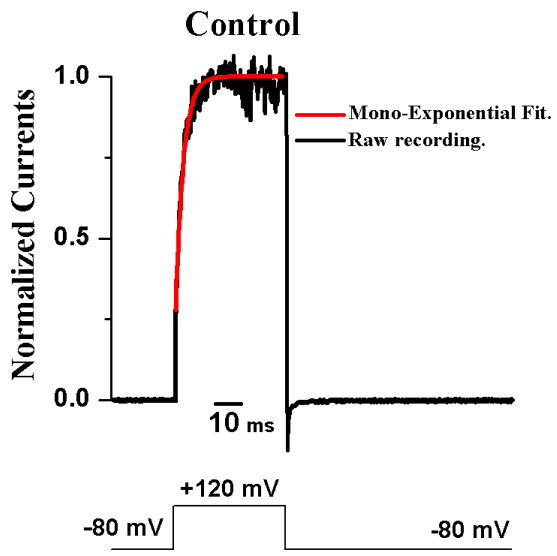

Figure 15. Example of monoexponentially fitting during activation voltage step. (From -80 mV up to +120 mV during 50 ms, in control condition).

-During the deactivation phase (Current relaxation) at -80 mV. The normalized current recorded in control condition was fitted to a monoexponential equation of deactivation. The fitting equation used was :

(B) $Y = -\exp(-t / \tau_d)$

Where:

t : time from the end of the pulse (ms)

τ_d **:** Deactivation time constant in control condition (ms).

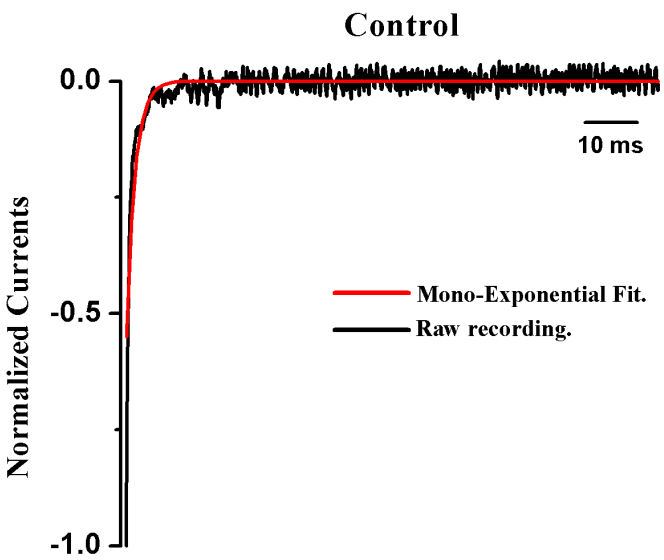

Figure 16. Example of monoexponentially fitting during deactivation phase at -80 mV in control condition.

- On the contrary, the activation phase (depolarizing potential) during voltage step from -80 mV up to 120 mV in the presence of TRPM8 agonist. In control condition, the normalized current recorded in the presence of TRPM8 agonists required a bi-exponential fitting during the activation, which gave result to two time constants of activation: the fast component that occured in the initial phase of activation called also the first time constant (τ_1), and the slow component that occured at the last period of activation called also second time constante (τ_2) both used for comparaison to control. The fitting equation used was :

$$\textbf{(C)}\ Y = A1\ (1-\exp(-t / \tau_1)) + (1-A1)\ (1-\exp(-t / \tau_2))$$

Where:

Y: The normalized current.

A1: Weight of the fast component.

τ_1: Fast time constant in the presence of TRPM8 agonist (ms).

A2 or (1-A1): The weight of the slow component of activation.

τ_2: Slow time constant in the presence of TRPM8 agonist.

t: Time from the start of the pulse.

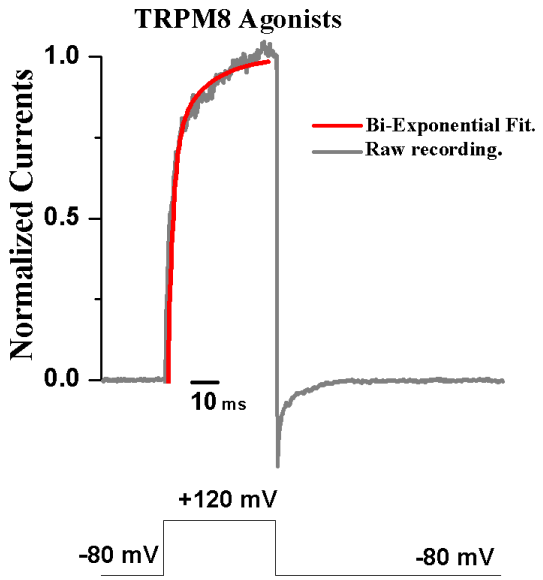

Figure 17. Example of Bi-exponential fitting of normalized current in the presence of TRPM8 agonist (RAP 30 µM) during activation voltage step. (From -80 mV up to +120 mV during 50 ms)

-During the deactivation phase (Current relaxation) at -80 mV. The normalized current recorded in the presence of TRPM8 agonists also required a bi-exponential fitting following this equation:

$$\textbf{(D)}\ Y = -A1 \exp(-t / \tau_1) - (1-A1) \exp(-t / \tau_2)$$

Where:

Y: The normalized current.

A1: Weight of the fast component of deactivation.

τ_1: Deactivation fast time constant in the presence of TRPM8 agonist (ms).

A2 or (1-A1): Eeight of the slow component of deactivation.

τ_2: Decativation slow time constant in the presence of TRPM8 (ms).

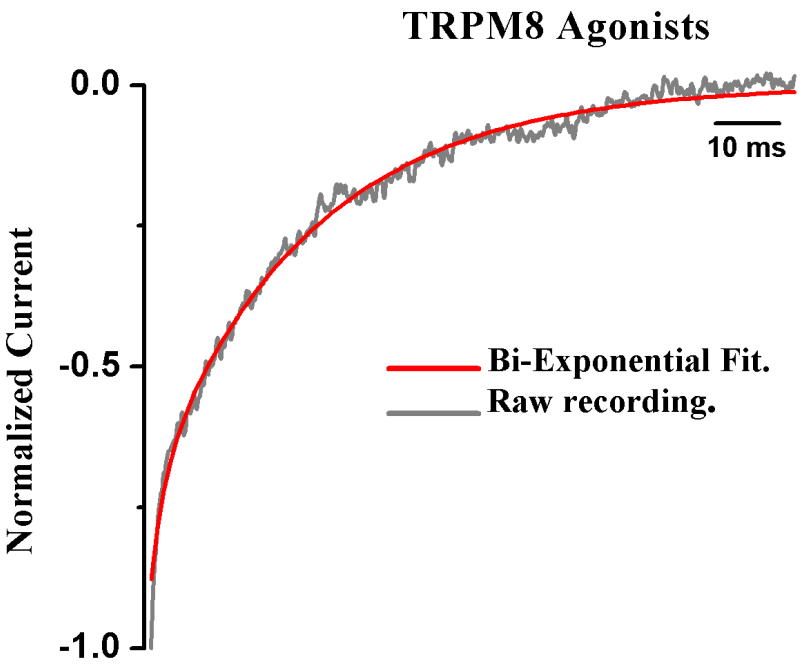

Figure 18. Example of Bi-exponential fitting during deactivation phase at -80 mV in the presence of TRPM8 agonist (Menthol 30 µM).

3.9.4 Software and statistics

Combination of both Origin 8.0 and GraphPad Prism version 9.5.1 were used to analyse the calcium imaging and patch clamp electrophysiology data and to prepare the figures. Spike 2 was used to analyse the skin nerve experiments. Data are reported as mean ± standard error of the mean (SEM), statistical analysis of the data was performed using GraphPad prism version 9.5.1 for Windows (GraphPad Software). Statistical significance was assessed by student's two-tailed t-test when comparing two means ($P<0.05$), and Chi two square when comparing two proportions. While one-way ANOVAs was performed for multiple comparisons of means. The assessment of normality of data distribution was performed with Shapiro-Wilk test. Several statistical hypothesis tests including ANOVA are robust to the violation of normality assumption when the sample size is large. Which is the case in most of our calcium imaging data´s sample size (>30). Additionally, the data distribution was supported by the evaluation of quantile-quantile (Q-Q) normality plot. If the data were not following a normal distribution the propre program offers an option to perform a non-parametric test. Asterisk are used for comparing the effect of different stimuli (*, p-value< 0.05; **, p-value< 0.01; ***, p-value< 0.001; ****, p-value< 0.0001).

3.10 Chemicals

Rapamycin (LC laboratories) was prepared in DMSO (stock 50 mM) and dissolved in prewarmed control solution (50 ºC), once inside the solution a precipitate of white color was seen, then just the application of a gentle shake made the solution homogenous. Due to its poor solubility in aqueous solution, it has limited our highest working concentration at 30 µM. G-RGM-145 and G-RGM-109 (Institute of medical chemistry) were dissolved in DMSO (20 mM), different concentrations were used with both compounds 3, 10 and 30 µM dissolved in control solution. Menthol (Scharlau, Spain), AMTB (N-(3-Aminopropyl)-2-[(3-methylphenyl) methoxy]-N-(2-thienylmethyl) benzamide hydrochloride; Tocris), RQ00203078 (Tocris), carbachol (Carbamoylcholine chloride, Sigma), all were prepared as stock and stored at -20 º C.

Compound	Stock (mM)	Solvent	Working Concentration (µM)
Rapamycin (RAP)	50	DMSO	30
Menthol	300	DMSO	30
WS-12	20	DMSO	0.5 and 10
AMTB	50	DMSO	10
RQ00203078	0.1	dH_2O	0.5
G-RGM-145	20	DMSO	3, 10 and 30
G-RGM-109	20	DMSO	3, 10 and 30

4. Results

4.1 The immunosuppressant macrolide Rapamycin activates cold-sensitive TRPM8 channels

I investigated the effects of rapamycin (RAP), a clinically approved drug widely used as immunosuppressant. I found that it has agonistic effects on the TRPM8 channel. The study covered a wide range of experiments, going from characterization in a heterologous expression system to studies in mouse cultured DRG neurons and, finally reaching the sensory terminals in the mouse skin. Beyond the characterization of the agonistic effect, I also characterized some TRPM8 mutants searching for the potential binding site of our drug on the channel.

4.1.1 Rapamycin activates heterologously expressed mouse TRPM8 channel

Using *in vitro* intracellular calcium imaging, I studied mouse TRPM8 (mTRPM8) responses to RAP in cells co-transfected with GFP. The HEK293 cells expressing mTRPM8 were activated by cooling ramp, and sequential application of RAP (30 µM) and WS-12 (10 µM) (Fig. 19A, blue trace).

The amplitude of RAP-evoked responses was markedly smaller compared to either cold or WS-12 (Cold=0.5 ± 0.1 vs RAP=0.22 ± 0.03 vs WS-12= 1.2 ± 0.1) (Fig. 19B). The RAP effect on TRPM8 channel was similar to a recent study characterizing another macrolide family member, tacrolimus (Arcas et al., 2019). In line with previous studies characterizing other chemical agonists, RAP potentiated cold-evoked responses (Voets et al., 2004; Mälkiä et al., 2007). The potentiation of cold responses was similar comparing RAP and WS-12 agonists (Cold=0.5 ± 0.1 vs RAP+cold=2.1 ± 0.2 vs WS-12+cold= 2.03 ± 0.15) (n=123, p-value< 0.0001) (Fig. 19B).

In addition, a fraction of cells that was not activated by cold (Cold insensitive), responded to cold in the presence of RAP or WS-12 (Fig. 19A, green trace). The fraction of cells unresponsive to cold or WS-12 did not show any change in the intracellular Ca^{2+} levels in the presence of RAP (Fig. 19A, grey trace) suggesting that they are not expressing wild type mTRPM8.

The percentage of cells activated by RAP (Fig. 19G) among all GFP+ HEK293 cells (n=201) was less than the percentage activated by cold or WS-12 (RAP = 49% vs Cold = 61% vs WS-12 = 85%) (p-value< 0.0001, chi-squared test) (Fig. 19D, I). In the presence of RAP, the percentage of cells activated by cold increased robustly, and a similar result was obtained with WS-12 (Cold=61% vs RAP+cold=91.5% vs WS-12+cold= 91%) (p-value< 0.0001, Chi-squared test) (Fig. 19D.H and J).

Thus, RAP behaves as an agonist of mouse TRPM8 channels, with effects on cold sensitivity similar to previous observations with different agonists (Brauchi et al., 2004; Voets et al., 2004; Arcas et al., 2019). In terms of potency, the result suggests that RAP is less potent than WS-12.

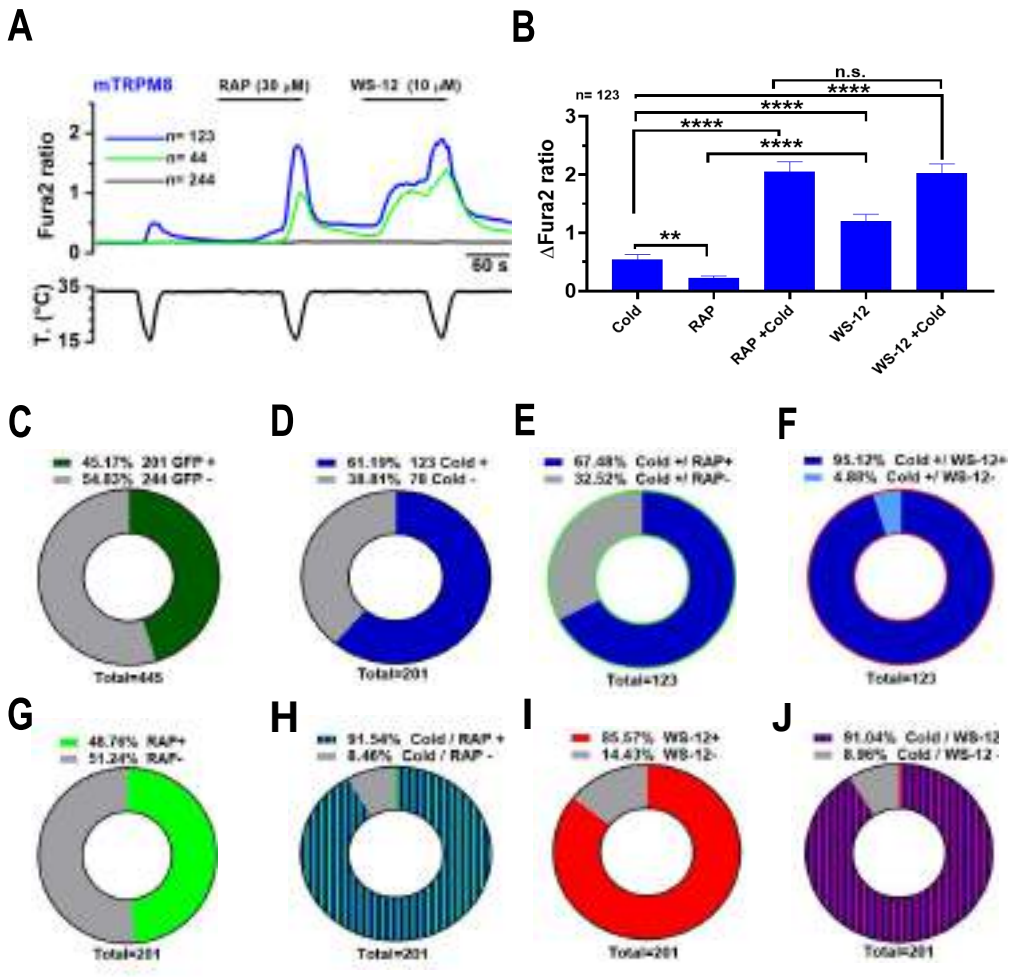

Figure 19. Rapamycin activated heterologously transfected mouse TRPM8 channel and potentiated cold evoked responses. A, Average ± SEM fura2 ratio response to cold, RAP (30 µM) and WS-12 (10 µM) in HEK293 cells transiently transfected with mouse TRPM8 and GFP. GFP (+) cold sensitive cells (n=123) are shown in blue (blue trace) and GFP (+) cold insensitive cells (n=44) are shown in green (green trace) while GFP (-) non transfected cells (n=244) are shown in grey. **B,** Bar histogram summarizing the responses of cold sensitive HEK293 cells transfected with mouse TRPM8 to different agonists. Statistical significance was calculated by a one-way ANOVA followed by Bonferroni post-hoc test. **C,** Pie graph showing the percentage of GFP (+) transfected and GFP (-) non-transfected cells out of total cells (n=445). **D,** Pie graph showing the percentage of cold sensitive cells (Cold+) and cold insensitive cells (Cold-) out of the total GFP+ transfected cells (n=201). **E,** Pie graph showing the percentage of cold sensitive cells that are either Rapamycin (30 µM) sensitive (Cold+ / RAP+) or Rapamycin insensitive (Cold+ / RAP-) cells out of total cold responders (n=123). **F,** Pie graph showing the percentage of cold sensitive cells that are either WS-12 (10 µM) sensitive (Cold+ / WS-12+) or WS -12 insensitive (Cold+ / WS-12 -) cells out of total cold responders (n=123). **G,** Pie graph showing the percentage of Rapamycin sensitive cells (RAP+) and insensitive cells (RAP-) out of the total GFP+ transfected cells (n=201). **H,** Pie graph showing the percentage of cold evoked percentage cell activation in the presence of rapamycin potentiating cold responses (Cold/RAP+) and the insensitive cells (Cold/RAP-) out of the total GFP+ transfected cells (n=201). **I,** Pie graph showing the percentage of WS-12 sensitive cells (WS-12+) and insensitive cells (WS-12-) out of the total GFP+ transfected cells (n=201). **J,** Pie graph showing the percentage of cold evoked percentage of cells activation in the presence of WS-12 (Cold/WS-12+) and insensitive cells (Cold/WS-12-) out of the total GFP+ transfected cells (n=201).

4.1.2 Rapamycin activates TRPM8 channels currents

Electrophysiological whole-cell patch clamp recordings following a voltage ramp protocol (see material and methods) showed that the application of cold or 30 µM RAP evoked robust whole-cell currents in HEK293 cell expressing mouse TRPM8 (Fig. 20A). In line with previous reports (Mälkiä et al., 2007; Voets et al., 2004; Arcas et al., 2019) the current-voltage relationship of both, cold-activated or RAP-activated currents, had the typical characteristics of TRPM8 recordings, showing a strong outward rectification and reversal potential around 0 mV (Fig. 20B). In addition, cold-evoked inward current was markedly potentiated by RAP (Cold= -11 ± 2 pA/pF vs Cold + RAP= -160 ± 37 pA/pF) (n=14; p-value< 0.05). Cold-evoked outward current was also potentiated by RAP (Cold=189 ± 19 pA/pF vs Cold + RAP= 360± 36 pA/pF) (n=14; p-value< 0.01) (Fig. 20C). The RAP potentiation of cold-evoked response was similar to that produced by WS-12.

These findings confirmed calcium imaging results and demonstrated the agonism of RAP on TRPM8 channels.

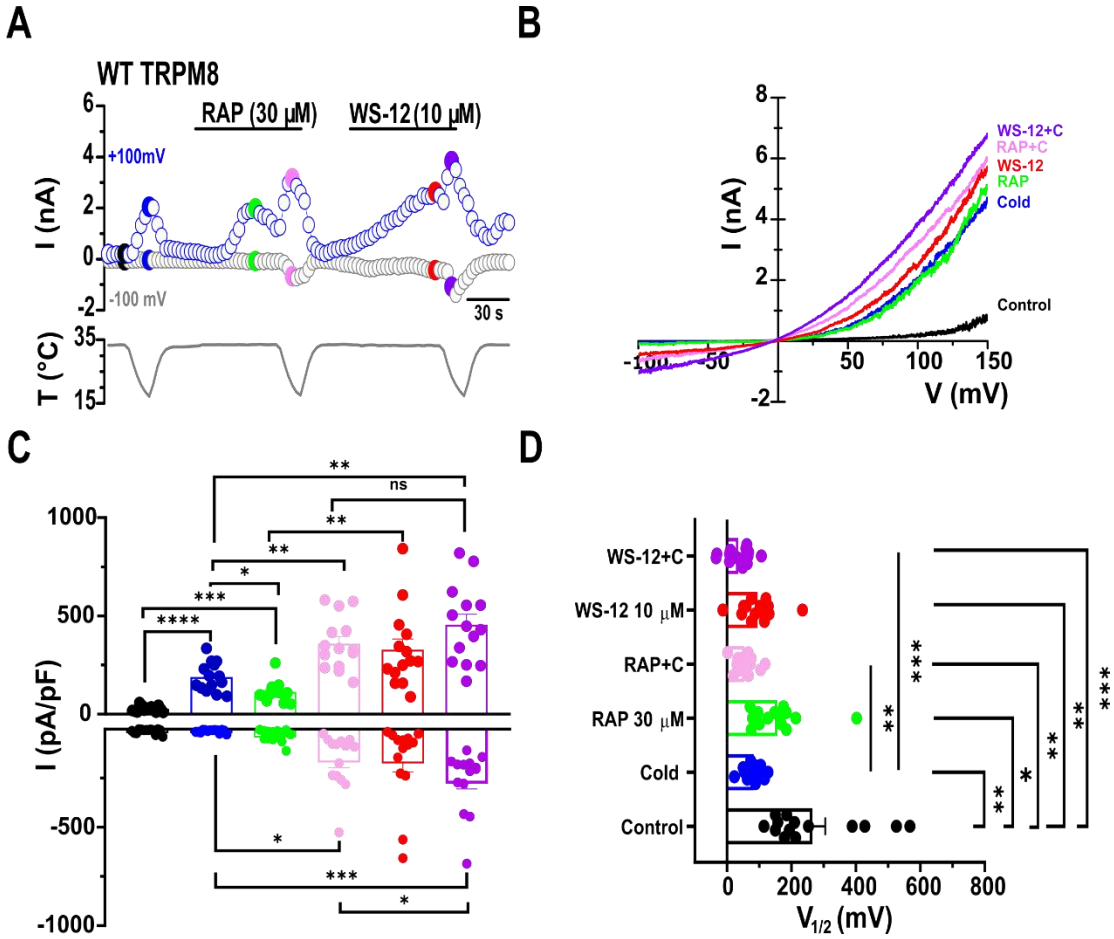

Figure 20. Rapamycin activated mouse TRPM8 expressed in HEK293 cells mediated whole-cell currents and provoked a leftward shift of its current voltage dependence. **A,** Representative time course of mTRPM8 whole cell currents screened at -100 mV and +100 mV in transiently transfected cells during sequential agonists application. The trace of simultaneous recording of the batch temperature during experiment is shown at the bottom. **B,** The current-voltage relationship (I-V) of responses presented in A, resulted with 800 ms voltage ramp from -100 to +150mV. The key colors of single traces coincide with specific time points in A**.** Rapamycin elicited a non-selective cationic currents TRPM8 dependent features and potentiated cold evoked responses. **C,** Bar histogram summarizing the mean ± SEM current density at +100 and -100 mV of the different stimuli presented in A, following the color code. Statistical differences were evaluated by one-way Anova followed by Bonferroni´s post-hoc test. ***D,*** Mean (n=14) values calculated from fitting the individual I-V curve to linear Boltzmann equation. Note rapamycin provoked a less significant leftward shift of $V_{1/2}$ compared to Cold and WS-12, statistical differences were evaluated by one-way anova followed by Bonferroni's post-hoc test.

4.1.3 Rapamycin induces typical biophysical effect on TRPM8 gating

4.1.3.1 Rapamycin shiftes voltage dependance towards more negative potentials

Previous studies characterizing the effect of TRPM8 agonists (cold, menthol and tacrolimus) on channel activation demonstrated that these agonists produce a marked shift in the voltage dependence of activation towards more negative potentials (Brauchi et al., 2004; Voets et al., 2004; Arcas et al., 2019). while, antagonists (BCTC and SKF96365) induce strong shift towards more positive potentials (Madrid et al., 2006; Mälkiä et al., 2007). To investigate the effect of RAP (30 µM) on the voltage-dependence of channel gating, I used mouse TRPM8 (mTRPM8) channels heterolougously expressed in HEK293 cells, and compared RAP effect to the both canonical TRPM8 agonists WS-12 (10 µM) that is most potent agonist, and Menthol (30 µM). These concentrations of WS-12 and menthol used produce a similar potentiation of current (Fig. 21A), in line with the literature (Ma et al., 2008).

Based on voltage ramp protocol performed at baseline temperature (33 ± 1 ˚C), RAP (30 µM) elicited a strong leftward shift of the voltage of half- maximal activation ($V_{1/2}$) compared to control (Control $V_{1/2}$ =265 ± 40 mV; RAP $V_{1/2}$ = 156 ± 23 mV) (n=14; $p< 0.05$). The cold-evoked $V_{1/2}$ shift was significantly potentiated by RAP (Cold $V_{1/2}$=83 ± 8 mV; Cold + RAP=55 ± 9 mV) (n=14; p-value< 0.01) (Fig. 20D).

Next, I applied voltage steps going from -80 mV up to +240 mV (see methods), in whole-cell mode, to characterize the amplitude and time course of evoked currents. These experiments were performed at room temperature (23 ± 1˚C) in order to confer a substantial baseline activation of mTRPM8 channels. The RAP used at 30 µM, in comparaison to two canonical agonists menthol used at 30 µM and its derivative WS-12 at 10 µM in order to obtain similar degree of TRPM8 channel activation as well as to make the comparison more meaningful. Moreover, the maximal conductance (G_{max}) value obtained by either agonist was used for current normalization. Shown in Fig. 21A are currents recorded from the same cell during 50 ms voltage steps ranging from -80 mV to +240 mV. The analysis of the current-voltage relationship (I-V) and the conductance-voltage (G/G_{max}-V) curves in the different conditions, is shown in figures 21C and 21E, which revealed a robust leftward shift of the voltage activation curve in the presence of the three agonists (Fig. 21B, D): from the control value $V_{1/2}$=148 ± 7 mV to $V_{1/2}$ =107 ± 5 mV in the presence of 30 µM RAP, while WS-12 and menthol produced even stronger shifts of the voltage of half maximal activation respectively (Control $V_{1/2}$ =148 ± 7 mV vs WS-12 $V_{1/2}$ =93 ± 12 mV and Menthol $V_{1/2}$ =79 ± 7 mV) (calculated from I-V) (Fig. 21D). Similar shift is calculated from the G/G -V plot, from control $V_{1/2}$ =148 ± 6 mV to $V_{1/2}$ =107 ± 5 mV in the presence of 30 µM RAP. WS-12 and menthol showed strong shift of the voltage of half maximal activation respectively $V_{1/2}$ =93 ± 12 mV and $V_{1/2}$ =79 ± 7 mV (Fig. 21F).

4.1.4 Rapamycin behaves as a TRPM8 type 1 agonist (or Menthol-like)

In 2016, Janssens and collaborators published a study describing the kinetic properties of TRPM8 gating by different chemical agonists that resulted in the definition of two types of agonists with distinct mechanisms. Type-1 agonists, exemplified by menthol, acted by inducing a stabilization of the open channel, manifested by slowing of the gating kinetic upon depolarizing to +120 mV and slowing the deactivation kinetisc of the channel following repolarization at -80 mV. In contrast, type-2 agonists, or AITC-like group, acted by destabilizing the closed channel conformation, whereby accelerating the opening kinetic and forced the channel to close faster (Janssens et al., 2016). Here, I investigated the effects of 30 µM RAP on TRPM8 channel gating kinetics by analysing the time constant of both the current activation during voltage step from -80 mV up to +120 mV, and their current relaxation at -80 mV in HEK293 expressing mTRPM8. To facilitate comparaison, currents were normalized to their steady-state values and the baseline was subtracted. In control conditions, during activation and deactivation phases, the traces were well fitted by a monoexponential equation respectively (A) and (B) (see methods), resulting in a single time constant (**τ**) (which I included in the graphs as **τ_1** for comparison with the fast component resulting after agonists application). In contrast, in the presence of different agonists a bi-exponential fitting, using equations (**C**) and (**D**) resprectively, was necesasary to fit both activation and deactivation traces, resulting into two time constants: a fast component (**τ_1**), and a second slower component (**τ_2**).

During the activation phase (voltage step going from -80 mV up to +120 mV), I observed that RAP (30 µM), WS-12 (10 µM) and menthol (30 µM) evoked a clear slowing of activation kinetics that is revealed by the requirement of the bi-exponontial equation fitting resulting in two time constants : a fast component or the first activation time constant τ_1 was similar after the application of different agonists (RAP τ_1= 2.7 ± 0.4 ms, Amplitude A1= 0.8; WS-12 τ_1 = 2.7 ± 0.4 ms, Amplitude A1= 0.8; Menthol τ1= 2.5 ± 0.3 ms, Amplitude A1= 0.7) compared to control (τ= 3.9 ± 0.5 ms), and the slow component or second time constante (τ_2) (RAP τ_2 = 17± 1 ms, Amplitude A2= 0.2 ; WS-12 τ_2 = 31 ± 5 ms, Amplitude A2= 0.2; Menthol τ_2 = 21 ± 2 ms, Amplitude A2= 0.3). Although RAP is slowing the activation kinetic, the effect was smaller than the slowing evoked by WS-12 or menthol. While in control conditon the kinetic of activation was faster, which only required fittiing to a monoexponential equation giving rise to a single time constante of activation (τ= 3.9 ± 0.5 ms) (represented in the graph as τ_1) (Fig. 22D).

Similar results were obtained during the deactivation phase time constants at -80 mV (current relaxation). RAP and WS-12 produced a marked slowing of the relaxation kinetics represented by the biexponential fitting that give rise to both slow component or second time constant τ_2 (RAP τ2 = 16 ± 1 ms, Amplitude A2= 0.4; WS-12 τ_2 = 27 ± 6 ms, Amplitude A2= 0.2) (p-value< 0.05), while menthol induced more stronger slowing of the slow time constante τ_2 (τ_2 = 24± 2 ms, Amplitude A2= 0.6), (Fig.

22F), and fast component or first time constant τ_1 that was slowed after RAP, WS-12 and Menthol applications. Compared to control condition where either in activation or deactivation phases showed a fast kinetic fitted with monoexponetial equation that give rise to single time constante (τ) (Fig. 22E).

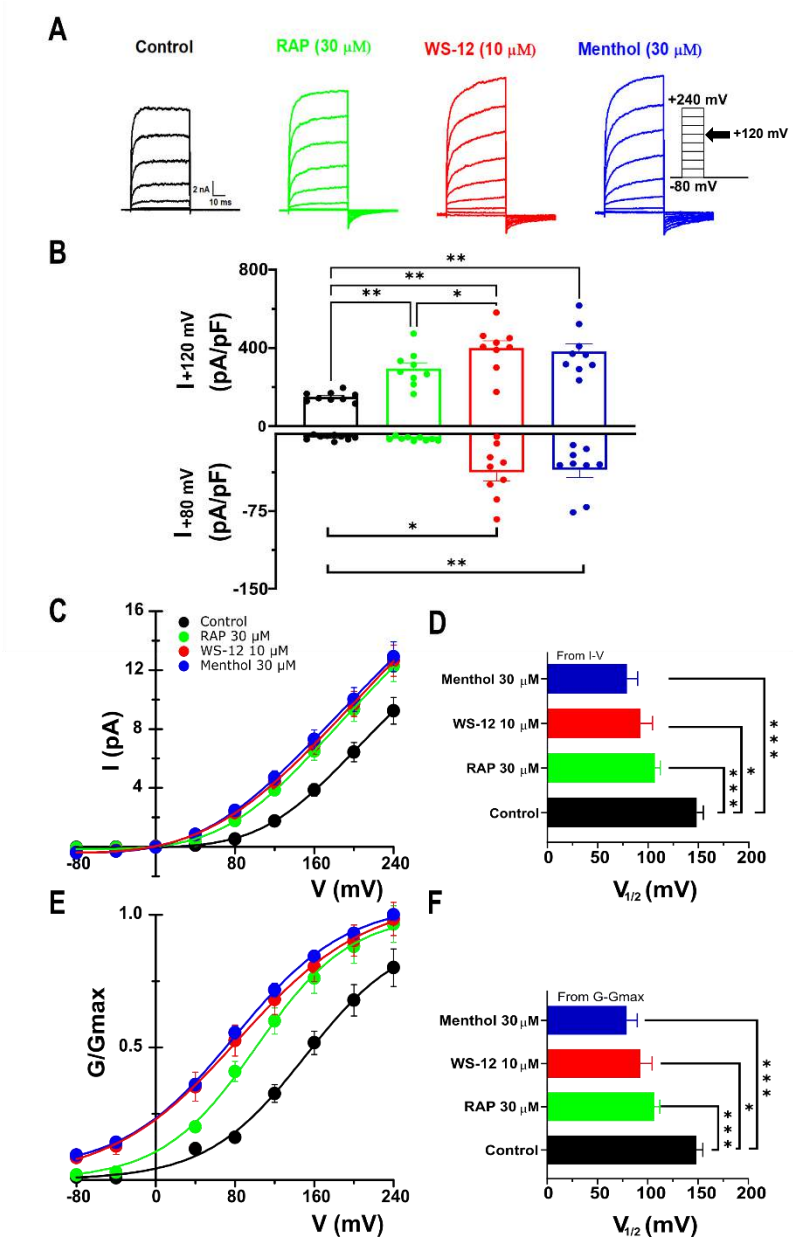

Figure 21. Biophysical characterization of rapamycin effects on TRPM8 gating. A, Representative whole-Cell TRPM8 currents in response to the given voltage steps protocol (from -80 to +240 mV during 50 ms, ΔV= 40 mV see material and methods) in control conditions and in the presence of RAP (30 µM), WS-12 (10 µM) menthol (30 µM) at 24 ˚C (ambient temperature). **B,** Bar histogram summarizing the mean ± SEM current density at +120 (outward current density) and -80 mV (inward current density) of the different stimuli presented in A, following the color code. Statistical differences were evaluated by one-way Anova followed by Bonferroni´s post-hoc test. **C**, Average ± SEM (n=9) steady-state I-V curves extracted from individual cells after application of protocol the lines represent the fitting to linearized Boltzmann equation (see methods). **D,** Mean (n=9) $V_{1/2}$ value calculated from fitting the individual I-V curve to linearized Boltzmann equation. **E,** Average (n=9) voltage dependence activation curve in control condition and in the presence of different agonists, conductance was calculated as the steady state current divided by the driving force (Driving force = V_{Test}-E_{rev}) and normalized to the estimated maximal conductance (Gmax) which is the G value at +240 mV in the presence of 30 µM menthol. **F,** Mean (n=9) $V_{1/2}$ value calculated from fitting the individual G/Gmax-V curve to Boltzmann equation. The statistical differences were analyzed by one way ANOVA, followed by Bonferroni's post-hoc test.

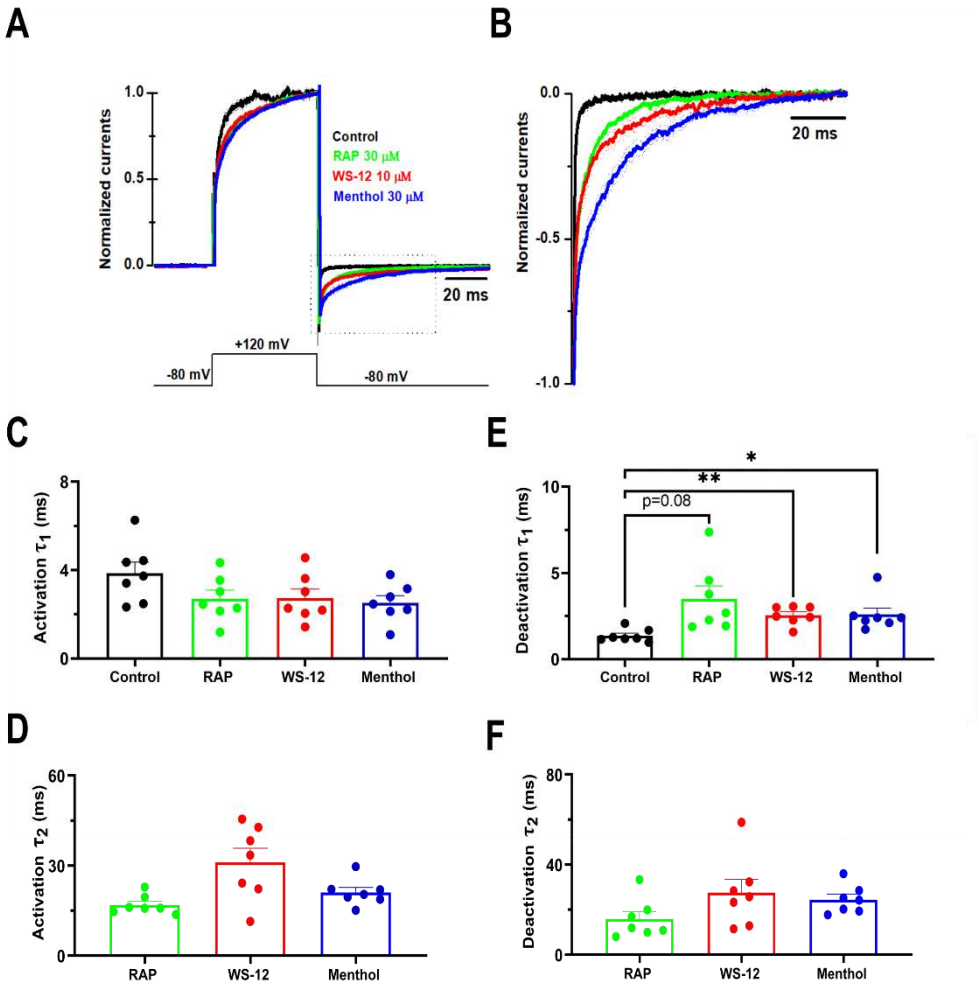

Figure 22. Characterization of the rapamycin effect on TRPM8 activation/deactivation kinetics. A, Normalized average ± SEM of TRPM8 currents during a voltage step from -80 to +120 mV in control condition and in the presence of different agonists normalized to their steady-state amplitude after baseline subtraction. **B,** Average ± SEM TRPM8 deactivation kinetics at -80 mV extracted from tail current after a voltage step to + 120 mV (box dotted line in A), in both control and in the presence of different agonists. The current was normalized to the maximum value and baseline was subtracted. **C,** Bar histogram showing Mean ± SEM of the faster component first time constant (τ_1) during activation phase from voltage step up to +120 mV, extracted from fitting single traces in control condition to a mono-exponential (τ) and agonists traces to a bi-exponential equations (τ_1). **D,** Bar histogram showing Mean ± SEM of Slow component or second time constant (τ_2) during activation phase after a voltage step to +120 mV. **E,** Bar histogram showing Mean ± SEM fast component or first time constant (τ_1) during deactivation phase at -80 mV. **F,** Bar histogram showing Mean ± SEM slow component or second time constant (τ_2) during deactivation phase at -80 mV. Note that for both activation and deactivation phases, in the control condition the activation traces following voltage step up to +120 mV were fitted to a mono-exponential equation resulting a single time constate (τ) used for comparison with different conditions, while with different agonists activation traces were fitted with a bi-exponential from the baseline up to 100% of current amplitude resulting two activation phase time constants : the fast component or first time constant (τ_1) of the first activation, and a slow component time constant (τ_2) of the second activation phase (See materials and methods), the same was applicable for deactivation phase at -80 mV. Statistical differences were evaluated using ANOVA one way followed by Bonferroni post-hoc test.

4.1.5 Rapamycin activates inward currents and elicites action potential firing in cold thermoreceptors

In this part, I investigated the effect of rapamycin (RAP) on native TRPM8 channel expressed in DRG sensory neurons obtained from a transgenic TRPM8$^{BAC\text{-}EYFP}$ mouse line (Morenilla-Palao et al., 2014). To test the rapamycin effect on excitability of cold thermorecptors, I performed whole-cell patch clamp recordings at a voltage of -60 mV, and observed that RAP (30 µM) activated inward current and potentiated cold-evoked inward current (Fig. 23A, B) in YFP+ neurons, identified by their green fluorescence during illumination with 488 nm blue light (Fig. 23D). RAP activation elicited a shift in the temperature threshold activation of cold-evoked inward current towards warmer temperatures (Fig. 23C). In the same neurons, menthol (30 µM) provoked a similar effect to RAP, also both agonists induced similar potentiation of cold evoked current (Fig. 23B). In whole-cell current-clamp configuration, rapamycin application elicited the firing of action potentials similar to the effects of cold in the same thermoreceptor neuron (Fig. 23E). Rapamycin slightly potentiated cold-evoked action potentials (Fig. 23F).

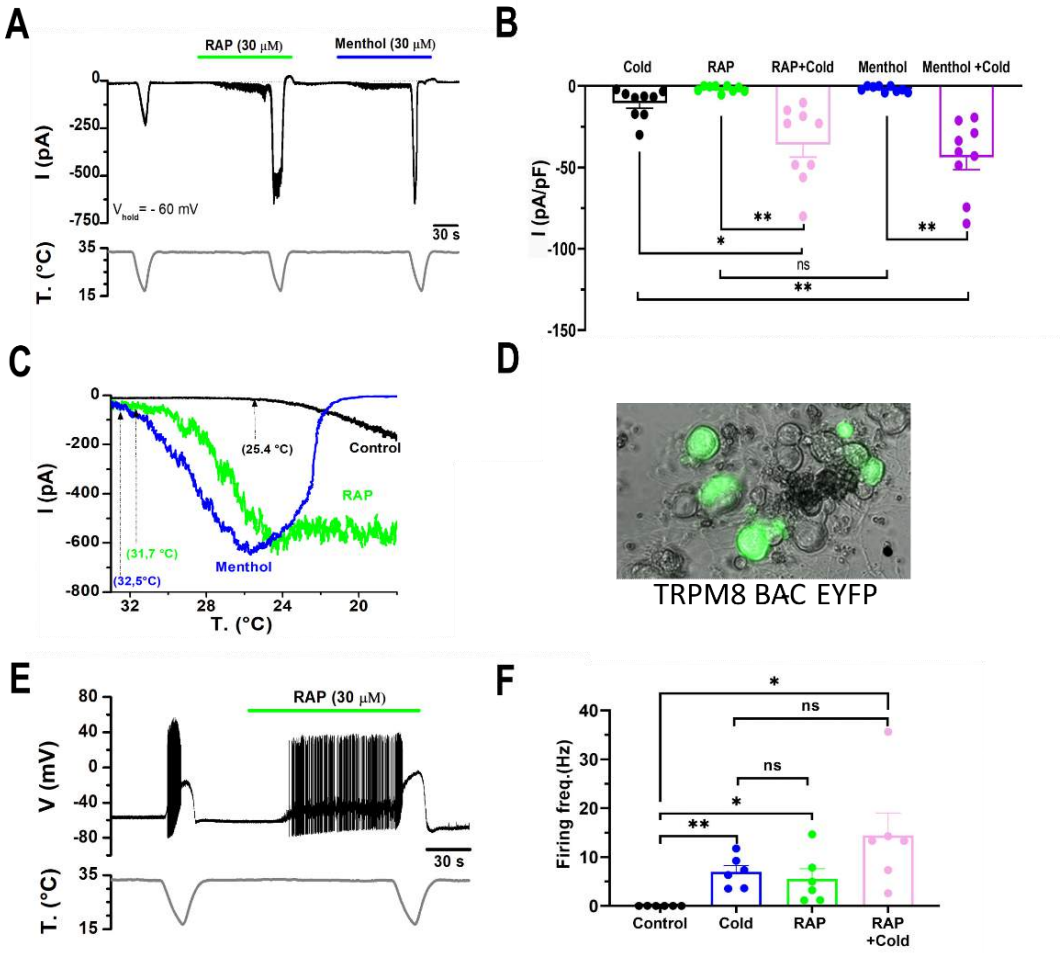

Figure 23. Rapamycin increased the excitability of cold sensitive DRG neurons. A, Representative whole-cell recording voltage-clamp configuration (V_{hold} = -60 mV) of the TRPM8 expressing cold sensitive DRG neurons identified by the expression of EYFP as shown in D, RAP (30 µM) evoked an inward current with similar amplitude to that identified by menthol (30 µM). Both RAP and menthol potentiated the response to cold. The bottom trace represented the simultaneous recording of the bath temperature during the protocol. **B,** Bar histogram summarizing the effects of agonists on the inward current amplitude during the protocol shown in A. Statistical analysis consisted to one way ANOVA followed by Bonferroni post-hoc. **C,** Current-temperature relationship of the same neuron in control (black trace) and in the presence of 30 µM RAP (green trace) or 30 µM menthol (Bleu trace). Note the clear shift of temperature threshold. **D,** Image field of the dissociated DRG neurons from transgenic mouse $TRPM8^{BAC\text{-}EYFP}$, shown a clear distinction of recorded TRPM8-expressing DRG neurons with a unique and high expression of EYFP green protein compared to negative neurons (Not expressing TRPM8 channel). **E,** Representative recording of cold sensitive DRG neurons in whole-cell current clamp configuration showing responses to cold and to the application of RAP (30 µM). **F,** Bar histogram summarizing the mean responses measured as average frequency during different stimuli application Firing frequency for cold was averaged from the first to the last spike during cooling ramp. Firing frequency in control condition was calculated during one minute before RAP application (Only 1/6 neuron fired action potentials in control condition). RAP provoked firing frequency was calculated from the first spike during RAP application to the start of the cold ramp. The statistical analysis consists of two paired T-test for Control vs cold (p=0.003), Control vs RAP (p= 0.04), Control vs RAP+ cold (p=0.02).

4.1.6 Rapamycin activates cutaneous cold thermoreceptors in mice

In 2019, the the study by Arcas et al showed that tacrolimus, another macrolide immunosuppressant, sensitised cold fibres in the saphenous nerve of mice. To evaluate whether rapamycin (RAP) activates, like tacrolimus, cold thermoreceptor endings, I have performed extracellular recordings from the shapenous nerve skin-nerve preparation, focusing on cutaneous cold fibres. The strategy was based on searching for unimodal cutaneous cold fibre, which are known to express TRPM8 channels and are key drivers of their cold sensitivity (Toro et al., 2015; Winter et al., 2017). I identified 7 cold fibres in the saphenous nerve, 5 out of 7 fibres showed an ongoing activity at the basal temperature of ~ 35 ºC while only two were silent. Upon application of cold solution to the isolated receptive field, the silent cold fibres started firing action potentials, while the rest of fibres characterized with an ongoing activity showed an increase in the number of action potentials. The first cold application induced an increase in the firing of action potentials in cutaneous cold thermoreceptors that was higher compared to their baseline activity (Before 1st Cold =18 ± 5 AP/60 s vs During 1st Cold= 75 ± 15 AP/60 s) (n=7; p-value< 0.01) (Fig. 24D). Next, after the application of 30 µM RAP, only 3 out of 7 fibres showed an increase in firing activity at the basal temperature (Fig. 24B, I and J). These RAP-sensitive cold fibres showed a similar maximum firing frequency compard to cold (Cold= 81± 59 Hz vs RAP=90 ± 66 Hz), and cold-evoked maximum firing frequency was robustly potentiated in the presence of RAP (Cold= 81 ± 58 Hz vs RAP+cold=205 ± 104 Hz) (n=3) (Fig. 24J). Moreover, among the 7 cold fibres recorded, 5 fibres shifted their cold-evoked firing threshold towards warmer temperatures in the presence of RAP (30 µM), in contrast, the remaining 2 fibers showed a shift of cold-evoked firing threshold towards colder temperature in the presence of RAP.(Fig. 24F). Thereafter, the temperature for reaching the maximum discharge rate during cooling shifted robustly towards warmer temperatures in the presence of RAP (Cold T. Freq =21 ± 3 ˚C vs RAP T.Freq=35 ± 1 ˚C) (Fig. 24K).

To sum up, RAP activated cold fibres terminals expressing TRPM8 channels that are innervating the mouse hairy skin by shifting their cold threshold towards warmer temperature, while rapamycin did not change the maximum firing during cooling.

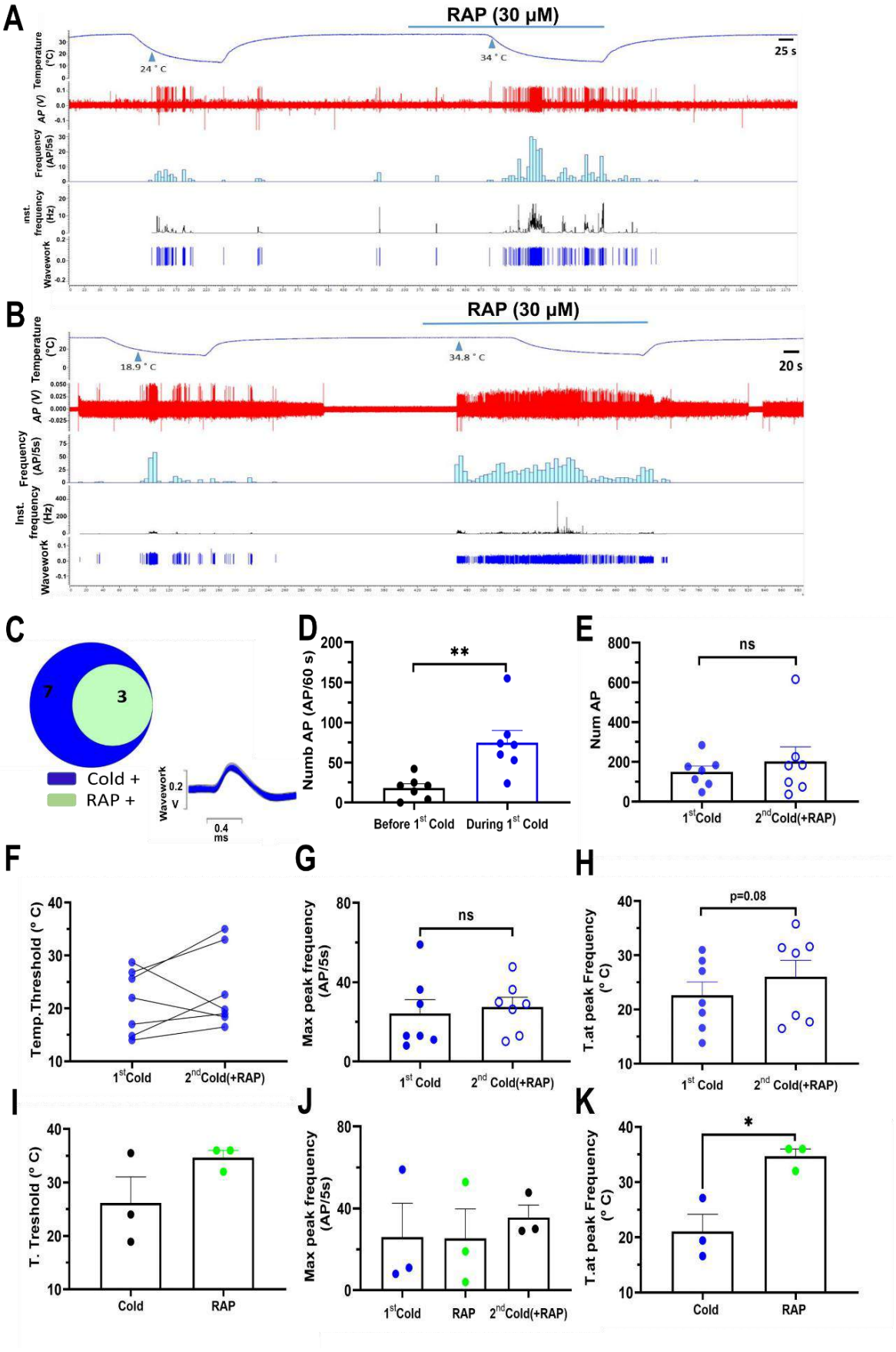
A
RAP (30 µM)
Temperature (°C)
24 ° C
34 ° C
25 s
AP (V)
Frequency (AP/5s)
inst. frequency (Hz)
Wavework
B
RAP (30 µM)
Temperature (°C)
18.9 ° C
34.8 ° C
20 s
AP (V)
Frequency (AP/5s)
Inst. frequency (Hz)
Wavework
C
7
3
Cold +
RAP +
Wavework
0.2 V
0.4 ms
D
Numb AP (AP/60 s)
**
Before 1st Cold
During 1st Cold
E
Num AP
ns
1st Cold
2nd Cold(+RAP)
F
Temp.Threshold (° C)
1st Cold
2nd Cold(+RAP)
G
Max peak frequency (AP/5s)
ns
1st Cold
2nd Cold(+RAP)
H
T.at peak Frequency (° C)
p=0.08
1st Cold
2nd Cold(+RAP)
I
T. Treshold (° C)
Cold
RAP
J
Max peak frequency (AP/5s)
1st Cold
RAP
2nd Cold(+RAP)
K
T.at peak Frequency (° C)
*
Cold
RAP

Figure 24. Rapamycin activated cutaneous cold thermoreceptors. A, Ex-vivo recording of a cold fiber activity in response to a decrease in the temperature of the receptive field before and after 30 µM RAP application. From top to bottom, temperature of the receptive field, raw voltage signal, firing frequency (AP/5s), instantaneous frequency and cleaned cold voltage signal. Note the absence of firing activity in the presence of 30 µM RAP alone, however RAP increased cold evoked action potentials firing (AP) (fiber not responding to RAP-).**B,** Ex-vivo recording of a cold fiber activity in response to a decrease in the temperature of the receptive field before and after 30 µM RAP application. Note that 30 µM RAP alone induces an increase of firing activity (Fiber responding to RAP+).**C,** Venn diagram showing the total number of cold sensitive fibers, within which 3 out 7 were responded to rapamycin (RAP+) (n=3)(see criteria in material and method).And an example of cold action potential shape of the 1st cold fiber shown in A.**D,** Bar histogram showing Mean ± SEM of the number of action potential 60 s before and during the application of 1st cold ramp in all cold fibers recorded (n=7). The statistical analysis consists of two paired student T-test (p= 0.006). **E,** Bar histogram showing Mean ± SEM of the number of action potentials during the first cold ramp, after the second cold ramp in the presence of RAP 30 µM. Not that RAP induced a non-significative increase of cold evoked action potentials (Cold= 149.6 ± 29.09 AP vs RAP= 202 ± 73.59 AP). **F,** Temperature threshold of the cold-evoked thermoreceptors firing in the absence and presence of RAP 30 µM. Not that 5 out of 7 fibers showed a shift of temperature threshold towards warmer temperatures. **G,** Bar histogram showed mean ± SEM of cold evoked the maximum peak frequency before and after RAP treatment. RAP induced an increase of peak frequency (Cold =24 ± 7 AP/5s vs Cold + RAP= 27 ± 4AP/5s). **H,** Bar histogram showing Mean ± SEM cold temperature evoked the maximal peak frequency in absence and presence of RAP. Not that RAP provoked a shift in cold temperature evoked maximum peak frequency towards warmer temperature (Cold= 22.59 ± 2.47 ˚C vs Cold+RAP= 26 ± 3.02˚C). **I,** Bar histogram showing Mean ± SEM of temperature threshold for activation of impulse discharge after cold and RAP treatment of the RAP+ fibers (n=3). Note that 30 µM RAP activated cold thermoreceptors at the basal temperature (RAP = 34 ± 1.33 ˚C vs Cold = 26.13 ± 4.9 ˚C). **J,** Bar histogram showing Mean ± SEM of cold evoked the maximum peak frequency before and after RAP treatment. RAP induced an increase cold evoked peak frequency (Cold =24 ± 7 AP/5s vs Cold + RAP= 27 ± 4 AP/5s). Not that RAP provoked similar maximum frequency like cold (Cold= 22.59 ± 2.47 ˚C vs Cold+RAP= 26 ± 3.02˚C) and that cold-evoked maximum frequency was markedly increased in the presence of (Cold= 26 ± 16.52 AP/5s vs RAP= 25.3 ± 14.4 AP/5s vs Cold+RAP AP/5s= 35.57 ± 6.07). **K,** Bar histogram showing Mean ± SEM of temperature evoked the maximal peak frequency following cold and RAP treatments. Not that RAP provoked a significative discharge activity at basal temperature (Cold= 21.03 ± 3.13 ˚C vs Cold+RAP= 34 ± 1.33˚C).

4.1.7 Rapamycin action on TRPM8 channels is independent from a key Menthol- and WS-12- binding residue

Mutagenesis studies have provided valuable insights into the effects of various TRPM8 agonists. The well-known TRPM8 agonist, menthol, was identified to bind to a cytosol-facing cavity formed by the S1-S4 segments of TRPM8. This binding involves several residues, including Y745 (S1), R842 (S4), and N799 (S3). Additionally, the TRP domain residues Y1005 and R1008 were identified as essential for menthol sensitivity (reviewed by (Plaza-Cayón et al., 2022)). Recent research has highlighted the significance of the isopropyl group of menthol, which exhibits a strong interaction (high coupling energy) with the TRPM8 residue I846 situated on segment 4. This interaction is crucial for the menthol-dependent binding to the channel (L. Xu et al., 2020; X. Chen et al., 2022).

Our objective was to investigate whether rapamycin follows a similar binding mechanism as menthol. To achieve this, I conducted calcium imaging and whole-cell patch-clamp electrophysiological recordings in HEK293 cells expressing either the wild-type or mTRPM8 mutants. I compared their activation profiles in response to rapamycin and other TRPM8 agonists.

4.1.7.1 Rapamycin activates the menthol-insensitive mutant Y745H and potentiates cold-evoked responses

The residue tyrosine Y745, located in transmembrane segment 1 according to cryo-EM structural analysis of the TRPM8 channel (Yin et al., 2018), is believed to be part of the menthol binding site. The Y745 residue's mutation of the aromatic residue tyrosine to histidine (Y745H) prevented the channel's activation by menthol (Bandell et al., 2006). Despite the mutant channel being menthol-insensitive, it retained activation by cold and voltage, similar to the wild-type TRPM8 (Bandell et al., 2006; Malkia et al., 2009). To test whether RAP shares menthol's action mechanism, I performed *in vitro* calcium imaging in HEK293 cells transiently expressing the Y745H-TRPM8 mutant. In contrast to results obtained with menthol, I found that RAP activated the mutant channel. The responses to RAP were smaller than the elevation in internal calcium produced by cold. Moreover, cold-evoked calcium elevation was strongly potentiated in the presence of RAP (30 µM) (Fig. 25A, B). In agreement with results reported previously for menthol (Bandell et al., 2006; Malkia et al., 2009), the Y745H mutant channel was also completely insensitive to WS-12, a menthol derivative. Additionally, WS-12 did not potentiate cold-evoked responses, confirming the essential role of this residue in menthol and WS-12 activation (Fig. 25A and B). Besides, cold evoked a higher percentage of GFP+ cells activation compared to both RAP and WS-12 (Cold=84 % vs WS-12=10 % vs RAP=23 %) (p-value < 0.0001, Chi-squared test) (Fig. 25D, G, and I). RAP efficiently potentiated the fraction of GFP+ cells activated by cold, but not WS-12 (Cold=84 % vs Cold+WS-12=64% vs Cold+RAP=97.33 %) (p-value < 0.0001, Chi-squared test) (Fig. 25 D, H, and J).

Compared to wild-type TRPM8, the segment 1 mutant Y745H presented a higher response to cold (WT TRPM8 Cold= 0.5 ± 0.1, n=123 vs Y745H Cold= 0.9 ± 0.1, n=150) (p-value < 0.05) (Fig. 43A). The RAP-evoked calcium response of the mutant channel was smaller compared to the wild type (WT TRPM8 RAP= 0.22 ± 0.03 vs Y745H RAP= 0.07 ± 0.03) (p-value = 0.45) (Fig. 43B). Additionally, cold-evoked responses were similarly potentiated in the presence of RAP in both groups (WT TRPM8 RAP+Cold= 2.1 ± 0.2 vs Y745H RAP+Cold= 1.8 ± 0.2) (p-value > 0.99) (Fig. 43D).

Next, I performed whole-cell patch clamp recordings on the Y745H mutant, applying a voltage ramp protocol from -100 to +150 mV, and 800 ms duration (see materials and methods). Cooling elicited a robust outward current measured at +100 mV (Control= 40 ± 8 pA/pF vs Cold= 177 ± 39 pA/pF) (n=6; p-value= 0.0091) (Fig. 26C). RAP (30 µM) activated a robust outward current measured at +100 mV (Control= 40 ± 8 pA/pF vs RAP= 114 ± 34 pA/pF) (n=6; p-value= 0.0384) (Fig. 26A). Additionally, the cold-evoked outward current measured at +100 mV (Cold= 177 ± 39 pA/pF vs RAP+cold= 264 ± 41 pA/pF) (n=6; p-value= 0.0412) (Fig. 26C) and inward current measured at -100 mV (Cold= -7 ± 1 pA/pF vs RAP + cold= -27±4 pA/pF) (n=6; p-value= 0.0052) (Fig. 26C) were robustly potentiated in the presence of RAP. As expected, application of WS-12 (10 µM) did not induce any currents.

The Y745H mutant channel preserved the characteristic outwardly rectifying current-voltage relationship (I-V) observed in wild-type channels, with a reversal potential (Erev) around 0 mV. These findings confirmed our calcium imaging results (Fig. 25B). Cooling elicited a marked leftward shift of the voltage-dependence of activation ($V_{1/2}$) (Control $V_{1/2}$= 155 ± 13 mV vs Cold $V_{1/2}$= 86 ± 14 mV) (n=6; p-value= 0.0011) (Fig. 26D). Subsequently, at basal temperature (33 ± 1˚C), RAP (30 µM) elicited a leftward shift of the voltage of half-maximal activation ($V_{1/2}$) towards negative potentials compared to control (Control $V_{1/2}$= 155 ± 13 mV vs RAP $V_{1/2}$= 119 ± 12 mV) (n=6; p-value= 0.0162) (Fig.26D). The cold-evoked voltage-dependent shift was robustly potentiated by RAP (Control $V_{1/2}$= 155 ± 13 mV; RAP+cold $V_{1/2}$= 63 ± 14 mV) (n=6; p-value= 0.0901) (Fig. 26D). In contrast, as expected, WS-12 did not shift the Y745H mutant voltage dependency (Control $V_{1/2}$= 155.1 ± 13 mV vs WS-12 $V_{1/2}$= 231 ± 55 mV) (n=6; p-value > 0.99) (Fig.26D).

Compared to wild-type TRPM8, in control condition, the Y745H mutant channel showed no clear difference comparing both generated outward and inward currents of activation measured respectively at +100 mV (WT TRPM8 Control= 28± 4 pA/pF vs Y745H Control= 40 ± 8 pA/pF; WT TRPM8 Cold= 189 ± 19 pA/pF vs Y745H Cold= 177 ± 39 pA/pF) (p-value > 0.99), and at -100 mV (WT TRPM8 Control= -12± 3 pA/pF vs Y745H Control= -7 ± 1 pA/pF; WT TRPM8 Cold= -11 ± 2 pA/pF vs Y745H Cold= -7 ± 1 pA/pF) (p-value > 0.99) in control condition or following cold activation (Fig.44A, B). RAP (30 µM) application elicited similar outward current measured at +100 mV (WT TRPM8 RAP= 114 ± 14 pA/pF vs Y745H RAP= 114 ± 34 pA/pF) (p-value > 0.99). In contrast, the inward current generated by RAP at -100 mV was markedly smaller in the mutant (WT TRPM8 RAP= -34 ± 8 pA/pF

vs Y745H RAP= -8 ± 1 pA/pF) (p-value= 0.08) in the Y745H group compared to wild-type TRPM8 (Fig. 44C). Moreover, cold-activated outward current in Y745H at +100 mV was potentiated similarly to wild-type TRPM8 in the presence of RAP (WT TRPM8 RAP+cold= 360± 36 pA/pF vs Y745H RAP+cold= 264 ± 41 pA/pF) (p-value > 0.99), whereas cold-activated inward current potentiation in the presence of RAP at -100 mV of the mutant Y745H was smaller compared to wild-type (WT TRPM8 RAP+cold= -160 ± 37 pA/pF, n=14 vs Y745H RAP+cold= -27 ± 4 pA/pF, n=6) (p-value < 0.01) (Fig. 44D).

Additionally, I extracted the cold temperature threshold from the periodic voltage-clamp protocol combined with a cooling ramp (Fig. 26A) (please consult methods). The Y745H-expressing HEK293 transfected cells showed a marked shift of the temperature threshold towards warmer temperatures compared to WT TRPM8 (WT TRPM8 T.threshold= 27.3 ± 0.3 ˚C, n=11 vs Y745H T.threshold= 30.7 ± 1.1 ˚C, n=6) (p-value < 0.05) (Fig. 45A).

Next, at basal conditions, the Y745H group voltage dependence ($V_{1/2}$) was heavely shifted towards negative voltages compared to WT, but not significantly different (WT TRPM8 Control $V_{1/2}$= 265 ± 39 mV, n=14 vs Y745H Control $V_{1/2}$= 155 ± 13 mV, n=6) (p-value= 0.09) (Fig. 45B). Furthermore, both cold or RAP (30 µM) evoked voltage dependence leftward shift were not significantly different between Y745H and WT TRPM8 groups (WT TRPM8 Cold $V_{1/2}$= 83 ± 8 mV, n=14 vs Y745H Cold $V_{1/2}$= 86 ± 14 mV, n=6, p-value > 0.99; WT TRPM8 RAP $V_{1/2}$= 156 ± 23 mV, n=14 vs Y745H RAP $V_{1/2}$= 119 ± 12 mV, n=6, p-value= 0.86) (Fig. 45C, D). Furthermore, cold-evoked voltage dependence shift potentiation in the presence of RAP was similar in both Y745H and wild TRPM8 groups (WT TRPM8 RAP+cold $V_{1/2}$= 55 ± 9 mV, n=14 vs Y745H RAP+cold $V_{1/2}$= 63 ± 14 mV, n=6) (p-value > 0.99) (Fig. 45E). Indeed, as previously described for Y745H, the menthol derivative WS-12 did not provoke any leftward shift of the voltage dependence compared to WT TRPM8 (Fig. 45F).

I explored further the effect of TRPM8 agonists on Y745H voltage-dependence of activation using a voltage steps protocol (from -80 mV to +240 mV, ΔV=40 mV) (see methods), which is performed at room temperature (23 ± 1˚C) (Fig. 27A). In whole-cell patch clamp configuration performed in HEK293 cells expressing Y745H TRPM8 mutant, I found that RAP (30 µM) potentiated voltage-activated outward and inward currents measured respectively at +120 mV (Control= 198 ± 30 pA/pF vs RAP (30 µM)= 280 ± 45 pA/pF, n=5) (p-value= 0.0459), and at -80 mV (Control= -6 ± 1 pA/pF vs Y745H RAP = -27 ± 11 pA/pF, n=5) (p-value= 0.06) (Fig. 27B). The analysis of current-voltage (I-V) and conductance-voltage (G/Gmax-V) relationships revealed a leftward shift of the voltage activation curve in the presence of RAP towards negative voltages (Fig. 27C, E), which was accompanied by a robust leftward shift of voltage of half-maximal activation ($V_{1/2}$) from the control value $V_{1/2}$= 140 ± 11 mV to $V_{1/2}$= 89 ± 26 mV in the presence of 30 µM RAP (calculated from I-V, n=5) (p-value= 0.0595) (Fig.27D). A similar result was calculated from G/Gmax-V (from a control value $V_{1/2}$= 136 ± 12 mV

to $V_{1/2}$= 82 ± 27 mV in the presence of RAP 30 µM (n=5) (p-value= 0.05) (Fig.27F). Despite that WS-12 at both low (0.5 µM) and high concentration (10 µM) did not potentiate voltage-evoked outward current measured at +120 mV, WS-12 (10 µM) elicited a small increase of voltage-evoked inward current measured at -80 mV (Y745H Control= -6 ± 1 pA/pF vs Y745H WS-12 (10 µM) = -15 ± 5 pA/pF, n=5) (p-value= 0.1437) (Fig. 27B). Finaly, further analysis of the mutant gating kinetics in presence of RAP showed wild type behviour with a slowing of either activation and deactivation gating kinetics (see annex Fig.65).

In summary, RAP mecanism of action on TRPM8 is distinct from the one of menthol (or WS-12).

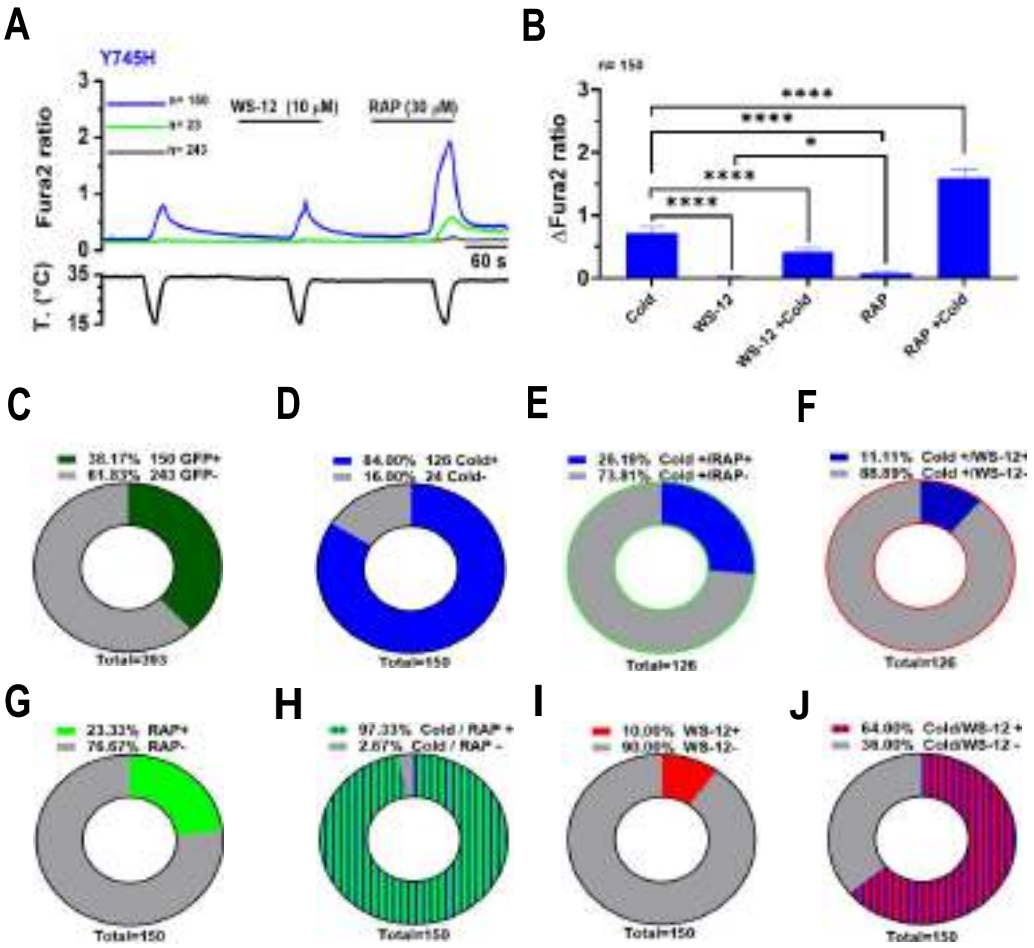

Figure 25. Rapamycin activated menthol- and WS-12- insensitive TRPM8 mutant Y745H channel and potentiated the cold evoked responses. A, Average ± SEM fura2 ratio responses to cold, RAP (30 µM) and WS-12 (10 µM) in HEK293 cells transiently transfected with Y745H TRPM8 and GFP. GFP (+) cold sensitive cells (n=150) are shown in blue (blue trace) and GFP (+) cold insensitive cells (n=23) are shown in green (green trace) while GFP (-) non transfected cells (n=243) are shown in grey. **B,** Bar histogram summarizing the responses of GFP+ HEK293 cells transfected with Y745H TRPM8 to different agonists (n=150). Statistical significance was calculated by a one-way ANOVA followed by Bonferroni post-hoc test. **C,** Pie graph showing the percentage of GFP (+) transfected and GFP (-) non-transfected cells out of total cells (n=393). **D,** Pie graph showing the percentage of cold sensitive cells (Cold+) and cold insensitive cells (Cold-) out of the total GFP+ transfected cells (n=150). **E,** Pie graph showing the percentage of cold sensitive cells that are either rapamycin (30 µM) sensitive (Cold+ / RAP +) or rapamycin insensitive (Cold+ / RAP -) cells out of total cold responders (n=126). **F,** Pie graph showing the percentage of cold sensitive cells that are either WS-12 (10 µM) sensitive (Cold+ / WS-12 +) or WS -12 insensitive (Cold+ / WS-12 -) cells out of total cold responders (n=126). **G,** Pie graph showing the percentage of Rapamycin sensitive cells (RAP+) and insensitive cells (RAP-) out of the total GFP+ transfected cells (n=150). **H,** Pie graph showing the cold evoked percentage of cells responses potentiation in the presence of rapamycin (Cold/RAP+) and the insensitive cells (Cold/RAP-) out of the total GFP+ transfected cells (n=150). **I,** Pie graph showing the percentage of WS-12 sensitive cells (WS-12+) and insensitive cells (WS-12-) out of the total GFP+ transfected cells (n=150). **J,** Pie graph showing the cold evoked percentage of cells responses potentiation in the presence of WS-12 (Cold/WS-12+) and the insensitive cells (Cold/WS-12-) out of the total GFP+ transfected cells (n=150).

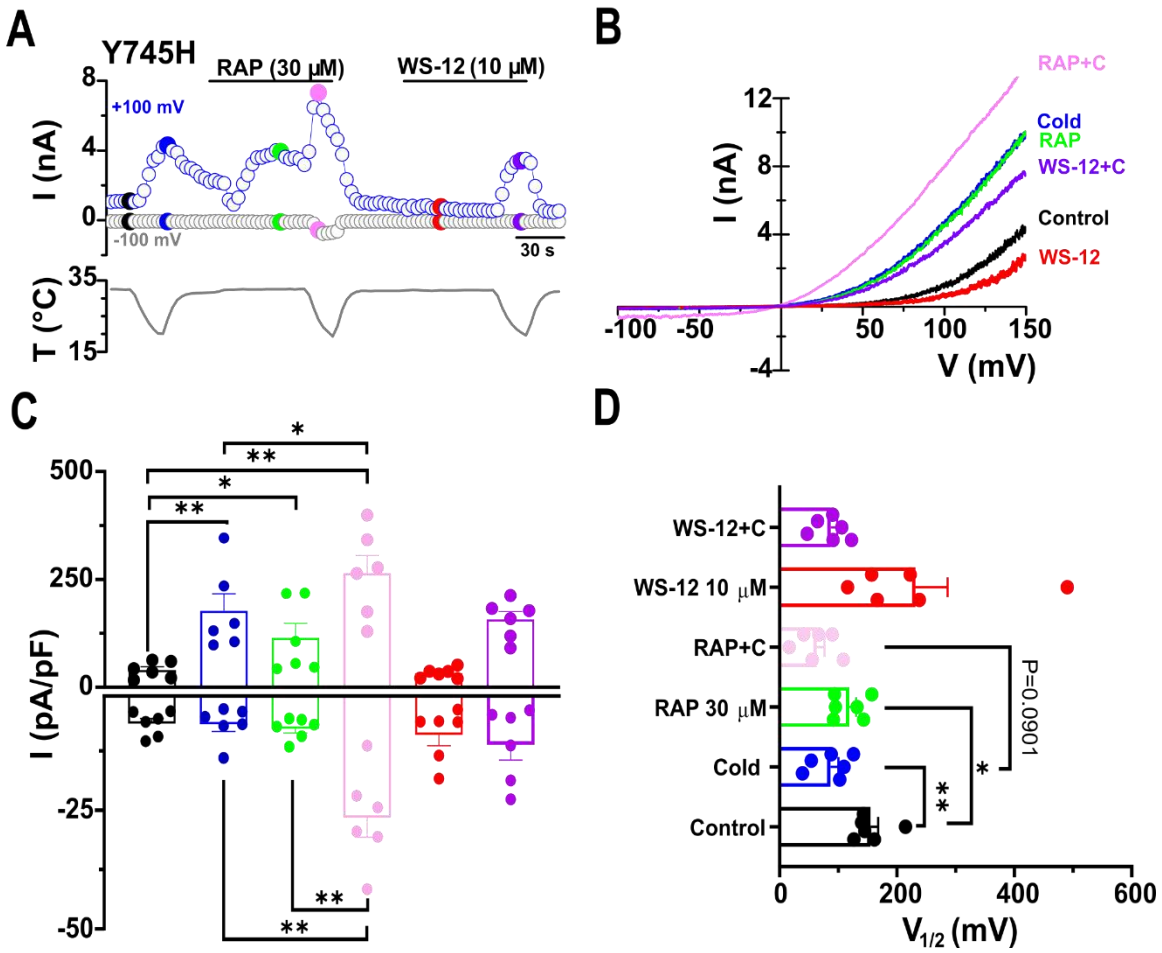

Figure 26. Rapamycin activated menthol-insensitive Y745H TRPM8 mutant whole-cell currents expressed in HEK293 cells and induced a leftward shift of the voltage dependence activation. **A,** Representative time course of Y745H TRPM8 mutant whole cell currents screened at -100 mV and +100 mV in transiently transfected HEK293 cells during sequential agonists application. The trace of simultaneous recording of the bath temperature during experiment is shown at the bottom. Note the insensitivity of the mutant to WS-12. **B,** The current-voltage relationship (I-V) of responses presented in A**,** obtained with 800 ms voltage ramp from -100 to +150mV. The key colors of single traces coincide with specific time points in A**.** Rapamycin elicited non-selective cationic currents with TRPM8-like features and potentiated cold evoked responses. **C,** Bar histogram summarizing the mean ± SEM current densities measured at +100 and -100 mV for the different stimuli presented in A, following the color code. Statistical differences were evaluated by one-way Anova followed by Bonferroni´s post-hoc test. ***D,*** Mean (n=6) values calculated from fitting the individual I-V curve to linear Boltzmann equation. Note rapamycin (RAP) provoked a significant leftward shift of $V_{1/2}$ likewise Cold, moreover, cold evoking $V_{1/2}$ shift significantly potentiated in the presence of RAP. Statistical differences were evaluated by one-way Anova followed by Bonferroni's post-hoc test.

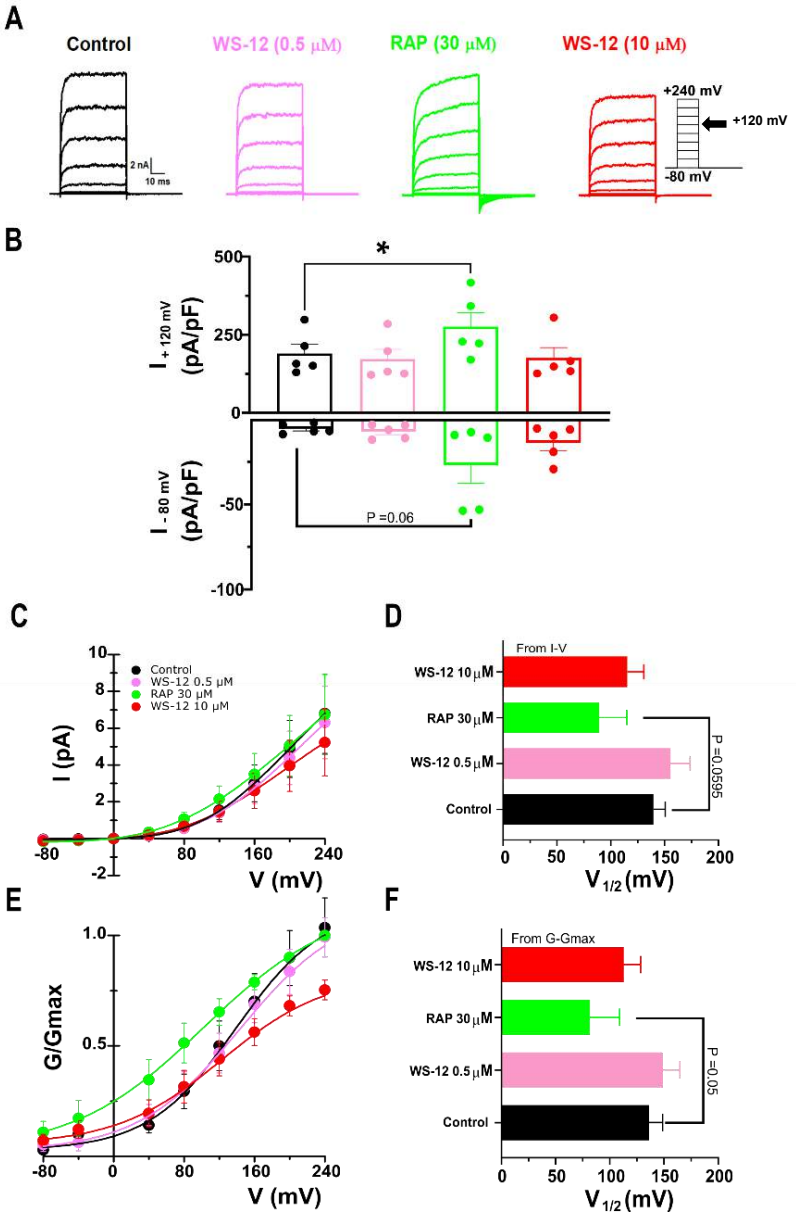

Figure 27. Biophysical characterization of rapamycin effects on menthol- and WS-12 insensitive Y745H TRPM8 mutant gating. A, Representative whole-Cell Y745H mutant TRPM8 currents in response to the voltage steps protocol applied (from -80 to +240 mV, ΔV= 40 mV see material and methods) in control conditions and in the presence of RAP (30 µM), WS-12 (0.5 and 10 µM) at 24 ˚C room temperature. **B,** Bar histogram summarizing the mean ± SEM current density at +120 and -80 mV of the different stimuli presented in A, following the color code. Statistical differences were evaluated by one-way Anova followed by Bonferroni´s post-hoc test. **C**, Average (n=5) steady-state I-V curves extracted from individual cells after application of protocol. The lines represent the fitting to linearized Boltzmann equation (see methods). **D,** Mean (n=5) $V_{1/2}$ value calculated from fitting the individual I-V curve to linearized Boltzmann equation. **E,** Average (n=5) voltage dependence activation curve in control condition and in the presence of different agonists, conductance was calculated as the steady state current divided by the driving force (Driving force = V_{Test}-E_{rev}) and normalized to the estimated maximal conductance (Gmax) which is the G value at +240 mV in the presence of 30 µM rapamycin. **F,** Mean (n=5) $V_{1/2}$ values calculated from fitting the individual G/Gmax-V curve Boltzmann equation. The statistical differences were analyzed by one way ANOVA, followed by Bonferroni's post-hoc test.

4.1.7.2 Rapamycin activation hypersensitivity following segment 4 (S4) mutations at I846 residue

The importance of the isoleucine residue at position 846 (I846) for menthol binding has been previously highlighted, with specific emphasis on the isopropyl group of menthol acting as a "leg" interacting strongly with the I846 residue, thus facilitating channel activation (L. Xu et al., 2020; X. Chen et al., 2022). In this series of experiments, I investigated the impact of various mutations at the I846 residue (I846A, I846T, I846V, and I846D) on the rapamycin sensitivity of the TRPM8 channel.

The initial mutation, I846A, involved substituting isoleucine with alanine. Although this substitution maintained the non-polar nature of the residue, it reduced the size of the lateral chain. Calcium imaging experiments were conducted in HEK293 cells expressing the I846A mutant. Interestingly, cells expressing the I846A mutant exhibited a higher fura2 ratio at rest (Blue trace, n=87) compared to non-transfected cells (Grey trace, n=165), suggesting a distinct phenotype compared to cells expressing the wild-type TRPM8 channel. This observation hinted at the possibility that the I846A mutant might be active at the resting temperature (~33 ºC) (Fig. 28A), a phenomenon explored further in this thesis.

Functionally, I observed that rapamycin (RAP) at 30 µM elicited stronger activation of the I846A mutant channel compared to cold. RAP also potentiated cold-evoked responses, with the potentiation markedly higher than that induced by WS-12 (10 µM) (Fig. 28B). Furthermore, RAP activated a larger percentage of cells expressing I846A compared to both WS-12 and cold (Cold= 66% vs RAP= 81% vs WS-12=66%) (p-value= 0.04, Chi-squared test) (Fig. 28D, G, I).

In comparison to the wild-type TRPM8, cells expressing the I846A mutant showed similar calcium amplitudes in response to cold. However, RAP at 30 µM elicited a significantly larger calcium amplitude response in the I846A mutant cells compared to the wild-type TRPM8 group (WT TRPM8 RAP= 0.22 ± 0.03, n=123 vs I846A RAP= 1 ± 0.2, n=87) (p-value< 0.0001) (Fig.43B). Cold-evoked responses potentiation in the presence of RAP was altered in the I846A group compared to the wild-type TRPM8 (WT TRPM8 RAP+cold = 2.1 ± 0.2 vs I846A RAP+cold= 1.2 ± 0.2, p-value< 0.01) (Fig. 43C). WS-12 (10 µM) activated calcium responses were strongly reduced in the I846A group compared to the wild-type TRPM8 (WT TRPM8 WS-12 = 1.2 ± 0.1 vs I846A WS-12= 0.8 ± 0.1) (p-value< 0.01) (Fig. 43D). Potentiation of cold-evoked responses in the presence of WS-12 was markedly diminished in the I846A group compared to the wild-type TRPM8 (WT TRPM8 WS-12+cold = 2 ± 0.2 vs I846A WS-12+cold= 0.9 ± 0.2, p-value< 0.0001) (Fig. 43E).

Subsequently, whole-cell patch-clamp recordings were performed using periodic voltage ramps (from -100 mV to +150 mV) (Fig.29A). Remarkably, HEK293 cells expressing I846A displayed a distinct basal current phenotype characterized by a higher outward current and less pronounced outward current rectification compared to wild-type mTRPM8 channels (Fig. 29A, B). Cold elicited robust currents both

at +100 mV (Control=173 ± 14 pA/pF vs Cold=283 ± 38 pA/pF) (n=6, p-value= 0.0283) and at -100 mV (Control =-20 ± 5 pA/pF vs Cold=-55 ± 5 pA/pF) (p-value=0.0008). Application of RAP (30 µM) also activated robust inward and outward currents. Average outward current measured at +100 mV was 173 ± 14 pA/pF in control and 318 ± 29 pA/pF after RAP application (n=6, p-value=0.0006), while inward current measured at -100 mV was 20 ± 5 pA/pF in control, and -60 ± 13 pA/pF in the presence of RAP (n=6, p-value=0.0059). Additionally, cold-evoked outward current (Cold=283 ± 38 pA/pF vs RAP+ cold= 317 ± 38 pA/pF) and inward current (Cold=-55 ± 5 pA/pF vs RAP+ cold= -77 ± 14 pA/pF) were not potentiated in the presence of RAP. WS-12 generated a strong outward current at +100 mV (Control=173± 14 pA/pF vs WS-12=275± 48 pA/pF) (p-value=0.0507) and markedly elicited inward current measured at -100 mV (Control=-20 ± 5 pA/pF vs WS-12=-76 ± 16 pA/pF) (n=6, p-value= 0.04). Moreover, WS-12 potentiated robust cold-evoked inward current (Cold=-55 ± 5 pA/pF vs WS-12+cold= -88 ± 11 pA/pF) (n=6, p-value= 0.0144), whereas it did not potentiate cold-evoked outward current (Fig. 29C).

Based on the current-voltage relationship (I-V), RAP activated the mutant channel I846A-TRPM8 by inducing a leftward shift of the voltage activation curve towards more negative potentials (Fig. 29B). This finding confirmed our calcium imaging results, validating the agonistic effect of RAP on mTRPM8. At the baseline temperature (33 ± 1˚C), following the fitting of voltage activation curves in both control or after agonists application to a Boltzmann equation. Cold induced a robust leftward shift of $V_{1/2}$ (Control $V_{1/2}$ = 91 ± 4 mV; Cold $V_{1/2}$ =33 ± 10 mV) (n=6, p-value = 0.0006) (Fig. 29D). The application of RAP (30 µM) also elicited a strong leftward shift of the $V_{1/2}$ towards negative potentials compared to control (Control $V_{1/2}$ = 91 ± 4 mV; RAP $V_{1/2}$ =69 ± 7 mV) (n=6, p-value = 0.0225) (Fig. 29D). WS-12 (10 µM) induced a similar shift like RAP but both were inferior to the shift generated by cold (Control $V_{1/2}$ = 91 ± 4 mV; WS-12 $V_{1/2}$ =67 ± 11 mV) (n=6, p-value = 0.0552) (Fig.29D). Neither RAP nor WS-12 potentiated cold-evoked $V_{1/2}$ shift (Cold $V_{1/2}$ = 33 ± 10 mV; RAP+ cold $V_{1/2}$ = 67 ± 12 mV, WS-12+ cold $V_{1/2}$ = 39 ± 8 mV) (Fig. 29D).

Compared to the wild-type TRPM8, in control condition, the I846A mutant channel showed larger mean outward current measured at +100 mV (WT TRPM8 Control = 28 ± 4 pA/pF vs I846A Control= 173 ± 14 pA/pF) (p-value< 0.0001), while the inward current measured at -100 mV was not significantly different (WT TRPM8 control = -12 ± 3 pA/pF vs I846A control= -20 ± 5 pA/pF) (Fig.44A). RAP (30 µM) application generated a higher outward current measured at +100 mV (WT TRM8 RAP = 114 ± 14 pA/pF, n=14 vs I846A RAP= 318 ± 29 pA/pF, n=6) (p-value< 0.01), and inward current, measuerd at -100 mV in the I846A group compared to wild-type mTRPM8 (WT TRPM8 RAP = -34 ± 8 pA/pF vs I846A RAP= -60 ± 13 pA/pF) (p-value=0.09) (Fig. 44C). Moreover, cold activated outward current in the I846A group at +100 mV was potentiated similarly to wild-type TRPM8 in the presence of RAP (WT TRPM8 RAP+cold = 360 ± 36 pA/pF vs I846A RAP+cold= 317 ± 38 pA/pF), whereas cold activated inward current potentiation in the presence of RAP at -100 mV was severely altered in the

I846A group compared to wild-type (WT TRPM8 RAP+cold = -160 ± 37 pA/pF, n=14 vs I846A RAP+cold= -77 ± 14 pA/pF, n=6) (Fig. 44D).

Next, I observed that I846A-expressing cells showed a shift in their cold-activation threshold towards warmer temperatures compared to wild-type channels (WT TRPM8 = 27.3 ± 0.3 ˚C, n=11 vs I846A=31 ± 1 ˚C, n=6) (p-value< 0.01) (Fig. 45A).

The I846A voltage dependence ($V_{1/2}$) was leftward shift compared to WT TRPM8 (WT TRPM8 control $V_{1/2}$=265 ± 40 mV, n=14 vs I846A control $V_{1/2}$=91 ± 4 mV, n=6) (p-value< 0.01) (Fig. 45B). In addition, either cold or RAP (30 µM) stimuli evoked a marked voltage dependence leftward shift of the $V_{1/2}$ in the I846A group towards more negative voltages compared to WT TRPM8 (WT TRPM8 Cold $V_{1/2}$=83 ± 8 mV, n=14 vs I846A Cold $V_{1/2}$=33 ± 10 mV, n=6; WT TRPM8 RAP $V_{1/2}$ =156 ± 23 mV, n=14 vs I846 RAP $V_{1/2}$=69 ± 7 mV, n=6) (p-value< 0.01) (Fig. 45C, E). Cold-evoked $V_{1/2}$ shift potentiation in the presence of RAP was similar in both I846A and WT TRPM8 groups (WT TRPM8 RAP+cold $V_{1/2}$=55 ± 9 mV, n=14 vs I846A RAP+cold $V_{1/2}$=67 ± 12 mV, n=6) (Fig. 45E). WS-12 elicited a leftward shift of $V_{1/2}$ in the I846A group was similar to WT TRPM8 (WT TRPM8 WS-12 $V_{1/2}$=95 ± 15 mV, n=14 vs I846A WS-12 $V_{1/2}$=67 ± 11 mV, n=6) (Fig. 45F). Moreover, cold-evoked $V_{1/2}$ shift potentiation in the presence of WS-12 was alike in both WT TRPM8 and I846A groups (WT TRPM8 WS-12+cold $V_{1/2}$=36 ± 11 mV, n=14 vs I846A WS-12+cold $V_{1/2}$=39 ± 8 mV, n=6) (Fig. 45G).

Altogether, these results indicate that the alanine mutation at I846 iduced: first a special phenotype with high calcium at rest, second a shift of the voltage dependence toward more negative potentials, and last, enhanced the senstitivity of the mutant channel to RAP.

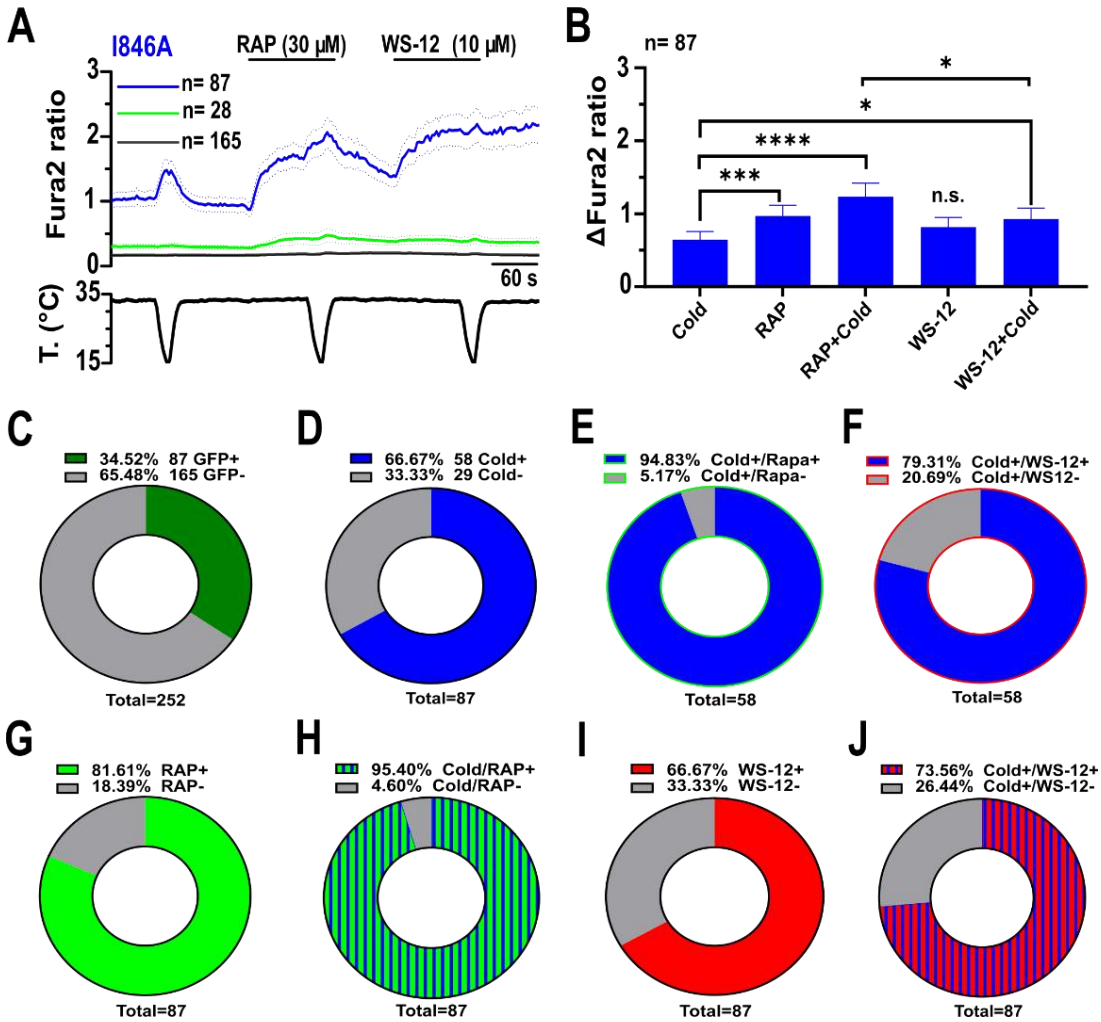

Figure 28. Rapamycin activated heterologously transfected mouse TRPM8 I846A mutant channel and potentiated cold evoked responses. A, Average ± SEM fura2 ratio response to cold, RAP (30 µM) and WS-12 (10 µM) in HEK293 cells transiently transfected with mouse TRPM8 I846A mutant and GFP. GFP (+) cold sensitive cells (n=87) are shown in blue (blue trace) and GFP (+) cold insensitive cells (n=28) are shown in green (green trace) while GFP (-) cells (n=165) are shown in grey. **B,** Bar histogram summarizing the responses of GFP+ HEK293 cells transfected with I846A mouse TRPM8 mutant to different agonists. Statistical significance was calculated by a one-way ANOVA followed by Bonferroni post-hoc test. **C,** Pie graph showing the percentage of GFP (+) transfected and GFP (-) non-transfected cells out of total cells (n=252). **D,** Pie graph showing the percentage of cold sensitive cells (Cold+) and cold insensitive cells (Cold-) out of the total GFP+ transfected cells (n=87). **E,** Pie graph showing the percentage of cold sensitive cells that are either rapamycin (30 µM) sensitive (Cold+ / RAP +) or rapamycin insensitive (Cold+ / RAP -) cells out of total cold responders (n=58). **F,** Pie graph showing the percentage of cold sensitive cells that are either WS-12 (10 µM) sensitive (Cold+ / WS-12 +) or WS -12 insensitive (Cold+ / WS-12 -) cells out of total cold responders (n=58). **G,** Pie graph showing the percentage of rapamycin sensitive cells (RAP+) and insensitive cells (RAP-) out of the total GFP+ transfected cells (n=201). **H,** Pie graph showing the percentage of cold evoking cells responses potentiation in the presence of rapamycin (Cold/RAP+) and the insensitive cells (Cold/RAP-) out of the total GFP+ transfected cells (n=87). **I,** Pie graph showing the percentage of WS-12 sensitive cells (WS-12+) and insensitive cells (WS-12-) out of the total GFP+ transfected cells (n=87). **J,** Pie graph showing the percentage of cold evoking cells responses potentiation in the presence of WS-12 (Cold/WS-12+) and the insensitive cells (Cold/WS-12-) out of the total GFP+ transfected cells (n=87).

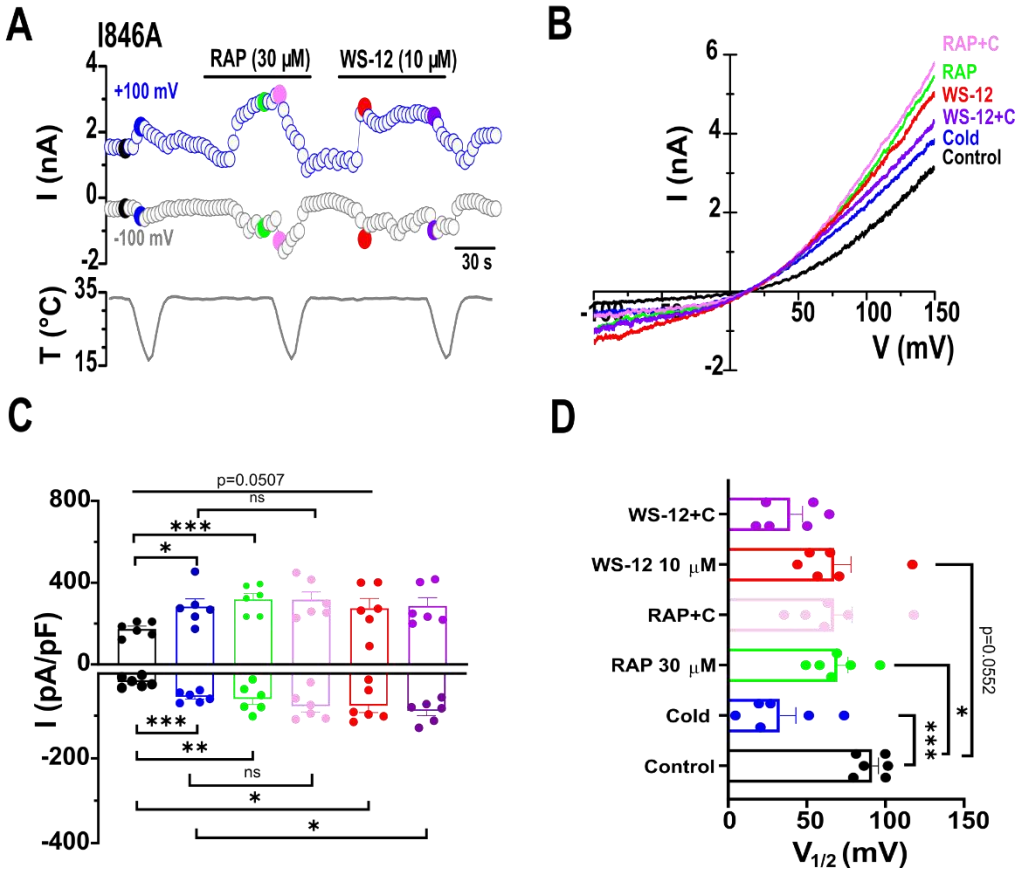

Figure 29. Rapamycin activated I846A TRPM8 mutant whole-cell currents expressed in HEK293 cells and induced a leftward shift of the mutant voltage dependence. **A,** Representative time course of I846A TRPM8 mutant whole cell currents extracted at -100 mV and +100 mV in transiently transfected HEK293 cells during sequential agonists application. The trace of simultaneous recording of the bath temperature during experiment is shown at the bottom. **B,** the current-voltage relationship (I-V) of responses presented in A**,** resulted after 800 ms voltage ramp from -100 to +150mV. The key colors of single traces coincided with specific time points in A**.** Rapamycin elicited a non-selective cationic currents TRPM8 dependent features and potentiates cold evoked responses. **C,** Bar histogram summarizing the mean ± SEM currents densities at +100 mV (outward current) and -100 mV (inward current) of different stimuli presented in A, following the color code. Statistical differences were evaluated by one-way Anova followed by Bonferroni´s post-hoc test. ***D,*** mean (n=6) voltage dependence $V_{1/2}$ values calculated from fitting the individual I-V curve to linear Boltzmann equation. Note rapamycin provoked a significative leftward shift of $V_{1/2}$, statistical differences were evaluated by one-way Anova followed by Bonferroni's post-hoc test.

The notable increase in response to RAP observed in the I846A mutant prompted an exploration of additional mutations within the same segment 4 residue to ascertain the potential role of isoleucine (I846) in rapamycin sensitivity. Consequently, we introduced Threonine (T), a polar uncharged amino acid with a longer side chain than alanine (A) but smaller compared to the isoleucine (I) side chain.

In vitro calcium imaging experiments conducted in HEK293 cells expressing the I846T mutant (GFP+) revealed, consistent with the distinct phenotype observed in I846A-expressing cells, a higher resting calcium level (Blue trace, n=60) compared with GFP- cells (Grey trace, n=95) (Fig. 30A). The application of RAP (30 µM) evoked a calcium response amplitude similar to cold but markedly higher than WS-12 (Fig. 30A, B). Cold-evoked activation was potentiated in the presence of RAP, with the potentiation of cold-evoked response in the presence of RAP being higher than in the presence of WS-12 (Fig. 30B). Regarding the percentage of cell activation, RAP activated a significant proportion of GFP+ cells compared to both cold and WS-12 (Cold=51% vs RAP=76% vs WS-12=61%) (p-value= 0.016, Chi-squared test) (Fig. 30D, G, and I). Cold-activated cell percentage potentiation in the presence of RAP was higher than in the presence of WS-12 (RAP+cold=91% vs WS-12+cold=65%) (p-value= 0.0004, Chi-squared test) (Fig. 30 H and J).

Compared to the wild-type TRPM8, the I846T mutant group exhibited a similar response to cold (WT TRPM8 Cold= 0.5 ± 0.1 vs I846A Cold= 0.6 ± 0.2) (Fig. 43A). However, the application of RAP (30 µM) elicited a response of larger amplitude in the I846T mutant compared to the wild-type TRPM8 group (WT TRPM8 RAP= 0.22 ± 0.03, n=123 vs I846T RAP= 0.6 ± 0.1, n=60) (p-value< 0.0001) (Fig. 43B). Additionally, cold-evoked responses potentiation in the presence of RAP was severely altered in the I846T group compared to the wild type (WT TRPM8 RAP+cold = 2.1 ± 0.2, n=123 vs I846T RAP+cold= 0.9 ± 0.2, n=60) (p-value< 0.01) (Fig. 43C). Moreover, the menthol derivative WS-12's activation of I846T cells was also drastically altered compared to the wild-type TRPM8 group (WT TRPM8 WS-12 = 1.2 ± 0.1, n=123 vs I846T WS-12 = 0.4 ± 0.1, n=60) (p-value< 0.001) (Fig. 43D). Cold-evoked response potentiation in the presence of WS-12 was markedly diminished in the I846T group compared to the wild type (WT TRPM8 WS-12+cold = 2 ± 0.2, n=123 vs I846T WS-12+cold = 0.5 ± 0.1, n=60) (p-value< 0.001) (Fig. 43E).

Next, using the periodic voltage ramp protocol (see Materials and Methods) (Fig. 31A), similarly to the results obtained with the I846A mutant, at rest (33 ºC), the cells expressing I846T mutants exhibited large outward currents measured at +100 mV (WT TRPM8 Control = 28 ± 4 pA/pF vs I846T Control= 263 ± 84 pA/pF) (p-value< 0.0001). Conversely, the inward current activation measured at -100 mV was similar (WT TRPM8 Control = -12 ± 3 pA/pF vs I846T Control= -13 ± 6 pA/pF) (Fig. 44A) compared to the wild-type TRPM8. Additionally, the baseline voltage activation curve was shifted to more negative potentials (Fig. 31A and B) compared to the WT TRPM8 phenotype (Fig. 20A and B). These results, together with the calcium imaging data, showing a high fura2 ratio at rest in cells

transfected with I846T, strongly suggest a constitutively active phenotype following S4 I846 residue mutations.

Concerning the activation phenotype of I846T HEK293 cells, cooling elicited both outward and inward currents, measured respectively at +100 mV (Control=263 ± 84 pA/pF vs Cold=323 ± 125 pA/pF) (n=5, p-value=0.4424) and -100 mV (Control=-13 ± 6 pA/pF vs Cold=-37 ± 9 pA/pF) (n=5, p-value=0.0101). The application of RAP (30 µM) robustly activated both outward current measured at +100 mV (Control=263 ± 84 pA/pF vs RAP=484 ± 126 pA/pF) (n=5, p-value=0.08) and inward current measured at -100 mV (Control=-13 ± 6 pA/pF vs RAP=-31 ± 9 pA/pF) (n=5, p-value= 0.0272) (Fig. 31C). Furthermore, cold-evoked outward current measured at +100 mV (Cold=323 ± 125 mV vs RAP+cold= 551 ± 158 pA/pF) (n=5, ns, p-value= 0.2087) and inward current measured at -100 mV (Cold=-37 ± 9 pA/pF vs RAP+cold = -65 ± 14 pA/pF) (n=5, p-value= 0.013) were both robustly potentiated in the presence of RAP (Fig. 31C). WS-12 (10 µM) activated both the I846T channel's outward current at +100 mV (Control= 263 ± 84 pA/pF vs WS-12= 516 ± 130 pA/pF) (n=5, p-value= 0.0341) and inward current at -100 mV (Control= -13 ± 6 pA/pF vs WS-12= -162 ± 54 pA/pF) (n=5, p-value= 0.0576) (Fig. 31C). The cold-evoked inward current was robustly potentiated in the presence of WS-12 (Cold=-37 ± 9 pA/pF vs WS-12+cold= -145 ± 37 pA/pF) (n=5, p-value= 0.0612) (Fig. 31C).

Moreover, regarding the voltage dependence ($V_{1/2}$) measured at basal temperature (33±1˚C), either cold (Control $V_{1/2}$ = 101 ± 10 mV Cold $V_{1/2}$ = 37 ± 14 mV) (n=5, p-value= 0.0107) or RAP (30 µM) stimuli elicited a robust leftward shift of $V_{1/2}$ compared to control (Control $V_{1/2}$ = 101 ± 10 mV vs RAP $V_{1/2}$ = 66 ± 4 mV) (n=5, p-value= 0.0225). Interestingly, the cold-evoked voltage dependence ($V_{1/2}$) shift was not potentiated by neither RAP nor WS-12 (Fig. 31D).

Compared to wild type TRPM8, RAP (30 µM) application provoked a significantly larger outward current measured at +100 mV (WT TRPM8 RAP = 114 ± 14 pA/pF, n=14 vs I846T RAP= 484 ± 126 pA/pF, n=5) (p-value< 0.0001), while the inward current generated at -100 mV was similar (WT TRPM8 RAP = -34 ± 8 pA/pF vs I846T RAP= -31 ± 9 pA/pF) in the I846T group (Fig.44C). Moreover, cold-activated outward current at +100 mV potentiation in the presence of RAP was higher in the I846T group compared to the WT TRPM8 group (WT TRPM8 RAP+ cold = 360 ± 36 pA/pF vs I846T RAP+cold= 551 ± 158 pA/pF), whereas the cold-activated inward current potentiation in the presence of RAP at -100 mV was markedly altered in the mutant I846T group compared to the wild type (WT TRPM8 RAP+ cold = -160 ± 37 pA/pF, n=14 vs I846T RAP+cold= -65 ± 14 pA/pF, n=5) (Fig. 44D).

The HEK293 cells expressing the I846T mutant exhibited a shift in their temperature threshold towards warmer temperatures compared to WT TRPM8 (WT TRPM8 = 27.3 ± 0.3 ˚C, n=11 vs I846T=29 ± 0.6 ˚C, n=5) (Fig. 45A).

At basal temperature, I846T group showed a strong leftward shift of $V_{1/2}$ towards negative potentials compared to WT TRPM8 (WT TRPM8 Control $V_{1/2}$ =265 ± 40 mV, n=14 vs I846T Control $V_{1/2}$ =101

± 10 mV, n=5) (p-value< 0.01) (Fig. 45B). Cooling robustly shifted the $V_{1/2}$ towards more negative potentials in I846T compared to wild-type TRPM8 (WT TRPM8 Cold $V_{1/2}$ = 83 ± 8 mV, n=14 vs I846T Cold $V_{1/2}$ = 37 ± 14 mV, n=5) (p-value= 0.09) (Fig. 45D). RAP (30 µM) evoked a marked leftward shift of $V_{1/2}$ in the I846T group towards negative potentials compared to WT TRPM8 (WT TRPM8 RAP $V_{1/2}$ =156 ± 23 mV, n=14 vs I846T RAP $V_{1/2}$ =66 ± 4 mV, n=5) (p-value< 0.05) (Fig. 45D). The Cold-evoked $V_{1/2}$ shift potentiation in the presence of RAP was similar between I846T and WT TRPM8 groups (WT TRPM8 RAP+cold $V_{1/2}$=55 ± 9 mV, n=14 vs I846T RAP+cold $V_{1/2}$ =39 ± 8 mV, n=5) (Fig. 45E). The application of WS-12 elicited a robust leftward shift of voltage dependence in the I846T group compared to WT TRPM8 (WT TRPM8 WS-12 $V_{1/2}$ =95 ± 15 mV, n=14 vs I846T WS-12 $V_{1/2}$ =57 ± 4 mV, n=5) (Fig. 45F). In contrast, cold-evoked $V_{1/2}$ leftward shift potentiation in the presence of WS-12 was diminished in I846T compared to WT TRPM8 groups (WT TRPM8 WS-12+Cold $V_{1/2}$ =36 ± 11 mV, n=14 vs I846T WS-12+Cold $V_{1/2}$ =51 ± 8 mV, n=5) (Fig. 45G).

Following the standard voltage steps protocol (see materials and methods) used on HEK293 cells expressing I846T (Fig. 32A), RAP (30 µM) potentiated voltage-activated outward and inward currents measured respectively at +120 mV (I846T Control= 228 ± 58 pA/pF vs I846T RAP = 350 ± 58 pA/pF, n=5) (p-value= 0.0154), and at -80 mV (I846T Control= -10 ± 3 pA/pF vs I846T RAP = -34 ± 11 pA/pF, n=5) (ns, p-value= 0.1229) (Fig. 32B). Moreover, the analysis of current-voltage (I-V) and conductance-voltage (G/Gmax-V) relationships revealed a leftward shift of the voltage activation curve in the presence of RAP (Fig. 32C, E), which was accompanied by a leftward shift in voltage of half maximal activation ($V_{1/2}$) from the control value $V_{1/2}$ =154 ± 42 mV to $V_{1/2}$ = 104 ± 6 mV in the presence of 30 µM RAP (calculated from I-V, n=5), similar results were calculated from G/Gmax-V. (Fig. 32D, F). Besides, the analysis of actual mutant gating kinetics showed a slowing of either activation or deactivation kinetics in the presence of RAP resmbling wild type channel behaviour (Fig.67 see annex).

In summary, our results indicate that the threonine mutation at I846 iduced : similar phenotype to I846A showing a high intracelluar calcium at rest, second a shift of the voltage dependence toward more negative potentials, and last, enhanced channel senstitivity to RAP.

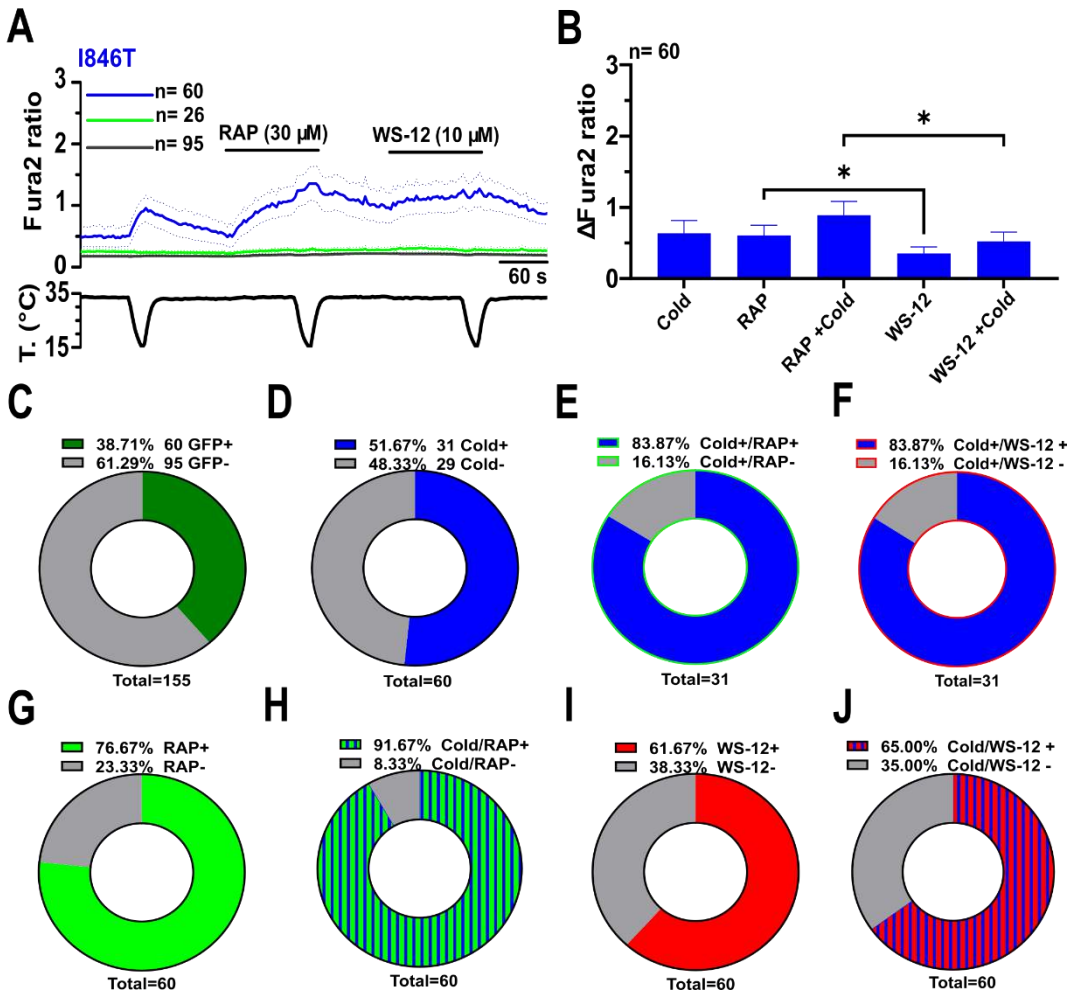

Figure 30. Rapamycin activated heterologously transfected mouse TRPM8 mutant I846T channel. A, Average ± SEM fura2 ratio response to cold, RAP (30 µM) and WS-12 (10 µM) in HEK293 cells transiently transfected with I846T TRPM8 mutant and GFP. GFP (+) cold sensitive cells (n=60) are shown in blue (blue trace) and GFP (+) cold insensitive cells (n=26) are shown in green (green trace) while GFP (-) cells (n=95) are shown in grey. **B,** Bar histogram summarizing the responses of GFP+ HEK293 cells transfected with mouse I846T TRPM8 mutant to different agonists. Statistical significance was calculated by a one-way ANOVA followed by Bonferroni post-hoc test. **C,** Pie graph showing the percentage of GFP (+) transfected and GFP (-) non-transfected cells out of total cells (n=155). **D,** Pie graph showing the percentage of cold sensitive cells (Cold+) and cold insensitive cells (Cold-) out of the total GFP+ transfected cells (n=60). **E,** Pie graph showing the percentage of cold sensitive cells that are either rapamycin (30 µM) sensitive (Cold+ / RAP +) or rapamycin insensitive (Cold+ / RAP -) cells out of total cold responders (n=31). **F,** Pie graph showing the percentage of cold sensitive cells that are either WS-12 (10 µM) sensitive (Cold+ / WS-12 +) or WS -12 insensitive (Cold+ / WS-12 -) out of total cold responders (n=31). **G,** Pie graph showing the percentage of rapamycin sensitive cells (RAP+) and insensitive cells (RAP-) out of the total GFP+ transfected cells (n=60). **H,** Pie graph showing the percentage of cold evoking cell responses in the presence of rapamycin (Cold/RAP+), and the insensitive cells (Cold/RAP-) out of the total GFP+ transfected cells (n=150). **I,** Pie graph showing the percentage of WS-12 sensitive cells (WS-12+) and insensitive cells (WS-12-) out of the total GFP+ transfected cells (n=60). **J,** Pie graph showing the percentage of cold evoking cell responses potentiation in the presence of WS-12 (Cold/WS-12+), and insensitive cells (Cold/WS-12-) out of the total GFP+ transfected cells (n=60).

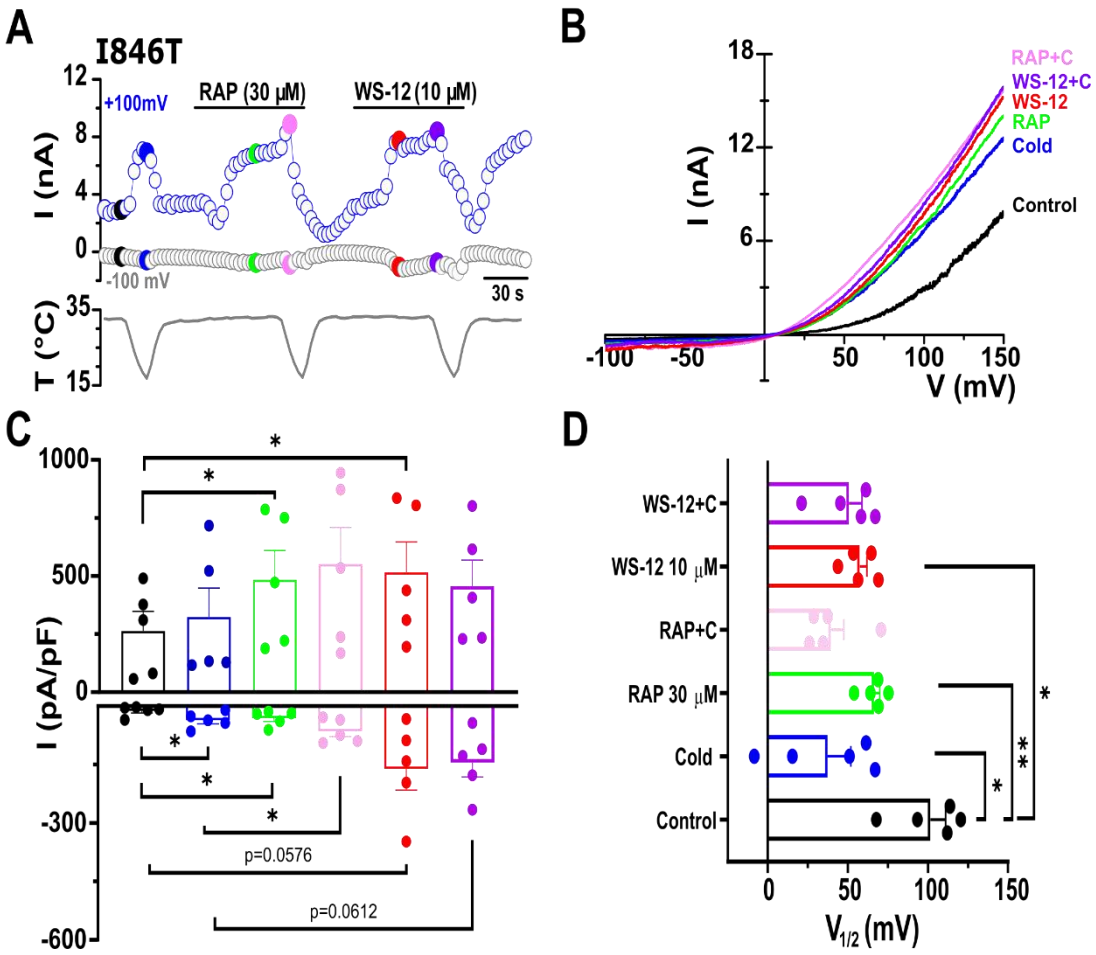

Figure 31. Rapamycin activated I846T TRPM8 mutant whole-cell currents expressed in HEK293 cells and induced a leftward shift of its voltage dependence. **A,** Representative time course of I846T TRPM8 mutant whole cell currents screened at -100 mV and +100 mV in transiently transfected HEK293 cells during sequential agonists application. The trace of simultaneous recording of the bath temperature during experiment is shown at the bottom. **B,** the current-voltage relationship (I-V) of responses presented in A**,** resulted with 800 ms voltage ramp from -100 to +150mV. The key colors of single traces coincide with specific time points in A**.** Rapamycin elicited a non-selective cationic currents TRPM8 dependent features and potentiates cold evoked responses. **C,** Bar histogram summarizing the mean ± SEM currents densities at +100 and -100 mV of the different stimuli presented in A, following the color code. Statistical differences were evaluated by one-way Anova followed by Bonferroni´s post-hoc test. **D,** mean (n=5) $V_{1/2}$ values calculated from fitting the individual I-V curve to linear Boltzmann equation. Note rapamycin provoke a significative leftward shift of $V_{1/2}$, statistical differences were evaluated by one-way Anova followed by Bonferroni's post-hoc test.

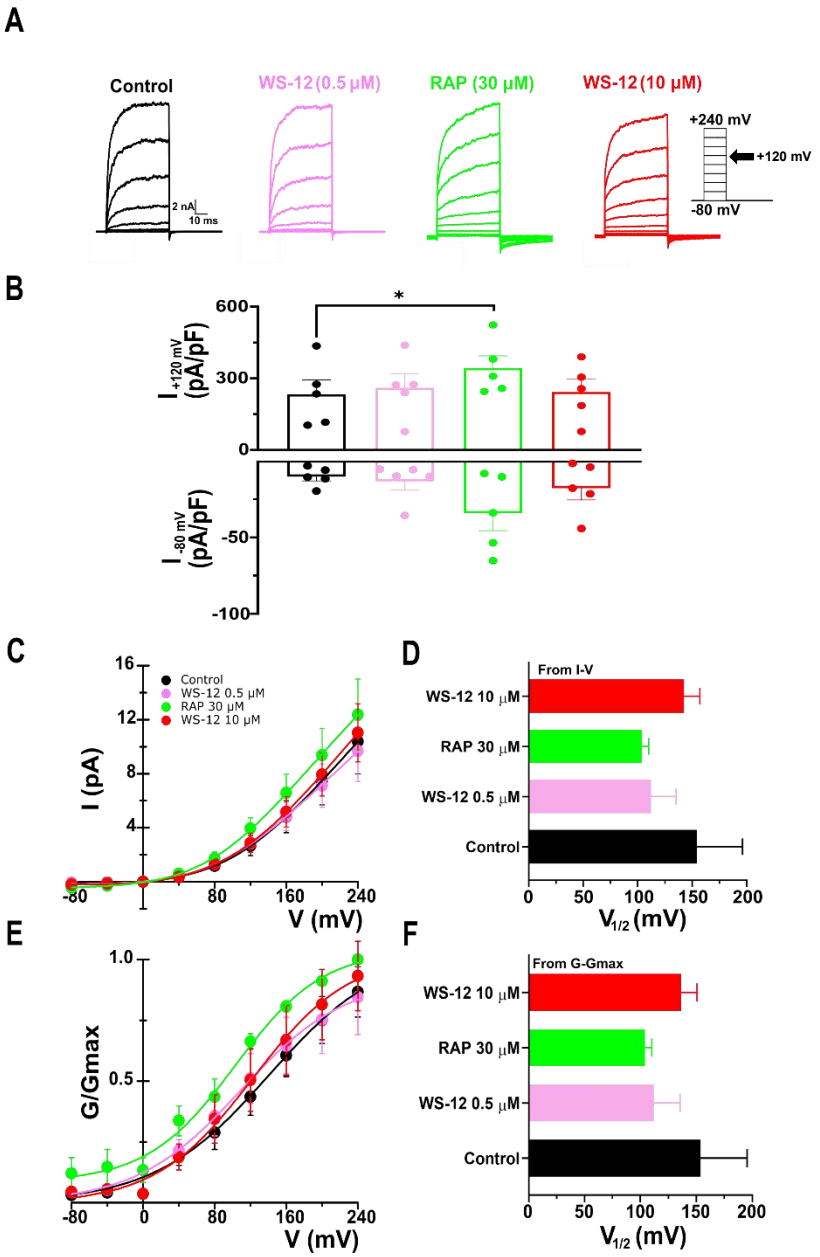

Figure 32. Biophysical characterization of Rapamycin effects on I846T TRPM8 mutant gating. A, Representative whole cell of I846T mutant TRPM8 currents in response to the given voltage steps protocol (from -80 to +240 mV during 50 ms, ΔV= 40 mV see material and methods) in control conditions and in the presence of RAP (30 µM), WS-12 (0.5 and 10 µM) at 24 ˚C room temperature. **B,** Bar histogram summarizing the mean ± SEM currents densities at +120 and -80 mV of the different stimuli presented in A, following the color code. Statistical differences were evaluated by one-way Anova followed by Bonferroni´s post-hoc test. **C**, Average (n=5) steady-state I-V curves extracted from individual cells after application of protocol the lines represent the fitting to linearized Boltzmann equation (see methods). **D,** Mean (n=5) $V_{1/2}$ value calculated from fitting the individual I-V curve to linearized Boltzmann equation. **E,** Average (n=5) voltage dependence activation curve in control condition and in the presence of different agonists, conductance was calculated as the steady state current divided by the driving force (Driving force = V_{Test}-E_{rev}) and normalized to the estimated maximal conductance (Gmax) which is the G value at +240 mV in the presence of 30 µM Rapamycin. **F,** Mean (n=5) $V_{1/2}$ value calculated from fitting the individual G/Gmax-V curve Boltzmann equation. The statistical differences were analyzed by one way ANOVA, followed by Bonferroni's post-hoc test.

In our exploration into the role of I846 residue in gating, we introduced an additional mutation: the substitution of isoleucine with valine (V). Valine, a nonpolar amino acid, possesses a larger side chain than alanine (A) but is smaller than isoleucine (I).

In the *in vitro* calcium imaging experiment conducted with HEK293 cells expressing the I846V mutant (Blue trace, n=81), a distinct pattern emerged compared to the previously characterized I846 residue mutants (I846A and I846T). This mutant displayed a less pronounced elevation in the fura-2 ratio at rest, in contrast to GFP- cells (Grey trace, n=350) (Fig. 33A). This result underscores once again the crucial role of the segment 4 residue isoleucine I846 in maintaining channel closure at 33 ºC.

Upon RAP (30 µM) application, I846V mutant cells exhibited larger responses than those induced by either cold or WS-12 (30 µM) stimuli (Fig. 33A, B). Additionally, the activation in response to cold was significantly potentiated in the presence of RAP, surpassing the potentiation observed in the presence of WS-12 (Fig. 33B). The percentage of GFP+ cells activated by RAP was higher compared to WS-12 (RAP=97% vs WS-12=80%) (p-value=0.0007, Chi-squared test) (Fig. 33G, I). Similarly, the percentage of cold-activated cells potentiation in the presence of RAP was larger than in the presence of WS-12 (RAP+cold=98% vs WS-12+cold=91%) (p-value=0.06, Chi-squared test) (Fig. 33H, J).

Compared to wild-type TRPM8, cells expressing the I846V mutant in segment 4 exhibited an enhanced response to cold (WT TRPM8 Cold=0.5 ± 0.1 vs I846V Cold=1.5 ± 0.2) (p-value<0.0001) (Fig. 43A). Furthermore, RAP (30 µM) elicited a markedly higher activation in HEK293 cells expressing the I846V mutant channel compared to the wild type (WT TRPM8 RAP=0.22 ± 0.03, n=123 vs I846V RAP=2.3 ± 0.2, n=81) (p-value<0.0001) (Fig. 43B). The potentiation of cold-evoked responses by RAP was more pronounced in the I846T mutant group compared to the wild type (WT TRPM8 RAP+cold=2.1 ± 0.2, n=123 vs I846T RAP+cold=2.7 ± 0.2, n=81) (p-value<0.01) (Fig. 43C). Subsequent calcium responses to WS-12 were similar in both wild-type and I846V groups (WT TRPM8 WS-12=1.2 ± 0.1, n=123 vs I846V WS-12=1.3 ± 0.2, n=81) (Fig. 43D). Similarly, the potentiation of cold-evoked responses by WS-12 was comparable in both groups (WT TRPM8 WS-12+cold=2 ± 0.2, n=123 vs I846T WS-12+cold=2.1± 0.2, n=81) (Fig. 43E).

Next, we characterized the I846V mutant electrophysiologically, using voltage ramps. In HEK293 cells expressing the I846V mutant (Fig. 34A), I found that, akin to previously described I846 mutants, the I846V mutant channel exhibited a higher outward current at +100 mV (WT TRPM8 Control = 28± 4 pA/pF vs I846V Control= 118 ± 26 pA/pF) (p-value< 0.05) (Fig. 44A). However, the basal inward currents at -100 mV were not significantly different between the I846V mutant and wild-type groups (WT TRPM8 Control = -12 ± 3 pA/pF vs I846V Control= -13 ± 7 pA/pF) (Fig. 36A).

In I846V-expressing cells, cooling induced robust outward currents: at +100 mV (Control=118 ± 26 pA/pF vs Cold=369 ± 87 pA/pF) (n=5, p-value=0.0234) (Fig. 34C) and non-significantly increased inward current at -100 mV (Control=-13 ± 7 pA/pF vs Cold=-34 ± 10 pA/pF) (n=5, ns, p-value=0.2455)

(Fig. 34C). RAP (30 µM) activated a pronounced outward current at +100 mV (Control=118 ± 26 pA/pF vs RAP=349 ± 58 pA/pF) (n=5, p-value=0.004) and elicited a markedly higher inward current at -100 mV (Control=-13 ± 7 pA/pF vs RAP=-75 ± 5 pA/pF) (n=5, p-value=0.0022) (Fig. 34C). Cold-evoked outward current at +100 mV (Cold=369 ± 87 pA/pF vs RAP+cold = 300 ± 38 pA/pF) (n=5, ns, p-value=0.4034) (Fig. 34C) was not potentiated by RAP. In contrast, in line with the calcium-imaging data, the inward current at -100 mV was robustly potentiated by RAP (Cold=-34 ± 10 mV vs RAP+cold= -81 ± 3 pA/pF) (n=5, p-value=0.0196) (Fig. 34C). Moreover, WS-12 (10 µM) activated a strong outward current at +100 mV, but exhibited an altered inward current at -100 mV in the I846V group compared to the wild type (Fig. 34C). Furthermore, WS-12 did not potentiate cold-evoked outward current (Cold=369 ± 87 pA/pF vs WS-12+cold = 386 ± 42 pA/pF) (n=5, ns, p-value=0.1211), but significantly potentiated cold-evoked inward current at -100 mV (Cold=-34 ± 10 pA/pF vs WS-12+cold= -110 ± 17 pA/pF) (n=5, p-value=0.0327) (Fig. 34C).

In comparison to the wild-type TRPM8 group, RAP (30 µM) application elicited a markedly higher both outward current, measured at +100 mV (WT TRPM8 RAP = 114 ± 14 pA/pF, n=14 vs I846V RAP= 349 ± 58 pA/pF, n=5) (p-value< 0.001) and inward current, measured at -100 mV (WT TRPM8 RAP = -34.4 ± 7.9 pA/pF vs I846V RAP= -74.8 ± 5.1 pA/pF) (p-value< 0.01) in I846V cells (Fig. 44C). Moreover, cold-activated outward current potentiation at +100 mV in the presence of RAP in I846V-transfected cells was slightly reduced compared to the WT TRPM8 group (WT TRPM8 RAP+ cold = 360 ± 36 pA/pF vs I846V RAP+cold= 300 ± 38 pA/pF) (Fig. 44D), while cold-activated inward current potentiation in the presence of RAP was markedly diminished in I846V compared to the wild type (WT TRPM8 RAP+ cold = -160 ± 37 pA/pF, n=14 vs I846V RAP+cold= -81 ± 3 pA/pF, n=5) (Fig. 44D). WS-12 elicited a strong outward current at +100 mV but showed an altered inward current at -100 mV in the I846V group compared to the wild type (Fig. 44E). Furthermore, WS-12 potentiated cold-evoked outward current at +100 mV was similar in both groups, in contrast, inward current potentiation in the presence of WS-12 at -100 mV was altered in the I846V group compared to the wild type (WT TRPM8 WS-12+ cold = -263 ± 42 pA/pF, n=14 vs I846V WS-12+cold= -110 ± 17 pA/pF, n=5) (Fig. 44F).

In the current-voltage relationship (I-V), RAP activation of the mutant channel I846V-TRPM8 preserved the typical WT TRPM8 characteristics, showing a leftward shift of the voltage activation curve towards more negative potentials and a reversal potential around 0 mV (Fig. 34B). Upon cooling, the $V_{1/2}$ was robustly shifted towards more negative potentials (Control $V_{1/2}$ = 124 ± 8 mV; Cold $V_{1/2}$ = 31 ± 24 mV) (n=5, p-value=0.0054) (Fig. 34D). At baseline temperature (33±1˚C), RAP (30 µM) shifted markedly $V_{1/2}$ towards negative potentials (Control $V_{1/2}$ = 124 ± 8 mV; RAP $V_{1/2}$ = 62 ± 12 mV) (n=5, p-value=0.0003) (Fig. 34D). In contrast to results observed in wild-type channels, RAP did not potentiate the shift of $V_{1/2}$ produced by cold (Cold $V_{1/2}$ = 31 ± 24 mV; RAP+cold $V_{1/2}$ = 63 ± 8 mV) (Fig. 34D). WS-12 also elicited a robust $V_{1/2}$ shift (Control $V_{1/2}$ = 124 ± 8 mV; WS-12 $V_{1/2}$ = 63 ± 10

mV) (n=5, p-value=0.0052) (Fig. 34D), whereas it did not potentiate cold-evoked $V_{1/2}$ shift (Cold $V_{1/2}$ = 31 ± 24 mV; WS-12+Cold $V_{1/2}$ = 24 ± 11 mV) (n=5, ns, p-value=0.7081) (Fig. 34D).

Upon analyzing the current time course recordings from I846V-expressing HEK293 cells (Fig. 34A), a noticeable shift in the temperature threshold towards warmer temperatures was observed compared to WT TRPM8 (WT TRPM8 = 27.3 ± 0.3 ˚C, n=11 vs I846T=31 ± 0.9 ˚C, n=5) (Fig. 45A).

The voltage dependence ($V_{1/2}$) of I846V was robustly leftward shifted compared to WT TRPM8 (WT TRPM8 Control $V_{1/2}$=265 ± 40 mV, n=14 vs I846V Control $V_{1/2}$ =124 ± 8 mV, n=5) (p-value< 0.05) (Fig. 45B). RAP (30 µM) evoked a higher voltage dependence $V_{1/2}$ leftward shift in the I846V group compared to WT TRPM8 (WT TRPM8 RAP $V_{1/2}$=156 ± 23 mV, n=14 vs I846V RAP $V_{1/2}$=62 ± 12 mV, n=5) (p-value< 0.05) (Fig. 45D). Cold-evoked $V_{1/2}$ shift potentiation in the presence of RAP was similar in both I846V and WT TRPM8 groups (WT TRPM8 RAP+cold $V_{1/2}$=55 ± 9 mV, n=14 vs I846V RAP+cold $V_{1/2}$=63 ± 8 mV, n=5) (Fig. 45E). WS-12 elicited a larger leftward shift of $V_{1/2}$ towards more negative potentials in I846V cells compared to WT TRPM8 (WT TRPM8 WS-12 $V_{1/2}$=95 ± 15 mV, n=14 vs I846V WS-12 $V_{1/2}$=63 ± 8 mV, n=5) (Fig. 37F), whereas cold-evoked voltage $V_{1/2}$ leftward shift potentiation in the presence of WS-12 was diminished in the I846V cell group compared to the WT TRPM8 group (WT TRPM8 WS-12+cold $V_{1/2}$=36 ± 11 mV, n=14 vs I846V WS-12+cold $V_{1/2}$=24 ± 11 mV, n=5) (Fig. 45G).

In summary, these results indicate that, in contrast to the previous mutants I846T and I846A, the valine induced less pronounced high basal calcium level. Furthermore, in line the previous reults valin mutation at residue I846 enhanced both rapamycin and cold sensitivity.

Subsequently, the voltage steps protocol (see materials and methods) was used at room temperature (23 ±1˚C) (Fig. 35A). The application of RAP (30 µM) robustly potentiated voltage-activated outward currents measured at +120 mV (I846V Control= 176 ± 45 pA/pF vs I846V RAP = 307 ± 58 pA/pF) (n=4, p-value=0.0092) and also induced inward current at -80 mV (I846V Control= -3 ± 0.8 pA/pF vs I846V RAP = -25 ± 12 pA/pF, n=4) (n=4, ns, p-value=0.1988) (Fig. 35B). WS-12, at both low (0.5 µM) (I846V Control= 176 ± 45 pA/pF vs I846V WS-12 (0.5 µM) = 386 ± 98 pA/pF) (n=4, p-value=0.034) and high (10 µM) concentrations (I846V Control= 176 ± 45 pA/pF vs I846V WS-12 (10 µM)= 355 ± 57 pA/pF) (n=4, p-value=0.0047), activated markedly outward current measured at +120 mV in HEK293 expressing I846V, whereas only WS-12 (10 µM) potentiated the voltage-evoked inward current at -80 mV (I846V Control= -3 ± 0.8 pA/pF vs I846V WS-12 (10 µM) = -45 ± 8 pA/pF, n=4) (n=4, ns, p-value=0.019) (Fig. 35B). Moreover, the analysis of both current-voltage (I-V) and conductance-voltage (G/Gmax-V) relationships revealed a leftward shift of the voltage activation curve in the presence of RAP (Fig. 35C, E) : $V_{1/2}$=153 ± 4 mV in control vs 123 ± 8 mV in the presence of 30 µM RAP (calculated from I-V, n=4, p-value=0.0452). Similar results were calculated from G/Gmax-V (Control $V_{1/2}$=152 ± 4 mV to $V_{1/2}$=113 ± 6 mV in the presence of RAP 30 µM, (n=4, p-value=0.0284)

(Fig. 35D, F). In addition, WS-12 also robustly shifted the voltage of half maximal activation ($V_{1/2}$) towards negative voltages (Fig. 35D, F). The effect of RAP on the gating kinetcs was similar to wild type behaviour showing a slowing of both activation and deactivation kinetics (see annex Fig.68).

In summary, our results indicate that the valin mutation at I846 iduced : on the contrary In contrast to phenotypes seen in I846A and I846T, the I846V did not show a high intracelluar calcium at rest. While, the shift of the voltage dependence toward more negative potentials, and enhanced channel senstitivity to RAP (this mutant show also hypersensitivity to cold) were persisting.

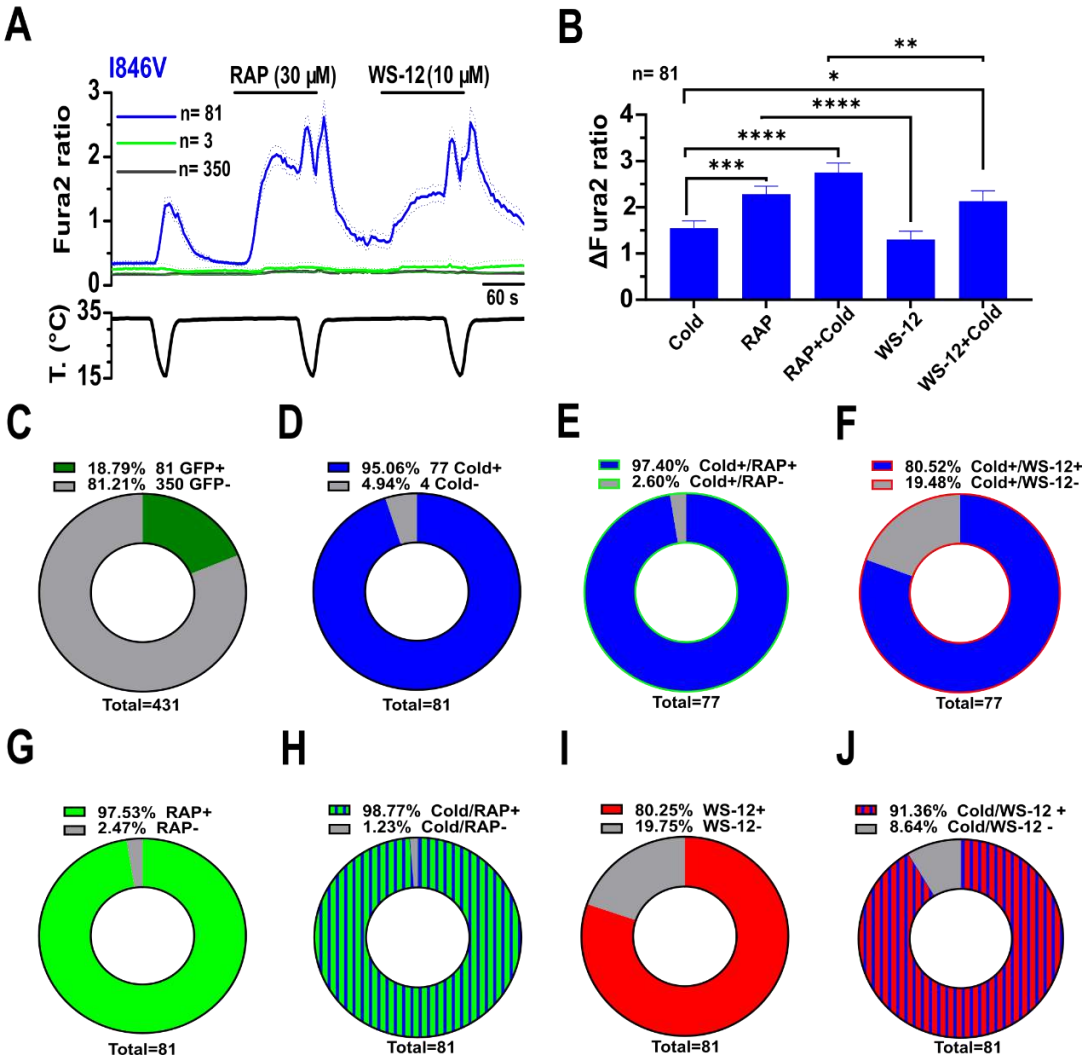

Figure 33. Rapamycin activated heterologously transfected I846V TRPM8 channel and potentiated cold evoked responses. A, Average ± SEM fura2 ratio response to cold, RAP (30 µM) and WS-12 (10 µM) in HEK293 cells transiently transfected with mouse TRPM8 I846V mutant and GFP. GFP (+) cold sensitive cells (n=81) are shown in blue (blue trace) and GFP (+) cold insensitive cells (n=3) are shown in green (green trace) while GFP (-) cells (n=350) are shown in grey. **B,** Bar histogram summarizing the responses of cold sensitive HEK293 cells transfected with mouse TRPM8 to different agonists. Statistical significance was calculated by a one-way ANOVA followed by Bonferroni post-hoc test. **C,** Pie graph showing the percentage of GFP (+) transfected and GFP (-) non-transfected cells out of total cells (n=431). **D,** Pie graph showing the percentage of cold sensitive cells (Cold+) and cold insensitive cells (Cold-) out of the total GFP+ transfected cells (n=81). **E,** Pie graph showing the percentage of cold sensitive cells that are either rapamycin (30 µM) sensitive (Cold+ / RAP+) or rapamycin insensitive (Cold+ / RAP-) cells out of total cold responders (n=77). **F,** Pie graph showing the percentage of cold sensitive cells that are either WS-12 (10 µM) sensitive (Cold+ / WS-12 +) or WS -12 insensitive (Cold+ / WS-12 -) out of total cold responders (n=77). **G,** Pie graph showing the percentage of rapamycin sensitive cells (RAP+) and insensitive cells (RAP-) out of the total GFP+ transfected cells (n=81). **H,** Pie graph showing the percentage of cold evoking cells responses potentiation in the presence of rapamycin (Cold/RAP+) and the insensitive cells (Cold/RAP-) out of the total GFP+ transfected cells (n=81). **I,** Pie graph showing the percentage of WS-12 sensitive cells (WS-12+) and insensitive cells (WS-12-) out of the total GFP+ transfected cells (n=81). **J,** Pie graph showing the percentage of cold evoking cell response potentiation in the presence of WS-12 (Cold/WS-12+) and insensitive cells (Cold- /WS-12-) out of the total GFP+ transfected cells (n=81).

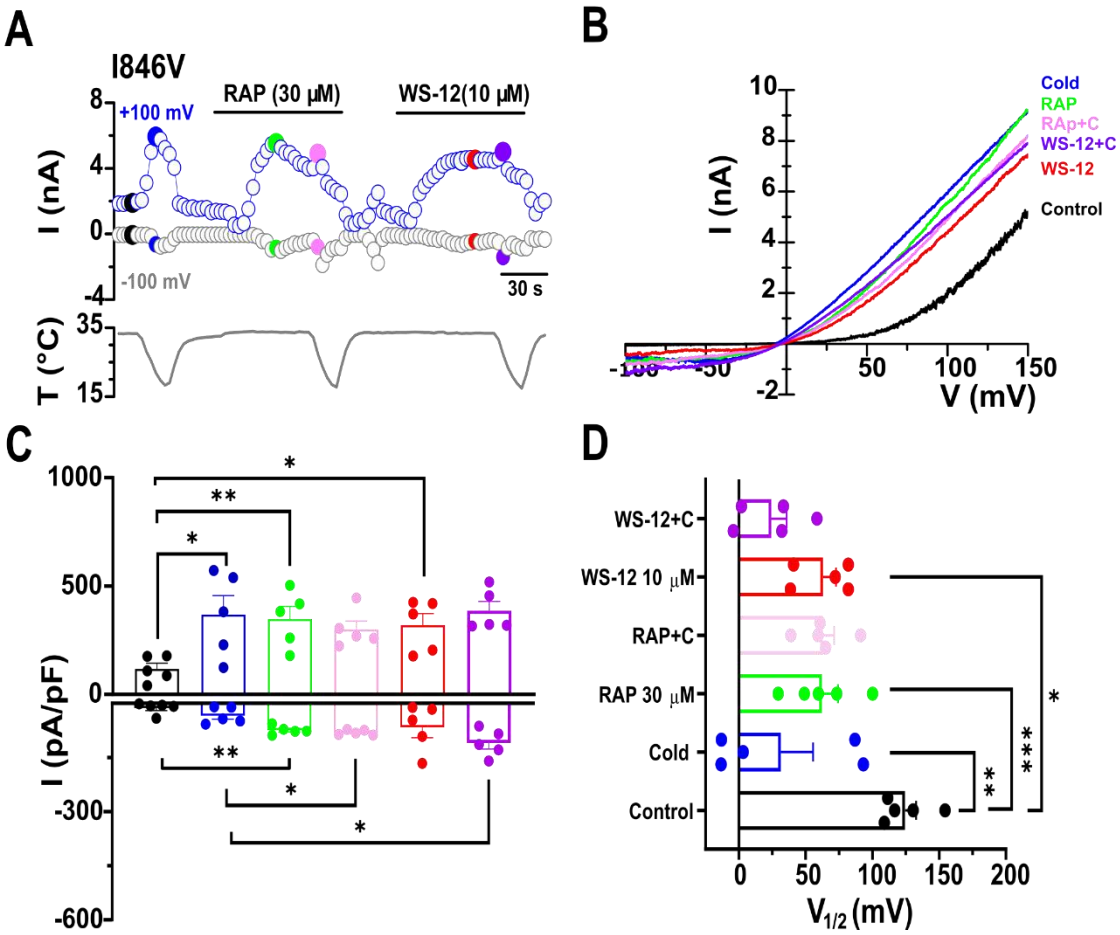

Figure 34. Rapamycin activated I846V TRPM8 mutant whole-cell currents expressed in HEK293 cells and induced a leftward shift of mutant TRPM8 voltage dependence. **A,** Representative time course of I846V TRPM8 mutant whole cell currents screened at -100 mV and +100 mV in transiently transfected HEK293 cells during sequential agonists application. The trace of simultaneous recording of the bath temperature during experiment is shown at the bottom. **B,** the current-voltage relationship (I-V) of responses presented in A**,** resulted with 800 ms voltage ramp from -100 to +150mV. The key colors of single traces coincide with specific time points in A**.** Rapamycin elicited a non-selective cationic currents TRPM8 dependent features and potentiates cold evoked responses. **C,** Bar histogram summarizing the mean ± SEM outward and inward currents densities measured respectively at +100 and -100 mV of the different stimuli presented in A, following the color code. Statistical differences were evaluated by one-way Anova followed by Bonferroni´s post-hoc test. ***D,*** Mean (n=5) $V_{1/2}$ values calculated from fitting the individual I-V curve to linear Boltzmann equation. Note rapamycin provoked a significative leftward shift of $V_{1/2}$, statistical differences were evaluated by one-way Anova followed by Bonferroni's post-hoc test.

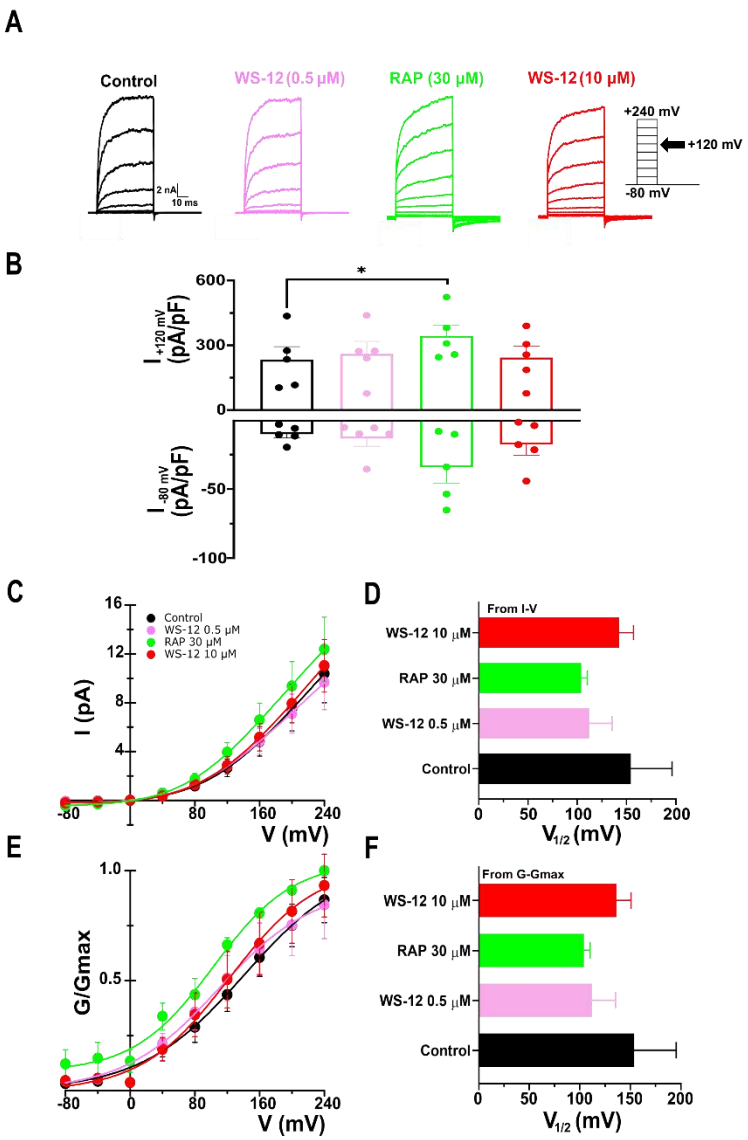

Figure 35. Biophysical characterization of Rapamycin effects on I846V TRPM8 mutant gating. A, Representative whole cell of I846V mutant TRPM8 currents in response to the given voltage steps protocol (from -80 to +240 mV during 50ms, ΔV= 40 mV see material and methods) in control conditions and in the presence of RAP (30 µM), WS-12 (0.5 and 10 µM) at 24 ˚C room temperature. **B,** Bar histogram summarizing the mean ± SEM currents densities at +120 (outward current density) and -80 mV (inward current density) of the different stimuli presented in A, following the color code. Statistical differences were evaluated by one-way Anova followed by Bonferroni´s post-hoc test. **C**, Average (n=4) steady-state I-V curves extracted from individual cells after application of protocol the lines represent the fitting to linearized Boltzmann equation (see methods). **D,** Mean (n=4) $V_{1/2}$ value calculated from fitting the individual I-V curve to linearized Boltzmann equation. **E,** Average (n=4) voltage dependence activation curve in control condition and in the presence of different agonists, conductance was calculated as the steady state current divided by the driving force (Driving force = V_{Test}-E_{rev}) and normalized to the estimated maximal conductance (Gmax) which is the G value at +240 mV in the presence of 30 µM rapamycin. **F,** Mean (n=4) $V_{1/2}$ value calculated from fitting the individual G/Gmax-V curve Boltzmann equation. The statistical differences were analyzed by one way ANOVA, followed by Bonferroni's post-hoc test.

Until this point, substitutions of the isoleucine I846 with non-polar amino acids, including alanine (A) and valine (V), or the polar amino acid threonine (T), demonstrated an enhancement of RAP sensitivity compared to wild-type TRPM8. Our findings suggested that isoleucine might play a crucial role in negatively modulating rapamycin sensitivity. To further investigate this hypothesis, we performed another mutation, introducing a charged amino acid residue, aspartic acid (D), instead of isoleucine. This change was expected to completely disrupt the hydrophobic nature of the site and assess whether it would lead to a complete suppression of RAP activation or maintain rapamycin hypersensitivity in the channel. It is important to note that aspartic acid (D) is a negatively charged amino acid, likely to disturb the original hydrophobic environment.

In *in vitro* calcium imaging experiments conducted on HEK293 cells expressing the I846D mutant, we observed a distinct phenotype compared to the previously characterized I846A, I846T, and I846V TRPM8 mutants. The GFP+ cells expressing I846D (Blue trace, n=65) did not exhibit the high internal fura2 ratio phenotype at rest compared to GFP- cells (Grey trace, n=136) (Fig. 36A). This result further supports the role of the segment 4 residue isoleucine (I846) in maintaining the normal closed pore structure at rest. However, the application of RAP (30 µM) to this mutant elicited responses with an amplitude markedly greater than that observed with cold (Fig. 36A, B), and cold-evoked activation was robustly potentiated in the presence of RAP. In contrast, HEK293 cells expressing I846D were completely insensitive to WS-12 and did not potentiate cold-evoked responses (Fig. 36A, B). Concerning the percentage of cell activation, RAP activated a greater percentage of HEK293 cells expressing I846D TRPM8 mutant compared to cold (Cold= 58% vs RAP=93%) (p-value < 0.0001, Chi-squared test) (Fig. 36D, E). The percentage of cold-activated cells was fully potentiated in the presence of RAP; on the contrary, WS-12 did not potentiate cold-evoked cell responses (Cold=58% vs RAP+cold=100% vs WS-12+cold=38%) (p-value < 0.0001, Chi-squared test) (Fig. 36D, H, and J).

Compared to wild-type TRPM8, the segment 4 mutant I846D presented a slightly reduced response to cold (WT TRPM8 Cold= 0.5 ± 0.1, n=123 vs I846D Cold= 0.3 ± 0.1, n=65) (Fig. 43A). RAP (30 µM) elicited a markedly higher activation amplitude in the I846D group compared to wild-type TRPM8 (WT TRPM8 RAP= 0.22 ± 0.03, n=123 vs I846D RAP= 0.8 ± 0.1, n=65) (p-value< 0.0001) (Fig. 43B). Additionally, cold-evoked response potentiation in the presence of RAP was drastically diminished in the I846D group compared to wild-type (WT TRPM8 RAP+cold = 2.1 ± 0.2, n=123 vs I846D RAP+cold= 1.1 ± 0.2, n=65) (p-value< 0.001) (Fig. 43C). As expected, the menthol derivative WS-12 was unable to activate I846D and did not potentiate cold-evoked activation compared to wild-type (Fig. 43D, E).

Furthermore, using a voltage ramp protocol (see materials and methods) in HEK293 cells expressing I846D TRPM8 mutant (Fig. 37A), we observed that, at rest (Control: absence of any stimulus), GFP+ cells expressing the I846D mutant showed a higher outward current at +100 mV, consistent with the

phenotype observed previously with S4 residue I846 mutants (I846A, I846T, and I846V). Cooling elicited both, outward current at +100 mV (Control=71 ± 7 pA/pF vs Cold = 173 ± 18 pA/pF) (n=5, p-value= 0.0011) and inward current at -100 mV (Control= -6 ± 2 pA/pF vs Cold= -30 ± 6 pA/pF) (n=5, p-value= 0.0324) (Fig. 37C). The application of RAP (30 µM) activated a marked outward current measured at +100 mV (Control=71 ± 7 pA/pF vs RAP=158 ± 6 pA/pF) (n=5, p-value= 0.0005) and increased inward current at -100 mV (Control= -6 ± 2 pA/pF vs RAP= -22± 8 pA/pF) (n=5, ns, p-value= 0.1387) (Fig. 37C). Cold-evoked outward current at +100 mV (Cold= 173 ± 18 pA/pF vs RAP+cold = 246 ± 22 pA/pF) (n=5, p-value=0.0105) and inward current at -100 mV (Cold=-30 ± 6 pA/pF vs RAP+cold= -100 ± 23 pA/pF) (n=5, p-value=0.0301) (Fig. 37C) were both markedly potentiated in the presence of RAP. Notably, WS-12 (10 µM) elicited a substantial outward and inward current measured at +100 mV and -100 mV, respectively. Despite failing to potentiate cold-evoked outward current at +100 mV, WS-12 significantly potentiated cold-evoked inward current at -100 mV (Cold=-30 ± 6 pA/pF vs WS-12+cold= -56 ± 7 pA/pF) (n=5, p-value=0.0432) (Fig. 37C).

RAP(30 µM), produced a leftward shift of the voltage dependance towards more negative potentials of the I846D-TRPM8 mutant (Control $V_{1/2}$ = 124 ± 8 mV; RAP $V_{1/2}$ = 87.1 ± 15.2 mV) (n=5, p-value= 0.0612) (Fig. 37B,D). The cold-evoked voltage dependence shift was potentiated by RAP (Cold $V_{1/2}$ = 53 ± 17 mV; RAP+cold $V_{1/2}$ = 34 ± 12 mV) (n=5, p-value= 0.0653) (Fig. 37D). WS-12 potentiated cold-evoked $V_{1/2}$ leftward shift (Cold $V_{1/2}$ = 53 ± 17 mV; WS-12+cold $V_{1/2}$ = 32 ± 17 mV) (n=5, p-value= 0.0594) (Fig. 37D).

Compared to wild-type TRPM8, at rest, the I846D mutant channel showed a higher outward current measured at +100 mV (WT TRPM8 Control = 28 ± 4 pA/pF vs I846D Control= 71 ± 7 pA/pF). This phenotype aligns with the previously described I846 mutants, while the inward current activation measured at -100 mV was diminished in the I846D group (WT TRPM8 Control = -12 ± 3 pA/pF vs I846D Control= -6 ± 2 pA/pF) (Fig. 44A). RAP (30 µM) application elicited a higher outward current measured at +100 mV (WT TRPM8 RAP = 114 ± 14 pA/pF, n=14 vs I846D RAP= 158 ± 6 pA/pF, n=5), while inward current generated at -100 mV (WT TRPM8 RAP = -34 ± 8 pA/pF vs I846D RAP= -22 ± 8 pA/pF) was diminished in the I846D group compared to wild-type TRPM8 (Fig. 44C). Moreover, cold activated both outward current at +100 mV (WT TRPM8 RAP+cold = 360 ± 36 pA/pF vs I846D RAP+cold= 246 ± 22 pA/pF), and inward current potentiation in the presence of RAP were diminished in I846D cells compared to WT TRPM8 (WT TRPM8 RAP+cold = -160 ± 37 pA/pF, n=14 vs I846D RAP+cold= -100 ± 23 pA/pF, n=5) (Fig. 44D). Interestingly, in line with our calcium results, WS-12 (10 µM) did not evoke either current activation at both +100 mV (WT TRPM8 WS-12 = 329 ± 53 pA/pF, n=14 vs I846D WS-12= 96 ± 7 pA/pF, n=5) (p-value<0.05) and at -100 mV (WT TRPM8 WS-12 = -165 ± 54 pA/pF, n=14 vs I846D WS-12= -20 ± 8 pA/pF, n=5) (p-value=0.08), nor contributed to cold-activated currents potentiation, thus supporting I846D mutant insensitivity to WS-12 (Fig. 44E and F).

The cold temperature threshold extracted from the time course current recording of HEK293 cells expressing I846D (Fig. 37A) showed a robust shift of the threshold towards warmer temperatures compared to WT TRPM8 (WT TRPM8 = 27.3 ± 0.3 ˚C, n=11 vs I846D = 31 ± 0.9 ˚C, n=7) (p-value< 0.01) (Fig. 45A). This result was corroborated with a marked leftward shift of the I846D voltage dependence ($V_{1/2}$) towards more negative potentials compared to the WT TRPM8 group (WT TRPM8 Control $V_{1/2}$=265 ± 40 mV, n=14 vs I846D Control $V_{1/2}$=124 ± 8 mV, n=5) (p-value< 0.05) (Fig. 45B).

Compared to wild type channel, RAP (30 µM) evoked a strong leftward shift of $V_{1/2}$ in the I846D group towards more negative potentials compared to WT TRPM8 (WT TRPM8 RAP $V_{1/2}$=156 ± 23 mV, n=14 vs I846D RAP $V_{1/2}$=87 ± 15 mV, n=5) (Fig. 45D). Cold-evoked $V_{1/2}$ leftward shift potentiation in the presence of RAP was shifted towards more negative potentials in the I846D group compared to WT TRPM8 (WT TRPM8 RAP+cold $V_{1/2}$ =55 ± 9 mV, n=14 vs I846D RAP+cold $V_{1/2}$ =34 ± 12 mV, n=5) (Fig. 45E). Interestingly, WS-12 did not affect the $V_{1/2}$ voltages in cells expressing I846D compared to WT TRPM8 (Fig. 45F). In contrast, cold-evoked $V_{1/2}$ shift potentiation in the presence of WS-12 was not different between I846D compared to WT TRPM8 groups (WT TRPM8 WS-12+cold $V_{1/2}$ =36 ± 11 mV, n=14 vs I846D WS-12+cold $V_{1/2}$ =32 ± 17 mV, n=5) (Fig. 45G).

Next, I analyzed responses of the I846D mutant to voltage steps. An exemplary cell is shown in figure 38A. The application of RAP (30 µM) resulted in a robust potentiation of voltage-activated outward currents measured at +120 mV (I846D Control= 257 ± 48 pA/pF vs I846D RAP = 384 ± 65 pA/pF) (n=5, p-value= 0.0371) and elicited a small inward current at -80 mV (I846D Control= -11 ± 5 pA/pF vs I846D RAP = -23 ± 9 pA/pF) (n=5, ns, p-value= 0.198) (Fig. 38B). Consistently with previous results obtained from the voltage ramp protocol, WS-12 (10 µM) failed to potentiate voltage-activated outward currents measured at +120 mV but induced a robust inward current at -80 mV (I846D Control= -11 ± 5 pA/pF vs I846D WS-12= -42± 14 pA/pF) (n=5, p-value= 0.0459) (Fig. 38B). Similarly, menthol (30 µM) exhibited an inability to potentiate voltage-evoked currents. Furthermore, the analysis of the current-voltage (I-V) and conductance-voltage (G/Gmax-V) relationships uncovered a notable leftward shift of the voltage activation curve toward negative potentials in the presence of RAP (Fig. 38C, E). This shift was accompanied by a highly significant alteration in the voltage of half maximal activation ($V_{1/2}$), moving from the control value of $V_{1/2}$=123 ± 11 mV to $V_{1/2}$= 101 ± 12 mV upon exposure to 30 µM RAP (calculated from G/Gmax-V) (n=5, p-value= 0.0015). Consistently, a similar result was observed in the I-V relationship, where $V_{1/2}$ transitioned from control $V_{1/2}$=127 ± 10 mV to $V_{1/2}$= 109 ± 18 mV in the presence of RAP 30 µM (Fig. 38D, F). Notably, both WS-12 and menthol induced a negligible shift in $V_{1/2}$.

Furthermore, the agonism of RAP on I846D mutant, was further supported by the analysis of RAP gating kinetics that was showing a clear slowing of both current acivation (upon depolarisation at +120

mV) and current deactivation (at -80 mV) times constantes (Check Annex Fig. 66) these results resembling those obtained with wild type channel (Fig. 22).

In summary, the acid aspartic mutation I846D, did not show a higher basal phenotype that was observed in previous I846A and I846T mutants. Besides, rapamycin hypersensitivity phenotype was conserved following different I846 residue mutations. Finaly, our result highlighted that I846D residue plays a crucial role in the WS-12/menthol channel activation since the mutant I846D lack completely channel sensitivity to both agonists.

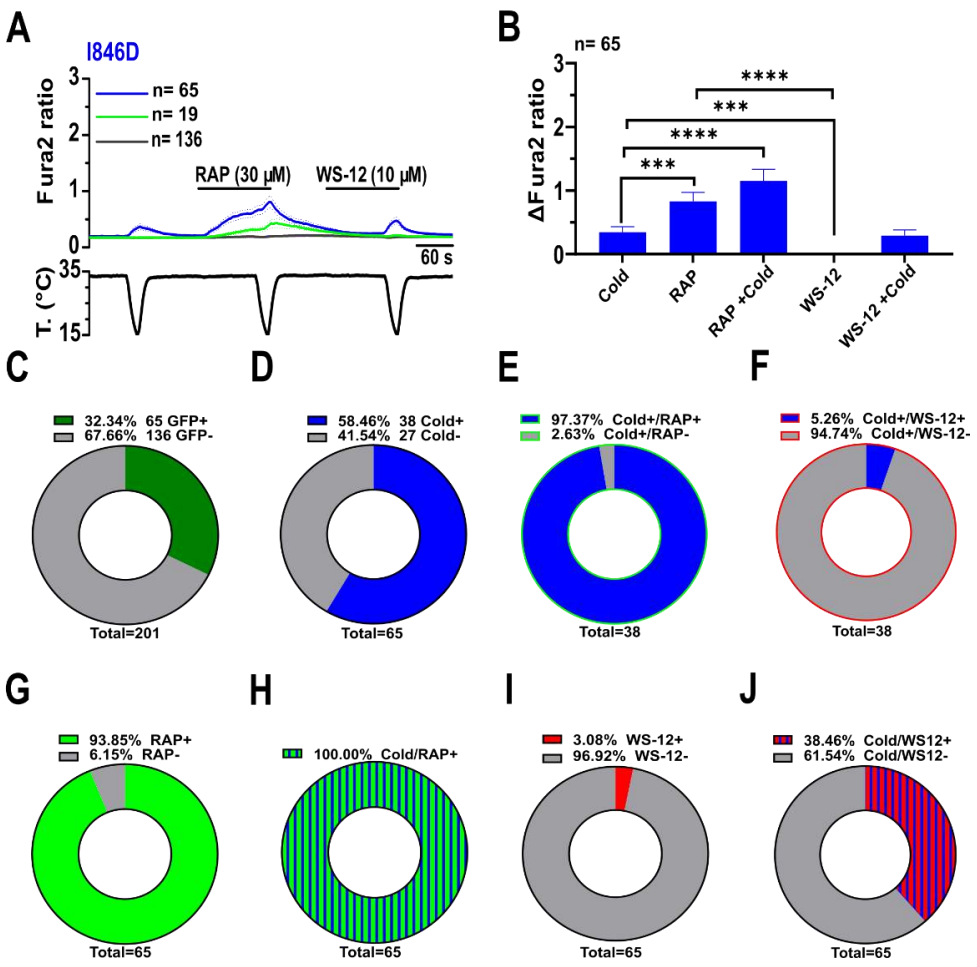

Figure 36. Rapamycin activated I846D TRPM8 mutant channel expressed in HEK293 cells and potentiated cold evoked responses. A, Average ± SEM fura2 ratio response to cold, RAP (30 µM) and WS-12 (10 µM) in HEK293 cells transiently transfected with mouse TRPM8 and GFP. GFP (+) cold sensitive cells (n=65) are shown in blue (blue trace) and GFP (+) cold insensitive cells (n=19) are shown in green (green trace) while GFP (-) cells (n=136) are shown in grey. **B,** Bar histogram summarizing the responses of cold sensitive HEK293 cells transfected with mouse TRPM8 to different agonists. Statistical significance was calculated by a one-way ANOVA followed by Bonferroni post-hoc test. **C,** Pie graph showing the percentage of GFP (+) transfected and GFP (-) non-transfected cells out of total cells (n=201). **D,** Pie graph showing the percentage of cold sensitive cells (Cold+) and cold insensitive cells (Cold-) out of the total GFP+ transfected cells (n=65). **E,** Pie graph showing the percentage of cold sensitive cells that were either rapamycin (30 µM) sensitive (Cold+/RAP+) or rapamycin insensitive (Cold+/ RAP -) cells out of total cold responders (n=38). **F,** Pie graph showing the percentage of cold sensitive cells that were either WS-12 (10 µM) sensitive (Cold+ / WS-12 +) or WS -12 insensitive (Cold+ / WS-12 -) cells out of total cold responders (n=38). **G,** Pie graph showing the percentage of rapamycin sensitive cells (RAP+) and insensitive cells (RAP-) out of the total GFP+ transfected cells (n=65). **H,** Pie graph showing the percentage of cold evoked cells responses potentiation in the presence rapamycin (Cold/RAP+) and the insensitive cells (Cold/RAP-) out of the total GFP+ transfected cells (n=65). **I,** Pie graph showing the percentage of WS-12 sensitive cells (WS-12+) and insensitive cells (WS-12-) out of the total GFP+ transfected cells (n=65). **J,** Pie graph showing the percentage of cold evoking cells responses potentiation in the presence of WS-12 (Cold/WS12+) and the insensitive cells (Cold/WS12-) out of the total GFP+ transfected cells (n=65).

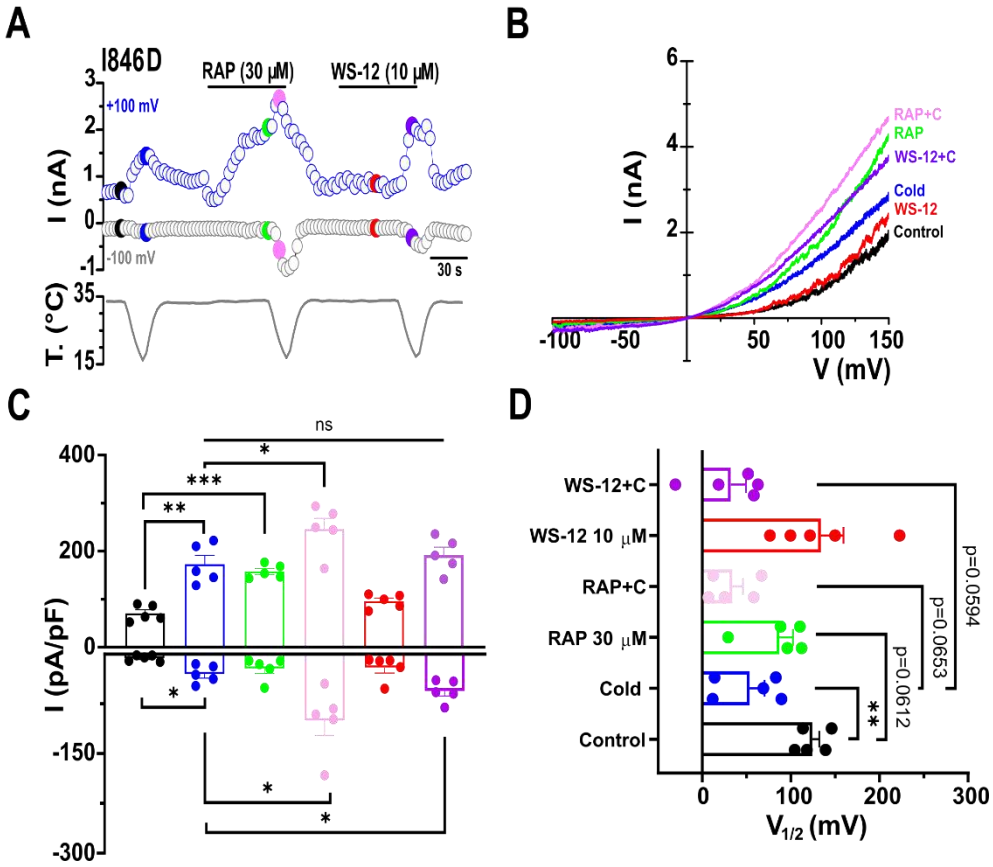

Figure 37. Rapamycin activated I846D TRPM8 mutant whole-cell currents expressed in HEK293 cells and induced a leftward shift of mutant TRPM8 voltage dependence. **A,** Representative time course of I846A TRPM8 mutant whole cell currents screened at -100 mV and +100 mV in transiently transfected HEK293 cells during sequential agonists application. The trace of simultaneous recording of the bath temperature during experiment is shown at the bottom. **B,** The current-voltage relationship (I-V) of responses presented in A**,** resulted with 800 ms voltage ramp from -100 to +150mV. The key colors of single traces coincide with specific time points in A**.** Rapamycin elicited a non-selective cationic currents TRPM8 dependent features and potentiates cold evoked responses. **C,** Bar histogram summarizing the mean ± SEM outward and inward current density measured respectively at +100 and -100 mV of the different stimuli presented in A, following the color code. Statistical differences were evaluated by one-way Anova followed by Bonferroni´s post-hoc test. **D,** Mean (n=5) $V_{1/2}$ values calculated from fitting the individual I-V curve to linear Boltzmann equation. Note rapamycin provoke a robust leftward shift of $V_{1/2}$, statistical differences were evaluated by one-way Anova followed by Bonferroni's post-hoc test.

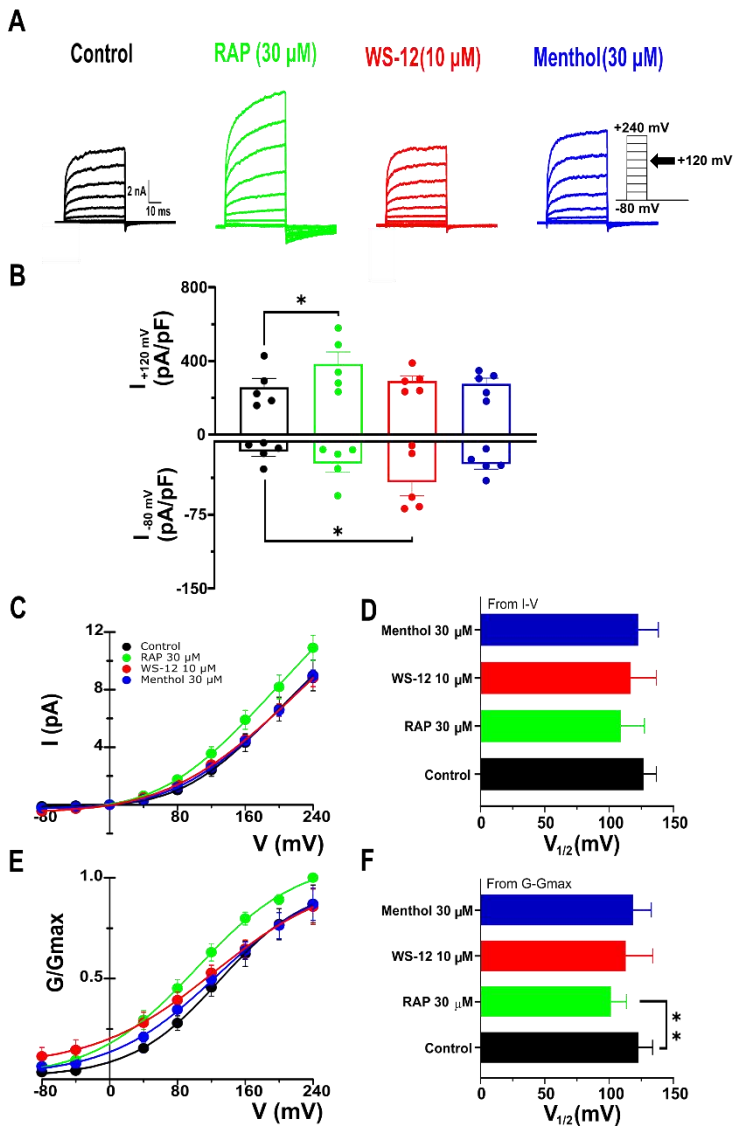

Figure 38. Biophysical characterization of rapamycin effects on I846D TRPM8 mutant gating. A, Representative whole-Cell I846D mutant TRPM8 currents in response to the given voltage steps protocol (from -80 to +240 mV, ΔV= 40 mV see material and methods) in control conditions and in the presence of RAP (30 µM), WS-12 (0.5 and 10 µM) at 24 ˚C room temperature. **B,** Bar histogram summarizing the mean ± SEM current density at +120 and -80 mV of the different stimuli presented in A, following the colour code. Statistical differences were evaluated by one-way Anova followed by Bonferroni´s post-hoc test. **C**, Average (n=5) steady-state I-V curves extracted from individual cells after application of protocol the lines represent the fitting to linearized Boltzmann equation (see methods). **D,** Mean (n=5) $V_{1/2}$ value calculated from fitting the individual I-V curve to linearized Boltzmann equation. **E,** Average (n=5) voltage dependence activation curve in control condition and in the presence of different agonists, conductance was calculated as the steady state current divided by the driving force (Driving force = V_{Test}-E_{rev}) and normalized to the estimated maximal conductance (Gmax) which is the G value at +240 mV in the presence of 30 µM Rapamycin. **F,** Mean (n=5) $V_{1/2}$ value calculated from fitting the individual G/Gmax-V curve Boltzmann equation. The statistical differences were analyzed by one way ANOVA, followed by Bonferroni's post-hoc test.

4.1.7.3 TRP domain mutations Y1005A and R1008A decrease TRPM8 sensitivity to rapamycin

The TRP domain is a critical region of the TRPM8 channel, influencing its function and activation by external ligands. Mutagenesis studies have provided insights into the role of specific TRP domain residues, such as Y1005 and R1008, in menthol activation. More specificallty, previous research (Bandell et al., 2006; Rohács et al., 2005) has demonstrated that mutations in these two residues lead to a significant reduction in menthol sensitivity. Consequently, Y1005 and R1008 are deemed essential for TRPM8 channel activation by agonists, as comprehensively reviewed by (Plaza-Cayón et al., 2022).

In vitro calcium imaging experiments were conducted in HEK293 cells expressing the Y1005A mutant.

Compared to wild-type TRPM8, the Y1005A mutant exhibited a small response to all the agonists (Fig. 39A): cold (WT TRPM8 Cold = 0.5 ± 0.1, n=123 vs Y1005A Cold = 0.11 ± 0.01, n=123) (Fig. 43A). RAP (30 µM) (WT TRPM8 RAP = 0.22 ± 0.03, n=123 vs Y1005A RAP = 0.07 ± 0.01, n=123) (Fig. 43B). WS-12 (WT TRPM8 WS-12 = 1.2 ± 0.1, n=123 vs Y1005A WS-12 = 0.02 ± 0.01, n=123) (Fig. 43B).

The results indicated a marked alterations in Y1005A responses to cold, RAP and WS-12 (Fig. 39B) in agrement with litterature. Given the mutants small responses to cold stimulus , nevertheless, the response was potentiated after combining cold with either RAP or WS-12 (Fig. 39A, B). The percentage of cells activated by cold,was also potentiated by RAP, and was greater than WS-12 (RAP+cold = 75% vs WS-12+cold = 66%) (p-value < 0.0304, Chi-squared test) (Fig. 39D, H, and J).

Moreover, cold-evoked response potentiation in the presence of RAP was severely diminished in the Y1005A group compared to wild type TRPM8 (WT TRPM8 RAP+cold = 2.1 ± 0.2, n=123 vs Y1005A RAP+cold = 0.42 ± 0.05, n=123) (p-value < 0.0001) (Fig. 43D). Similarly, the menthol analogue WS-12 activation was drastically altered in Y1005A compared to wild type (WT TRPM8 WS-12 = 1.2 ± 0.1, n=123 vs Y1005A WS-12 = 0.02 ± 0.01, n=123) (p-value < 0.0001) (Fig. 43D). Furthermore, cold-evoked response potentiation in the presence of WS-12 was severely reduced in Y1005A compared to WT TRPM8 (WT TRPM8 WS-12+cold = 2 ± 0.2, n=123 vs Y1005A WS-12+cold = 0.3 ± 0.03, n=123) (p-value < 0.0001) (Fig. 43E).

Next, whole-cell patch-clamp recordings were performed using a voltage ramp protocol in HEK293 cells expressing the Y1005A mutant channel (Fig. 40A). Cooling induced a significant outward current at +100 mV (Control=17 ± 2 pA/pF vs Cold=96 ± 31 pA/pF) (n=6, p-value= 0.0492), without generating an inward current at -100 mV. In contrast to calcium imaging data, the application of RAP (30 µM) elicited outward current at +100 mV (Control=17 ± 2 pA/pF vs RAP=99 ± 34 pA/pF) (n=6, p-value= 0.0577) (Fig. 40A, C). Cold-evoked outward current at +100 mV (Cold= 96 ± 31 pA/pF vs RAP+cold= 238 ± 69 pA/pF) (n=6, p-value=0.0135), and inward current at -100 mV (Cold=-4 ± 1 pA/pF vs

RAP+cold= -21 ± 7 pA/pF) (n=6, p-value=0.0606) were both robustly potentiated in the presence of RAP. WS-12 (10 µM) induced a larger outward current at +100 mV (Control=17 ± 2 pA/pF vs WS-12=61 ± 13 pA/pF) and inward current at -100 mV (Control=-5 ± 1 pA/pF vs WS-12= -10 ± 2 pA/pF) (n=6, p-value=0.0582) (Fig. 40C). Additionally, WS-12 markedly potentiated both cold-evoked outward current (Cold=96± 31 pA/pF vs WS-12+cold= 184 ± 20 pA/pF) (n=6, p-value= 0.0053) and inward current (Cold=-4 ± 1 pA/pF vs WS-12+cold= -13 ± 2 pA/pF) (n=6, p-value= 0.0142) (Fig.40A, C).

The current-voltage relationship (I-V) of RAP activation of the TRP domain mutant channel Y1005A-TRPM8 preserved some typical characteristics of WT TRPM8 including a leftward shift of the voltage activation curve towards more negative potentials(Fig. 40B, in contrast, the reversal potential (Erev) in 5 out of 6 was more negative in contrast to to wild type channel which Erev more around 0 mV. Additionally, the effect of TRPM8 agonists on channel voltage dependence at baseline temperature (33±1˚C) was examined. I should notify that at basal temperature, half of the cells (n=3) were having their voltage dependence $V_{1/2}$ less Than 200 mV, while the othere half (n=3) had their $V_{1/2}$ more than 400 mV. This dispersion of data should make us more careful when discussing these elctrophysiological results obtained (need to perform more recordings in ordre to obtaine homogenous recordings).

RAP (30 µM) induced a leftward shift of the voltage of half maximal activation $V_{1/2}$ towards more negative potentials compared to control (Control $V_{1/2}$ = 304 ± 88 mV; RAP $V_{1/2}$ = 130 ± 34 mV) (n=6, ns, p-value= 0.1551). Cold-evoked voltage dependence leftward shift was strongly potentiated by RAP (Cold $V_{1/2}$ = 136 ± 33 mV vs RAP+cold $V_{1/2}$= 40 ± 12 mV) (n=6, p-value= 0.0221) (Fig. 40D). WS-12 induced a leftward shift of $V_{1/2}$ (Control $V_{1/2}$ = 304 ± 88 mV vs WS-12 $V_{1/2}$ = 167 ± 54 mV) (n=6, ns, p-value= 0.1008), and potentiated cold-evoked $V_{1/2}$ shift towards more negative voltages (Cold $V_{1/2}$ = 136 ± 33 mV; WS-12+cold $V_{1/2}$ = 58 ± 10 mV) (n=6, p-value= 0.0663) (Fig. 40D).

Compared to wild-type TRPM8, at basal temperature, the TRP domain mutant Y1005A channel showed small outward current measured at +100 mV (WT TRPM8 Control = 28 ± 4 pA/pF vs Y1005A Control= 17 ± 2 pA/pF) (Fig. 44A). Upon RAP (30 µM) application, the Y1005A mutant channel exhibited approximately similar outward current measured at +100 mV compared to wild-type TRPM8 (WT TRPM8 RAP = 114 ± 14 pA/pF, n=14 vs Y1005A RAP= 99 ± 34 pA/pF, n=6). However, RAP-evoked inward current at -100 mV was markedly smaller in Y1005A mutant cells (WT TRPM8 RAP = -34 ± 8 pA/pF vs Y1005A RAP= -5 ± 1 pA/pF) (p-value= 0.06) (Fig. 44C). Cold-activated outward current potentiation in the presence of RAP measured at +100 mV in Y1005A transfected HEK293 cells was decreased compared to the WT TRPM8 group (WT TRPM8 RAP+cold = 360 ± 36 pA/pF vs Y1005A RAP+cold= 238 ± 69 pA/pF). Similarly, inward current potentiation in the presence of RAP measured at -100 mV was severely reduced in the Y1005A mutant group compared to the WT TRPM8 group (WT TRPM8 RAP+cold = -160 ± 37 pA/pF, n=14 vs Y1005A RAP+cold= -21 ± 7 pA/pF, n=6) (p-

value< 0.01) (Fig.44D). WS-12 evoking both outward and inward currents respectively at +100 mV (WT TRPM8 WS-12 = 329 ± 53 pA/pF vs Y1005A WS-12= 61 ± 13 pA/pF) (p-value< 0.01) and at -100 mV (WT TRPM8 WS-12 = -165 ± 54 pA/pF, n=14 vs Y1005A WS-12 = -10 ± 2 pA/pF, n=6) (p-value< 0.05) were drastically altered in the Y1005A group compared to the wild type. Furthermore, WS-12 failed to potentiate cold-evoked both outward current at +100 mV (WT TRPM8 WS-12+cold = 456 ± 53 pA/pF vs Y1005A WS-12+cold= 184 ± 20 pA/pF) (p-value< 0.001) and inward current at -100 mV (WT TRPM8 WS-12+cold = -263 ± 42 pA/pF, n=14 vs Y1005A WS-12+cold = -13 ± 2 pA/pF, n=6) (p-value< 0.0001) (Fig. 40F) compared to the wild-type group.

The temperature threshold extracted from the current time course recorded from cells expressing the Y1005A mutant following cooling (Fig.40A) showed approximately shifted towards warmer Temperature compared to WT TRPM8 (WT TRPM8 = 27.3 ± 0.3 ˚C, n=11 vs Y1005A=29 ± 2 ˚C, n=6) (Fig. 45A).

In control conditions, the voltage dependence ($V_{1/2}$) of Y1005A was rightward shifted towards positive voltages compared to WT TRPM8 (WT TRPM8 Control $V_{1/2}$=265 ± 40 mV, n=14 vs Y1005A Control $V_{1/2}$=304 ± 88 mV, n=6) (Fig.45B). RAP (30 µM) evoked approximately similar leftward shift of the voltage dependence in the Y1005A group compared to WT TRPM8 (WT TRPM8 RAP $V_{1/2}$=156 ± 23 mV, n=14 vs Y1005A RAP $V_{1/2}$=130 ± 34 mV, n=6) (Fig. 45D). Cold-evoked voltage dependence leftward shift potentiation in the presence of RAP in the Y1005A group was similar to the WT TRPM8 group (WT TRPM8 RAP+cold $V_{1/2}$=55 ± 9 mV, n=14 vs Y1005A RAP+cold $V_{1/2}$=40 ± 12 mV, n=5) (Fig. 45E). Next, WS-12 elicited a leftward shift of voltage dependence ($V_{1/2}$) was markedly altered in the Y1005A group compared to WT TRPM8 (WT TRPM8 WS-12$V_{1/2}$=95 ± 15 mV, n=14 vs Y1005A WS-12 $V_{1/2}$=167 ± 54 mV, n=6) (Fig.45F). In the same direction, cold-evoked voltage dependence leftward shift potentiation in the presence of WS-12 was notably reduced in the Y1005A group compared to the WT TRPM8 (WT TRPM8 WS-12+cold $V_{1/2}$=36 ± 11 mV, n=14 vs Y1005A WS-12+cold $V_{1/2}$=58 ± 10 mV, n=6) (Fig. 45G).

In summary, based on calcium imaging data, The Y1005A mutants showed diminished response profile to all tested agonists (Cold, RAP and WS-12) these results are in line with literature (Bandell et al., 2006; Voets et al., 2007a), which fully support the crucial role of the TRP domain in the agonists allosteric modulation of channel coupling channel gating (Taberner et al., 2014). In contrast, taken the heterogenous cells behaviour, during patch clamp electrophysiology of cells expressing the Y1005A mutant showed a normal response profile to RAP compared wild type channel (4 out 6 cells RAP responders), while the profile response to WS-12 was resembling those of calcium imaging data showing a clear WS-12 sensitivity reduction. Thus, the consistent diminished sensitivity to WS-12 in both experiments support the critical implication of this residue in coupling the opening of the channel

by menthol and derivatives WS-12 (Bandell et al., 2006; Voets et al., 2007a). Whereas the RAP activation, observed during electrophysiology, may support a distinct biding pocket than menthol.

(Important note : in order to re-confirm my result with patch showing that Y1005A is activated by RAP we should repeat this specific patch experiment to avoid the bias introduced by cells behavioural heterogeneity seen in my batch of cells recording, until then my interpretation will take only the consistent result obtained from calcium imaging experiment).

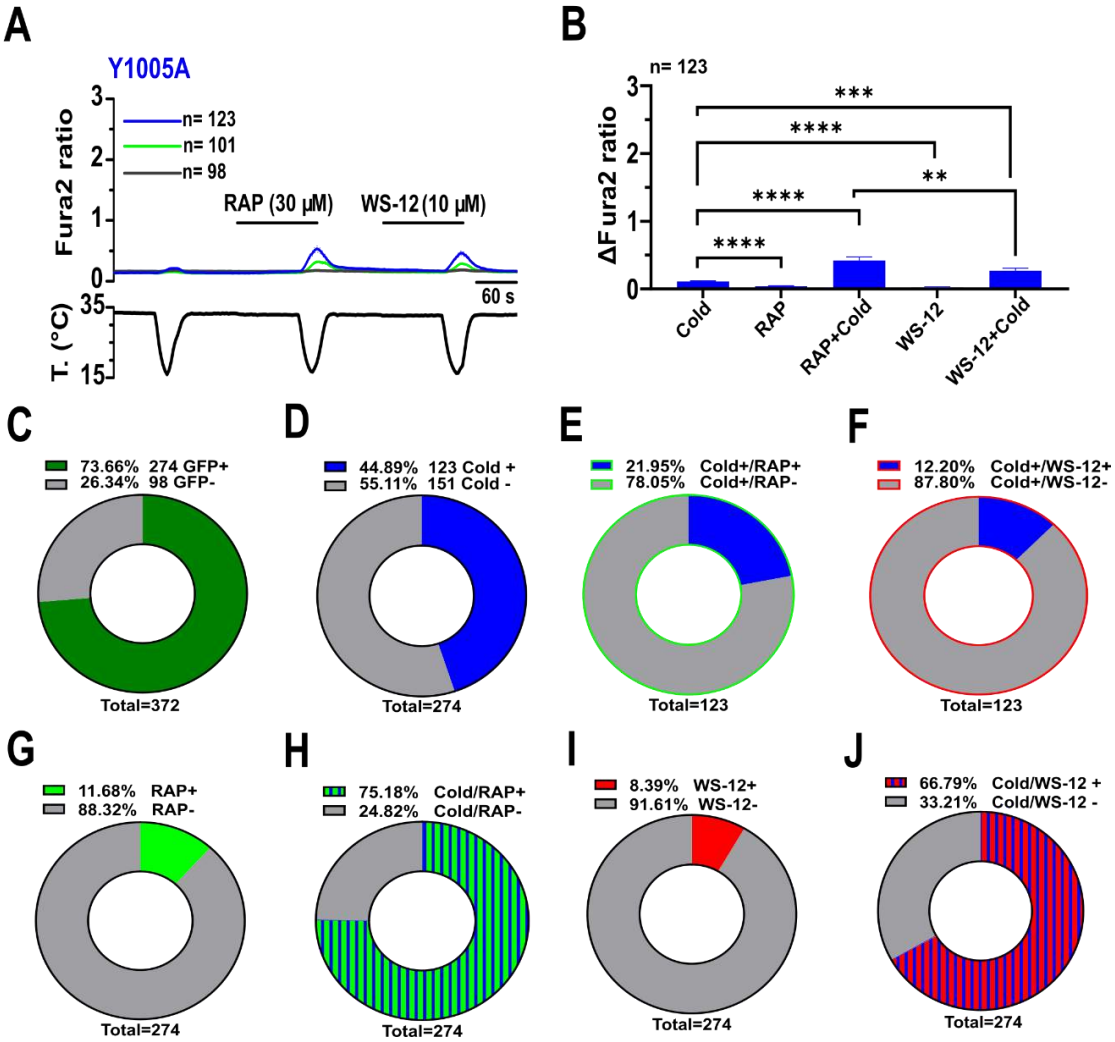

Figure 39. Rapamycin sensitized cold evoked responses in heterologously transfected HEK293 expressing Y1005A TRPM8 mutant channel. A, Average ± SEM fura2 ratio response to cold, RAP (30 µM) and WS-12 (10 µM) in HEK293 cells transiently transfected with mouse TRPM8 and GFP. GFP (+) cold sensitive cells (n=123) are shown in blue (blue trace) and GFP (+) cold insensitive cells (n=101) are shown in green (green trace) while GFP (-) cells (n=98) are sown in grey. **B,** Bar histogram summarizing the responses of cold sensitive HEK293 cells transfected with mouse TRPM8 Y1005A mutant to different agonists(n=123). Statistical significance was calculated by a one-way ANOVA followed by Bonferroni post-hoc test. **C,** Pie graph showing the percentage of GFP (+) transfected and GFP (-) non-transfected cells out of total cells (n=372). **D,** Pie graph showing the percentage of cold sensitive cells (Cold+) and cold insensitive cells (Cold-) out of the total GFP+ transfected cells (n=274). **E,** Pie graph showing the percentage of cold sensitive cells that are either rapamycin (30 µM) sensitive (Cold+ / RAP +) or rapamycin insensitive (Cold+ / RAP -) cells out of total cold responders (n=123). **F,** Pie graph showing the percentage of cold sensitive cells that are either WS-12 (10 µM) sensitive (Cold+ / WS-12 +) or WS -12 insensitive (Cold+ / WS-12 -) cells out of total cold responders (n=123). **G,** Pie graph showing the percentage of rapamycin sensitive cells (RAP+) and insensitive cells (RAP-) out of the total GFP+ transfected cells (n=274). **H,** Pie graph showing the percentage of cold evoking cells responses potentiation in the presence rapamycin (Cold/RAP+) and the insensitive cells (Cold- /RAP-) out of the total GFP+ transfected cells (n=274). **I,** Pie graph showing the percentage of WS-12 sensitive cells (WS-12+) and insensitive cells (WS-12-) out of the total GFP+ transfected cells (n=274). **J,** Pie graph showing the percentage of cold evoking cells responses potentiation in the presence of WS-12 (Cold/WS-12+) and insensitive cells (Cold- /WS-12-) out of the total GFP+ transfected cells (n=274).

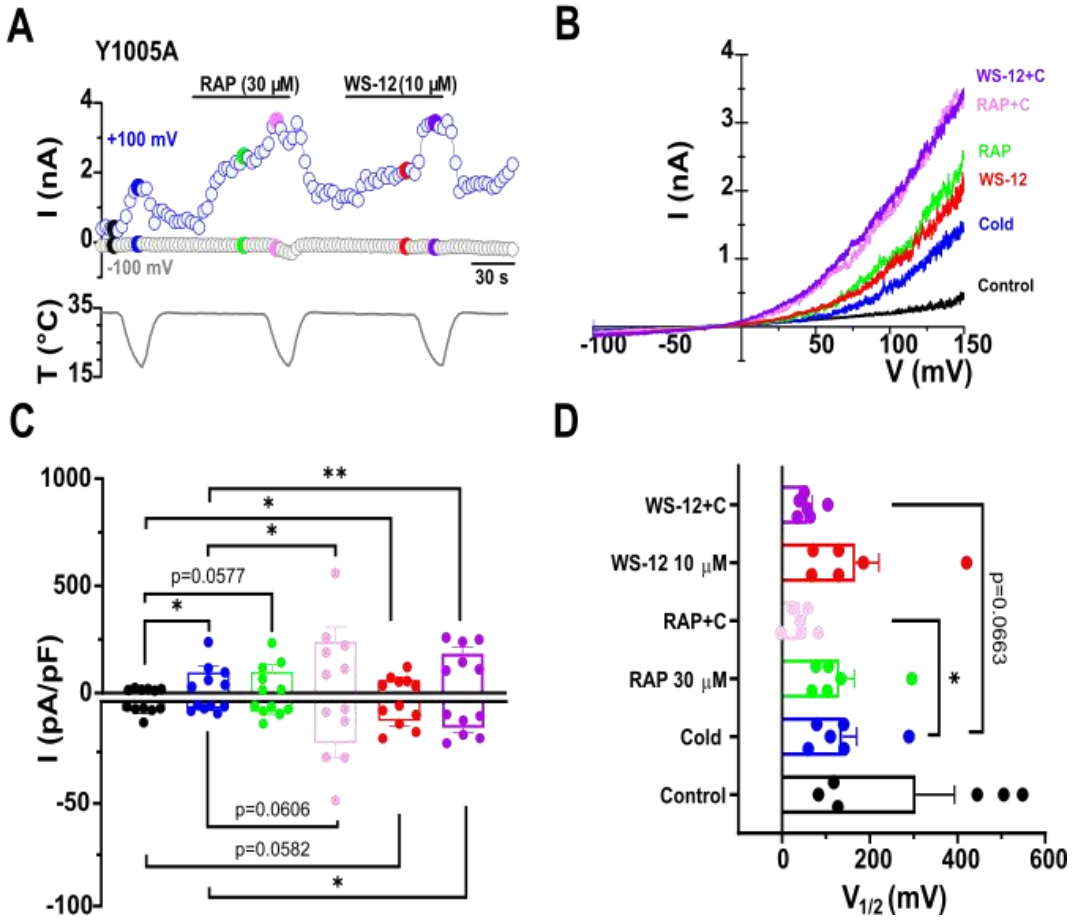

Figure 40. Rapamycin activated Y1005A TRPM8 mutant whole-cell currents expressed in HEK293 cells and induced a leftward shift of mutant TRPM8 voltage dependence. **A,** Representative time course of Y1005A TRPM8 mutant whole cell currents screened at -100 mV and +100 mV in transiently transfected HEK293 cells during sequential agonists application. The trace of simultaneous recording of the bath temperature during experiment is shown at the bottom. **B,** The current-voltage relationship (I-V) of responses presented in A**,** resulted with 800 ms voltage ramp from -100 to +150mV. The key colors of single traces coincided with specific time points in A**.** Rapamycin elicited a non-selective cationic currents TRPM8 dependent features and potentiates cold evoked responses. **C,** Bar histogram summarizing the mean ± SEM current density at +100 and -100 mV of the different stimuli presented in A, following the color code. Statistical differences were evaluated by one-way Anova followed by Bonferroni´s post-hoc test. **D,** Mean (n=6) values calculated from fitting the individual I-V curve to linear Boltzmann equation. Note rapamycin provoked a clear leftward shift of $V_{1/2}$ statistical differences were evaluated by one-way Anova followed by Bonferroni's post-hoc test.

The results of calcium imaging experiments performed on the second TRP domain mutant R1008A (Fig. 41A) where qualitatively similar to those obtained with the Y1005A mutant described in the previous section. Compared to wild-type TRPM8, R1008A showed very small reponses to cold (WT 0.5 ± 0.1, n=123 vs R1008A 0.05 ± 0.01, n=164) (p-value< 0.0001), while both RAP(WT TRPM8 RAP= 0.22 ± 0.03, n=123 vs R1008A RAP= 0.02 ± 0.0103 n=164) (p-value< 0.0001) (Fig. 43B) and WS-12 (WT TRPM8 WS-12 = 1.2 ± 0.1 , n=123 vs R1008A WS-12= 0.01 ± 0.01, n=164) (p-value< 0.0001) (Fig. 43D) did not elicite any reponses (Fig. 43B).

However, responses could be potentiated when combining RAP or WS-12 with cold (Fig. 41A,B). Moreover, cold-evoked cells activation percentage was potentiated in the presence both agonists, but was greater with WS-12 (30 µM) (Cold=24% vs RAP+cold=79% vs WS-12+cold=92%) (p-value = 0.0201, Chi-squared test) (Fig. 41D, H, and J). The cold potentiation by either RAP or WS-12 remain very altred compared to wild type channel : (WT TRPM8 RAP+cold = 2 ± 0.2, n=123 vs R1008A RAP+cold= 0.35 ± 0.03, n=164) (p-value< 0.0001) (Fig. 43C), (WT TRPM8 WS-12+cold = 2.03 ± 0.15, n=164 vs R1008A WS-12+cold= 0.34 ± 0.04, n=164) (p-value< 0.0001) (Fig. 43E).

The electrophysiological recordings confirmed the results obtained with calcium imaging:

Following whole-cell patch-clamp recordings using standard voltage ramp protocol (see the material and methods) performed in HEK293 cells expressing R1008A (Fig. 42A), cooling induced an increase in the outward current measured at +100 mV (Control=11 ± 2 pA/pF vs Cold=35 ± 11 pA/pF) (n=7, p-value= 0.04) but not inward current. While, RAP (30 µM) failed to activate outward current measured at +100 mV (Control=11 ± 2 pA/pF vs RAP=23 ± 10 pA/pF) (n=7) (Fig. 42A, C). Cold-evoked both outward current measured at +100 mV (Cold= 35 ± 11 pA/pF vs RAP+cold= 167 ± 49 pA/pF) (n=7, p-value= 0.0609) (Fig. 42C) was potentiated in the presence of RAP. WS-12 (10 µM) elicited outward current measured at +100 mV (Control=11 ± 2 pA/pF vs WS-12=30 ± 8 pA/pF) (n=7, p-value= 0.0059) (Fig. 42C). Besides, WS-12 potentiated cold-evoked outward current measured at +100 mV (Cold=35 ± 11 pA/pF vs WS-12+cold= 175 ± 36 pA/pF) (n=7, p-value= 0.014) (Fig. 42A, C).

From the current-voltage relationship (I-V) of agonists activating the TRP domain mutant R1008A-TRPM8 channel, neither RAP nor WS-12 induced a leftward shift of the voltage activation curve towards negative potentials compared to cold (Fig. 42B).

Compared to wild-type TRPM8, at basal condition, the TRP domain mutant R1008A channel showed reduced outward current measured respectively at +100 mV (WT TRPM8 Control = 28 ± 4 pA/pF, n=14 vs R1008A Control= 11 ± 2 pA/pF, n=7), and a diminished inward current measured at -100 mV (WT TRPM8 Control = -12 ± 3 pA/pF vs R1008A Control= -5 ± 1 pA/pF) (Fig.44A). R1008A cells presented a robust alteration of cold-evoked outward and inward currents compared to wild-type TRPM8 measured respectively at +100 mV (WT TRPM8 Cold = 189 ± 19 pA/pF, n=14 vs R1008A

Cold= 35 ± 11 pA/pF, n=7) and at -100 mV (WT TRPM8 Cold = -11 ± 2 pA/pF, n=14 vs R1008A Cold= -3 ± 1 pA/pF, n=7) (Fig. 44B).

Next, RAP (30 µM) application elicited a markedly altered either outward current measured at +100 mV (WT TRPM8 RAP = 114 ± 14 pA/pF, n=14 vs R1008A RAP= 23 ± 10 pA/pF, n=7), and inward current generated at -100 mV (WT TRPM8 RAP = -34 ± 8 pA/pF vs R1008A RAP= -6 ± 2 pA/pF) (p-value< 0.05) in R1008A group compared to wild type TRPM8 (Fig. 44C). Cold-activated outward current potentiation in the presence of RAP at +100 mV was severely altered in R1008A transfected HEK293 compared to WT TRPM8 group (WT TRPM8 RAP+cold = 360 ± 36 pA/pF vs R1008A RAP+cold= 167 ± 49 pA/pF) (p-value=0.07), in the same line cold-activated inward current potentiation in the presence of RAP measured at -100 mV was markedly reduced in R1008A cells compared to WT TRPM8 group (WT TRPM8 RAP+cold = -160.1 ± 37 pA/pF, n=14 vs R1008A RAP+cold= -11 ± 3 pA/pF, n=7) (p-value< 0.001) (Fig. 44D). WS-12 generated both outward current at +100 mV (WT TRPM8 WS-12 = 329 ± 53 pA/pF vs R1008A WS-12= 35 ± 7 pA/pF) (p-value< 0.001), and inward current at -100 mV (WT TRPM8 WS-12 = -165 ± 54 pA/pF vs R1008A WS-12= -13 ± 4 pA/pF) (p-value< 0.05) were severely altered in R1008A cells compared to wild type (Fig.44E). Cold-evoked outward current at +100 mV (WT TRPM8 WS-12+cold = 456 ± 53 pA/pF vs R1008A WS-12+cold= 175 ± 36 pA/pF) (p-value< 0.001) and inward current at -100 mV (WT TRPM8 WS-12+cold = -263 ± 42 pA/pF vs R1008A WS-12+cold= -30 ± 8 pA/pF) (p-value< 0.0001) potentiation in the presence of WS-12 were significantly decreased in R1008A group compared to wild type TRPM8 (Fig. 44F).

Notabely, the cold temperature threshold was extracted from the current time course following cooling (Fig. 42A) in HEK293 cell expressing R1008A mutant and showed a significant shift of the threshold toward colder temperature compared to WT TRPM8 (WT TRPM8 = 27.3 ± 0.3 ˚C, n=11 vs R1008A=21 ± 0.8 ˚C, n=5) (p-value< 0.0001) (Fig. 45A). In control condition, the voltage dependence ($V_{1/2}$) of R1008A estimate was not possible since the values expected were extremly high, therfore we did not fit the activation curves (I-V) to a Boltzmann equation.

I conclude that The TRP doamin muation R1008A, likwise Y1005A, is essential for different used TRPM8 agonists tested (Cold , RAP and WS-12) channel activation . The current result supported again the relevance of TRPM8 domain in the allosteric effect modulation of TRPM8 channel(Taberner et al., 2014). Besides, knowing that the R1008 residue is a PIP_2 binding site and that the PIP2 is essential for channel activation thus could also explain the decreased sensisivity of this mutant channel to different tested agonists includig RAP (Rohács et al., 2005).

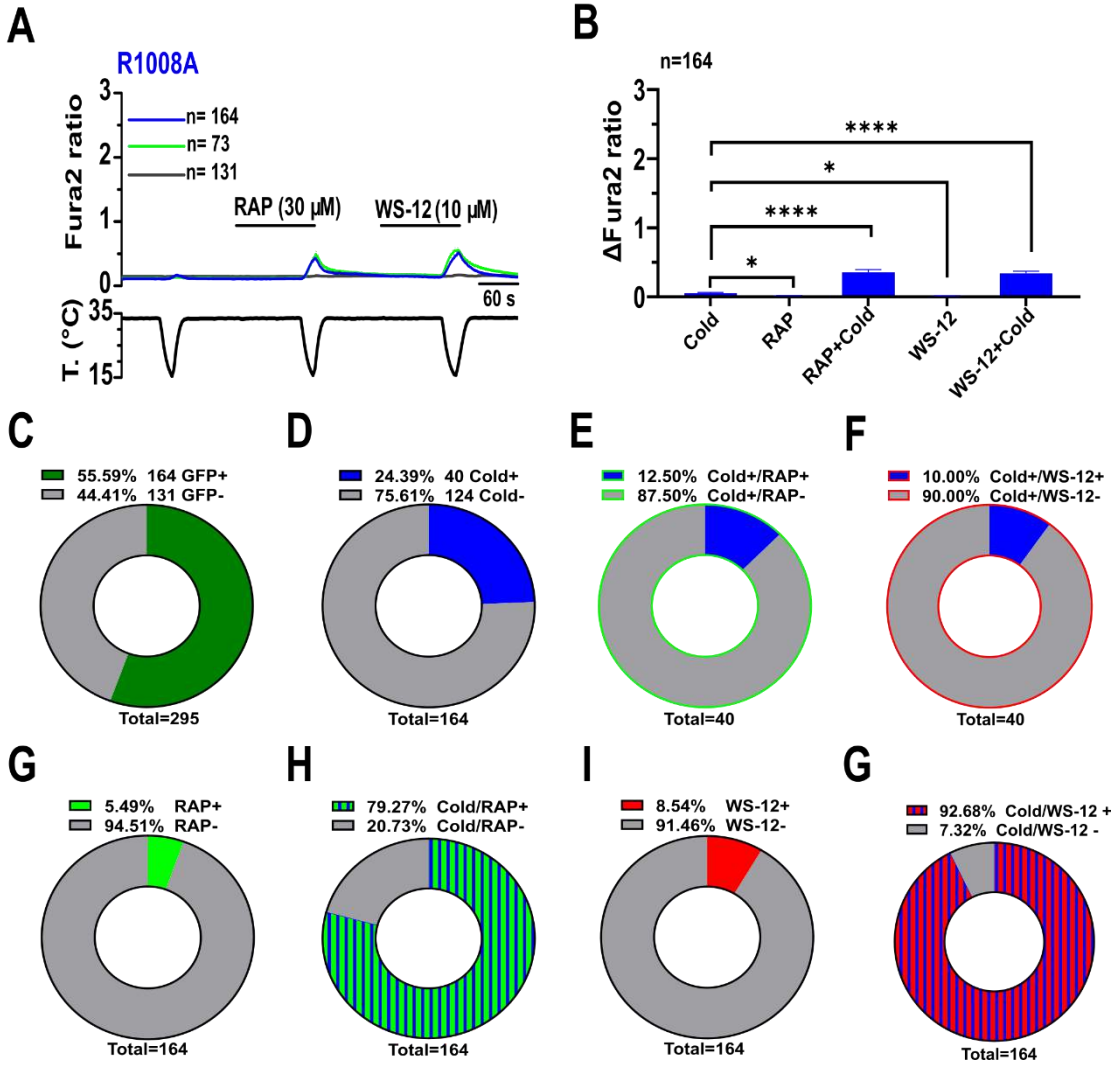

Figure 41. Rapamycin did not activate heterologously transfected HEK293 cells expressing R1008A TRPM8 mutant channel, but it potentiated cold evoked responses. A, Average ± SEM fura2 ratio response to cold, RAP (30 µM) and WS-12 (10 µM) in HEK293 cells transiently transfected with R1008A mouse TRPM8 mutant and GFP. GFP (+) cold sensitive cells (n=124) are shown in blue (blue trace) and GFP (+) cold insensitive cells (n=73) are shown in green (green trace) while GFP (-) cells (n=131) are shown in grey. **B,** Bar histogram summarizing the responses of GFP+ HEK293 cells transfected with R1008A mouse TRPM8 to different agonists (n=164). Statistical significance was calculated by a one-way ANOVA followed by Bonferroni post-hoc test. **C,** Pie graph showing the percentage of GFP (+) transfected and GFP (-) non-transfected cells out of total cells (n=295). **D,** Pie graph showing the percentage of cold sensitive cells (Cold+) and cold insensitive cells (Cold-) out of the total GFP+ transfected cells (n=164). **E,** Pie graph showing the percentage of cold sensitive cells that either rapamycin (30 µM) sensitive (Cold+ / RAP +) or rapamycin insensitive (Cold+ / RAP -) cells out of total cold responders (n=40). **F,** Pie graph showing the percentage of cold sensitive cells that are either WS-12 (10 µM) sensitive (Cold+ / WS-12 +) or WS -12 insensitive (Cold+ / WS-12 -) cells out of total cold responders (n=40). **G,** Pie graph showing the percentage of rapamycin sensitive cells (RAP+) and insensitive cells (RAP-) out of the total GFP+ transfected cells (n=164).**H,** Pie graph showing the percentage of cold evoking cells responses potentiation in the presence of rapamycin (Cold/RAP+) and the insensitive cells (Cold/RAP-) out of the total GFP+ transfected cells (n=164). **I,** Pie graph showing the percentage of WS-12 sensitive cells (WS-12+) and insensitive cells (WS-12-) out of the total GFP+ transfected cells (n=164).**J,** Pie graph showing the percentage of cold evoking cells responses potentiation in the presence of WS-12 (Cold/WS-12+) and insensitive cells (Cold/WS-12-) out of the total GFP+ transfected cells (n=164).

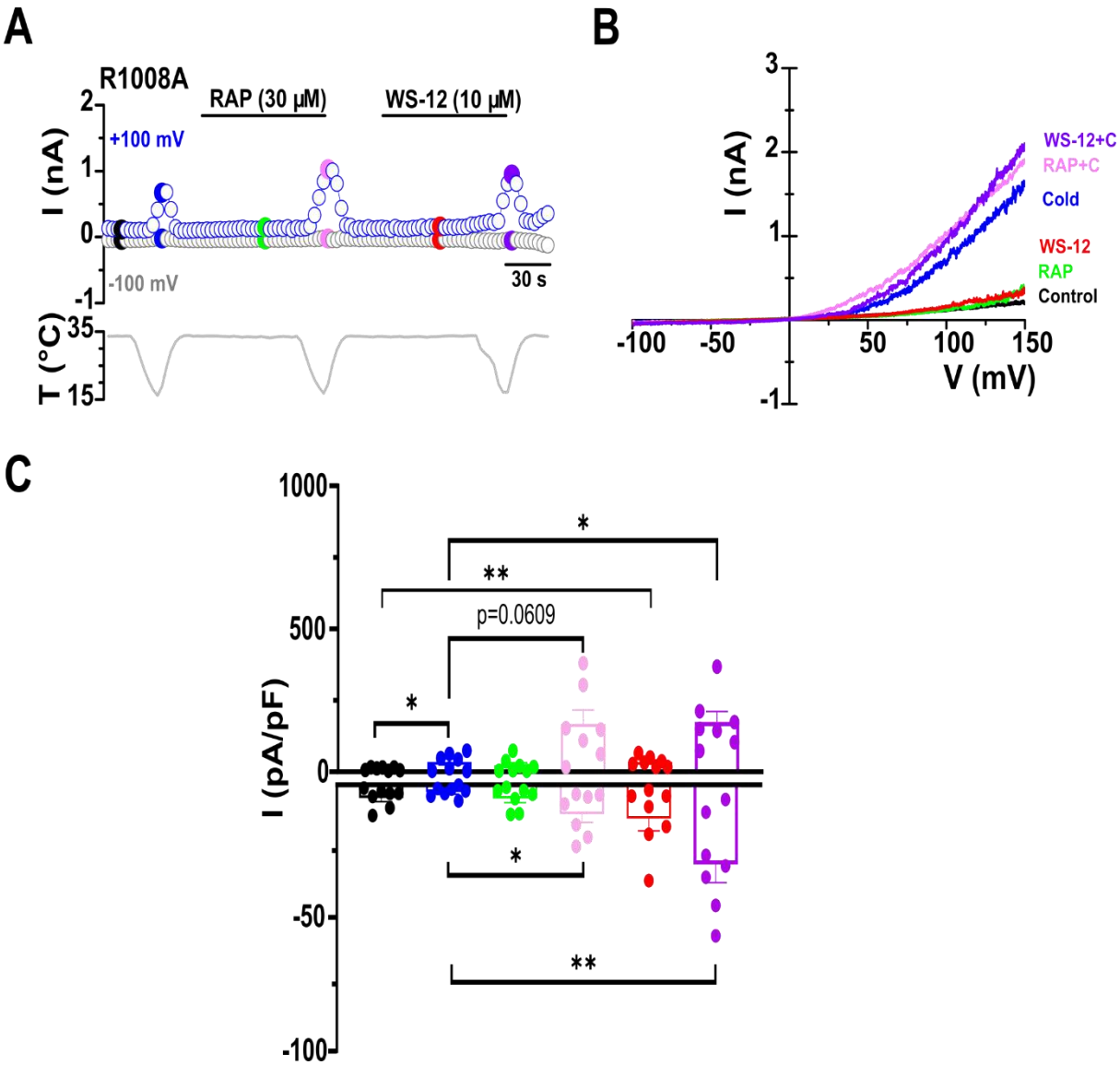

Figure 42. Rapamycin activated negligible R1008A TRPM8 mutant whole-cell currents expressed in HEK293 cells and induced a leftward shift of mutant TRPM8 voltage dependence. **A,** Representative time course of I846A TRPM8 mutant whole cell currents screened at -100 mV and +100 mV in transiently transfected HEK293 cells during sequential agonists application. The trace of simultaneous recording of the bath temperature during experiment is shown at the bottom. **B,** The current-voltage relationship (I-V) of responses presented in A**,** resulted with 800 ms voltage ramp from -100 to +150 mV. The key colors of single traces coincide with specific time points in A**.** Rapamycin elicited a non-selective cationic currents TRPM8 dependent features and potentiates cold evoked responses. **C,** Bar histogram summarizing the mean ± SEM current density at +100 and -100 mV of the different stimuli presented in A (n=7), following the color code. Statistical differences were evaluated by one-way Anova followed by Bonferroni´s post-hoc test.

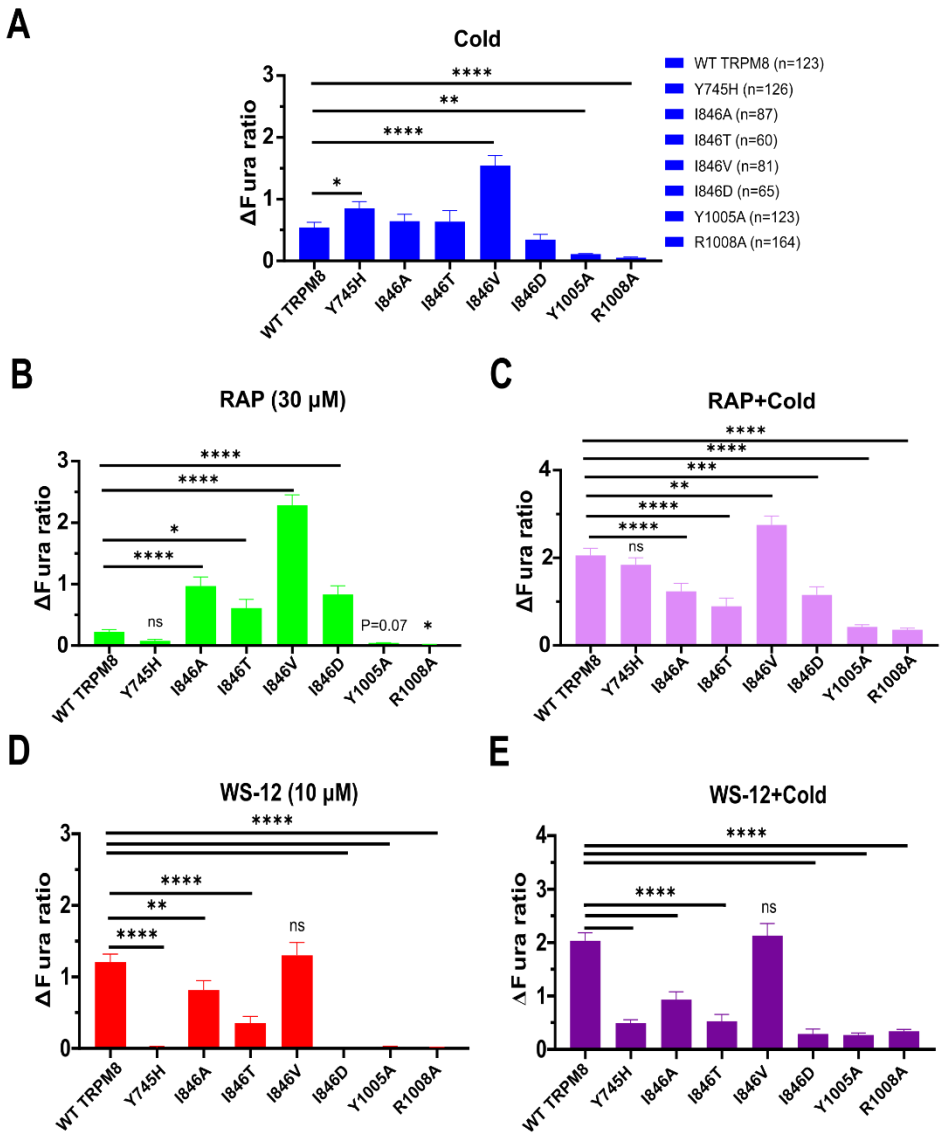

Figure 43. Summary of TRPM8 Calcium imaging response amplitude of mouse wild type (WT) TRPM8 compared to different TRPM8 mutants following the application of different TRPM8 agonists. A, Bar histogram summarizing the mean ± SEM calcium amplitude responses of GFP+ HEK293 cells transfected with mouse TRPM8 (WT or mutants) to cold. **B,** Bar histogram summarizing the mean ± SEM calcium amplitude responses of GFP+ HEK293 cells transfected with mouse TRPM8 (WT or mutants) to rapamycin (30 μM). **C,** Bar histogram summarizing the mean ± SEM calcium amplitude responses of GFP+ HEK293 cells transfected with mouse TRPM8 (WT or mutants) to cold in the presence of rapamycin. **D,** Bar histogram summarizing the mean ± SEM calcium amplitude the responses of GFP+ HEK293 cells transfected with mouse TRPM8 (WT or mutants) to WS-12 (10 μM). **E,** Bar histogram summarizing the mean ± SEM calcium amplitude responses of GFP+ HEK293 cells transfected with mouse TRPM8 (WT or mutants) to cold in the presence of WS-12. Statistical significance was calculated by a one-way ANOVA followed by Bonferroni post-hoc test. Asterisk are used for comparing the effect of different stimuli (*, p-value< 0.05; **, p-value< 0.01; ***, p-value< 0.001; ****, p-value< 0.0001).

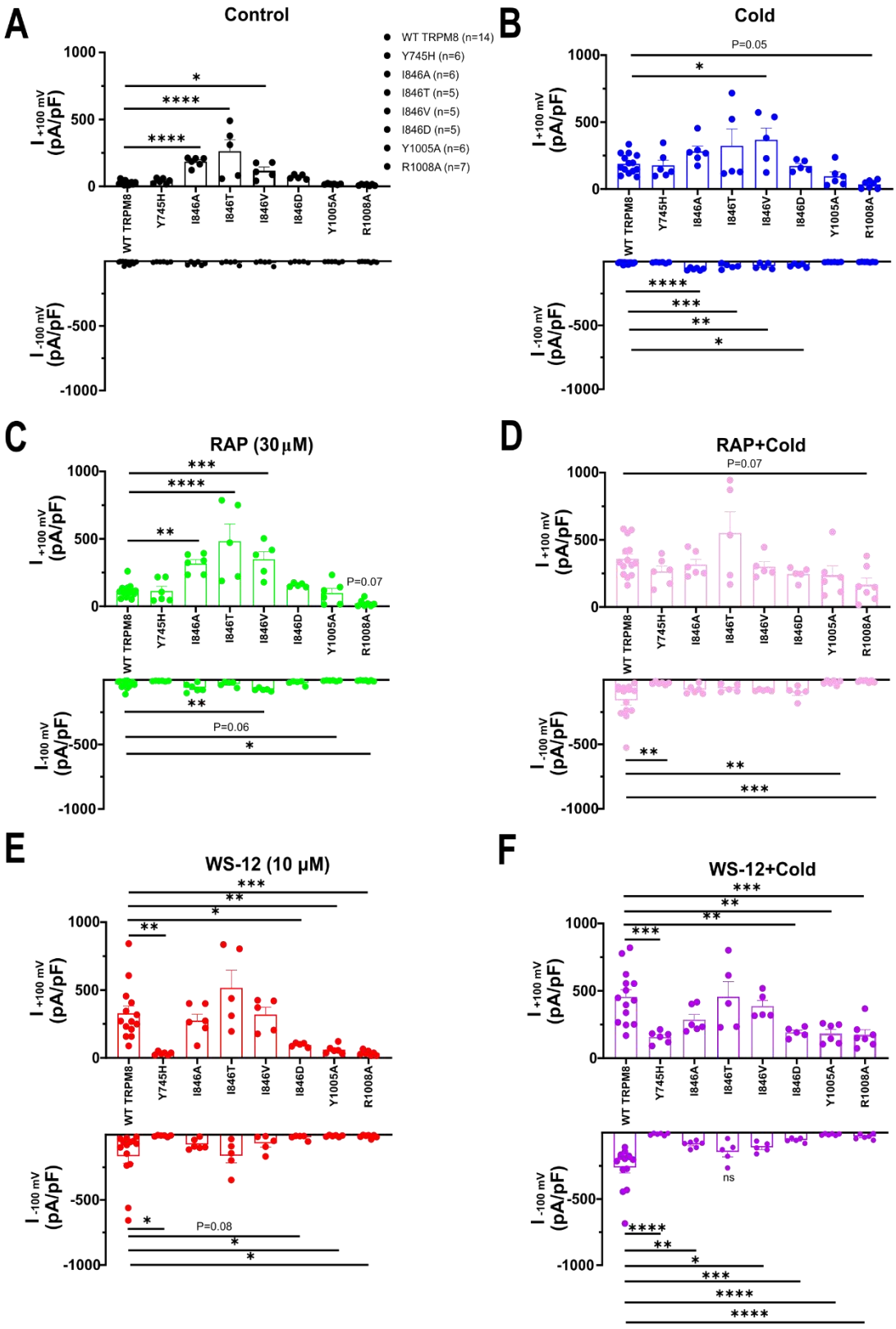
A
Control
WT TRPM8 (n=14)
Y745H (n=6)
I846A (n=6)
I846T (n=5)
I846V (n=5)
I846D (n=5)
Y1005A (n=6)
R1008A (n=7)
B
Cold
P=0.05
C
RAP (30 µM)
P=0.07
P=0.06
D
RAP+Cold
P=0.07
E
WS-12 (10 µM)
P=0.08
F
WS-12+Cold
ns
I +100 mV (pA/pF)
I -100 mV (pA/pF)
WT TRPM8
Y745H
I846A
I846T
I846V
I846D
Y1005A
R1008A

Figure 44. Summary of TRPM8 Current density responses of wild type TRPM8 compared to TRPM8 mutants following the application of different TRPM8 agonists. The outward and inward current densities obtained respectively at +100 mV and -100 mV were extracted from the voltage ramp protocol (-100 mV up to +150 mV, 800 ms; see materials and methods) applied in HEk293cells expressing both wild type TRPM8 or different TRPM8 mutants tested. **A,** Bar histogram summarizing the mean ± SEM current densities responses of GFP+ HEK293 cells transfected with mouse TRPM8 (wild type or mutants) in control condition. **B,** Bar histogram summarizing the mean ± SEM current densities responses of GFP+ HEK293 cells transfected with mouse TRPM8 (wild type or mutants) to cold. **C,** Bar histogram summarizing the mean ± SEM current densities responses of GFP+ HEK293 cells transfected with mouse TRPM8 (wild type or mutants) to rapamycin (30 μM). **D,** Bar histogram summarizing the mean ± SEM current densities responses of GFP+ HEK293 cells transfected with mouse TRPM8 (wild type or mutants) to cold in the presence of rapamycin. **E,** Bar histogram summarizing the mean ± SEM current densities responses of GFP+ HEK293 cells transfected with mouse TRPM8 (wild type or mutants) to WS-12 (10 μM). Statistical significance was calculated by a one-way ANOVA followed by Bonferroni post-hoc test.

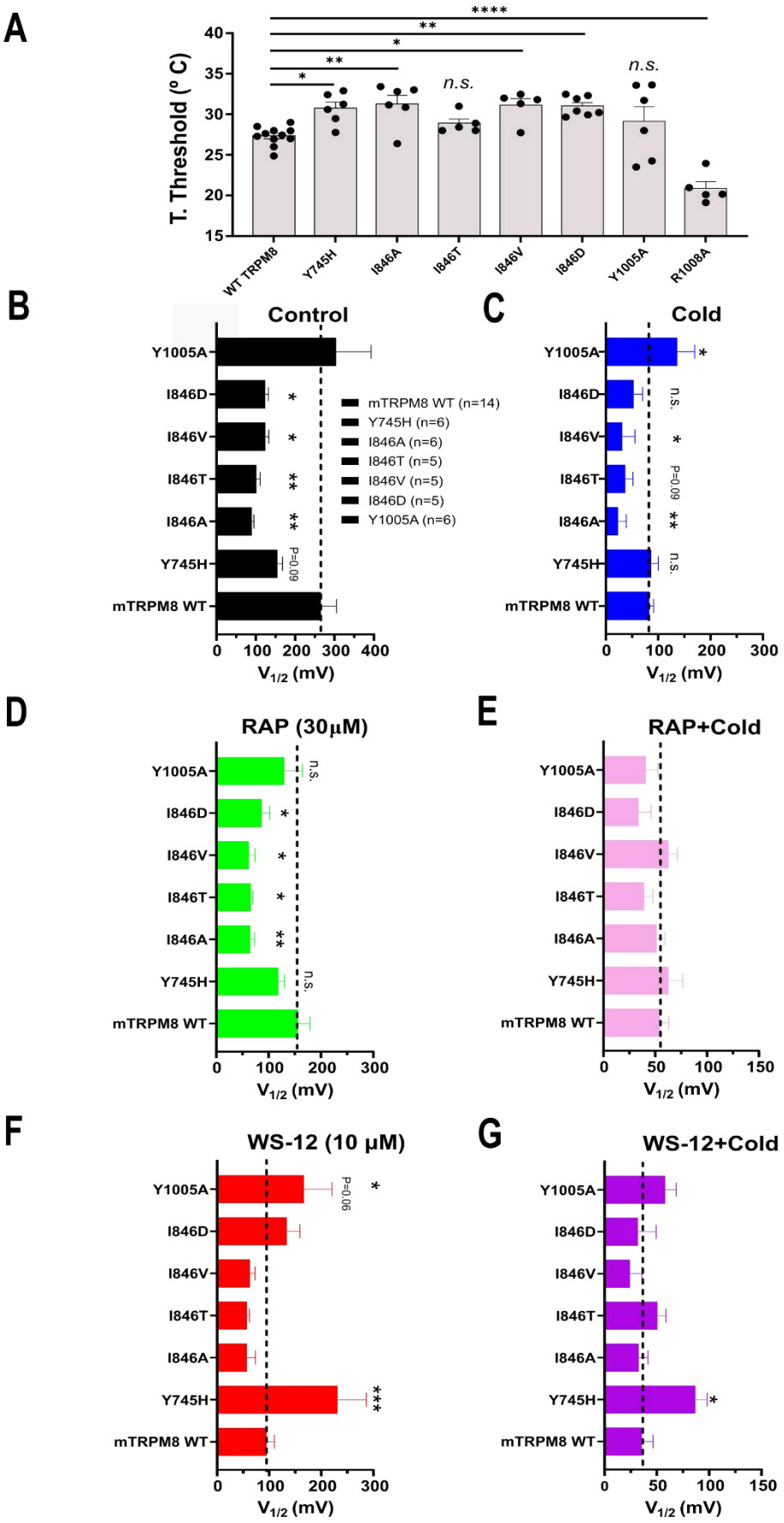
A
T. Threshold (º C)
WT TRPM8
Y745H
I846A
I846T
I846V
I846D
Y1005A
R1008A
n.s.
B
Control
mTRPM8 WT (n=14)
Y745H (n=6)
I846A (n=6)
I846T (n=5)
I846V (n=5)
I846D (n=5)
Y1005A (n=6)
P=0.09
V1/2 (mV)
C
Cold
D
RAP (30µM)
E
RAP+Cold
F
WS-12 (10 µM)
G
WS-12+Cold

Figure 45. Summary of cold temperature threshold of mouse TRPM8 (WT and mutants), and their voltage of half maximal activation $V_{1/2}$ (mV) following TRPM8 agonists application. A, Bar histogram summarizing the mean ± SEM of the cold temperature threshold obtained from transfected HEK293 cells either with wild type TRPM8 or mutants. The temperature threshold was obtained during the voltage ramp protocol, and it is the temperature from which the current activation increase was occurred. Statistical significance was calculated by a one-way ANOVA followed by Bonferroni post-hoc test. **B**, Bar histogram summarizing the mean ± SEM of voltage of half maximal activation ($V_{1/2}$) obtained from HEK293 cells transfected with mouse TRPM8 (wild type or mutants) in control condition. The $V_{1/2}$ were data obtained from fitting individual current-voltage (I-V) curve following different treatments during voltage ramp protocol from -100 mV to + 150 mV. **C**, Bar histogram summarizing the mean ± SEM of voltage of half maximal activation ($V_{1/2}$) obtained from HEK293 cells transfected with mouse TRPM8 (wild type or mutants) to cold. **D**, Bar histogram summarizing the mean ± SEM of voltage of half maximal activation ($V_{1/2}$) obtained from HEK293 cells transfected with mouse TRPM8 (wild type or mutants) to rapamycin (30 μM). **E**, Bar histogram summarizing the mean ± SEM of voltage of half maximal activation ($V_{1/2}$) obtained from HEK293 cells transfected with mouse TRPM8 (wild type or mutants) to cold in the presence of rapamycin. **F**, Bar histogram summarizing the mean ± SEM of voltage of half maximal activation ($V_{1/2}$) obtained from HEK293 cells transfected with mouse TRPM8 (wild type or mutants) to WS-12 (10 μM). **F**, Bar histogram summarizing the mean ± SEM of voltage of half maximal activation ($V_{1/2}$) obtained from HEK293 cells transfected with mouse TRPM8 (wild type or mutants) to Cold in the presence WS-12. Statistical significance was calculated by a one-way ANOVA followed by Bonferroni post-hoc test.

4.2 The segment 4 TRPM8 mutants I846A and I846T are constitutively active at rest, and alter the AMTB blockade efficacy

TRPM8 channels are calcium permeable (Voets et al., 2004, 2007a; Yin et al., 2018, 2022; Palchevskyi et al., 2022). Mutants I846A and I846T TRPM8 show higher resting calcium levels compared to both wild type TRPM8 and to GFP- (not expressing TRPM8 channel) cells. Thus, I hypothesized that TRPM8 may be constitutively open at rest. To test this hypothesis, I examined the effect of the specific TRPM8 blocker AMTB (10 µM) on basal calcium levels in both mutants.

The GFP+ cells expressing wild type TRPM8 channel (blue trace n=26) showed similar basal calcium levels compared to GFP- (i.e. non transfected cells) (Grey trace n=44) (Fig. 46A), and the application of AMTB (10 µM) did not modify this level (Fig. 46A, B). In contrast, cells expressing either I846A or I846T had much higher resting calcium levels compared to wild type or non-transfected cells. At baseline, the fura2 ratio of either I846A group (WT TRPM8 ratio = 0.16 ± 0.01, n=26 vs I846A ratio= 0.48 ± 0.06, n=33) (p-value < 0.0001) or I846T group (WT TRPM8 ratio = 0.16 ± 0.01, n=26 vs I846T ratio= 0.24 ± 0.02, n=72) (ns, p-value= 0.5573) were higher than wild type group (Fig. 46G). Note that the baseline in I846A mutant group is markedly higher compared to I846T mut ant group (I846A ratio= 0.48 ± 0.06, n=33 vs I846T ratio= 0.24 ± 0.02, n=72) (p-value < 0.0001).

Application of AMTB (10 µM), markedly decreased the elevated fura2 ratios observed in cells expressing either mutant I846A (Control = 0.48± 0.06 vs AMTB= 0.26 ± 0.03, n=33) (p-value< 0.0001; Tow-Tailed, Unpaired-T-test) or I846T (Fura2 ratio Before AMTB = 0.24 ± 0.02 vs Fura2 ratio After AMTB= 0.16 ± 0.01, n=72) (p-value< 0.0001; Tow-Tailed, Unpaired-T-test) (Fig. 46D, F).

These results suggest that block of the open mutant channels by AMTB decreases the steady influx of calcium at the resting potential of the cell. In contrast, no changes were obdrtvrd in the cells expressing WT TRPM8, consistent with the idea that wildtype channels are close at 33 ºC.

As expected AMTB, completely suppressed cold-evoked responses in cells expressing wildtype TRPM8 (Fig. 46A). In contrast, cells expressing I846A or I846T mutants showed only a partial reduction in cold-evoked responses in the presence of AMTB (Fig. 46C, E) (WT TRPM8 AMTB+cold = 0.002 ± 0.001, n=26 vs I846A AMTB+cold = 0.35 ± 0.07, n=33) (p-value< 0.0001) and (WT TRPM8 AMTB+cold = 0.002 ± 0.001, n=26 vs I846T AMTB+cold = 0.07 ± 0.02, n=72) (ns, p-value=0.5405) compared to wild type (Fig. 46H). The partial AMTB inhibition phenotype obderved was bigger in I846A muatnt compared to I846T (I846A AMTB+cold = 0.35 ± 0.01, n=26 vs I846T AMTB+cold = 0.07 ± 0.02, n=72) (p-value< 0.0001) compared to wild type (Fig. 46H).

To investigate the mechanism leading to the elevated resting calcium levels in the mutant channels, I perfomed whole-cell patch-clamp recordings. At rest (33 ºC), HEK293 cells expressing the I846A mutant showed large outward currents mesured at +100 mV compared to the wild type TRM8 group

(WT TRPM8 Control = 36 ± 9 pA/pF, n=6 vs I846A Control = 111 ± 23 pA/pF, n=5) (p-value< 0.05; Tow-Tailed, Unpaired-T-test) (Fig. 47E). The application of AMTB (10 µM) significantly decreased outward current both in wild type TRPM8 (WT TRPM8 Control = 36 ± 9 pA/pF vs WT TRPM8 AMTB = 21 ± 5 pA/pF, n=6) (p-value< 0.05; Tow-Tailed, paired-T-test), and in the I846A mutant (I846A Control = 111 ± 23 pA/pF vs I846A AMTB = 13 ± 6 pA/pF, n=5) (p-value< 0.05; Tow-Tailed, paired-T-test). The decrease was very marked in cells expressing I846A, suggesting the presence of a large basal current that is AMTB-sensitive (Fig. 47E). The recovery of cold-evoked currents after AMTB block was minimal in wild type channels (Fig. 47A). In contrast, the recovery was small but evident in the I846A mutant (Fig. 47A, B). The fast recovery from AMTB blockad in I846A groupe compared to wild type could suggeste a decreaed affinity to AMTB at 10 µM following S4 I846 muation.

I conclude that mutations I846A and I846T in TM segment 4 generate constitutively active channels. These mutants are also blocked by AMTB, but they may have lower affinity to the blocker, something that needs to be explored further.

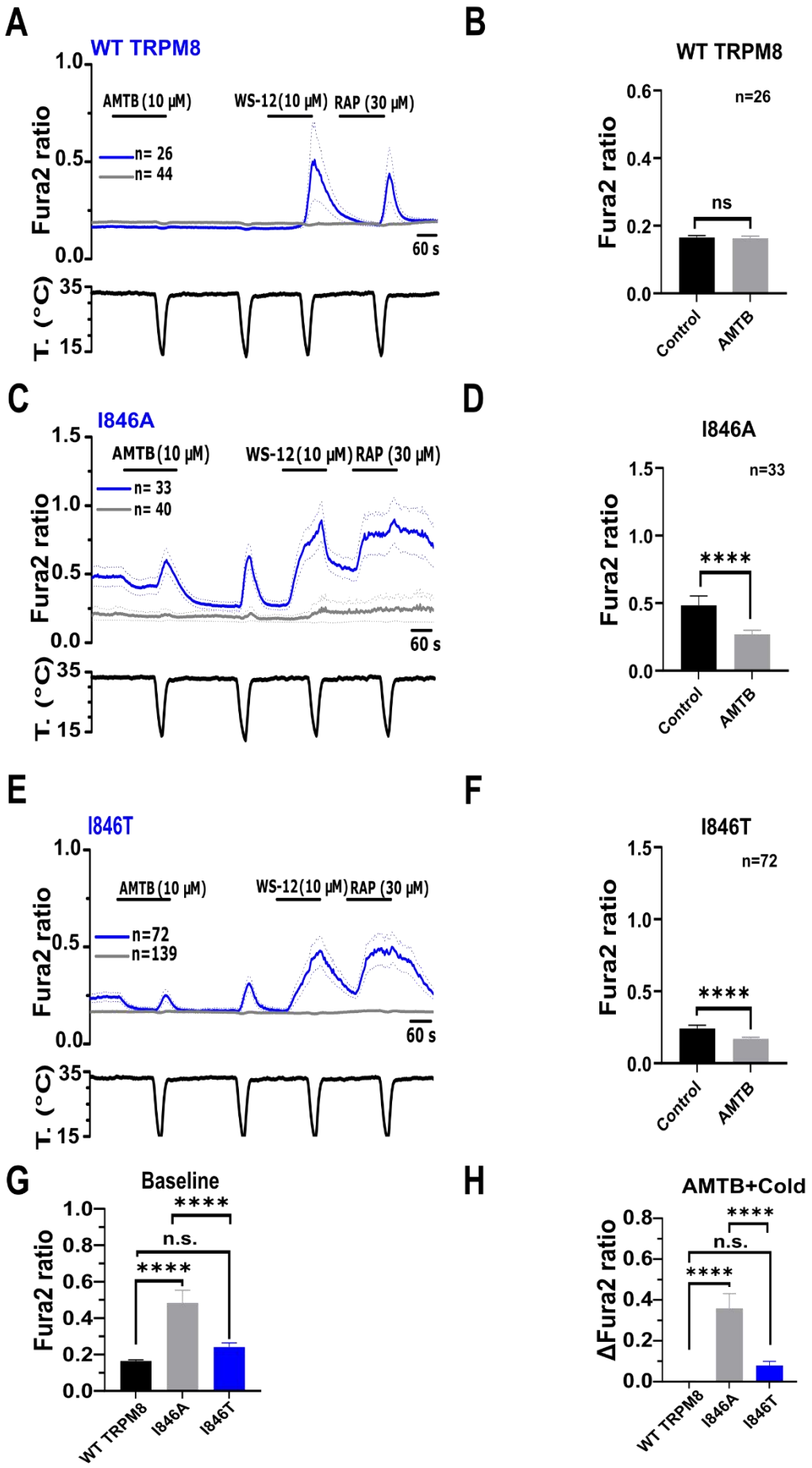
A
WT TRPM8
AMTB (10 μM)
WS-12(10 μM)
RAP (30 μM)
n= 26
n= 44
Fura2 ratio
T. (°C)
60 s
B
WT TRPM8
n=26
ns
Control
AMTB
C
I846A
n= 33
n= 40
D
I846A
n=33
****
E
I846T
n=72
n=139
F
I846T
n=72
G
Baseline
n.s.
H
AMTB+Cold
ΔFura2 ratio
WT TRPM8
I846A
I846T

Figure 46. AMTB reversed the constitutively active ´´open pore `` phenotype observed in TRPM8 S4 mutants (I846A and I846T), and the S4 mutations affected the AMTB inhibitory efficacy. A, Average ± SEM fura2 ratio response to AMTB (10 µM), cold, WS-12 (10 µM) and RAP (30 µM) in HEK293 cells transiently transfected with wild type TRPM8 and GFP. The mean ± SEM ratio of GFP (+) cold-sensitive cells (n=26) is shown in blue (blue trace) and GFP (-) cells (n=44) is shown in grey. Note the strong blockade of AMTB as well as the long wash out time. **B,** Bar histogram summarizing the responses of GFP+ HEK293 cells transfected with wild type mouse TRPM8 to different agonists (n=26). Statistical significance was calculated by unpaired student-T test. **C, D.** Analysis of the I846A mutant. Note the decrease in AMTB blockade effect and the faster recovery of responses. **E, F,** Analysis of AMTB effect on the I846T mutant. **G,** Bar histogram summarizing the fura2 ratio baseline of three different GFP+ HEK293 cells group transfected with wild type, I846A or I846T mouse TRPM8. Statistical significance was calculated by a one-way ANOVA followed by Bonferroni post-hoc test. **H,** Bar histogram summarizing fura2 ratio calculated during cooling in the presence of AMTB (AMTB+cold) comparing three GFP+ HEK293 cells transfected groups with wild type TRPM8, I846A or I846T. Statistical significance was calculated by a one-way ANOVA followed by Bonferroni post-hoc test.

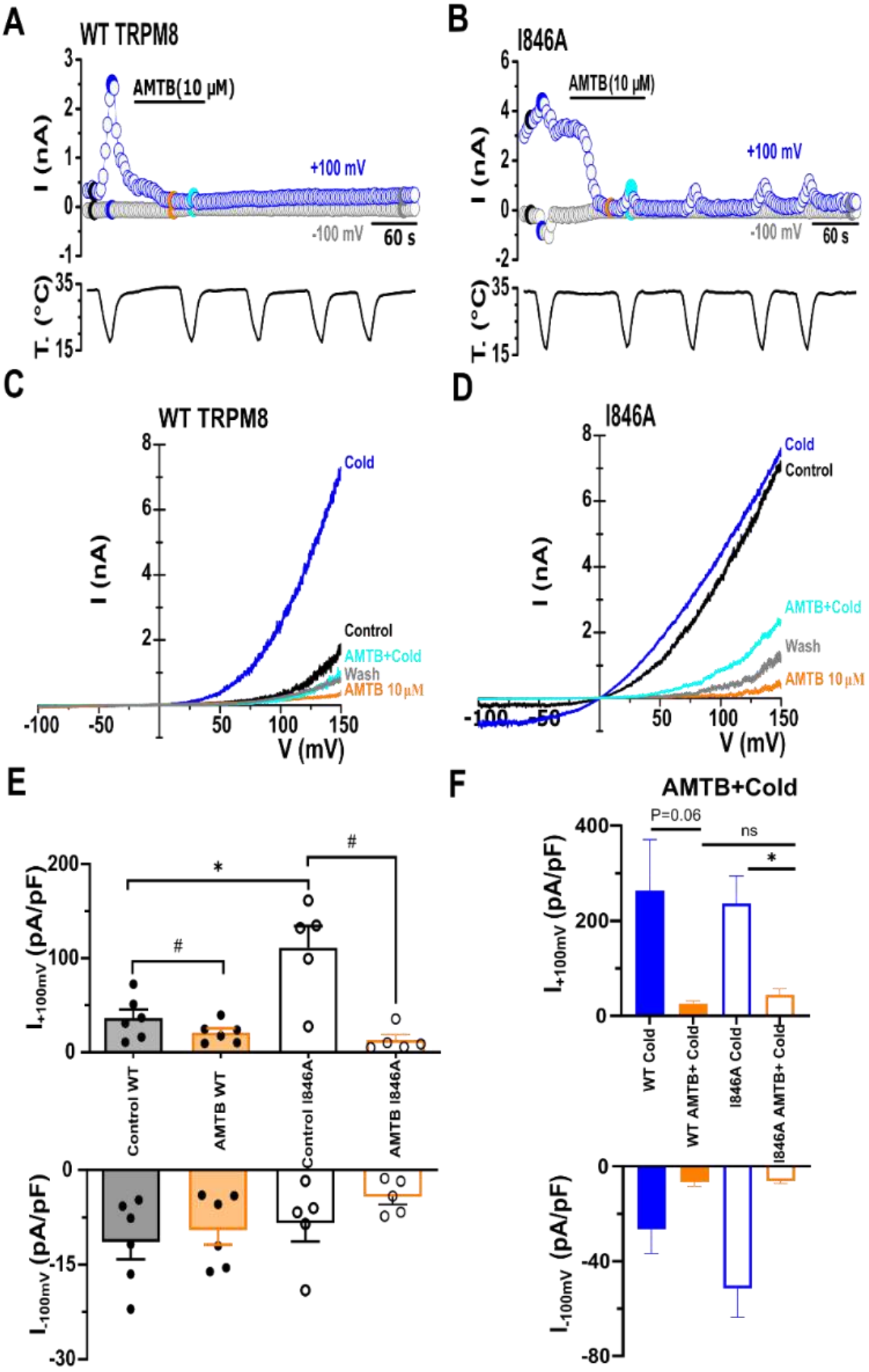
A
WT TRPM8
AMTB(10 μM)
+100 mV
-100 mV
60 s
I (nA)
T. (°C)
B
I846A
AMTB(10 μM)
+100 mV
-100 mV
60 s
I (nA)
T. (°C)
C
WT TRPM8
Cold
Control
AMTB+Cold
Wash
AMTB 10 μM
I (nA)
V (mV)
D
I846A
Cold
Control
AMTB+Cold
Wash
AMTB 10 μM
I (nA)
V (mV)
E
I+100mV (pA/pF)
Control WT
AMTB WT
Control I846A
AMTB I846A
I-100mV (pA/pF)
F
AMTB+Cold
P=0.06
ns
I+100mV (pA/pF)
WT Cold
WT AMTB+ Cold
I846A Cold
I846A AMTB+ Cold
I-100mV (pA/pF)

Figure 47. AMTB reversed the open pore phenotype observed in TRPM8 mutant I846A and decreased the high outward current density at control condition. A, Representative time course of wild typeTRPM8 (WT TRPM8) whole cell currents calculated at -100 mV and +100 mV in transiently transfected HEK293 cells during sequential Cold application in the presence or absence of AMTB. The trace of simultaneous recording of the bath temperature during experiment is shown at the bottom. **B,** Representative time course of I846A TRPM8 (WT TRPM8) whole cell currents screened at -100 mV and +100 mV in transiently transfected HEK293 cells during cold application in the presence and absence of the blocker AMTB. The trace of simultaneous recording of the bath temperature during experiment is shown at the bottom. **C,** WT TRPM8 current-voltage relationship (I-V) of responses presented in A**,** resulted with 800 ms voltage ramp from -100 to +150mV. The key colours of single traces coincide with specific time points in A**.** AMTB elicited a rightward shift of voltage activation curve and blocked cold evoking leftward shift of the voltage activation curve. **D,** The I846A current-voltage relationship (I-V) of responses presented in A**,** resulted with 800 ms voltage ramp from -100 to +150 mV. The key colours of single traces coincide with specific time points in B**.** AMTB elicited a rightward shift of voltage activation curve and blocked cold evoking leftward shift of the voltage activation curve. **E,** Bar histogram summarizing the mean ± SEM current density at +100 and -100 mV in control condition and in the presence of AMTB comparing HEK293 expressing wild type TRPM8 or I846A represented respectively in A and B. Statistical differences were evaluated by Student-t test (paired comparison within the same group and unpaired comparison between different groups). **E,** Bar histogram summarizing the mean ± SEM current density at +100 and -100 mV during cooling in the presence or absence of AMTB in HEK293 expressing wild type TRPM8 or I846A represented respectively in A and B. Statistical differences were evaluated by Student-t test (paired comparison within the same group and unpaired comparison between different groups).

Conclusion of this chapter:

- Segment 4 mutations at residue I846 created a constitutively active TRPM8 channel characterized by an open pore at resting temperature, which is reversed by TRPM8 blocker AMTB.
- AMTB antagonism efficacy is decreased following mutation at segment 4 residue I846.

4.3 The segment 4 TRPM8 mutants I846A and I846T show an altered channel trafficking

As shown in the previous sections, the segment 4 mutants I846A and I846T were characterized by eleveated resting calcium levels. Very often, mutations lead to defects in proper channel assembly detected by a quality control mechanism and leading alteration in the normal trafficking of the protein towards the plasma membrane and its retention within the endoplasmic reticulum (Ellgaard & Helenius, 2003). Here, I investigated whether this may be happening with these two mutants.

Previous studies showed that TRPM8 can tetramerazie and form functional ion channels in the ER compartment (Phelps & Gaudet, 2007; Pertusa et al., 2014) . The activity of these channels can be monitored with calcium imaging techniques. The protocol involved the sequential application of cold pulses, the first in the presence of extracellular calcium (2.4 mM), followed by calcium free solution (Ø Ca^{2+}).

In HEK293 cells expressing wildtype TRPM8 channels, application of a cold ramp in the presence of 2.4 mM Ca^{2+} evoked an increase of fura2 ratio (Fig. 48A). In contrast, in Ca^{2+}- free solution (Ø Ca^{2+}), the application of a cold ramp did not evoke activation (Fig. 48A, B), suggesting that calcium signals depend exclusively on calcium influx from the outside, through the opening of channels at the plasma membrane. Also noteworthy, removing extracellular calcium during a few minutes did not modify baseline calcium levels suggesting very low membrane flux of calcium (Pertusa et al., 2012).

As shown previously, cells expressing either I846A or I846T mutants showed elevated calcium levels at rest, compared to either untransfected (i.e GFP-) cells or to cells expressing wildtype channels (Fig. 48 C, E): (WT TRPM8 ratio = 0.2 ± 0.01, n=47 vs I846A ratio= 0.8 ± 0.2, n= 55) (p-value= 0.0003) and (WT TRPM8 ratio = 0.2 ± 0.01, n= 47 vs I846T ratio= 0.6 ± 0.1, n=62) (p-value = 0.01) (Fig. 40G). After switching to calcium-free extracellular solution, intracellular calcium levels decreased sharply in both mutants: I846A (BL ratio (2.4 mM Ca^{2+}) = 0.8 ± 0.2 vs BL Fura2 ratio (Ø Ca^{2+}) = 0.4 ± 0.1, n=55) (p-value< 0.001; Twow-Tailed, Unpaired-T-test) (Fig. 40I), or I846T (BL Fura2 ratio (+Ca^{2+}) = 0.58 ± 0.05 vs BL Fura2 ratio (Ø Ca^{2+}), = 0.25 ± 0.01, n=62) (p-value< 0.0001; Two-Tailed, Unpaired-T-test) (Fig. 40J). In contrast to results obtained in wildtype channels, cold activation in calcium-free solution (Ø Ca^{2+}) led to small but detectable calcium responses in cells expressing both mutants (Fig. 40B, D).

The results indicate that mutant channels form functional units in the endoplasmic reticulum, suggesting that they tetramerize properly. Moreover, the larger response of these channels to cold may be intrinsic or could be due to different filling of the stores.

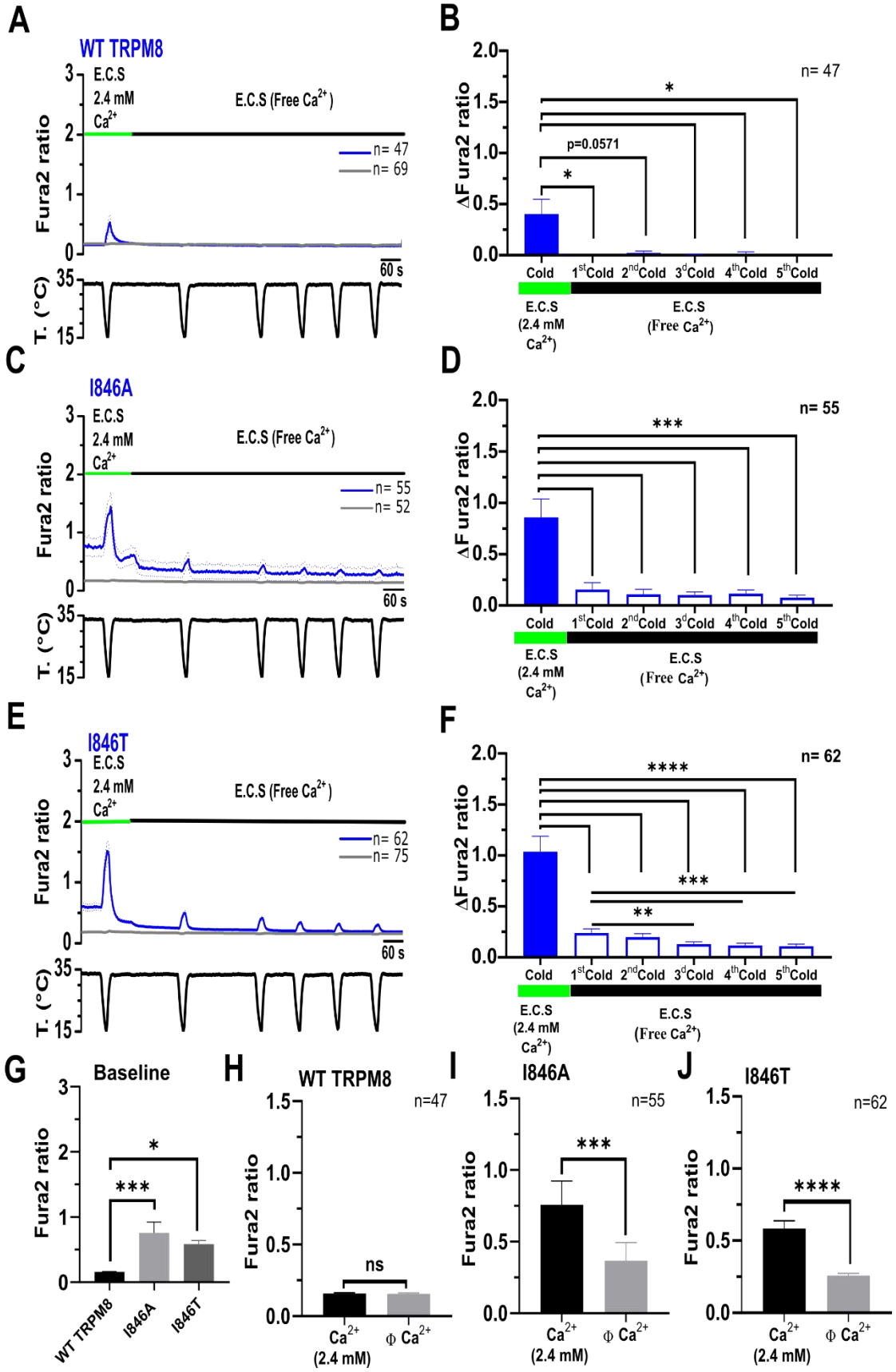
A
WT TRPM8
E.C.S
2.4 mM
Ca2+
E.C.S (Free Ca2+)
n= 47
n= 69
Fura2 ratio
60 s
T. (°C)
B
n= 47
ΔFura2 ratio
p=0.0571
Cold
1stCold
2ndCold
3dCold
4thCold
5thCold
E.C.S
(2.4 mM
Ca2+)
E.C.S
(Free Ca2+)
C
I846A
n= 55
n= 52
D
n= 55
E
I846T
n= 62
n= 75
F
n= 62
G
Baseline
WT TRPM8
I846A
I846T
H
WT TRPM8
n=47
ns
Ca2+
(2.4 mM)
Φ Ca2+
I
I846A
n=55
J
I846T
n=62

Figure 48. The segment 4 (S4) mouse TRPM8 mutants (I846A and I846T) are accumulated into endoplasmic reticulum (RE). A, Average ± SEM fura2 ratio response to cold ramps during two phases either in the presence of calcium ions into the extracellular control solution (+ Ca^{2+}) (Green line located up in the graph showing de period of application) or in the absence of calcium ions called calcium free in the extracellular control solution (Ø Ca^{2+})(black bar located up in the graph showing the period of application), in HEK293 cells transiently transfected with wild type mouse TRPM8 and GFP. GFP (+) cold sensitive cells (n=47) are shown in blue (blue trace) and GFP (-) cells (n=69) are shown in grey. **B,** Bar histogram summarizing the mean ± SEM amplitude responses of GFP+ HEK293 cells transfected with wild mouse TRPM8 to different cold ramps either in standard control solution (+ Ca^{2+}) or in calcium free control solution (Ø Ca^{2+}) (n=47). **C,** Average ± SEM fura2 ratio response to cold ramps during two phases either in the presence of calcium ions into the extracellular control solution (+ Ca^{2+}) (Green line located up in the graph showing de period of application) or in the absence of calcium ions called calcium free extracellular control solution (Ø Ca^{2+})(black bar located up in the graph show the period of application), in HEK293 cells transiently transfected with I846A mouse TRPM8 mutant and GFP. GFP (+) cold sensitive cells (n=55) are shown in blue (blue trace) and GFP (-) cells (n=52) are shown in grey. **D,** Bar histogram summarizing the mean ± SEM calcium amplitude responses of GFP+ HEK293 cells transfected I846A mouse TRPM8 mutant to different cold ramps either in standard control solution (+ Ca^{2+}) or in calcium free control solution (Ø Ca^{2+}) (n=55). **E,** Average ± SEM fura2 ratio responses to cold ramps during two phases either in the presence of calcium ions into the extracellular control solution (+ Ca^{2+}) (Green line located up in the graph showing de period of application) or in the absence of calcium ions called calcium free control solution (Ø Ca^{2+})(black bar located up in the graph show the period of application), in HEK293 cells transiently transfected I846T mouse TRPM8 mutant and GFP. GFP (+) cold sensitive cells (n=62) are shown in blue (blue trace) and GFP (-) cells (n=75) are shown in grey. **F,** Bar histogram summarizing the mean ± SEM calcium amplitude responses of GFP+ HEK293 cells transfected with I846T mouse TRPM8 mutant to different cold ramps either in standard control solution (+ Ca^{2+}) or in calcium free control solution (Ø Ca^{2+})(n=62). Statistical significance was calculated by a one-way ANOVA followed by Bonferroni post-hoc test. Asterisk are used for comparing the effect of different stimuli (*, p-value< 0.05; **, p-value< 0.01; ***, p-value< 0.001; ****, p-value< 0.0001). **G,** Bar histogram summarizing the mean ± SEM fura2 ratio at the baseline during standard control solution phase (+ Ca^{2+}) of GFP+ HEK293 cells transfected with mouse TRPM8 wild type, I846A mutant or I846T. Statistical significance was calculated by a one-way ANOVA followed by Bonferroni post-hoc test. **H,** Bar histogram summarizing the mean ± SEM fura2 ratio at the baseline during both phases in presence of standard extracellular control solution (+ Ca^{2+}) or in the presence of extracellular calcium free solution of GFP+ HEK293 cells transfected with mouse TRPM8 wild type. **I,** Bar histogram summarizing the mean ± SEM fura2 ratio at the baseline during both phases in presence of standard extracellular control solution (+ Ca^{2+}) or in the presence of extracellular calcium free solution of GFP+ HEK293 cells transfected with mouse TRPM8 I846A mutant. **J,** Bar histogram summarizing the mean ± SEM fura2 ratio at the baseline during both phases in presence of standard extracellular control solution (+ Ca^{2+}) or in the presence of extracellular calcium free solution of GFP+ HEK293 cells transfected with mouse TRPM8 I846T mutant. Unpaired student-T test was used for statistical differences.

Conclusions of this chapter:

- TRPM8 segment 4 mutations at residue I846 created an open pore channel phenotype, constitutively active at rest.
- Segemt4 mutants tetramerize properly and are functional. A fraction is retained in the endoplasmic reticulum since they contributed into the release of calcium from the stores (ER). Thus, mutation at S4 I846 altered channel trafficking towards the plasma membrane.

4.4 Agonist G-RGM-145 is a novel activator of the cold sensor TRPM8

The compound G-RGM-145 is a new chemically synthesized molecule (confidential structure) supplied by our collaborators at the Institute of Medicinal Chemistry (IQM) in Madrid. Their preliminary findings indicate that G-RGM-145 is a novel TRPM8 agonist. Here, I performed the characterization of G-RGM-145 agonistic effect on native TRPM8-expressing DRG sensory neurons, and in heterogousely transfected HEK293 cells expressing wildtype and mutated mouse TRPM8, to explore the mechanism of action on the channel.

4.4.1 G-RGM-145 activated TRPM8-expressing DRG sensory neurons and potentiated their cold responses

TRPM8 is expressed in a small population of DRG and trigeminal sensory neurons activated by cold and cooling compounds (McKemy et al., 2002; Peier et al., 2002; Dhaka et al., 2008). I used a BAC transgenic mouse line expressing enhanced YFP under the TRPM8 promoter TRPM8BAC-EYFP (Morenilla-Palao et al., 2014) as an efficacious methodology to reliably identify TRPM8 sensory neurons.

Application of a low concentration of G-RGM-145 (3 µM) activated a small 15 % YFP (+) of TRPM8 expressing thermoreceptor neurons (4 out of 26), while 10 µM G-RGM-145 activated a larger percentage 38 % (10 out of 26). In contrast, cold activated a larger percentage of about 88% of YFP(+) neurons (23 out of 26) compared to agonist G-RGM-145 (p-value ≤0.0001, Chi-squared test). The agonist effect of G-RGM-145 was very specific for TRPM8-expressing cold thermoreceptors: YFP (-) neurons (i.e. neurons not expressing TRPM8) were not activated by cold or G-RGM-145 (0 out 212), but they presented a normal response to 30 mM KCl (Fig. 49D). I also tested the effect of the canonical TRPM8 agonist WS-12 on the same cultures. G-RGM-145 (10 µM) was markedlly less potent than WS-12 (10 µM): (G-RGM-145 = 0.13 ± 0.04 vs WS-12 =0.71 ± 0.10, n=26) (p-value< 0.01) (Fig. 49E). Cold-evoked responses were robustly potentiated in the presence of 10 µM G-RGM-145 (Cold= 1.1 ± 0.1 vs G-RGM-145+cold =1.5 ± 0.2, n=26) (p-value< 0.05) (Fig. 49E). Consitent with the weaker agonist effect, this potentiation was smaller than the one observed with WS-12: (G-RGM-145+cold =1.5 ± 0.2 vs WS-12+cold= 1.9 ± 0.2) (n=26 p-value< 0.05) (Fig. 49E).

YFP+ neurons obtained from TRPM8 BAC-EYFP, can be separated into two subpopulations according to their fluorescence intensity (Ordás et al., 2021): the intensely fluorescent YFP+ neurons (IF-YFP (+)) and the weakly fluorescent neurons (WF-YFP (+)) (Fig.49G). IF-YFP neurons express lower TRPM8 levels (Hernández-Ortego et al., 2022). IF-YFP (+) neurons were smaller compared to the WF-YFP (+): (IF-YFP+ diameter = 13.1 ± 0.6 µm vs WF-YFP- diameter = 17.3 ± 0.6 µm) (p-value< 0.001;

two-Tailed, Unpaired-T-test) (Fig. 49H). Neurons activated by Ag145 had a small diameter (less than 20 µm) independently of their fluorscence intensity (Fig. 49I).

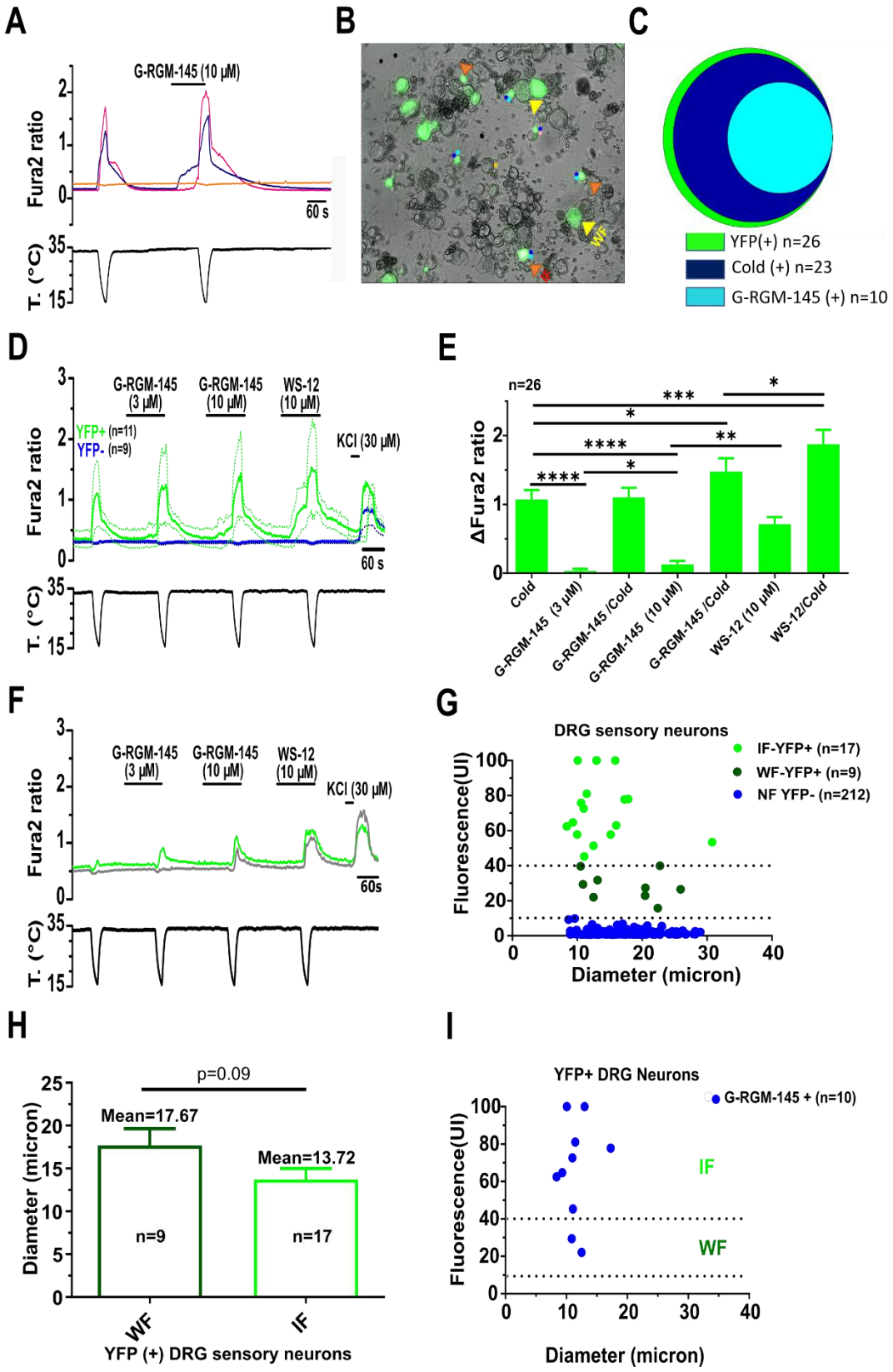

Figure 49. G-RGM-145 activated cold sensitive neurons selectively. A, Ratiometric $[Ca^{2+}]_i$ measurement from fura2-loaded cultured DRG neurons from TRPM8BAC-EYFP mice, showing two cold sensitive neurons (Blu and magenta traces) that increased their $[Ca^{2+}]_i$ level during cooling ramp, and one cold insensitive neuron (orange trace). Of the two cold-sensitive neurons, one (blue trace) responded distinctly to G-RGM-145 (10 µM) while the other did not. However, both neurons showed a potentiation of their cold-evoked response in the presence of G-RGM-145. The cold insensitive neuron did not respond to G-RGM-145.i. **B,** representative DRG culture image from TRPM8BAC-EYFP mouse. The traces shown in A correspond to the neurons marked with the same coloured arrowss . **C,** Venn diagram showing neurons in DRG culture presented in ´´B`` YFP (+) neurons (green, n=16), response to cold (bleu, n=5) and response to G-RGM-145 (cyan, n=4). **D,** Mean ± SEM ratiometric $[Ca^{2+}]_i$ level in fura2-loaded DRG neurons in response to different agonists. **E,** Bar histograms showing the average amplitude of responses to tested TRPM8 agonists. Statistical significance was calculated by a one-way ANOVA followed by Bonferroni post-hoc test. **F,** Time course fura2 ratio of YFP (+) cold insensitive but was recruited in the presence of G-RGM-145 (3 µM or 10 µM). **G,** Graph showing different clusters from DRG from TRPM8BAC-EYFPmice based on the normalized fluorescence (UI) correlated with DRG neurons diameter (µm, micron). YFP (+) DRG neurons were divided into two subgroups: intensely fluorescent neurons (IF-YFP (+), n=9) and weakly fluorescent neurons (WF-YFP (+), n=17), while the YFP (-) (n=212) were not fluorescent cells. The neurons dimeters were determined based on calibration bar of 20 µm. **H,** Bar histogram of mean ± SEM neurons diameter of both YFP (+) subgroups IF-YFP (+) and WF-YFP (+). Note that IF-(YFP+) are smaller than WF-YFP (+). **I,** Graph showing the YFP (+) DRG neurons presented in G that were activated by G-RGM-145.

4.4.2 TRPM8 is the exclusive transducer mediating G-RGM-145 responses within DRG sensory neurons

To confirm that G-RGM-145 activation of calcium signals was mediated through TRPM8 in cold-sensitive DRG neurons, I used a pharmacological strategy, based on the application of of different TRPM8 blockers. Indeed, as shown in figure 50A and 50C AMTB (10 µM) and RQ00203078 (0.5 µM) abolished responses to G-RGM-145 in cold- sensitive DRG neurons. Cold-evoked potentiation of the calcium increase in the presence of G-RGM-145 was also markedlly suppressed by these two TRPM8 antagonists (Fig. 50B, D).

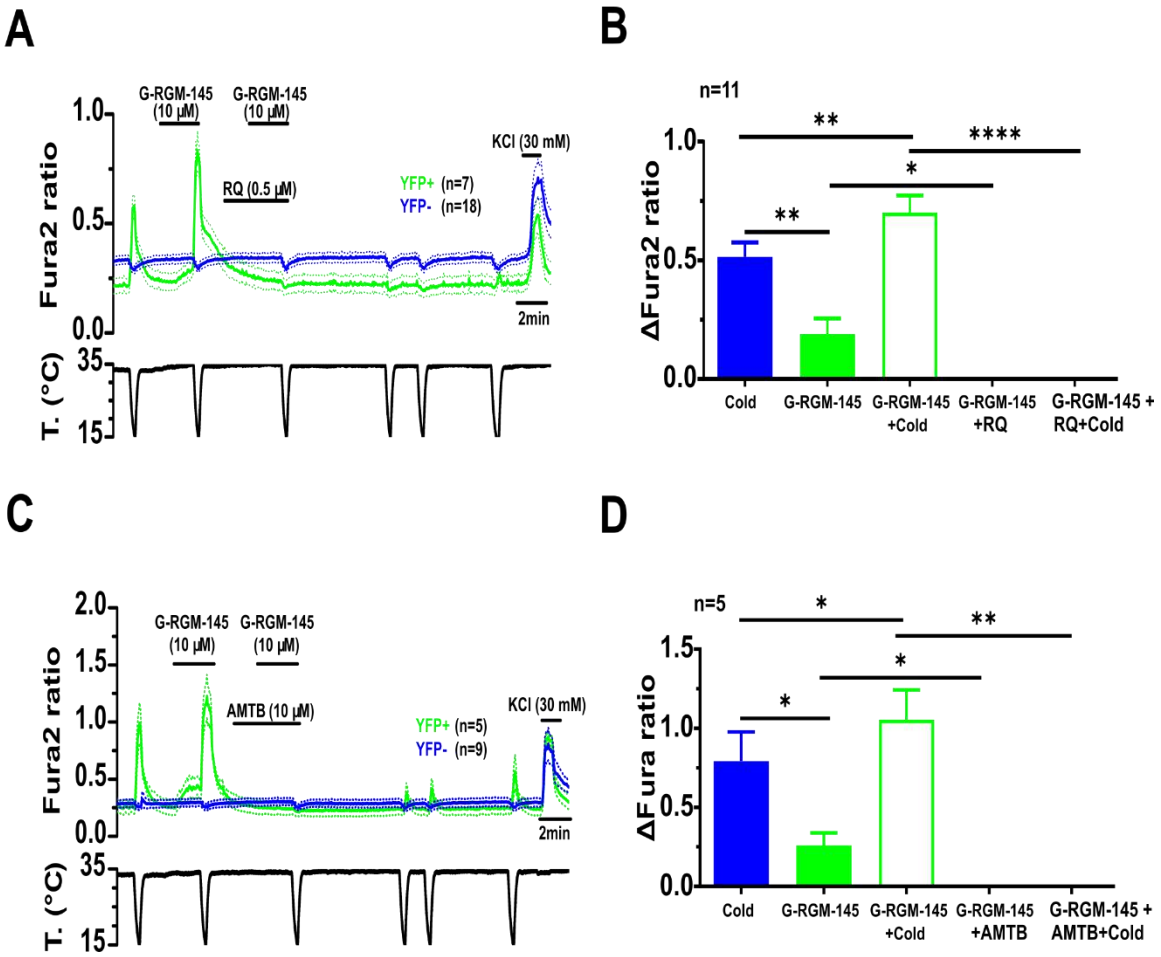

Figure 50.TRPM8 antagonists suppressed the excitatory effects of G-RGM-145 on mice sensory DRG neurons. A, Average ratiometric [Ca^{2+}] level in fura2-loaded cultured DRG neurons from a $TRPM8^{BAC\text{-}EYFP}$ mouse, showing the responses to cold and G-RGM-145 in control condition and in the presence of TRPM8 blocker RQ00203078 (0.5 µM). **B,** Bar histogram summarizing the effect TRPM8 antagonist RQ00203078 (n=11) on both cold- and G-RGM-145-evoked responses. Statistical significance was calculated by a one-way ANOVA followed by Bonferroni post-hoc test. **C,** Similar protocol shown in A, but this time in the presence of the blocker AMTB (10 µM) . Note the very slow recovery of the cold response **D,** Bar histogram summarizing the effect of AMTB (10 µM) (n=5) on cold- and G-RGM-145-evoked responses. Statistical significance was calculated by a one-way ANOVA followed by Bonferroni post-hoc test.

4.4.3 G-RGM-145 activates heterologously expressed mouse TRPM8 channel

Using intracellular calcium imaging *in vitro*, I verified the effects of G-RGM-145 on heterologously co-expressed mouse TRPM8 (mTRPM8) and GFP. The HEK293 cells expressing mTRPM8 (GFP+) were activated by either cold, or G-RGM-145 (30 µM) or WS-12 (10 µM) (Blue trace, n=30). In contrast, none of the non-transfected HEK293 cells (GFP-) was sensitive to TRPM8 agonists (Grey trace, n=190) (Fig. 51A).

G-RGM-145 (30 µM) induced a significantly larger amplitude of calcium signal compared to both agonists cold (Cold = 0.5 ± 0.1 vs G-RGM-145 = 0.9 ± 0.1) (n=130, p-value< 0.0001) and WS-12 (G-RGM-145 ratio=0.9 ± 0.1 vs WS-12 ratio= 0.5 ± 0.1) (n=130, p-value< 0.0001) (Fig. 51B). Cold-evoked responses were markedely potentiated in the presence of G-RGM-145 or WS-12 (Cold = 0.5 ± 0.1 vs G-RGM-145+cold =1.1 ± 0.1 vs WS-12+cold= 1.1 ± 0.1) (n=130, p-value< 0.0001). The cold evoked responses potentiation was similar in presence of either G-RGM-145 (30 µM) or WS-12 (10 µM) (Fig. 51B).

The percentage of cells activated by G-RGM-145 (Fig. 51G) of all transfected GFP+ HEK293 cells (n=130) was similar to the percentage activated by both cold (Fig. 51D) or WS-12 (Fig. 51I) (G-RGM-145 = 66% vs Cold= 56% vs WS-12= 59%) (p-value = 0.2235, Chi-square test). In the presence of G-RGM-145, the percentage of cells activated by cold increased (Fig. 51H), and a similar result was obtained with WS-12 (Fig. 51J) (Cold=56% vs G-RGM-145+cold=68% vs WS-12+cold= 69%) (p-value = 0.0664, Chi-squared test) (Fig. 51G).

Taken together, the results show that G-RGM-145 acts as a robust agonist of mouse TRPM8 channel, in neurons and in expression systems.

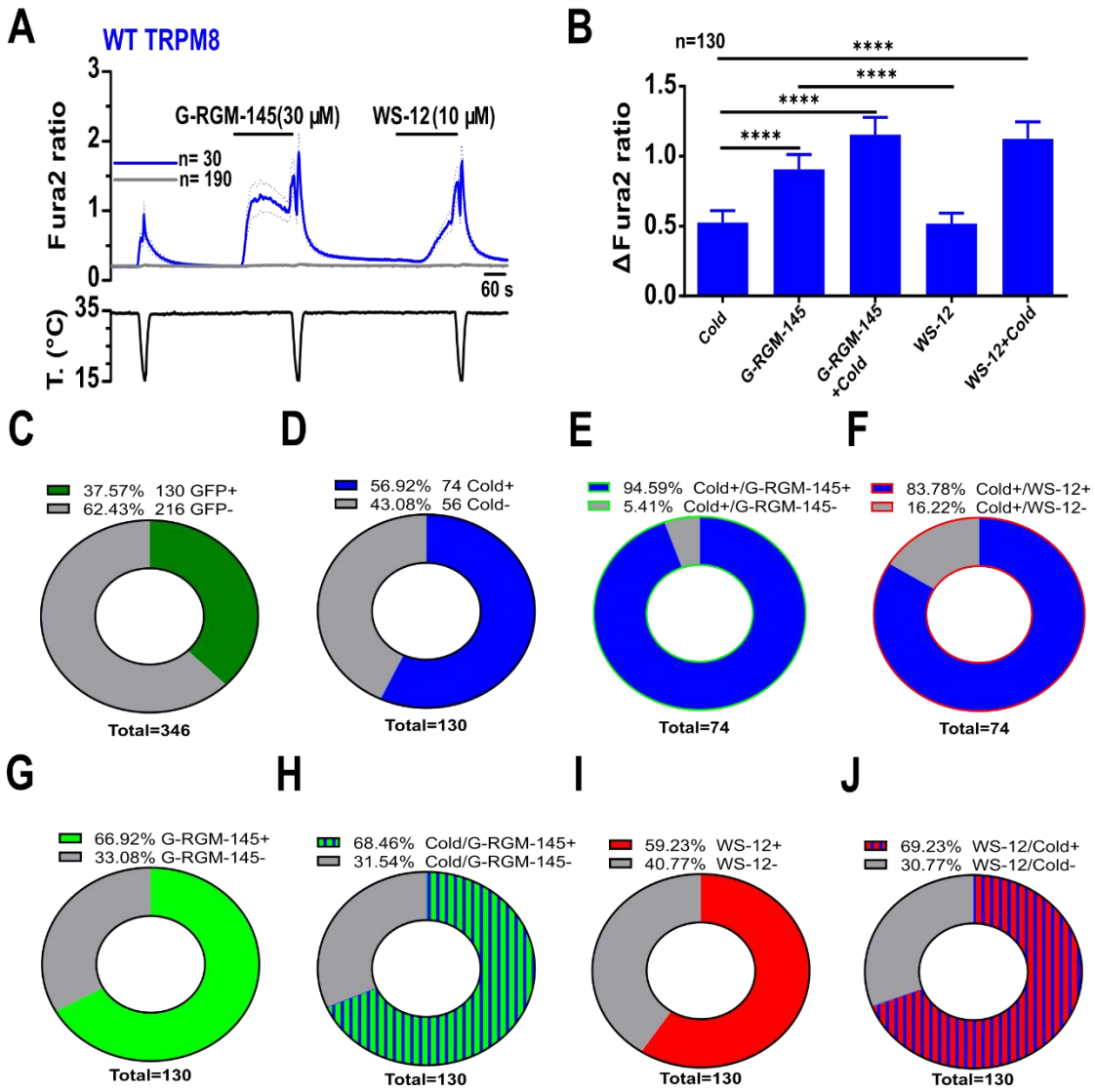

Figure 51. G-RGM-145 activated heterologously transfected mouse TRPM8 channel and potentiated cold evoked responses. A, Representative coverslip showing average ± SEM fura2 ratio response to cold, G-RGM-145 (30 µM) and WS-12 (10 µM) in HEK293 cells transiently transfected with mouse TRPM8 and GFP. GFP (+) cold- sensitive cells (n=30) are shown in blue (blue trace) and GFP (-) cells that are not transfected and insensitive to agonists (n=190) are shown in grey. **B,** Bar histograms summarizing the effect of (average ± SEM amplitude) od different agonist on cold-sensitive HEK293 cells transfected with mouse TRPM8. Statistical significance was calculated by a one-way ANOVA followed by Bonferroni post-hoc test. **C,** Pie graph showing the percentage of GFP (+) transfected and GFP (-) non-transfected cells out of total cells (n=346). **D,** Pie graph showing the percentage of cold sensitive cells (Cold+) and cold insensitive cells (Cold-) out of the total GFP+ transfected cells (n=130). **E,** Pie graph showing the percentage of cold-sensitive cells that are either G-RGM-145 (30 µM) sensitive (Cold+ / G-RGM-145 +) or G-RGM-145 insensitive (Cold+ / G-RGM-145 -) cells out of total cold responders (n=74). **F,** Pie graph showing the percentage of cold sensitive cells that are either WS-12 (10 µM) sensitive (Cold+ / WS-12 +) or WS -12 insensitive (Cold+ / WS-12 -) cells out of total cold responders (n=74). **G,** Pie graph showing the percentage of G-RGM-145 sensitive cells (G-RGM-145 +) and insensitive cells (G-RGM-145 -) out of the total GFP+ transfected cells (n=130). **H,** Pie graph showing the percentage cold evoked responses percentage potentiation in the presence of G-RGM-145 (Cold/ G-RGM-145 +) and the insensitive cells (Cold/ G-RGM-145 -) out of the total GFP+ transfected cells (n=130). **I,** Pie graph showing the percentage of WS-12 sensitive cells (WS-12+) and insensitive cells (WS-12-) out of the total GFP+ transfected cells (n=130). **J,** Pie graph showing the percentage of cells showing the cold evoked responses potentiation in the presence of WS-12 (Cold/WS-12+) and insensitive cells (Cold/WS-12-) out of the total GFP+ transfected cells (n=130).

4.4.4 G-RGM-145 activation of TRPM8 is mediated through the menthol- and WS-12 binding site

In this section of the thesis, I explored the possible mechanism of action of G-RGM-145 on TRPM8. In particular, I tried to determine whether the activation is dependent on the menthol binding pocket (Bandell et al., 2006; L. Xu et al., 2020; X. Chen et al., 2022). To verify this hypothesis, calcium imaging experiments were performed *in vitro*, comparing wild-type mouse TRPM8 to several mouse TRPM8 mutants known to be essential for menthol TRPM8 activation, including Y745A (S1), R1008A (TRPd), and R842A (S4) (reviewed by Plaza-Cayón et al., 2022).

The residue Y745 in segment 1 of TRPM8 has been identified as part of the menthol binding site. Its mutation to histidine (Y745H) renders the TRPM8 channel completely insensitive to menthol and abolishes cold potentiation (Bandell et al., 2006; Malkia et al., 2009). Calcium imaging experiments revealed that HEK293 cells expressing the Y745H mutant lacked G-RGM-145 activation (Fig. 52A, B). In comparasison to to HEK293 cells expressing WT TRPM8 the amplitude was reduced 90 fold: (n=130, WT TRPM8 G-RGM-145 = 0.9 ± 0.1 vs Y745H G-RGM-145 = 0.01 ± 0.002, n=256) (p-value< 0.0001) (Fig. 55B). Additionally, G-RGM-145 evoked cold response potentiation in the wild-type group was severely altered in the Y745H group (Fig. 55C). Very similar results were obtained with WS-12. This complete insensitivity to G-RGM-145 and suppression of cold-evoked potentiation confirmed that Y745 is essential for G-RGM-145 binding, indicating that G-RGM-145 action mechanism is similar to menthol and its derivative WS-12.

The voltage sensor S4 residue R842 is known to be crucial for agonist activation of TRPM8 by cold, menthol, or icilin (Reviewed by Plaza-Cayón et al., 2022). The R842A mutant, characterized by reduced responses to both menthol and cold (Voets et al., 2007b), showed a clear alteration of channel sensitivity to various TRPM8 agonists, including G-RGM-145 (Fig. 53A,B). The R842A channel was only recruited during a cold ramp in the presence of either G-RGM-145 or WS-12 (Fig. 53A, B). Compared to the WT TRPM8 group, G-RGM-145 activation and potentiation of cold-evoked responses were severely altered in the R842A group (Fig. 55B,C), similar to the results seen with cold and WS-12 (Fig. 55A,D). These findings confirmed the essential role of the S4 arginine residue R842 for the activation of all tested TRPM8 agonists, including the novel compound G-RGM-145.

Finally, the TRP domain residue R1008, known previously to be essential for several TRPM8 agonists' activation, including menthol, icilin, and IP3 (Reviewed by Plaza-Cayón et al., 2022), was investigated. The mutation of this residue to alanine (R1008A) significantly decreased sensitivity to menthol (Rohács et al., 2005). Calcium imaging results showed that both G-RGM-145 and WS-12 were unable to directly activate the channel, in contrast to cold (Fig. 54A, B). Compared to the wild-type group, G-RGM-145 activation and potentiation of cold-evoked responses were severely impaired in the R1008A group (Fig.

55B), similar to the results obtained for cold and WS-12 (Fig. 55A, D). Cold-evoked response potentiation in the presence of G-RGM-145 in the WT TRPM8 group was drastically altered in R1008A transfected cells (Fig. 55C). Thus, the R1008A TRPM8 mutant was insensitive to G-RGM-145, implying that the residue R1008 is essential for G-RGM-145 activation, similar to the menthol analogue WS-12.

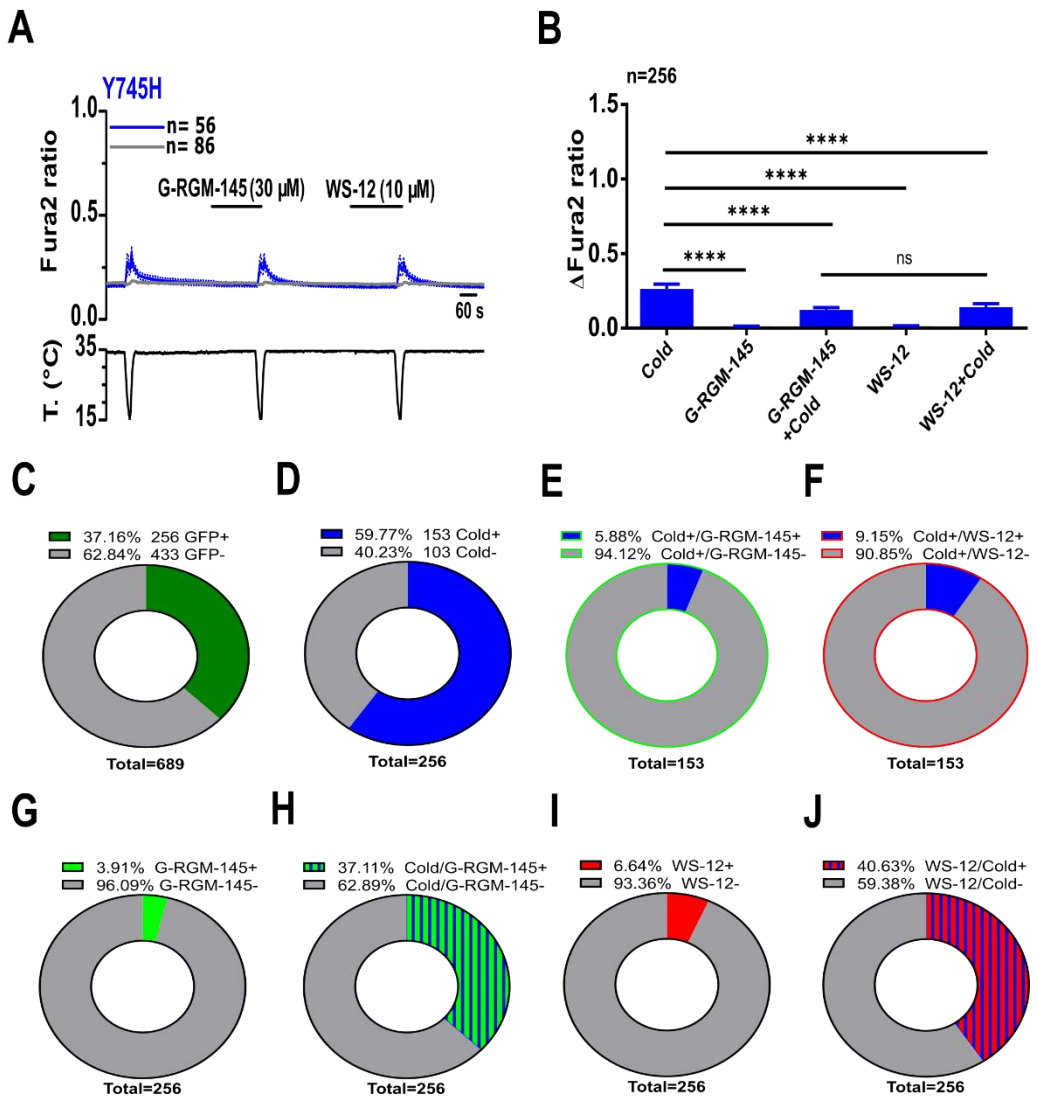

Figure 52. G-RGM-145 did not activate menthol- and WS-12- insensitive TRPM8 mutant Y745H TRPM8 channel heterologously expressed in HEk293 cells, and did not potentiate cold evoked responses. A, Representative coverslip showing average ± SEM fura2 ratio response to cold, G-RGM-145 (30 µM) and WS-12 (10 µM) in HEK293 cells transiently transfected with Y745H TRPM8 and GFP. GFP (+) cold sensitive cells (n=56) are shown in blue (blue trace) and GFP (-) agonists insensitive cells (n=86) are shown in grey. **B,** Bar histograms summarizing the responses of cold sensitive HEK293 cells transfected with Y745H TRPM8 to different agonists. Statistical significance was calculated by a one-way ANOVA followed by Bonferroni post-hoc test. **C,** Pie graph showing the percentage of GFP (+) transfected and GFP (-) non-transfected cells out of total cells (n=689). **D,** Pie graph showing the percentage of cold sensitive cells (Cold+) and cold insensitive cells (Cold-) out of the total GFP+ transfected cells (n=256). **E,** Pie graph showing the percentage of cold sensitive cells that are either G-RGM-145 (30 µM) sensitive (Cold+ / G-RGM-145 +) or G-RGM-145 insensitive (Cold+ / G-RGM-145 -) cells out of total cold responders' cells (n=153). **F,** Pie graph showing the percentage of cold sensitive cells that are either WS-12 (10 µM) sensitive (Cold+ / WS-12 +) or WS -12 insensitive (Cold+ / WS-12 -) cells out of total cold responders' cells (n=153). **G,** Pie graph showing the percentage of G-RGM-145 sensitive cells (G-RGM-145 +) and insensitive cells (G-RGM-145 -) out of the total GFP+ transfected cells (n=256). **H,** Pie graph showing the cold activated percentage of cells potentiation in the presence of G-RGM-145 (Cold/ G-RGM-145 +) and the insensitive cells (Cold/ G-RGM-145 -) out of the total GFP+ transfected cells (n=256). **I,** Pie graph showing the percentage of WS-12 sensitive cells (WS-12+) and insensitive cells (WS-12-) out of the total GFP+ transfected cells (n=256). **J,** Pie graph showing the cold activated percentage of cells potentiation in the presence of WS-12 potentiating cold responses (Cold/WS-12+) and the insensitive cells (Cold/WS-12-) out of the total GFP+ transfected cells (n=256).

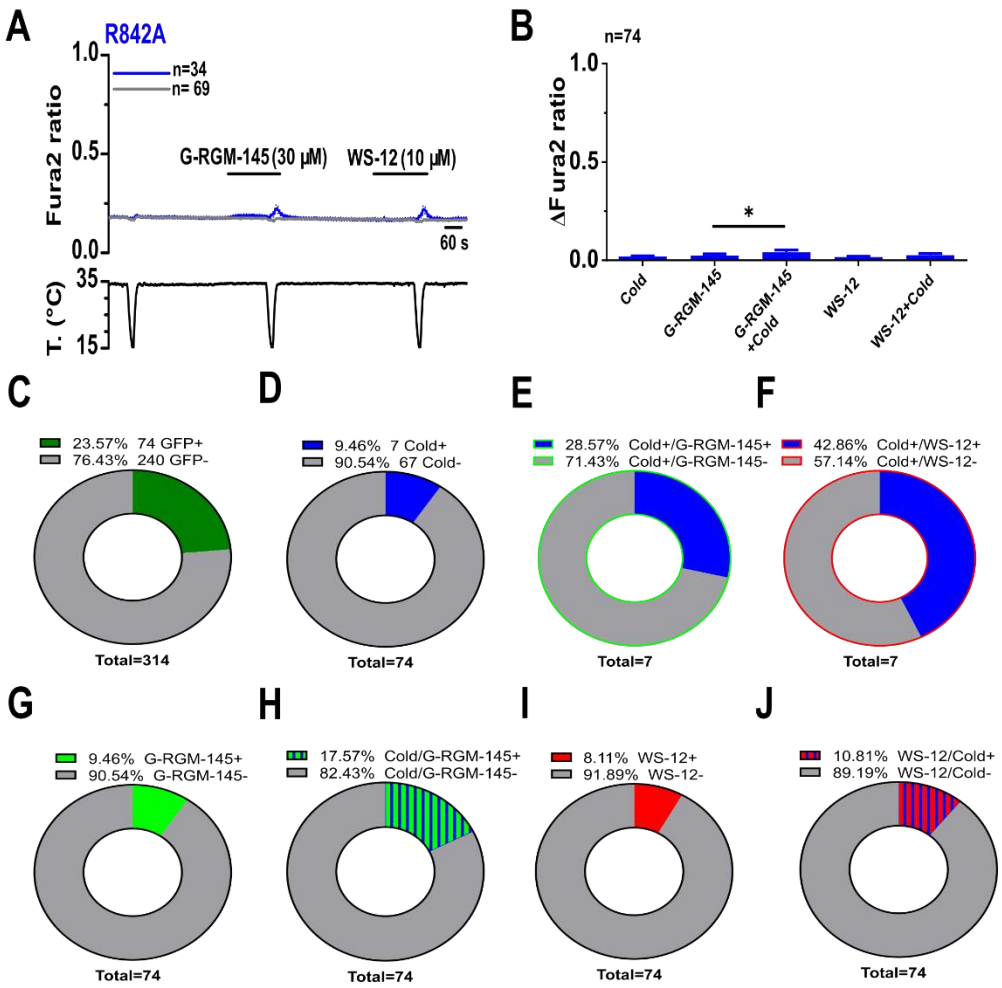

Figure 53. G-RGM-145 did not activate R842A TRPM8 channel heterologously expressed in HEK293 cells, and did not potentiate cold evoked responses. A, Representative coverslip showing Average ± SEM fura2 ratio response to cold, G-RGM-145 (30 µM) and WS-12 (10 µM) in HEK293 cells transiently transfected with R842A mouse TRPM8 mutant and GFP. GFP (+) cold sensitive cells (n=34) are shown in blue (blue trace) GFP (-) agonists insensitive cells (n=69) are shown in grey. **B,** Bar histogram summarizing the responses of GFP+ HEK293 cells transfected with R842A mouse TRPM8 to different agonists. Statistical significance was calculated by a one-way ANOVA followed by Bonferroni post-hoc test. **C,** Pie graph showing the percentage of GFP (+) transfected and GFP (-) non-transfected cells out of total cells (n=314). **D,** Pie graph showing the percentage of cold sensitive cells (Cold+) and cold insensitive cells (Cold-) out of the total GFP+ transfected cells (n=74). **E,** Pie graph showing the percentage of cold sensitive cells that either G-RGM-145 (30 µM) sensitive (Cold+ / G-RGM-145+) or G-RGM-145 insensitive (Cold+ / G-RGM-145 -) cells out of total cold responders (n=7). **F,** Pie graph showing the percentage of cold sensitive cells that are either WS-12 (10 µM) sensitive (Cold+ / WS-12 +) or WS -12 insensitive (Cold+ / WS-12 -) cells out of total cold responders' cells (n=7). **G,** Pie graph showing the percentage of G-RGM-145 sensitive cells (G-RGM-145 +) and insensitive cells (G-RGM-145 -) out of the total GFP+ transfected cells (n=74).**H,** Pie graph showing the percentage of cold evoking cells responses potentiation in the presence of G-RGM-145 (Cold/G-RGM-145 +) and the insensitive cells (Cold/ G-RGM-145-) out of the total GFP+ transfected cells (n=74). **I,** Pie graph showing the percentage of WS-12 sensitive cells (WS-12+) and insensitive cells (WS-12-) out of the total GFP+ transfected cells (n=74).**J,** Pie graph showing the percentage of cold evoking cells responses potentiation in the presence of WS-12 (Cold/WS-12+) and insensitive cells (Cold/WS-12-) out of the total GFP+ transfected cells (n=74).

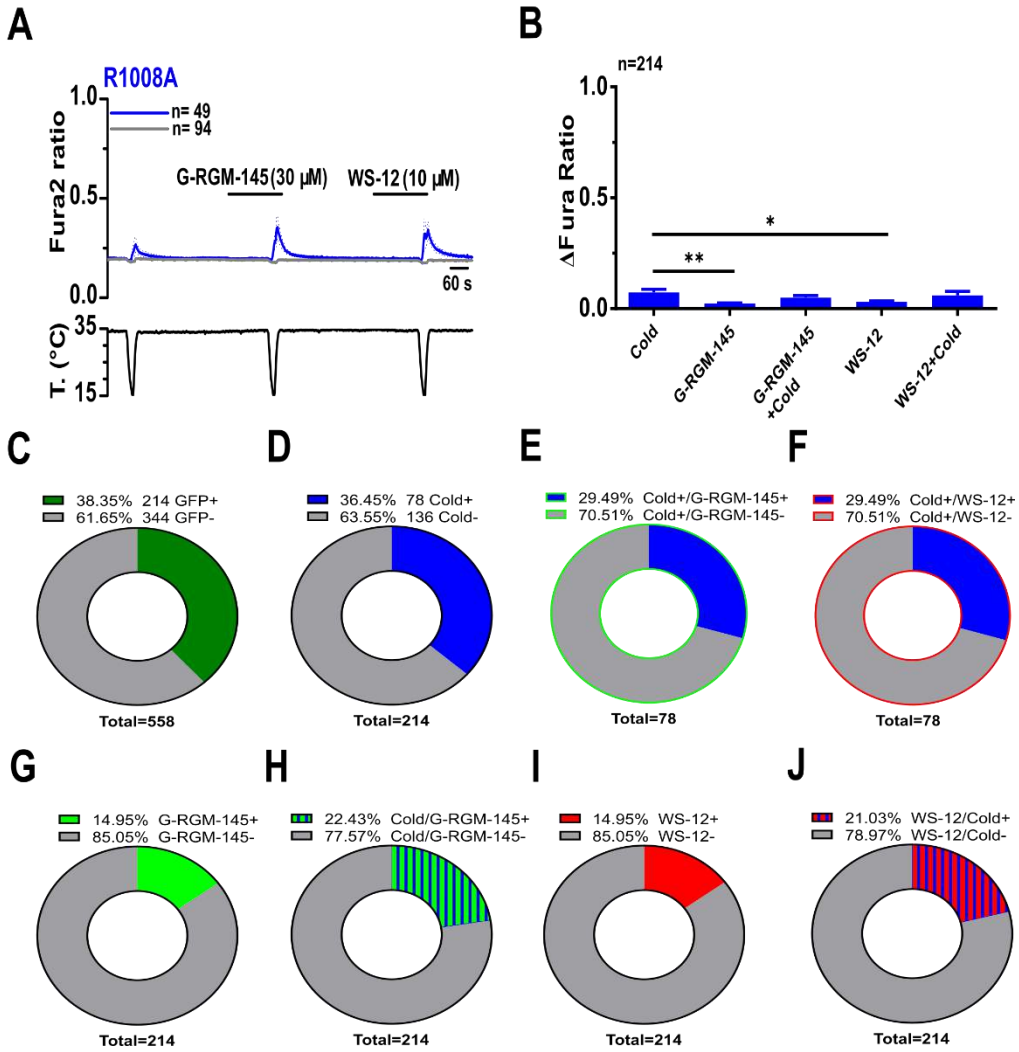

Figure 54. G-RGM-145 did not activate R1008A TRPM8 channel heterologously expressed in HEK293 cells and did not potentiate cold evoked responses. A, Representative coverslip showing Average ± SEM fura2 ratio response to cold, G-RGM-145 (30 µM) and WS-12 (10 µM) in HEK293 cells transiently transfected with R1008A mouse TRPM8 mutant and GFP. GFP (+) cold sensitive cells (n=49) are shown in blue (blue trace) GFP (-) agonists insensitive cells (n=94) are shown in grey. **B,** Bar histogram summarizing the responses of GFP+ HEK293 cells transfected with R842A mouse TRPM8 to different agonists. Statistical significance was calculated by a one-way ANOVA followed by Bonferroni post-hoc test. **C,** Pie graph showing the percentage of GFP (+) transfected and GFP (-) non-transfected cells out of total cells (n=558). **D,** Pie graph showing the percentage of cold sensitive cells (Cold+) and cold insensitive cells (Cold-) out of the total GFP+ transfected cells (n=214). **E,** Pie graph showing the percentage of cold sensitive cells that either G-RGM-145 (30 µM) sensitive (Cold+ / G-RGM-145 +) or G-RGM-145 insensitive (Cold+ / G-RGM-145-) cells out of total cold responders (n=78). **F,** Pie graph showing the percentage of cold sensitive cells and WS-12 (10 µM) sensitive (Cold+/ WS-12 +) or WS -12 insensitive (Cold+/ WS-12 -) cells out of total cold responders' cells (n=78). **G,** Pie graph showing the percentage of G-RGM-145 sensitive cells (G-RGM-145+) and insensitive cells (G-RGM-145-) out of the total GFP+ transfected cells (n=214).**H,** Pie graph showing the percentage of cold evoking cells responses potentiation in the presence of G-RGM-145 (Cold/G-RGM-145 +) and the insensitive cells (Cold/G-RGM-145 -) out of the total GFP+ transfected cells (n=214). **I,** Pie graph showing the percentage of WS-12 sensitive cells (WS-12+) and insensitive cells (WS-12-) out of the total GFP+ transfected cells (n=214).**J,** Pie graph showing the percentage of cold evoking cells responses potentiation in the presence of WS-12 (Cold/WS-12+) and insensitive cells (Cold/WS-12-) out of the total GFP+ transfected cells (n=214).

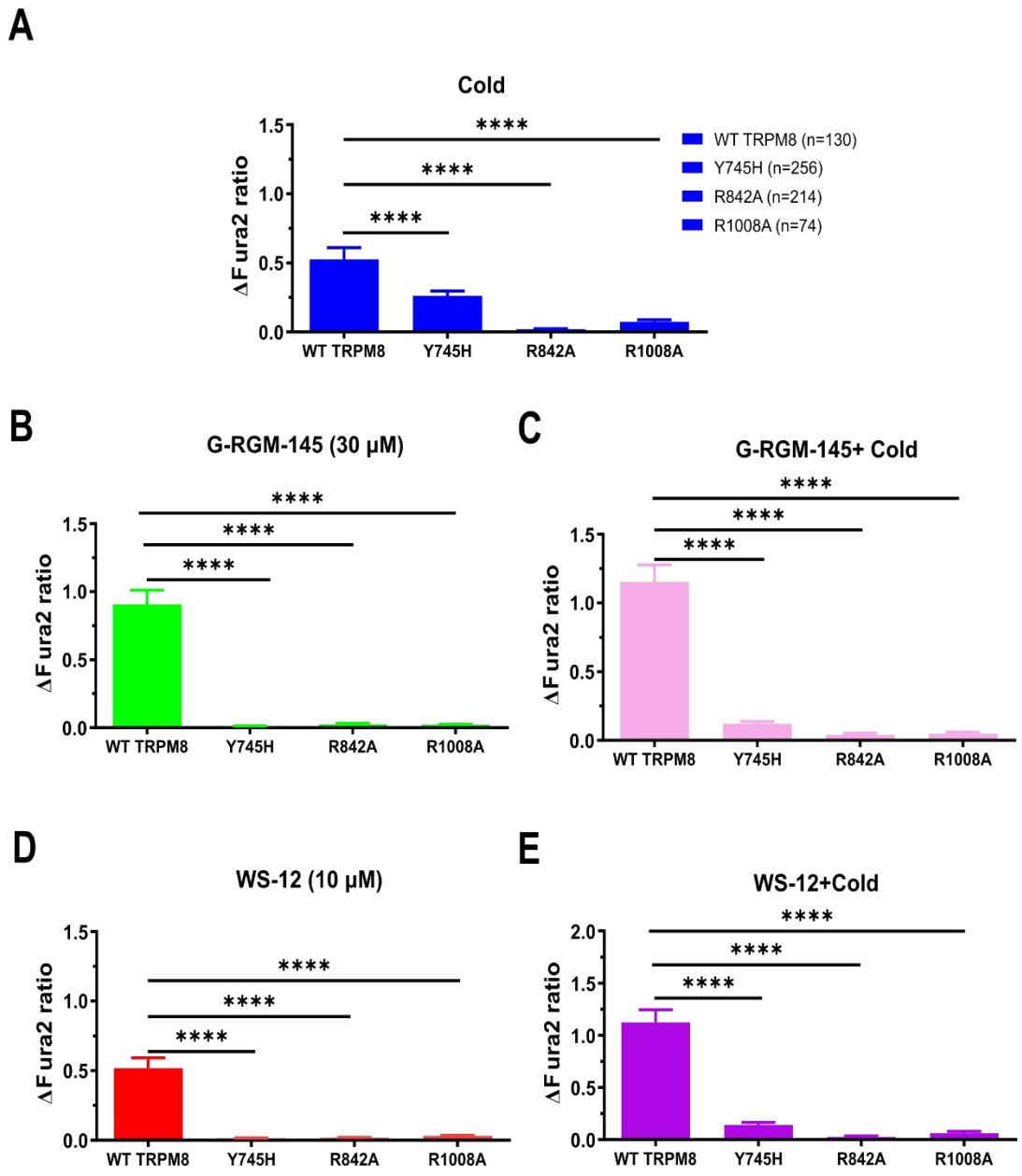

Figure 55. Summary of TRPM8 Calcium imaging response amplitude of mouse wild type (WT) TRPM8 compared to different TRPM8 mutants following the application of different TRPM8 agonists. A, Bar histogram summarizing the mean ± SEM calcium amplitude responses of GFP+ HEK293 cells transfected with mouse TRPM8 (WT or mutants) to cold. **B,** Bar histogram summarizing the mean ± SEM calcium amplitude responses of GFP+ HEK293 cells transfected with mouse TRPM8 (WT or mutants) to G-RGM-145 (30 μM). **C,** Bar histogram summarizing the mean ± SEM calcium amplitude responses of GFP+ HEK293 cells transfected with mouse TRPM8 (WT or mutants) to cold in the presence of G-RGM-145. **D,** Bar histogram summarizing the mean ± SEM calcium amplitude the responses of GFP+ HEK293 cells transfected with mouse TRPM8 (WT or mutants) to WS-12 (10 μM). **E,** Bar histogram summarizing the mean ± SEM calcium amplitude responses of GFP+ HEK293 cells transfected with mouse TRPM8 (WT or mutants) to cold in the presence of WS-12. Statistical significance was calculated by a one-way ANOVA followed by Bonferroni post-hoc test.

Conclusion of this chapter:

- Agonist G-RGM-145 is a novel selective mouse TRPM8 agonist.
- TRPM8 is the exclusive mediator of G-RGM-145 activation in DRG cold sensitive neurons.
- Agonist G-RGM-145 is acting through the menthol binding residue (Y745).

4.5 Agonist G-RGM-109 is a novel activator of the cold sensor mouse TRPM8

A The compound G-RGM-109 is also a new, chemically synthesized compound that is thought to have agonist effects on TRPM8. I tested G-RGM-109 agonism on native TRPM8-expressing DRG sensory neurons, and in HEK293 cells heterogously expressing mouse TRPM8. Moreover, as in the case of G-RGM-145 describes in the previous section, I investigated the potential binding site taking advantage of the previously known TRPM8 mutants.

4.5.1 G-RGM-109 activates TRPM8-espressing DRG sensory neurons and potentiates their cold responses

Like in the characetrization of G-RGM-145, I used the BAC transgenic mouse line expressing enhanced YFP under the TRPM8 promoter (TRPM8 $^{BAC\text{-}EYFP}$) (Morenilla-Palao et al., 2014).

Using fura2 calcium imaging on cultured DRG sensory neurons, G-RGM-109 (3 µM) activated about half of total number of TRPM8-expressing thermoreceptors (13 out of 21). This percentage was similar (10 out of 21) in 4 coverslips probed with 10 µM G-RGM-109. In contrast, cold (20 out of 21) and 10 µM WS-12 (19 out 21) activated a larger number TRPM8-expressing neurons respectively and YFP (-) neurons (neurons not expressing TRPM8) were not activated by cold or either of two TRPM8 agonists (0 out 241), while they had a normal response to 30 mM KCl (Fig. 56A). At the same concentration, G-RGM-109 (10 µM) was markedly less potent than WS-12 (10 µM) (G-RGM-109 = 0.2 ± 0.1 vs WS-12 =0.5 ± 0.1, n=21) (p-value< 0.01) (Fig. 56B). G-RGM-109 at low concentration (3 µM) evoked significantly bigger activation than at high concentration (10 µM) probed in 4 coverslips (G-RGM-109 (3 µM) = 0.2 ± 0.03 vs G-RGM-109 (10 µM) = 0.16 ± 0.05) (p-value< 0.05). Cold evoked responses were robustly increased in in the presence of low G-RGM-109 concentrations (Cold= 0.7 ± 0.1 vs G-RGM-109 (3 µM)+cold =0.9 ± 0.1) (p-value= 0.08) (Fig. 56B) and high concentration mesured in 3 coverslips (Cold= 0.51 ± 0.06 vs G-RGM-109 (3 µM)+cold =0.68 ± 0.08) (p-value= 0.0137) (Fig. 56D).

G-RGM-109 (10 µM) was significatively less potent than WS-12 at the same concentration (G-RGM-109 (10 µM) = 0.16 ± 0.02 vs WS-12 (10 µM) = 0.49 ± 0.06) (n=30, p-value < 0.0001). In addition, G-RGM-109 showed similar cold evoked response potentiation to WS-12 (G-RGM-109 + cold= 0.7 ± 0.1 vs WS-12+cold= 0.8 ± 0.1). (Fig. 56C, D).

YFP+ neurons represented as small fraction among all DRG neurons as mentioned previously the TRPM8 BAC-EYFP DRG neurons YFP+ neurons, and in line with result obtained with G-RGM-145 agonist, the G-RGM-109 activated also both IF-YFP+ and WF-YFP+ sensory neurons of small size mostly characterized with a diameter less than 20 µm (Fig. 56G).

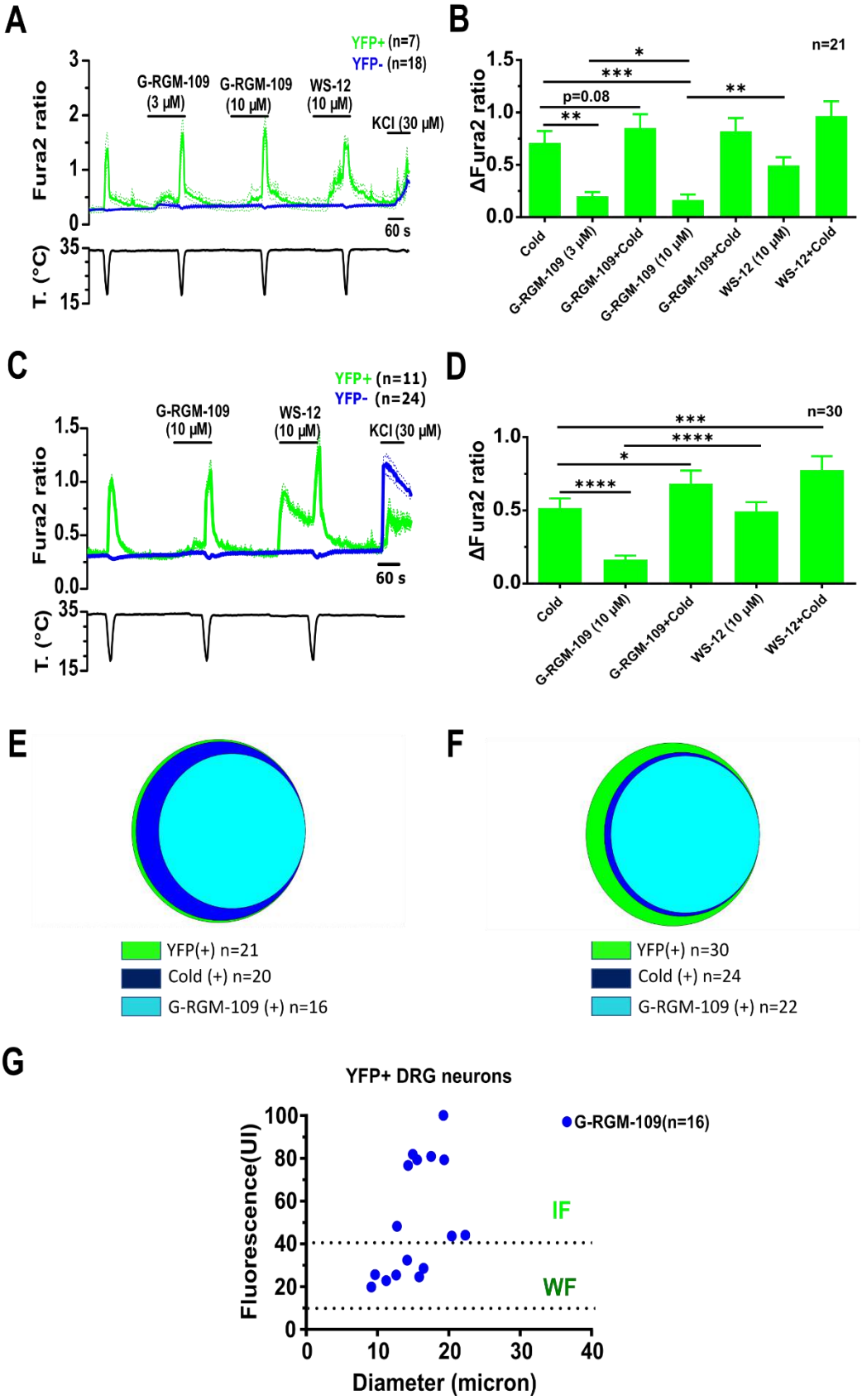
A
YFP+ (n=7)
YFP- (n=18)
G-RGM-109 (3 μM)
G-RGM-109 (10 μM)
WS-12 (10 μM)
KCl (30 μM)
Fura2 ratio
60 s
T. (°C)
B
n=21
ΔFura2 ratio
p=0.08
Cold
G-RGM-109 (3 μM)
G-RGM-109+Cold
G-RGM-109 (10 μM)
G-RGM-109+Cold
WS-12 (10 μM)
WS-12+Cold
C
YFP+ (n=11)
YFP- (n=24)
G-RGM-109 (10 μM)
WS-12 (10 μM)
KCl (30 μM)
Fura2 ratio
60 s
T. (°C)
D
n=30
ΔFura2 ratio
Cold
G-RGM-109 (10 μM)
G-RGM-109+Cold
WS-12 (10 μM)
WS-12+Cold
E
YFP(+) n=21
Cold (+) n=20
G-RGM-109 (+) n=16
F
YFP(+) n=30
Cold (+) n=24
G-RGM-109 (+) n=22
G
YFP+ DRG neurons
G-RGM-109(n=16)
IF
WF
Fluorescence(UI)
Diameter (micron)

Figure 56. G-RGM-109 activates cold sensitive neurons selectively and potentiates their cold-evoked responses. A, Representative ratiometric [Ca2+] level in fura2-loaded DRG neurons culture from TRPM8$^{BAC\text{-}EYFP}$mouse, showing mean ± SEM response to cold, G-RGM-109 (3 µM or 10 µM) and WS-12 (10 µM). **B,** Bar histogram of the respective averages Statistical significance was calculated by a one-way ANOVA followed by Bonferroni post-hoc test. **C,** Representative ratiometric [Ca^{2+}] level in fura2-loaded DRG neurons culture from TRPM8$^{BAC\text{-}EYFP}$ mouse, showing Mean ± SEM response to cold, G-RGM-109 (10 µM) and WS-12 (10 µM). **D,** Summary histograms of the averages obtained in C. Statistical significance was calculated by a one-way ANOVA followed by Bonferroni post-hoc test. **E,** Venn diagram showing neurons in DRG culture presented in ´´B`` YFP (+) neurons (green, n=21), response to cold (bleu, n=20) and response to G-RGM-109 (cyan, n=16). **F,** Venn diagram showing neurons in DRG culture presented in ´´D`` YFP (+) neurons (green, n=30), response to cold (bleu, n=24) and response to G-RGM-145 (cyan, n=22). **G,** Graph showing the YFP (+) DRG neurons presented in B,E that were activated by G-RGM-109.

4.5.2 TRPM8 mediates G-RGM-109 responses in mouse DRG sensory neurons

Following the pharmacological strategy outlined previously, I used the TRPM8 blocker AMTB to determine the role of TRPM8 in the response to G-RGM-109. As shown in figure 57A,application of AMTB (10 µM) abolished G-RGM-109-evoked calcium responses. The effect of AMTB was only partially reversible (Fig. 57A, B). These results support the sceoficity of G-RGM-109 effects on TRPM8.

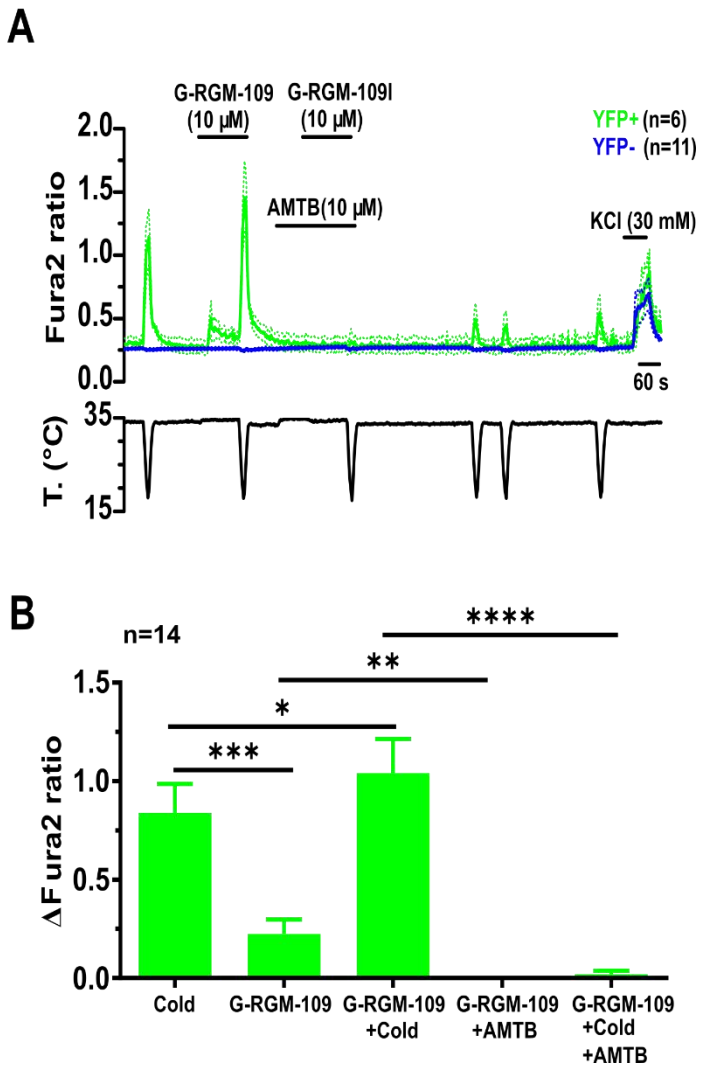

Figure 57. TRPM8 antagonist AMTB abolished the excitatory effects of G-RGM-109 on cold-sensitive DRG neurons. A, Representative ratiometric [Ca^{2+}] level in fura2-loaded cultured DRG neurons from $TRPM8^{BAC\text{-}EYFP}$ mouse, showing the responses to cold and G-RGM-109 in control condition and in the presence of AMTB (10 µM). **B,** Bar histogram summarizing the effects of AMTB on cold and G-RGM-109 evoked responses (n=14). Statistical significance was calculated by a one-way ANOVA followed by Bonferroni post-hoc test.

4.5.3 G-RGM-109 activates heterologously-expressed mouse TRPM8 channels

I performed calcium imaging experiments on HEK293 cells co-transfected withwild type mTRPM8 and GFP. GFP+ cells were activated by cold, G-RGM-109 (30 µM) and WS-12 (10 µM) (Blue trace, n=44). Inn contrast non of the GFP(-) HEK293 cells was activated by TRPM8 agonists (Grey trace, n=44) (Fig. 58A).

Responses to G-RGM-109 (30 µM) were significantly smaller in amplitude when compared to cold and WS-12 (Cold=0.31 ± 0.03, G-RGM-109 =0.06± 0.01, WS-12= 0.74 ± 0.05) (Fig. 58B). Cold evoked responses were strongly potentiated in the presence of G-RGM-109, but the effect was weaker than results obtained In the same cells with WS-12: (Cold=0.31 ± 0.03 vs G-RGM-109 +cold= 0.96 ± 0.07 vs WS-12+cold= 1.51 ± 0.09). (Fig. 58B).

In agreement with the weak agonist action of G-RGM-109-HCl, only a small percentage of GFP(+) neurons responded. This percentage was lower than that observed with cold of WS-12 : (G-RGM-109= 33%,cold = 76%, WS-12 = 80%) (p-value < 0.0001, Chi-squared test) (Fig. 58D, G and I). The combination of cold and chemical stimuli increased the number of responsive cells: (Cold=76% vs G-RGM-109 +cold=92% vs WS-12+cold= 90%) (p-value < 0.0001, Chi-squared test) (Fig. 58D, H and J).

In summary, G-RGM-109 behaves as a relatively weak agonist of mouse TRPM8 channels.

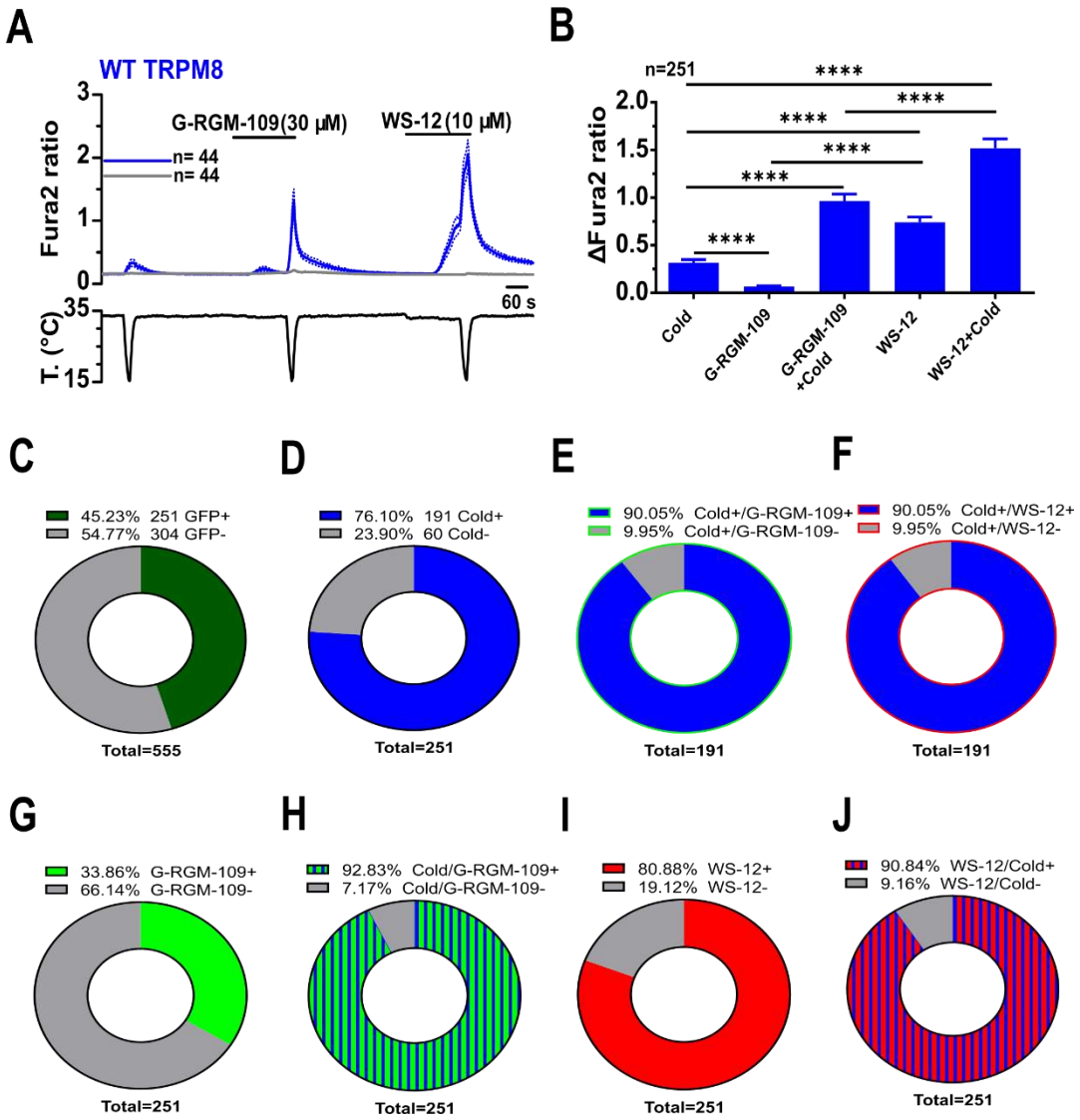

Figure 58. G-RGM-109 activated wild type mouse TRPM8 channel heterologously transfected in HEK293 cells and potentiated cold evoked responses. A, Representative coverslip showing Average ± SEM fura2 ratio response to cold, G-RGM-109 (30 µM) and WS-12 (10 µM) in HEK293 cells transiently transfected with mouse TRPM8 and GFP. GFP (+) cold sensitive cells (n=44) are shown in blue (blue trace) and GFP (-) cells that are (not transfected) agonists insensitive (n=44) are shown in grey. **B,** Bar histogram summarizing the Average ± SEM amplitude responses of cold sensitive HEK293 cells transfected with mouse TRPM8 to different agonists (n=251). Statistical significance was calculated by a one-way ANOVA followed by Bonferroni post-hoc test. Asterisk are used for comparing the effect of different stimuli (*, p-value< 0.05; **, p-value< 0.01; ***, p-value< 0.001; ****, p-value< 0.0001). **C,** Pie graph showing the percentage of GFP (+) transfected and GFP (-) non-transfected cells out of total cells (n=555). **D,** Pie graph showing the percentage of cold sensitive cells (Cold+) and cold insensitive cells (Cold-) out of the total GFP+ transfected cells (n=251). **E,** Pie graph showing the percentage of cold sensitive cells that are either G-RGM-109 (30 µM) sensitive (Cold+ / G-RGM-109 +) or G-RGM-109 insensitive (Cold+ / G-RGM-109 -) cells out of total cold responders (n=191). **F,** Pie graph showing the percentage of cold sensitive cells that are either WS-12 (10 µM) sensitive (Cold+ / WS-12 +) or WS -12 insensitive (Cold+ / WS-12 -) cells out of total cold responders (n=191). **G,** Pie graph showing the percentage of G-RGM-109 sensitive cells (G-RGM-109 +) and insensitive cells (G-RGM-109 -) out of the total GFP+ transfected cells (n=251). **H,** Pie graph showing the percentage cold evoked responses potentiation in the presence of G-RGM-109 (Cold/G-RGM-109 +) and the insensitive cells (Cold/G-RGM-109 -) out of the total GFP+ transfected cells (n=251). **I,** Pie graph showing the percentage of WS-12 sensitive cells (WS-12+) and insensitive cells (WS-12-) out of the total GFP+ transfected cells (n=251). **J,** Pie graph showing the percentage of cells showing the cold evoked responses potentiation in the presence of WS-12 (Cold/WS-12+) and insensitive cells (Cold/WS-12-) out of the total GFP+ transfected cells (n=251).

4.5.4 G-RGM-109 activation is mediated through menthol- and WS-12 binding site

Next, I used calcium imaging to explore the possible role of residues important for menthol effects on the agonism by G-RGM-109.

Te menthol-insensitive TRPM8 Y745H mutant swas also unresponsive to G-RGM-109 (Fig.59A). The calcium responses to G-RGM-109 were very small in the Y745H group compared to cells expressing WT TRPM8 (n=251, WT TRPM8 G-RGM-109 =0.06± 0.01 vs Y745H G-RGM-109 =0.02 ± 0.01, n=200)(p-value< 0.0001)(Fig.62B). G-RGM-109-induced potentiation of cold responses was also minimal (Fig. 62C).

In summary, thes results confirm that Y745 is essential for the activity of G-RGM-109, similar to Menthol and its derivative WS-12.

Next, we tested the effects of the single-point mutation R842A. Similarly to cold or WS-12, this mutant did nor respond to G-RGM-109 and the potentiation during cooling was also minimal (Fig. 59A,B). These results are in line with previous literature (Voets et al., 2007a) and confirmed that the R842 residue is critical for gating of TRPM8 by different agonists, including G-RGM-109.

Mutant R1008A was also insensitive to G-RGM-109. However, the mutant maintained small but detectable responses to cold, which were significantly potentiated in the presence of G-RGM-109 (Fig. 61B). A summary is presented in Fig.62.

These results led to the conclusion that alanine mutation at residue R1008 within the TRP domain mutation severely affects the sensitivity of the TRPM8 channel to G-RGM-109 and other agonists.

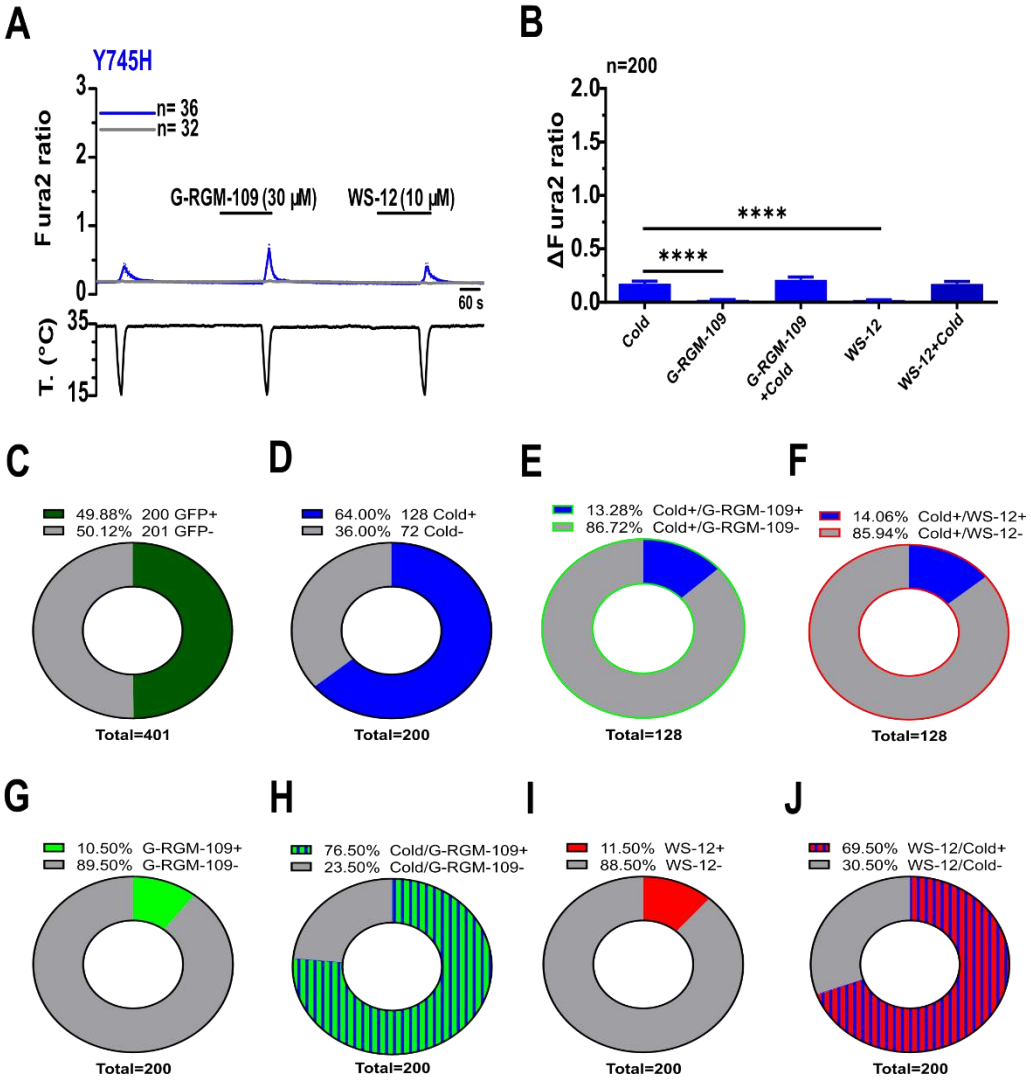

Figure 59. G-RGM-109 did not activate menthol- and WS-12- insensitive TRPM8 mutant Y745H TRPM8 channel heterologously transfected in HEK293 cells, and did not potentiate cold evoked responses. A, Representative coverslip showing average ± SEM fura2 ratio response to cold, G-RGM-109 (30 µM) and WS-12 (10 µM) in HEK293 cells transiently transfected with Y745H TRPM8 and GFP. GFP (+) cold sensitive cells (n=36) are shown in blue (blue trace) and GFP (-) agonists insensitive cells (n=32) are shown in grey. **B,** Bar histogram summarizing the responses of GFP+ HEK293 cells transfected with Y745H TRPM8 to different agonists (n=200). Statistical significance was calculated by a one-way ANOVA followed by Bonferroni post-hoc test. **C,** Pie graph showing the percentage of GFP (+) transfected and GFP (-) non-transfected cells out of total cells (n=401). **D,** Pie graph showing the percentage of cold sensitive cells (Cold+) and cold insensitive cells (Cold-) out of the total GFP+ transfected cells (n=200). **E,** Pie graph showing the percentage of cold sensitive cells that are either G-RGM-109 (30 µM) sensitive (Cold+ / G-RGM-109 +) or G-RGM-109 insensitive (Cold+ / G-RGM-109 -) cells out of total cold responders (n=128). **F,** Pie graph showing the percentage of cold sensitive cells that are either WS-12 (10 µM) sensitive (Cold+ / WS-12 +) or WS -12 insensitive (Cold+ / WS-12 -) cells out of total cold responders' cells (n=153). **G,** Pie graph showing the percentage of G-RGM-109 sensitive cells (G-RGM-109 +) and insensitive cells (G-RGM-109 -) out of the total GFP+ transfected cells (n=200). **H,** Pie graph showing the cold activated percentage of cells potentiation in the presence of G-RGM-109 (Cold/ G-RGM-109 +) and the insensitive cells (Cold/ G-RGM-109 -) out of the total GFP+ transfected cells (n=200). **I,** Pie graph showing the percentage of WS-12 sensitive cells (WS-12+) and insensitive cells (WS-12-) out of the total GFP+ transfected cells (n=200). **J,** Pie graph showing the cold activated percentage of cells potentiation in the presence of WS-12 potentiating cold responses (WS-12/Cold +) and the insensitive cells (WS-12/Cold -) out of the total GFP+ transfected cells (n=200).

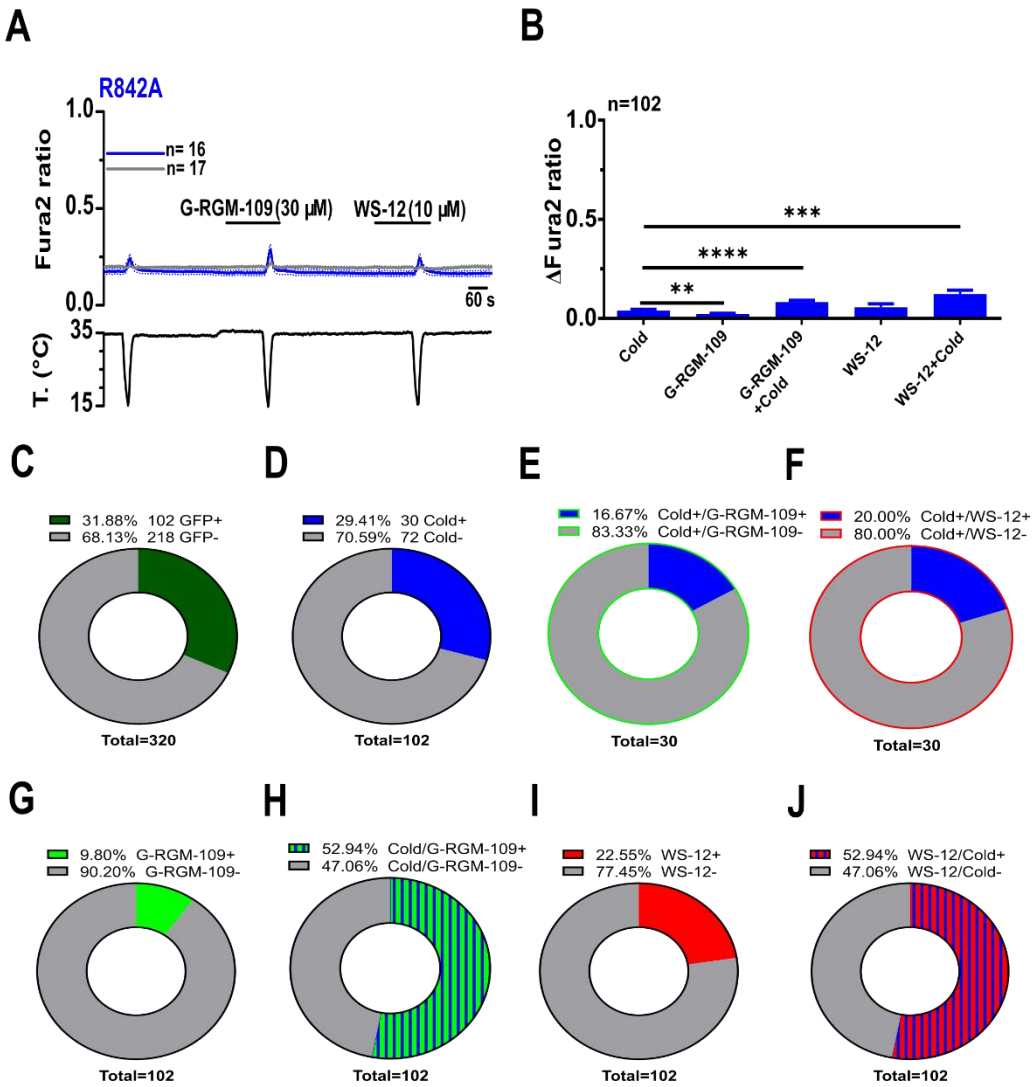

Figure 60. G-RGM-109 not did activate R842A TRPM8 mutant channel heterologously transfected in HEK293 cells but potentiated cold evoked responses. A, Representative coverslip showing Average ± SEM fura2 ratio response to cold, G-RGM-109 (30 µM) and WS-12 (10 µM) in HEK293 cells transiently transfected with R842A mouse TRPM8 mutant and GFP. GFP (+) cold sensitive cells (n=16) are shown in blue (blue trace) GFP (-) agonists insensitive cells (n=17) are shown in grey. **B,** Bar histogram summarizing the responses of GFP+ HEK293 cells transfected with R842A mouse TRPM8 to different agonists (n=102). Statistical significance was calculated by a one-way ANOVA followed by Bonferroni post-hoc test. **C,** Pie graph showing the percentage of GFP (+) transfected and GFP (-) non-transfected cells out of total cells (n=320). **D,** Pie graph showing the percentage of cold sensitive cells (Cold+) and cold insensitive cells (Cold-) out of the total GFP+ transfected cells (n=102). **E,** Pie graph showing the percentage of cold sensitive cells that either G-RGM-109 (30 µM) sensitive (Cold+ / G-RGM-109 +) or G-RGM-109 insensitive (Cold+ / G-RGM-109 -) cells out of total cold responders (n=30). **F,** Pie graph showing the percentage of cold sensitive cells that are either WS-12 (10 µM) sensitive (Cold+ / WS-12 +) or WS -12 insensitive (Cold+ / WS-12 -) cells out of total cold responders (n=30). **G,** Pie graph showing the percentage of G-RGM-109 sensitive cells (G-RGM-109 +) and insensitive cells (G-RGM-109-) out of the total GFP+ transfected cells (n=102). **H,** Pie graph showing the percentage of cold evoking cells responses potentiation in the presence of G-RGM-109 (Cold/G-RGM-109+) and the insensitive cells (Cold/ G-RGM-109 -) out of the total GFP+ transfected cells (n=102). **I,** Pie graph showing the percentage of WS-12 sensitive cells (WS-12+) and insensitive cells (WS-12-) out of the total GFP+ transfected cells (n=102).**J,** Pie graph showing the percentage of cold evoking cells responses potentiation in the presence of WS-12 (WS-12/Cold +) and insensitive cells (WS-12/Cold -) out of the total GFP+ transfected cells (n=102).

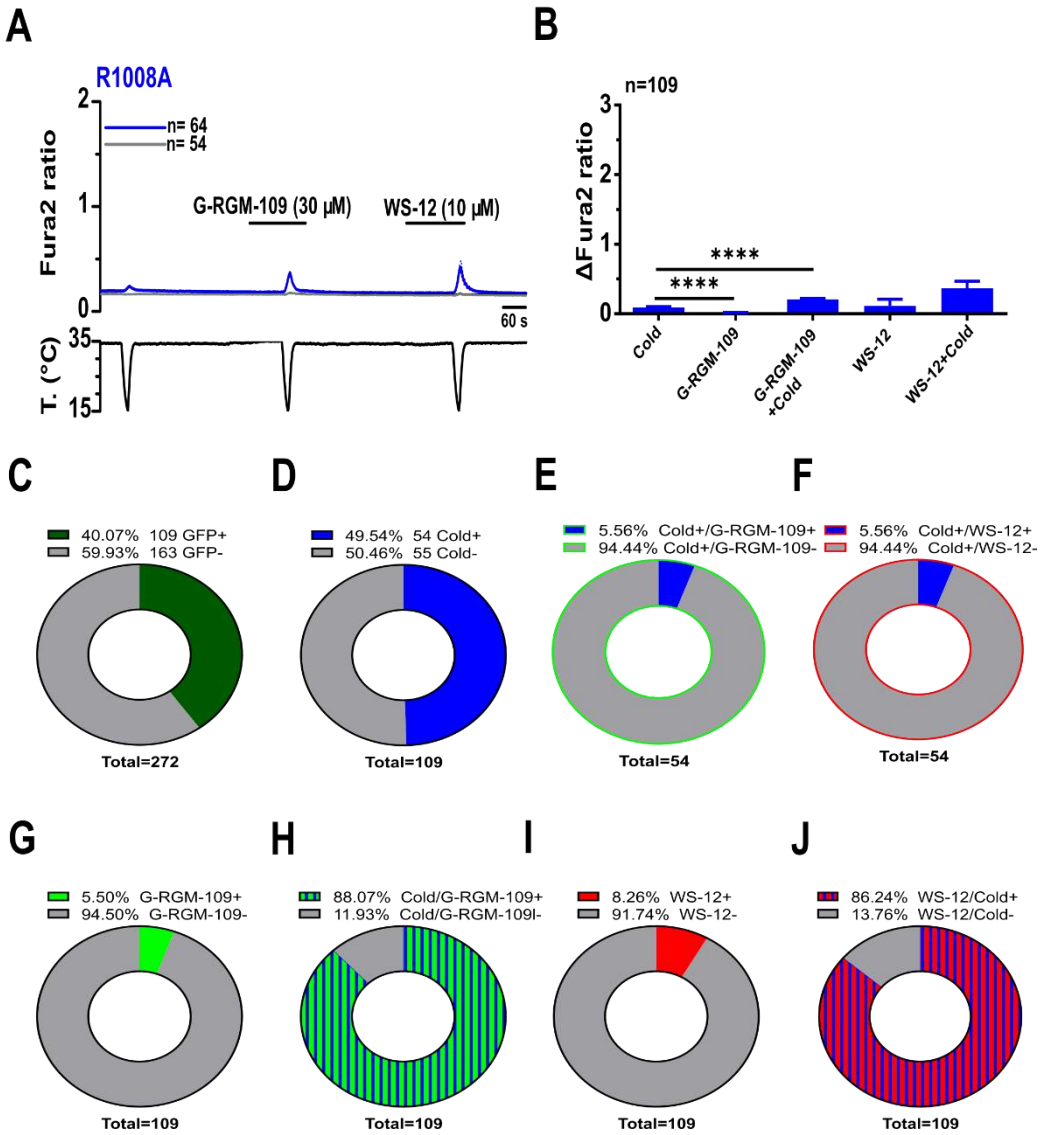

Figure 61. G-RGM-109 did not activate R1008A TRPM8 mutant channel heterologously transfected in HEK293 cells while it potentiated cold evoked responses. A, Representative coverslip showing Average ± SEM fura2 ratio response to cold, G-RGM-109 (30 µM) and WS-12 (10 µM) in HEK293 cells transiently transfected with R1008A mouse TRPM8 mutant and GFP. GFP (+) cold sensitive cells (n=64) are shown in blue (blue trace) GFP (-) agonists insensitive cells (n=54) are shown in grey. **B,** Bar histogram summarizing the responses of GFP+ HEK293 cells transfected with R842A mouse TRPM8 to different agonists (n=109). Statistical significance was calculated by a one-way ANOVA followed by Bonferroni post-hoc test. **C,** Pie graph showing the percentage of GFP (+) transfected and GFP (-) non-transfected cells out of total cells (n=272). **D,** Pie graph showing the percentage of cold sensitive cells (Cold+) and cold insensitive cells (Cold-) out of the total GFP+ transfected cells (n=109). **E,** Pie graph showing the percentage of cold sensitive cells that either G-RGM-109 (30 µM) sensitive (Cold+ / G-RGM-109 +) or G-RGM-109 insensitive (Cold+ / G-RGM-109 -) cells out of total cold responders (n=54). **F,** Pie graph showing the percentage of cold sensitive cells that are either WS-12 (10 µM) sensitive (Cold+ / WS-12 +) or WS -12 insensitive (Cold+ / WS-12 -) cells out of total cold responders' cells (n=54). **G,** Pie graph showing the percentage of G-RGM-109 sensitive cells (G-RGM-109 +) and insensitive cells (G-RGM-109 -) out of the total GFP+ transfected cells (n=109).**H,** Pie graph showing the percentage of cold evoking cells responses potentiation in the presence of G-RGM-109 (Cold/ G-RGM-109 +) and the insensitive cells (Cold/ G-RGM-109 -) out of the total GFP+ transfected cells (n=109). **I,** Pie graph showing the percentage of WS-12 sensitive cells (WS-12+) and insensitive cells (WS-12-) out of the total GFP+ transfected cells (n=109).**J,** Pie graph showing the percentage of cold evoking cells responses potentiation in the presence of WS-12 (Cold/WS-12+) and insensitive cells (Cold/WS-12-) out of the total GFP+ transfected cells (n=109).

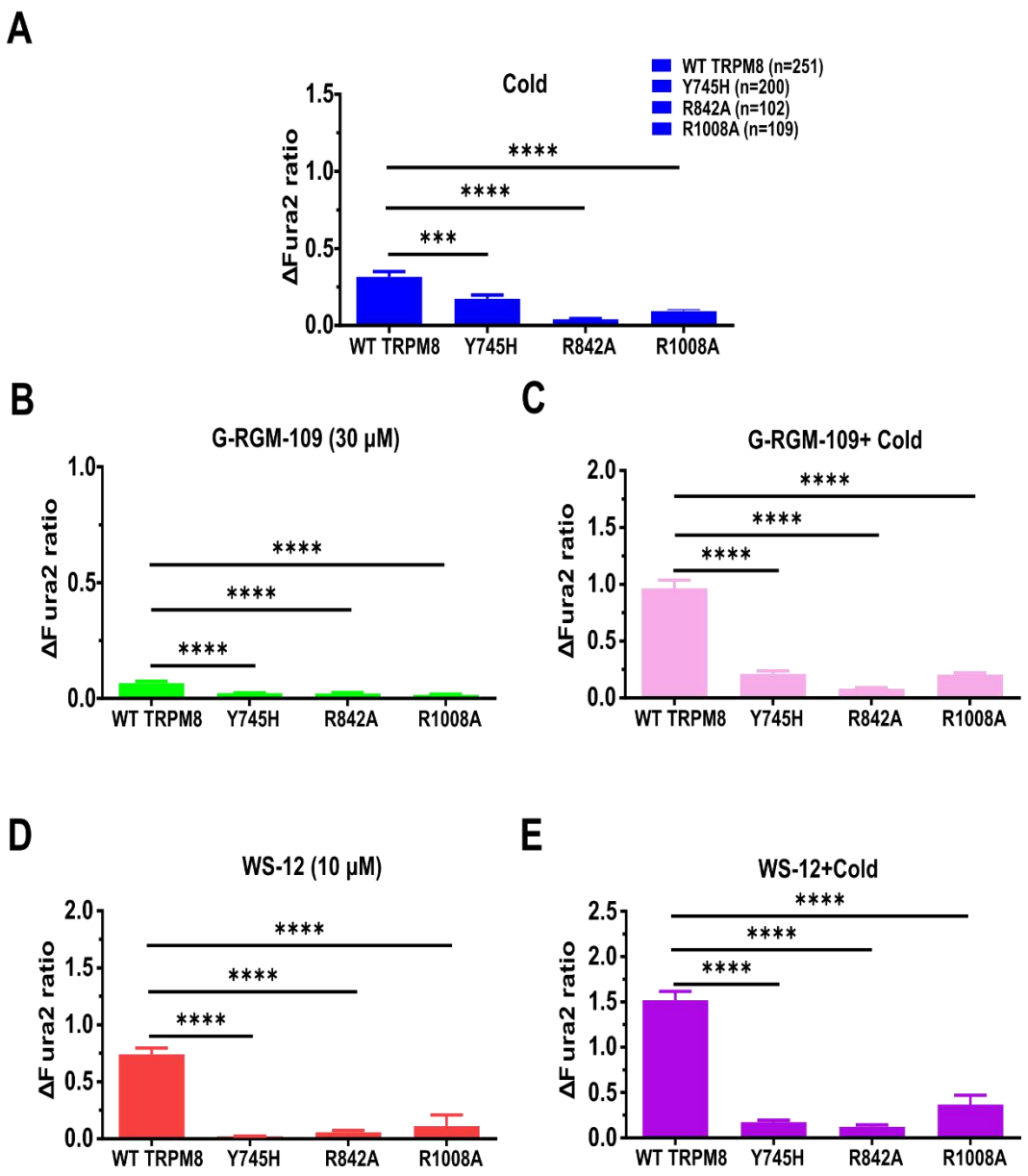

Figure 62. Summary of TRPM8 Calcium imaging response amplitude of mouse wild type (WT) TRPM8 compared to different TRPM8 mutants following the application of different TRPM8 agonists. A, Bar histogram summarizing the mean ± SEM calcium amplitude responses of GFP+ HEK293 cells transfected with mouse TRPM8 (WT or mutants) to cold. **B,** Bar histogram summarizing the mean ± SEM calcium amplitude responses of GFP+ HEK293 cells transfected with mouse TRPM8 (WT or mutants) to G-RGM-109 (30 μM). **C,** Bar histogram summarizing the mean ± SEM calcium amplitude responses of GFP+ HEK293 cells transfected with mouse TRPM8 (WT or mutants) to cold in the presence of G-RGM-109. **D,** Bar histogram summarizing the mean ± SEM calcium amplitude the responses of GFP+ HEK293 cells transfected with mouse TRPM8 (WT or mutants) to WS-12 (10 μM). **E,** Bar histogram summarizing the mean ± SEM calcium amplitude responses of GFP+ HEK293 cells transfected with mouse TRPM8 (WT or mutants) to cold in the presence of WS-12. Statistical significance was calculated by a one-way ANOVA followed by Bonferroni post-hoc test.

Conclusions of this chapter:

- G-RGM-109 is a weak and selective TRPM8 agonist.
- G-RGM-109 is less potent than WS-12.
- G-RGM-109 activation is dependent on menthol binding site Y745(S1).

5. Discussion

5.1 The immunosuppressant macrolide rapamycin is a novel TRPM8 Agonist

During this research project, I verified that the immunosuppressant macrolide rapamycin (RAP), a clinically approved drug, exhibits an agonistic effect on the TRPM8 ion channel. This was determined through a combination of *in vitro* calcium imaging and electrophysiological patch-clamp experiments. The experiments were conducted using either the HEK293 cell line, which was transfected heterologously, or cold-sensitive DRG neurons expressing TRPM8. These results support the description of RAP effects described previously by Arcas (Arcas Santos, 2019). I also tested the effects of RAP on different TRPM8 mutants to gain further insight on its interaction with the channel.

5.1.1 Pharmacological and biophysical characteristics of rapamycin agonism on TRPM8

RAP at 30 µM induced both, calcium influx activity and robust TRPM8 currents in HEK293 cell expressing mouse TRPM8. The RAP potency was lower compared to WS-12, a potent agonist (Ma et al., 2008). Similarly, to other TRPM8 agonists characterized previously, RAP potentiated cold-evoked calcium elevation and whole-cell currents closely resembled those evoked by menthol and it's derivative WS-12. I found that rapamycin activated the channel by causing a change in voltage-dependence, leading to channel activation at physiological potentials. Our finding is consistent with previously characterized TRPM8 agonists such as cold, menthol (Brauchi et al., 2004; Voets et al., 2004; Malkia et al., 2009), and the previously characterized immunosuppressant macrolide tacrolimus (Arcas et al., 2019). RAP slowed the gating kinetics of activation, resembling the effects observed with menthol and WS-12, classified as type I agonist (Janssens et al., 2016), and similar to observations made with menthol, thymol, incline, linalool. According to the analysis of these authors, this change reflects a slowing in the closing of the channel at the microscopic level. It is worth noting that tacrolimus, a different macrolide agonist of TRPM8, is also classified as a type I agonist and tacrolimus (Arcas et al., 2019).

I did also find that the application of 30 µM RAP activated an inward currents in a manner similar to menthol. Furthermore, in sensory DRG neurons RAP induced action potential firings at a frequency comparable to the response elicited by cold stimulation recorded in TRPM8-expressing thermoreceptor neurons. Similar results were obtained previously with the macrolide tacrolimus (Arcas et al., 2019). Moreover, I found also that RAP activated cold-sensitive thermoreceptor fibres innervating the dermis of mouse skin, shifting the activation threshold of these fibres towards warmer temperatures. When compared to the cold , RAP (30 µM) elicited a similar peak frequency response. However, its potency in enhancing the cold response was lower. This could be attributed to the limited accessibility of the drug in the *in vitro* skin preparation, which lacked vascularization.

I also obtained additional evidence supporting that RAP responses were mediated by the activation of the TRPM8 channel. First, RAP-evoked calcium increase was entirely absent in HEK293 cells that did not express TRPM8. Additionally, in our manuscript (Arcas et al., 2024 under review), we showed that RAP-induced currents in both TRPM8-expressing HEK293 cells and cold-sensitive dorsal root ganglia (DRG) neurons were completely blocked by two structurally unrelated TRPM8 blockers: BCTC (50 μM) and AMTB (10 μM). These findings strongly suggest that the effects of RAP are specifically mediated through the activation of TRPM8 channel.

In addition, I aimed to identify the potential binding site (LBS) of RAP on the mouse TRPM8 protein. Several methods have been used to study the molecular residues underlying the modulation of TRPM8 channel activation. These strategies go from classic site point-directed mutagenesis approaches (Chuang et al., 2004; Erler et al., 2006; Malkia et al., 2009; Pertusa et al., 2014; Beccari et al., 2017), to the construction of chimeric proteins (Chuang et al., 2004; Pertusa et al., 2014, 2018; Taberner et al., 2014) and, more recently, the application of the recent revolutionary single particle cryo-Electron Microscope (cryo-EM) techniques that have revolutionizing the field of structural biology (Yin et al., 2018, 2022; Palchevskyi et al., 2022; Pertusa et al., 2023). Noteworthy, computational methods have significantly advanced during the last decade, emerging as powerful tools for the prediction of ligand binding sites (LBS) on protein structures (J. Yang et al., 2013; Clark et al., 2020). Some authors suggest that the combination of both, experimental and computational methods, could enhance the accuracy and efficiency of ligand binding site (LBS) identification (J. Zhao et al., 2020; Guterres & Im, 2023). Therefore, I explored the possible residues involved in the activation of the TRPM8 ion channel by RAP using the site targeted mutagenesis technique. Thus, I ruled out the possibility of a shared mechanism of action between RAP and menthol after testing some key residues known to be critical for menthol activation. These residues are Y745, located in segment 1 (tested with Y745A mutation), and I846 in segment 4 (tested with I846A, I846T, I846V and I846D mutations). To complement this approach, I also tested the involvement of TRP domain residues Y1005 and R1008 (tested with Y1005A and R1008A mutations), known to be important in the activation mechanism of TRPM8 to different agonists.

Our results demonstrated that RAP activated the menthol-insensitive mutant Y745H by shifting the voltage-dependence of channel activation towards more negative potentials. Additionally, RAP induced potentiation of cold-evoked responses in this mutant. Interestingly, the segment 4 mutants at residue I846 (I846A, I846T, I846V, and I846D) exhibited an amplified response to RAP, indicating an enhanced sensitivity to RAP activation. In contrast, the I846D mutant showed a complete insensitivity to menthol and its structural analogue WS-12. This finding confirms the previously established critical role of the I846 residue in the binding and activation of TRPM8 by menthol (L. Xu et al., 2020). Furthermore, the TRP domain mutants Y1005A and R1008A showed a complete insensitivity to RAP and WS-12, in line with previous findings, highlighting both the crucial role of these residues in channel activation (Bandell et al., 2006; Rohács et al., 2005), and beyond, the pivotal role of TRP domain in tuning stimuli sensing

to pore opening that makes it essential for allosteric activation of TRPM8 channel (Taberner et al., 2014). Noteworthy, the presence of RAP significantly potentiated the response to cold stimulation of TRP domain mutants, which support the role of TRP domain residues Y1005 and R1008 in the coupling mechanism that leads to the opening of the TRPM8 channel in response to various stimuli.

Furthermore, RAP activates TRPM8 at the nerve terminals of saphenous cold-sensitive fibres that innervate mouse skin. I hypothesized that rapamycin sensitive fibres (n=3) that were firing action potentials upon exposure to rapamycin at the basal temperature are mostly expressing the TRPM8 thermoreceptor as their main transducer, and could be considered as the unimodal cutaneous cold fibres known previously in having TRPM8 receptor as their primary driver of cold sensitivity (Toro et al., 2015; Winter et al., 2017). In contrast, the remaining cold fibres (n=4) could be classified into two clusters, the first group are fibres (n=2 out 4) that showed both an increase of the cold evoked action potentials and a shift in the temperature threshold to warmer values in the presence of RAP, which might also be expressing TRPM8 as their prime excitability engine. While the second group of cold fibres (n=2 out 4) are those that showed a shift of the temperature threshold towards colder temperature after application of RAP, which could probably be expressing a different cold transducer most likely TRPA1 (Winter et al., 2017). Our skin nerve results are only preliminary, since our limited number of RAP fibres responders, which required to perform more experiments in order to expands the number of cold fibres, subsequently drawing a final conclusion.

To sum up, RAP has been established as an effective novel TRPM8 agonist. It has demonstrated the ability to activate both recombinant mTRPM8 and endogenous TRPM8 channels expressed in cold-activated mouse DRG sensory neurons.

This finding expanded the repertoire of TRPM8 agonists available for further research and for potential therapeutic applications. Moreover, I confirmed that RAP action mechanism is distinct from that of menthol, which enhance our understanding of the underlying mechanisms of TRPM8 channel activation. Finally, future research could take advantage of recent cryo-EM (cryogenic electron microscopy) findings on mouse TRPM8 (Yin et al., 2018, 2022) to uncover the binding site of RAP on the channel.

5.1.2 Therapeutical implications of RAP effects on TRPM8

My findings expand the repertoire of specific TRPM8 agonists, although further advancements in this field are still needed. I show that RAP can be used to identify and modulate TRPM8 expressing sensory neurons. Moreover, the residues involved in TRPM8 activation by RAP were found to be different from the canonical agonist menthol. Thus, the elucidation of the specific residues involved in RAP mediating TRPM8 activation is an important open question. Its solution would provide novel insights into the molecular mechanisms driving TRPM8 activation.

As previously mentioned in the introduction, TRPM8 is involved in many physiological functions such as warm perception, as reviewed by Paricio-Montesinos et al., (2020), thermoregulation and energy balance (Reimúndez et al., 2018), basal tearing, and sexual behaviour (Parra et al., 2010; Mohandass et al., 2020). Dysfunctions and/or dysregulations of the TRPM8 ion channel are linked to several pathologies such as different types of cancer (Tsavaler et al., 2001; Oh et al., 2018), migraine (González-Muñiz et al., 2019; Alarcón-Alarcón et al., 2022), dry eye disease (DED) (Parra et al., 2010; J. M. Yang et al., 2017a, 2018; Alcalde et al., 2018) and cold pain (Xing et al., 2007; Knowlton et al., 2013; Piña et al., 2019). Giving its multiple physiological roles, TRPM8 is considered a promising therapeutic target for the treatment of TRPM8-dependent dysregulations including pain. Notably, TRPM8 has been reported as the exclusive mechanism responsible for both menthol-evoked analgesia (Y. Liu et al., 2020b), and cold-induced analgesia (Knowlton et al., 2013). Additionally, TRPM8 activation by icilin has been found to have an effective anti-inflammatory effect in the colon during colitis (Ramachandran et al., 2013). Moreover, activation of the TRPM8-specific somatosensory pathway by either menthol or cold has been observed to provide relief from itch sensation (Palkar et al., 2018). Thus, there are extensive research efforts targeted at the development of novel selective and potent TRPM8 modulators, including agonists and antagonists, with the goal of treating or improving TRPM8-dependent diseases. RAP could represent an effective pharmacological therapy targeting several TRPM8 dependent pathologies, particularly pain and itch. In the future, it will be necessary to conduct experimental tests of RAP in animal models and clinical trials in humans to further evaluate its efficacy and safety in those contexts.

Rapamycin (Sirolimus), initially discovered as an antifungal agent (Arriola Apelo & Lamming, 2016), together with its analogs (rapalogs), such as Temsirolimus and Everolimus, are clinically approved drugs by the United States Food and Drug Administration (FDA) for clinical use in human pathologies starting from 1999. These drugs have been used primarily as immunosuppressors following solid organ transplantation, particularly in kidney and heart transplants. Furthermore, rapamycin and rapalogs also have been shown to be efficacious in the treatment of various forms of cancer, including renal carcinoma and neuroendocrine tumours of pancreatic origin, exhibiting cytostatic but not cytotoxic effects (J. Li et al., 2014).

Activation of TRPM8 was found to regulate basal tearing and blinking (Parra et al., 2010; Quallo et al., 2015). Based on these findings, TRPM8 agonists have been proposed as a potential therapy for DED, and the effectiveness of different TRPM8 agonists in improving DED symptoms have been reported (Belmonte and Gallar, 2011; Yang et al., 2017). In the same line, a study reported that RAP treatment-based on liposomes improved DED symptoms in a dog model by increasing lacrimal production and reducing inflammation (Linares-Alba et al., 2016). One year later, this finding was further supported by a study conducted in a mouse model of Sjogren´s syndrome, which demonstrated that topical RAP treatment reduced autoimmune-mediated lacrimal gland inflammation and stimulated tear secretion (Shah et al., 2017). Moreover, a nanoparticle-based eye drop containing adapted aqueous RAP (MET-

RAP) showed effectiveness in the treatment of an eye uveitis mouse model, suggesting an anti-inflammatory effect. This effect was achieved through the regulation of immune cells by inhibiting Th17 cells and upregulation of T-reg cells (Badri et al., 2022). In light of my discoveries, the relevance of RAP activation of TRPM8 in DED should be considered. In support of a role is the recent finding that tacrolimus regulates tearing and blinking by a TRPM8-dependent mechanism (Arcas et al., 2019). Although there is still limited evidence regarding the relevance of TRPM8 activation by RAP in topical dermatitis, our results have shown the activation of cutaneous cold thermoreceptors by RAP. This opens up possibilities for potential topical use in skin conditions. In this context, a recent study showed that topical application of RAP improved skin inflammation in a mouse model of IMQ-induced psoriasis (Kim et al., 2021). Despite the therapeutic potential of RAP, it is important to note that its use can be associated with serious side effects, including gastrointestinal, respiratory, and haematological issues. These side effects may be attributed to the inhibition of mTORC2, a canonical intracellular receptor target of RAP, rather than mTORC1. Chronic systemic treatment with RAP can impact several vital functions mediated by mTORC2 (J. Li et al., 2014).

Our findings defined TRPM8 as new pharmacological target for RAP, a clinically approved drug. The effects of RAP on TRPM8 could partially explain the role of RAP in the treatment of DED and dermatitis. Our discovery holds significance within the realm of drug reprofiling (or repositioning), a concept that entails repurposing a drug for a different medical indication than originally intended during its initial marketing. This strategy offers several advantages over developing entirely new drugs, leveraging the established pharmacokinetics and known safety profile of the repurposed drug. Additionally, it can result in significant time and cost savings compared to the intricate process of developing novel medications. (Doan et al., 2011; Jourdan et al., 2020).

5.1.3 Segment 4 residue I846 mutation induces a constitutively active TRPM8 channel

As shown previously in the results section, the introduction of single point mutations at residue I846 in segment 4, where the hydrophobic amino acid isoleucine (I) was substituted with different amino acids (Alanine, threonine, valine and and acid aspartic) resulted into enhanced responses to RAP. In contrast, the I846D mutant was insensitive to menthol and its analogue WS-12, which could be caused by the complete alteration of the hydrophobic character of residue isoleucine I846 that affected the binding of menthol and WS-12 through their isopropyl function group, in line with the literature (L. Xu et al., 2020).

The main function of ion channels is to regulate the flow of ions across cellular membranes. Alterations in their ability to open or close in response to stimuli is the molecular base of different channelopathies (Harraz & Delpire, 2024)

HEK293 cells expressing the laboratory generated mutants I846A, I846T and I846V had elevated basal internal calcium levels, in the absence of any stimuli. This suggests that these TRPM8 mutants have an open pore at rest, allowing the influx of calcium ions from the extracellular environment. The continuous influx could lead to alterations in the filling of endoplasmic reticulum calcium stores. A similar phenotype was previously observed in CHO cells expressing the I846V TRPM8 mutant (Bandell et al., 2006). Moreover, in whole-cell voltage-clamp experiments, HEK293 cells expressing these I846 mutations showed large outward currents at rest (33 ºC). Interestingly, our calcium imaging results supported the existence of extracellular calcium entry at rest, together with calcium store release from endoplasmic reticulum (ER) and/or Golgi apparatus (GA) (Xue et al., 1994; Missiaen et al., 2004).

Notably, our findings could be explained based on various studies demonstrating the expression of TRPM8 in both plasma and endoplasmic reticulum membranes(Thebault et al., 2005; Bidaux et al., 2007; Mahieu et al., 2007). Additionally, other research groups have reported the presence of truncated TRPM8 variants in the endoplasmic reticulum of lung epithelial cells(Sabnis et al., 2008). Subsequently, another isoform of the TRPM8 channel with four domains (4TM-TRPM8) was identified within the endoplasmic reticulum membrane of keratinocytes (Bidaux et al., 2015) or in prostate cells (Bidaux et al., 2018).

Subsequently, these TM4 mutants at residue I846 are characterized as constitutively active channels at resting potentials, indicating a gain of function phenotype. Electrophysiologically, this gain of function phenotype was manifested in a shift in the voltage dependence of activation towards more negative potentials compared to the wild type. Interestingly, neither the preservation of non-polar property of the isoleucine 846 residue by using alanine or valine amino acids, nor the complete alteration of the physico-chemical properties with threonine (polar) or aspartic acid (negatively charged) residues, was able to rescue the wild type TRPM8 voltage dependence. This suggests that the alteration of the voltage

dependence is more related to hydrophobic side chain size, as isoleucine has a larger nonpolar side chain compared to both alanine and valine.

A constitutively active phenotype was previously described for other members of the TRP channel family such as TRPML subfamily members TRPML2 and TRPML3. Specifically, mutations TRPML2-A424P and TRPML3-A419P caused pigmentation defect and hearing loss in mice (Lev & Minke, 2010; Lev et al., 2010). The *drosophila* TRP-F550I mutant (caused photoreceptor degeneration in *drosophila*), located in transmembrane segment 5, altered their resting activity and made them constitutively active, leading to outward rectification and opening at negative potentials (Yoon et al., 2000).

An open pore phenotype at basal conditions was also reported in TRPM8 channels following mutation at S27P located at N-terminus (Pertusa et al., 2014). The constitutive activity was observed both in calcium imaging (high intracellular $[Ca^{2+}]_i$) and in patch clamp recordings (outward rectification), and both phenotypes were reversed by the application of a specific TRPM8 blocker such as AMTB, which shifted the voltage dependence towards more positive potentials resulting in closed channels at the resting membrane potential. The use of TRPM8 blockers could be considered as an effective therapeutic approach for the treatment of this leaky channel phenotype. Besides, recent studies reported additional gain of function TRPM8 variants including R30Q (Gualdani et al., 2021) and D665N, V915M single mutations (Ghovanloo et al., 2024).

Similar constitutively active phenotypes had been reported in several studies investigating mutations in other ion channels associated with various diseases. For example, variants of the IP3R3 receptor were found to exhibit constitutively active leaky channels associated with human neuropathy (Terry et al., 2022). Moreover, the voltage gated potassium channel (KCNQ3) mutants had been widely associated with hyperexcitability related disorders including neuropathic pain and epilepsy. The R230C mutation in the voltage sensor (S4) of KCNQ3 turned the channel constitutively conductive at physiological potentials by shifting the voltage dependence towards more negative values, which was entirely attributed to the alteration of both the positive charge and the size of the side chain properties of the arginine residue (Barro-Soria, 2019). Furthermore, a gain of function phenotype was observed in a missense mutation in the D II S4-S5 linker of the Nav1.7 voltage gated sodium channel. The G856R or G586D mutants showed an enhanced persistent current at resting potentials, that was related to the shift of voltage dependence toward hyperpolarized potentials (Tanaka et al., 2017).

Thus, the identification of a constitutively active TRPM8 channel harbouring a single mutation could eventually implicate TRPM8 in a clinically relevant channelopathy (Gualdani et al., 2021; Ghovanloo et al., 2024). Additional studies of these constitutively active mutants are needed. For example, the expression of these ´´gain of function`` mutants in their native context, in in DRG neuronal cultures. Thereafter, investigating their effects at the organism level (pain behaviour, thermoregulation etc) using transgenic mouse models expressing these specific constitutive TRPM8 mutants.

5.1.4 Some I846 mutations cause alteration in channel trafficking

Tetramerization is essential for proper TRPM8 channel function. The synthesis of TRPM8 protein subunits happen within the endoplasmic reticulum, where likely the assembly of TRPM8 subunits into homo-tetramers initiate. Ultimately, the proper folding and maturation of the functional TRPM8 terminate in Golgi complex, before trafficking towards the plasma membrane (Erler et al., 2006; Phelps & Gaudet, 2007).

Two point mutations of the isoleucine residue at the position 846, I846A and I846T produced a different phenotype. Specifically, these two mutants presented an intracellular calcium transient response to cold ramps in calcium free solution (Ø Ca^{2+}) that was not observed in wild type. This calcium release must be coming from intracellular stores and further suggests a perturbation in the mutants TRPM8 channel trafficking. The hypothesis suggests that the mutant channels might be being massively trapped and/or extensively expressed at the membrane of the endoplasmic reticulum and/or Golgi apparats. Upon their activation released store calcium into the cytoplasm in calcium free solution (Ø Ca^{2+}). Together, these results lead us to suggest the possibility that both mutant channels are retained in the endoplasmic reticulum (ER) and/or Golgi apparatus. Noteworthy, In order to test our hypothesis we need to perform additional experiments such as : 1) Immunofluorescence of heterologous overexpression of our mutants channel fused to YFP- fluorescent victor (I846A-YFP and I846T-YFP) and visualize using confocal microscopy the expression pattern within plasma and organelles (ER and GA) membranes, compared to wild type channel expression (Phelps & Gaudet, 2007; Asuthkar et al., 2015). Or, 2) Perform calcium imaging, in calcium free solution (Ø Ca^{2+}) condition, and inhibit the gain of function mutants expression at ER/GA membranes that are responsible for calcium store leak, either using Thapsigarpin (plasma membrane permeable) TRPM8 antagonist, or using the short haipin RNA (shRNA) to silence the expression of TRPM8 channel (Sabnis et al., 2008).

Several previous studies reported TRPM8 mutants with altered traffic. For example, the deletion of different fragments of the N-terminus can produce channels with defect N-glycosylated state (Asn934) measured by western blot assay, and which are mostly localized in endoplasmic reticulum and/or Golgi organelles revealed combining confocal microscopy and immunofluorescence (Phelps & Gaudet, 2007; Pertusa et al., 2014). Another study demonstrated that the lack of C-terminus colloid coil (1064-1104 residues) of the TRPM8 channel produced a retention of the channel in the ER (Tsuruda et al., 2006).

Furthermore, accumulation in the ER was also observed with other TRP channel, including TRPV4 splice variants (Arniges et al., 2006), or TRPV5 mutants at the N-terminus channels (de Groot et al., 2011) reporting their ER retention could be explained by different mechanisms. First, the mutation could be due to the suppression of some trafficking signal encoded by the altered segment that could be affecting the proper targeting of the channels to plasma membrane. Second, the mutant sequence could

lead to channel misfolding that could be detected by a quality control mechanism resulting into mutants' retention within the ER. Finally, the exposition of the bi-arginine retention motif (R*X*R) in non-assembled channel subunits (normally hidden in the tetramerized structure).

Our investigation discriminates between these three possibilities and only admitted the first hypothesis, while ruling out the other hypothesis since the mutants are properly folded to a functional channel oligomer. I have conducted a functional study using calcium imaging as a validated technique to assess functionally both the plasma membrane but, more crucially, in HEK293 cells expressing the ER mTRPM8 mutants (I846A and I846T). The TRPM8 channel activity within ER was previously described and its activation required the simultaneous application of cold and menthol (Pertusa et al., 2012, 2014). Our results showed that both mutants channels were functional following just cold application, which indicating clearly that both, I846A and I846T mutants, were properly folded and assembled into functional tetramers. Interestingly, I showed that their expression in ER contributed into the cold hypersensitivity through the release of internal calcium stores, and that ER mutants TRPM8 activation required only cold stimulus confirming again the mutants' hypersensitivity to TRPM8 agonists. In contrast, wild type TRPM8 channels located within the ER whose activation requires the simultaneous application of cold and menthol (Pertusa et al., 2012). Furthermore, unpublished data from our laboratory, based on western blot experiment, clearly showed the absence of the glycosylated band in the I846A mutant compared to the wild type where two bands are typically observed: Glycosylated (~ 130 kDa) and Non-glycosylated (Pertusa et al., 2012), this leads us to suggest that the S4 mutants are mainly localized within the ER. Noteworthy, the absence of glycosylation may reflect that these mutants do not transit through Golgi apparatus due to failure to passe the quality control at ER. Thus, the mutation at I846 seemed to not affect the biogenesis of functional channel but rather suppresses the glycosylation state leading to mutants channel accumulation in the RE. Theoretically, we can suggest that the mutation at I846 of the segment 4 would affect the normal trafficking of the channel towards the plasma membrane, although the presence of these non-glycosylated channels in plasma membrane could be explained as an escape from the quality control barrier exerted at ER without undergoing the canonical process through Golgi apparatus, which in line with previously reported work on some mutants and chimeras (de Groot et al., 2011; Pertusa et al., 2014).

5.1.5 Isoleucine at position 846 plays a pivotal role in the modulation of both RAP and WS-12 sensitivity

The investigation into the role of the I846 residue revealed an inhibitory modulation effect on RAP sensitivity. Notably, an increase in RAP channel sensitivity was observed following single substitutions of the isoleucine (I846) residue with hydrophobic amino acids (alanine, threonine, and valine) or an insertion of the negatively charged acid aspartic. These mutations suggest that structural changes induced by these amino acid substitutions lead to an enhanced RAP response phenotype.

Crystallography and/or Cryo-EM structural studies are recommended to evaluate the interactions between different amino acids in segment 4 of the protein.
Electrophysiological recordings from different mutants at I846 (I846A, I846T, I846V, and I846D) revealed that the potentiation in response to RAP is attributed to a marked leftward shift of ~86 mV in the voltage dependence of activation. This shift increases the probability of channel opening at more physiological membrane potentials. The variety of amino acid substitutions, including alanine, valine, threonine, or acid aspartic, with distinct physicochemical properties, indicates that the isoleucine residue plays a critical role in this inhibition. Moreover, the results suggest that these substitutions may perturbate the TRPM8 protein structure, considering the role of the isoleucine hydrophobic side chain in tuning both the structure and stability of proteins (Kathuria et al., 2016; AL Mughram et al., 2023).

Importantly, the study demonstrated a clear loss of TRPM8 channel sensitivity to WS-12 and menthol when the isoleucine residue (I846) was mutated to the acid aspartic (D) amino acid, but not with alanine, threonine, or valine. This finding suggests that the hydrophobic environment induced by isoleucine is critical for WS-12 binding rather than the residue itself. The result is reminiscent of studies showing a lack of menthol sensitivity in TRPM8 mutants L1009R and Y745H (Bandell et al., 2006; Voets et al., 2007a). Tritiated menthol studies identified a defect in specific menthol binding in the Y745H mutant, while a decrease in menthol efficacy was observed in the L1009R mutant (Voets et al., 2007a).

TRM8 mutants (Location)	**TRPM8** **Agonists**	**Phenotypes**
Y745**H** (TM1)	**-Rapamycin** **-WS-12** **-Cold** -Voltage	**-Wild type response.** **-Insensitive.** **-Wild type response.** -Wild type phenotype
I846**A** (TM4)	**-Rapamycin** **-WS-12** **-Cold** **-Volatge**	-Constitutively active. -Trafficking alteration. **-Hypersensitive** **-Wild type response.** **-Wild type response.** -Alteration of cold potentiation by TRPM8 agonists. -leftward shifted (more negative)
I846**T** (TM4)	**-Rapamycin** **-WS-12** **-Cold** **-Volatge**	-Constitutively active. -Trafficking alteration. **-Hypersensitive** **-Wild type response.** **-Wild type response.** -Alteration of cold potentiation by TRPM8 agonists. - leftward shifted (more negative)
I846**V** (TM4)	**-Rapamycin** **-WS-12** **-Cold** **-Volatge**)	-Constitutively active. **-Hypersensitive** **-Wild type response.** **-Hypersensitive.** - leftward shifted (more negative)
I846**D** (TM4)	**-Rapamycin** **-WS-12 (menthol)** **-Cold** **-Volatge**	-Constitutively active. **-Hypersensitive** **-Insensitive (partially).** **-Wild type response.** -Alteration of cold potentiation by TRPM8 agonists. - leftward shifted (more negative)

Y1005**A** (TRPd)	**-Rapamycin** **-WS-12** **-Cold**	**- Altered sensitivity (from Calcium data).** **-Altered sensitivity.** **- Altered sensitivity.** -Altered of cold potentiation by TRPM8 agonists
R1008**A** (TRPd)	**Rapamycin** **-WS-12** **-Cold**	**- General alteration of the mutant channel's sensitivity to all TRPM8 agonists.**

Table 2. Summary of mouse TRPM8 mutants' response phenotypes to TRPM8 agonists.

Note, TM : transmembrane domain. TRPd: TRP domain.

5.2 G-RGM-145 and G-RGM-109 are two novel TRPM8 agonists

Two new chemically synthesized molecules, G-RGM-145 and G-RGM-109, developed by our collaborators at the Institute of Medicinal Chemistry (IQM) in Madrid, were studied. These molecules showed selective agonist activity on native mouse TRPM8-expressing neurons and in the heterologously expressed mTRPM8 channel. Moreover, their mechanism of action involves TRPM8 residues that are also important for menthol agonism.

5.2.1 TRPM8 channels in mouse DRG neurons are activated by G-RGM-145 and G-RGM-109

In TRPM8$^{BAC\text{-}EYFP}$ mice, both G-RGM-145 and G-RGM-109 activated the majority of TRPM8-expressing cold-sensitive neurons, as identified by EYFP fluorescence and by their response to a cold ramp from 33 to 18 ˚C. Only a negligible fraction of the EYFP (-) neurons (i.e., those not expressing TRPM8) were recruited in the presence of Ag145 during cooling, suggesting a highly specific effect of Agonist G-RGM-145 on TRPM8-expressing neurons.

Moreover, both agonists, G-RGM-145 and G-RGM-109, evoked calcium influx in TRPM8-expressing DRG sensory neurons at low concentrations (3 μM) and higher concentrations (10 μM), and they both potentiated cold evoked responses. The potency of both drugs in neuronal culture seems to be lower compared to WS-12. The potentiation of cold evoked responses by G-RGM-145 was similar to the effect obtained with WS-12, whereas the cold-evoked potentiation was significantly lower in the presence of G-RGM-109.

To confirm that the effects observed were mediated exclusively by TRPM8, a pharmacological strategy was employed, using specific TRPM8 blockers. The calcium influx induced by both novel agonists was

completely suppressed in the presence of TRPM8 blockers, AMTB (10 μM) or RQ00203078 (0.5 μM). This result indicates that the activation by each agonist was selectively mediated by endogenous mouse TRPM8.

In the same line, similar results were obtained in HEK293 cell line showing that the potentiation of cold-evoked responses in the presence of G-RGM-145 was similar to that of the menthol analogue WS-12. In contrast, the potentiation of cold evoked responses by G-RGM-109 was lower than that obtained with WS-12. Thus, results suggested that G-RGM-109 is a weaker agonist compared to G-RGM-145.

5.2.2 G-RGM-145 and G-RGM-109 HCl act through the menthol binding site

After validating that both novel TRPM8 agonists (G-RGM-145 and G-RGM-109) activated heterologously transfected mTRPM8 and potentiated cold-evoked responses in the HEK293 system, I conducted single targeted mutagenesis studies to explore the potential binding residues involved in TRPM8 activation by both agonists.

Furthermore, our results from single targeted mutagenesis confirmed the importance of the critical residues for menthol activation. Three mutants, Y745H, R842 and R1008A, showed complete insensitivity to all the agonists tested, including G-RGM-145, G-RGM-109 and the menthol analogue WS-12. Additionally, the application of agonists in these mutants failed to potentiate cold evoked responses, indicating that these residues play a crucial role in the activation of TRPM8 by all tested agonists.

I conclude that these novel chemically synthesized molecules, G-RGM-145 and G-RGM-109, are agonists of mouse TRPM8 channels, and their effect was shown to be selectively mediated by TRPM8 in DRG sensory neurons. Furthermore, I did show that these agonists activated the TRPM8 channel directly through their interaction with the menthol binding residue Y745 (S1). However, both G-RGM-145 and G-RGM-109 were found to be less potent at tested concentration (10 μM) compared to WS-12.

To further understand their pharmacology and efficacy, future experiments should investigate the cross-interactions of these two agonists within the same TRP family. Additionally, conducting electrophysiological recordings with the patch-clamp technique in both cell lines and neuronal culture would help to confirm the results obtained from calcium imaging experiments.

While these preliminary results are promising and expand the potential drug arsenal, further studies are needed to assess the therapeutic effects of these two novel agonists on TRPM8-dependent diseases in animal models, which may open new possibilities for potential therapeutical applications of these novel TRPM8 agonists.

5.2.3 Novel TRPM8 Agonists : From basic characterization to the clinical trial

The discovery, development of novel TRPM8 agonists has been extensively discussed in a recent review by Izquierdo and collaborators (Izquierdo et al., 2021). A major goal of these recent effort converges into the development of novel TRPM8 agonists with fast onset activation, long-lasting cooling effects, and without the side effects that are produced by the natural compounds, such as irritation and bitter tasting resulting from crossed pharmacology with other ion channels. The identification of these molecules, could be useful in different industries, including their use as cooling compounds in cosmetics and food ingredients.

Several companies directed their attention towards developing new chemically synthesized TRPM8 agonists, which are structurally menthol-independent, or menthol derivatives based on the replacement of menthol cyclohexane moiety by phenyl, adamantly or branched alkyl moieties, in order to enhance potency and achieve nanomolar scale agonist effects. Among the agonists, the most potent and biologically effective molecules reported so far is Cryosim C3 (J. M. Yang et al., 2017a; González-Muñiz et al., 2019; Izquierdo et al., 2021).

Moreover, the majority of cooling agonists identified have shown potential in stimulating physiological functions as well as improving TRPM8 dependent pathologies. Some have demonstrated efficacy in promoting thermogenesis by stimulating energy expenditure, which could be considered as potential treatment for obesity (Liskiewicz et al., 2023). Other TRPM8 agonists also showed efficacy in alleviating sensory discomfort (Wei, 2015), and treating gastrointestinal tract disorders (Wei, 2017). Notably, Cryosim-3 has been successfully used topically to treat mild dry eye disease, with a full absence of the usual side effects associated with use of agonists, such as irritation and pain (J. M. Yang et al., 2018).

The newly, chemically synthetized G-RGM-145 and G-RGM-109 showed a very selective activation of TRPM8-expressing DRG neurons, suggesting a reduced risk of side effects associated with crossed pharmacology targeting other ions channels. However, the potency of these two agonists seems to be markedly weaker compared to the reference agonist WS-12 at tested concentrations. This may render these agonists less attractive for potential clinical use. Although the preliminary data highlights their selective TRPM8 agonism and shared mechanism of action with menthol, a comprehensive study of these two TRPM8 agonists is still lacking. Thus, I cannot draw final conclusions at this stage, since further experiments are needed to confirm the data and expand the results especially in evaluating the efficacy of both drugs to treat TRPM8-dependent disorders.

Finally, addressing these additional questions through further research and experiments will be crucial to fully understand the potential of G-RGM-145 and G-RGM-109 as therapeutics for TRPM8-related dysregulations. This perspective will help to determine their suitability for clinical use and potentially contribute to the development of effective treatments for TRPM8-mediated disorders.

TRM8 mutants	TRPM8 Agonists	Phenotypes
Y745**H** **(TM2)**	- G-RGM-145 - G-RGM-109 -WS-12 -Cold	-Insensitive. -Insensitive. -Insensitive. -Wild type response.
R842**A** **(TM4)**	- G-RGM-145 - G-RGM-109 -WS-12 -Cold	-Insensitive. -Insensitive. -Insensitive. -Altered response.
R1008**A** **(TRPd)**	- G-RGM-145 - G-RGM-109 -WS-12 -Cold	-Severely altered response to all TRPM8 agonists.

Table 3. Summary of mouse TRPM8 mutants' response phenotype to both agonists : G-RGM-145 and G-RGM-109.

6. Conclusions:

1. Rapamycin activates the heterologously expressed mouse TRPM8 ion channel and potentiates cold-evoked responses.
2. Rapamycin elicits robust mTRPM8 currents and potentiates cold-evoked currents.
3. At biophysical level, TRPM8 activation by rapamycin is accompanied by a shift in the activation curve towards more negative membrane potentials.
4. Rapamycin increases the excitability of TRPM8-expressing cold sensory DRG neurons.
5. Rapamycin activates mutant channels that are insensitive to menthol, suggesting the presence of an alternative binding site for TRPM8 agonism.
6. The residue I846, located at transmembrane domain 4, appears to be critical for proper channel function. Mutations at this residue affected its thermal and chemical sensitivity, and alters channel traffic.
7. The compounds G-RGM-145 and G-RGM-109 selectively activate TRPM8-expressing cold sensory mouse DRG neurons and potentiate their cold-evoked responses.
8. G-RGM-145 and G-RGM-109 exhibit lower potency compared to the canonical agonist, WS-12.
9. Mutation Y745H prevents the agonism of both compounds, suggesting that agonism depends on a functional menthol binding pocket.

7. Conclusiones

1. La rapamicina activa el canal iónico TRPM8 de ratón expresado heterólogamente y potencia sus respuestas evocadas por el frío.
2. La rapamicina induce mTRPM8 corrientes robustas y potencia las corrientes evocadas por el frío.
3. A nivel biofísico, la activación del canal TRPM8 por la rapamicina se acompaña de un desplazamiento en la curva de activación hacía potenciales de membrana más negativos.
4. La rapamicina aumenta de manera selectiva la excitabilidad de las neuronas sensoras del frío de los ganglios raquideos que expresan TRPM8.
5. La rapamicina activa canales mutantes que son insensibles al mentol, lo que sugiere la presencia de un sitio de unión alternativo para el agonismo de TRPM8.
6. El residuo I846, ubicado en el dominio transmembrana 4, parece ser crítico para el correcto funcionamiento del canal. La mutaciones es este residuo afectaron su sensibilidad térmica y quimica y alteraron el tráfico del canal.
7. G-RGM-145 y G-RGM-109 activan selectivamente las neuronas los ganglios raquídeos que expresan TRPM8 y lo que respuestas evocadas por el frío.
8. Tanto G-RGM-145 como G-RGM-109 exhiben menor potencia que el agonista canónico de TRPM8, WS-12.
9. La mutación Y745H impide el agonismo de ambos compuestos, lo que sugiere que el agonismo depende de un sitio del agonista de TRPM8 mentol.

8. Bibliography

Abe, J., Hosokawa, H., Okazawa, M., Kandachi, M., Sawada, Y., Yamanaka, K., Matsumura, K., & Kobayashi, S. (2005). TRPM8 protein localization in trigeminal ganglion and taste papillae. *Molecular Brain Research*, *136*(1–2), 91–98. https://doi.org/10.1016/j.molbrainres.2005.01.013

Aizawa, N., Ohshiro, H., Watanabe, S., Kume, H., Homma, Y., & Igawa, Y. (2019). RQ-00434739, a novel TRPM8 antagonist, inhibits prostaglandin E2-induced hyperactivity of the primary bladder afferent nerves in rats. *Life Sciences*, *218*, 89–95. https://doi.org/10.1016/j.lfs.2018.12.031

AL Mughram, M. H., Catalano, C., Herrington, N. B., Safo, M. K., & Kellogg, G. E. (2023). 3D interaction homology: The hydrophobic residues alanine, isoleucine, leucine, proline and valine play different structural roles in soluble and membrane proteins. *Frontiers in Molecular Biosciences*, *10*. https://www.frontiersin.org/articles/10.3389/fmolb.2023.1116868

Alarcón-Alarcón, D., Cabañero, D., de Andrés-López, J., Nikolaeva-Koleva, M., Giorgi, S., Fernández-Ballester, G., Fernández-Carvajal, A., & Ferrer-Montiel, A. (2022). TRPM8 contributes to sex dimorphism by promoting recovery of normal sensitivity in a mouse model of chronic migraine. *Nature Communications*, *13*, 6304. https://doi.org/10.1038/s41467-022-33835-3

Alcalde, I., Íñigo-Portugués, A., González-González, O., Almaraz, L., Artime, E., Morenilla-Palao, C., Gallar, J., Viana, F., Merayo-Lloves, J., & Belmonte, C. (2018). Morphological and functional changes in TRPM8-expressing corneal cold thermoreceptor neurons during aging and their impact on tearing in mice. *Journal of Comparative Neurology*, *526*(11), 1859–1874. https://doi.org/10.1002/cne.24454

Almaraz, L., Manenschijn, J.-A., de la Peña, E., & Viana, F. (2014). TRPM8. In B. Nilius & V. Flockerzi (Eds.), *Mammalian Transient Receptor Potential (TRP) Cation Channels: Volume I* (pp. 547–579). Springer. https://doi.org/10.1007/978-3-642-54215-2_22

Almeida, M. C., Hew-Butler, T., Soriano, R. N., Rao, S., Wang, W., Wang, J., Tamayo, N., Oliveira, D. L., Nucci, T. B., Aryal, P., Garami, A., Bautista, D., Gavva, N. R., & Romanovsky, A. A. (2012). Pharmacological Blockade of the Cold Receptor TRPM8 Attenuates Autonomic and Behavioral Cold Defenses and Decreases Deep Body Temperature. *The Journal of Neuroscience*, *32*(6), 2086–2099. https://doi.org/10.1523/JNEUROSCI.5606-11.2012

Alvers, A. L., Wood, M. S., Hu, D., Kaywell, A. C., Dunn, W. A., & Aris, J. P. (2009). Autophagy is required for extension of yeast chronological life span by rapamycin. *Autophagy*, *5*(6), 847–849.

Andersson, D. A., Chase, H. W. N., & Bevan, S. (2004). TRPM8 activation by menthol, icilin, and cold is differentially modulated by intracellular pH. *The Journal of Neuroscience: The Official Journal of the Society for Neuroscience*, *24*(23), 5364–5369. https://doi.org/10.1523/JNEUROSCI.0890-04.2004

Andersson, D. A., Nash, M., & Bevan, S. (2007). Modulation of the Cold-Activated Channel TRPM8 by Lysophospholipids and Polyunsaturated Fatty Acids. *The Journal of Neuroscience*, *27*(12), 3347–3355. https://doi.org/10.1523/JNEUROSCI.4846-06.2007

Arcas, J. M., González, A., Gers-Barlag, K., González-González, O., Bech, F., Demirkhanyan, L., Zakharian, E., Belmonte, C., Gomis, A., & Viana, F. (2019). The Immunosuppressant Macrolide Tacrolimus Activates Cold-Sensing TRPM8 Channels. *The Journal of Neuroscience*, *39*(6), 949–969. https://doi.org/10.1523/JNEUROSCI.1726-18.2018

Arcas Santos, J. M. (2019). *The cold-activated TRPM8 channel: Agonism by macrolide immunosuppressants and modulation by Gq protein-coupled receptors signaling pathways* [Universidad Miguel Hernández-CSIC]. http://dspace.umh.es/bitstream/11000/5145/1/Tesis%20Arcas%20Santos%2C%20Jos%C3%A9%20Miguel%20.pdf

Arniges, M., Fernández-Fernández, J. M., Albrecht, N., Schaefer, M., & Valverde, M. A. (2006). Human TRPV4 Channel Splice Variants Revealed a Key Role of Ankyrin Domains in Multimerization and Trafficking *. *Journal of Biological Chemistry*, *281*(3), 1580–1586. https://doi.org/10.1074/jbc.M511456200

Arriola Apelo, S. I., & Lamming, D. W. (2016). Rapamycin: An InhibiTOR of Aging Emerges From the Soil of Easter Island. *The Journals of Gerontology Series A: Biological Sciences and Medical Sciences*, *71*(7), 841–849. https://doi.org/10.1093/gerona/glw090

Asuthkar, S., Demirkhanyan, L., Sun, X., Elustondo, P. A., Krishnan, V., Baskaran, P., Velpula, K. K., Thyagarajan, B., Pavlov, E. V., & Zakharian, E. (2015). The TRPM8 Protein Is a Testosterone Receptor. *The Journal of Biological Chemistry*, *290*(5), 2670–2688. https://doi.org/10.1074/jbc.M114.610873

Babes, R.-M., Selescu, T., Domocos, D., & Babes, A. (2017). The anthelminthic drug praziquantel is a selective agonist of the sensory transient receptor potential melastatin type 8 channel. *Toxicology and Applied Pharmacology*, *336*, 55–65. https://doi.org/10.1016/j.taap.2017.10.012

Badr, M. Y., Halwani, A. A., Odunze, U., Eskandarpour, M., Calder, V. L., Schätzlein, A. G., & Uchegbu, I. F. (2022). The topical ocular delivery of rapamycin to posterior eye tissues and the suppression of retinal inflammatory disease. *International Journal of Pharmaceutics*, *621*, 121755. https://doi.org/10.1016/j.ijpharm.2022.121755

Ballou, L. M., & Lin, R. Z. (2008). Rapamycin and mTOR kinase inhibitors. *Journal of Chemical Biology*, *1*(1–4), 27–36. https://doi.org/10.1007/s12154-008-0003-5

Bandell, M., Dubin, A. E., Petrus, M. J., Orth, A., Mathur, J., Hwang, S. W., & Patapoutian, A. (2006). High-throughput random mutagenesis screen reveals TRPM8 residues specifically required for activation by menthol. *Nature Neuroscience*, *9*(4), 493–500. https://doi.org/10.1038/nn1665

Barro-Soria, R. (2019). Epilepsy-associated mutations in the voltage sensor of KCNQ3 affect voltage dependence of channel opening. *The Journal of General Physiology*, *151*(2), 247–257. https://doi.org/10.1085/jgp.201812221

Bautista, D. M., Jordt, S.-E., Nikai, T., Tsuruda, P. R., Read, A. J., Poblete, J., Yamoah, E. N., Basbaum, A. I., & Julius, D. (2006). TRPA1 Mediates the Inflammatory Actions of Environmental Irritants and Proalgesic Agents. *Cell*, *124*(6), 1269–1282. https://doi.org/10.1016/j.cell.2006.02.023

Bautista, D. M., Siemens, J., Glazer, J. M., Tsuruda, P. R., Basbaum, A. I., Stucky, C. L., Jordt, S.-E., & Julius, D. (2007). The menthol receptor TRPM8 is the principal detector of environmental cold. *Nature*, *448*(7150), Article 7150. https://doi.org/10.1038/nature05910

Bavencoffe, A., Gkika, D., Kondratskyi, A., Beck, B., Borowiec, A.-S., Bidaux, G., Busserolles, J., Eschalier, A., Shuba, Y., Skryma, R., & Prevarskaya, N. (2010). The Transient Receptor Potential Channel TRPM8 Is Inhibited via the α2A Adrenoreceptor Signaling Pathway. *The Journal of Biological Chemistry*, *285*(13), 9410–9419. https://doi.org/10.1074/jbc.M109.069377

Bavencoffe, A., Kondratskyi, A., Gkika, D., Mauroy, B., Shuba, Y., Prevarskaya, N., & Skryma, R. (2011). Complex Regulation of the TRPM8 Cold Receptor Channel. *The Journal of Biological Chemistry*, *286*(11), 9849–9855. https://doi.org/10.1074/jbc.M110.162016

Beccari, A. R., Gemei, M., Lo Monte, M., Menegatti, N., Fanton, M., Pedretti, A., Bovolenta, S., Nucci, C., Molteni, A., Rossignoli, A., Brandolini, L., Taddei, A., Za, L., Liberati, C., & Vistoli, G. (2017). Novel selective, potent naphthyl TRPM8 antagonists identified through a combined ligand- and structure-based virtual screening approach. *Scientific Reports*, *7*(1), Article 1. https://doi.org/10.1038/s41598-017-11194-0

Behrendt, H.-J., Germann, T., Gillen, C., Hatt, H., & Jostock, R. (2004). Characterization of the mouse cold-menthol receptor TRPM8 and vanilloid receptor type-1 VR1 using a fluorometric imaging plate reader (FLIPR) assay. *British Journal of Pharmacology*, *141*(4), 737–745. https://doi.org/10.1038/sj.bjp.0705652

Belmonte, C., Acosta, M. C., & Gallar, J. (2004). Neural basis of sensation in intact and injured corneas. *Experimental Eye Research*, *78*(3), 513–525. https://doi.org/10.1016/j.exer.2003.09.023

Belmonte, C., Acosta, M. C., Merayo-Lloves, J., & Gallar, J. (2015). What Causes Eye Pain? *Current Ophthalmology Reports*, *3*(2), 111–121. https://doi.org/10.1007/s40135-015-0073-9

Belmonte, C., Garcia-Hirschfeld, J., & Gallar, J. (1997). Neurobiology of ocular pain. *Progress in Retinal and Eye Research*, *16*(1), 117–156. https://doi.org/10.1016/S1350-9462(96)00027-4

Benemei, S., & Dussor, G. (2019). TRP Channels and Migraine: Recent Developments and New Therapeutic Opportunities. *Pharmaceuticals*, *12*(2), 54. https://doi.org/10.3390/ph12020054

Berridge, M. J. (2017). Vitamin D deficiency accelerates ageing and age-related diseases: A novel hypothesis. *The Journal of Physiology*, *595*(22), 6825–6836. https://doi.org/10.1113/JP274887

Bessou, P., Burgess, P. R., Perl, E. R., & Taylor, C. B. (1971). Dynamic properties of mechanoreceptors with unmyelinated (C) fibers. *Journal of Neurophysiology*, *34*(1), 116–131. https://doi.org/10.1152/jn.1971.34.1.116

Bidaux, G., Borowiec, A., Gordienko, D., Beck, B., Shapovalov, G. G., Lemonnier, L., Flourakis, M., Vandenberghe, M., Slomianny, C., Dewailly, E., Delcourt, P., Desruelles, E., Ritaine, A., Polakowska, R., Lesage, J., Chami, M., Skryma, R., & Prevarskaya, N. (2015). Epidermal TRPM8 channel isoform controls the balance between keratinocyte proliferation and differentiation in a cold-dependent manner. *Proceedings of the National Academy of Sciences*, *112*(26), E3345–E3354. https://doi.org/10.1073/pnas.1423357112

Bidaux, G., Flourakis, M., Thebault, S., Zholos, A., Beck, B., Gkika, D., Roudbaraki, M., Bonnal, J.-L., Mauroy, B., Shuba, Y., Skryma, R., & Prevarskaya, N. (2007). Prostate cell differentiation status determines transient receptor potential melastatin member 8 channel subcellular localization and function. *Journal of Clinical Investigation*, *117*(6), 1647–1657. https://doi.org/10.1172/JCI30168

Bidaux, G., Gordienko, D., Shapovalov, G., Farfariello, V., Borowiec, A., Iamshanova, O., Lemonnier, L., Gueguinou, M., Guibon, R., Fromont, G., Paillard, M., Gouriou, Y., Chouabe, C., Dewailly,

E., Gkika, D., López-Alvarado, P., Carlos Menéndez, J., Héliot, L., Slomianny, C., & Prevarskaya, N. (2018). 4TM-TRPM8 channels are new gatekeepers of the ER-mitochondria Ca2+ transfer. *Biochimica et Biophysica Acta (BBA) - Molecular Cell Research*, *1865*(7), 981–994. https://doi.org/10.1016/j.bbamcr.2018.04.007

Bini, G., Cruccu, G., Hagbarth, K.-E., Schady, W., & Torebjörk, E. (1984). Analgesic effect of vibration and cooling on pain induced by intraneural electrical stimulation. *PAIN*, *18*(3), 239. https://doi.org/10.1016/0304-3959(84)90819-4

Bödding, M., Wissenbach, U., & Flockerzi, V. (2007). Characterisation of TRPM8 as a pharmacophore receptor. *Cell Calcium*, *42*(6), 618–628. https://doi.org/10.1016/j.ceca.2007.03.005

Borhani Haghighi, A., Motazedian, S., Rezaii, R., Mohammadi, F., Salarian, L., Pourmokhtari, M., Khodaei, S., Vossoughi, M., & Miri, R. (2010). Cutaneous application of menthol 10% solution as an abortive treatment of migraine without aura: A randomised, double-blind, placebo-controlled, crossed-over study. *International Journal of Clinical Practice*, *64*(4), 451–456. https://doi.org/10.1111/j.1742-1241.2009.02215.x

Brauchi, S., Orio, P., & Latorre, R. (2004). Clues to understanding cold sensation: Thermodynamics and electrophysiological analysis of the cold receptor TRPM8. *Proceedings of the National Academy of Sciences*, *101*(43), 15494–15499. https://doi.org/10.1073/pnas.0406773101

Buijs, T. J., & McNaughton, P. A. (2020). The Role of Cold-Sensitive Ion Channels in Peripheral Thermosensation. *Frontiers in Cellular Neuroscience*, *14*. https://www.frontiersin.org/articles/10.3389/fncel.2020.00262

Burgos-Vega, C. C., Ahn, D. D.-U., Bischoff, C., Wang, W., Horne, D., Wang, J., Gavva, N., & Dussor, G. (2016). Meningeal transient receptor potential channel M8 activation causes cutaneous facial and hindpaw allodynia in a preclinical rodent model of headache. *Cephalalgia*, *36*(2), 185–193. https://doi.org/10.1177/0333102415584313

Burstein, R., Cutrer, M. F., & Yarnitsky, D. (2000). The development of cutaneous allodynia during a migraine attack Clinical evidence for the sequential recruitment of spinal and supraspinal nociceptive neurons in migraine. *Brain*, *123*(8), 1703–1709. https://doi.org/10.1093/brain/123.8.1703

Carvalho, A. L., Treyball, A., Brooks, D. J., Costa, S., Neilson, R. J., Reagan, M. R., Bouxsein, M. L., & Motyl, K. J. (2021). TRPM8 modulates temperature regulation in a sex-dependent manner

without affecting cold-induced bone loss. *PLOS ONE*, *16*(6), e0231060. https://doi.org/10.1371/journal.pone.0231060

Caterina, M. J., Rosen, T. A., Tominaga, M., Brake, A. J., & Julius, D. (1999). A capsaicin-receptor homologue with a high threshold for noxious heat. *Nature*, *398*(6726), 436–441. https://doi.org/10.1038/18906

Caterina, M. J., Schumacher, M. A., Tominaga, M., Rosen, T. A., Levine, J. D., & Julius, D. (1997). The capsaicin receptor: A heat-activated ion channel in the pain pathway. *Nature*, *389*(6653), 816–824. https://doi.org/10.1038/39807

Chen, G.-L., Lei, M., Zhou, L.-P., Zeng, B., & Zou, F. (2016). Borneol Is a TRPM8 Agonist that Increases Ocular Surface Wetness. *PLOS ONE*, *11*(7), e0158868. https://doi.org/10.1371/journal.pone.0158868

Chen, X., Xu, L., Zhang, H., Wen, H., & Yang, F. (2022). Differential Activation of TRPM8 by the Stereoisomers of Menthol. *Frontiers in Pharmacology*, *13*, 898670. https://doi.org/10.3389/fphar.2022.898670

Chuang, H., Neuhausser, W. M., & Julius, D. (2004). The Super-Cooling Agent Icilin Reveals a Mechanism of Coincidence Detection by a Temperature-Sensitive TRP Channel. *Neuron*, *43*(6), 859–869. https://doi.org/10.1016/j.neuron.2004.08.038

Clapham, D. E. (2009). Transient Receptor Potential (TRP) Channels. In L. R. Squire (Ed.), *Encyclopedia of Neuroscience* (pp. 1109–1133). Academic Press. https://doi.org/10.1016/B978-008045046-9.01634-X

Clark, J. J., Orban, Z. J., & Carlson, H. A. (2020). Predicting binding sites from unbound versus bound protein structures. *Scientific Reports*, *10*(1), Article 1. https://doi.org/10.1038/s41598-020-72906-7

Colbert, H. A., Smith, T. L., & Bargmann, C. I. (1997). OSM-9, A Novel Protein with Structural Similarity to Channels, Is Required for Olfaction, Mechanosensation, and Olfactory Adaptation in *Caenorhabditis elegans*. *The Journal of Neuroscience*, *17*(21), 8259–8269. https://doi.org/10.1523/JNEUROSCI.17-21-08259.1997

Colburn, R. W., Lubin, M. L., Stone, D. J., Wang, Y., Lawrence, D., D'Andrea, M. R., Brandt, M. R., Liu, Y., Flores, C. M., & Qin, N. (2007). Attenuated Cold Sensitivity in TRPM8 Null Mice. *Neuron*, *54*(3), 379–386. https://doi.org/10.1016/j.neuron.2007.04.017

Cosens, D. J., & Manning, A. (1969). Abnormal Electroretinogram from a Drosophila Mutant. *Nature*, *224*(5216), 285–287. https://doi.org/10.1038/224285a0

Cox, L. S., & Mattison, J. A. (2009). Increasing longevity through caloric restriction or rapamycin feeding in mammals: Common mechanisms for common outcomes? *Aging Cell*, *8*(5), 607–613. https://doi.org/10.1111/j.1474-9726.2009.00509.x

Davies, S. J., Harding, L. M., & Baranowski, A. P. (2002). A Novel Treatment of Postherpetic Neuralgia Using Peppermint Oil. *The Clinical Journal of Pain*, *18*(3), 200.

Davis, K. D. (1998). Cold-induced pain and prickle in the glabrous and hairy skin. *Pain*, *75*(1), 47–57. https://doi.org/10.1016/S0304-3959(97)00203-0

de Groot, T., van der Hagen, E. A. E., Verkaart, S., te Boekhorst, V. A. M., Bindels, R. J. M., & Hoenderop, J. G. J. (2011). Role of the Transient Receptor Potential Vanilloid 5 (TRPV5) Protein N Terminus in Channel Activity, Tetramerization, and Trafficking. *The Journal of Biological Chemistry*, *286*(37), 32132–32139. https://doi.org/10.1074/jbc.M111.226878

DelMonte, D. W., & Kim, T. (2011). Anatomy and physiology of the cornea. *Journal of Cataract and Refractive Surgery*, *37*(3), 588–598. https://doi.org/10.1016/j.jcrs.2010.12.037

Denis, V., & Cyert, M. S. (2002). Internal Ca2+ release in yeast is triggered by hypertonic shock and mediated by a TRP channel homologue. *Journal of Cell Biology*, *156*(1), 29–34. https://doi.org/10.1083/jcb.200111004

Descoeur, J., Pereira, V., Pizzoccaro, A., Francois, A., Ling, B., Maffre, V., Couette, B., Busserolles, J., Courteix, C., Noel, J., Lazdunski, M., Eschalier, A., Authier, N., & Bourinet, E. (2011). Oxaliplatin-induced cold hypersensitivity is due to remodelling of ion channel expression in nociceptors. *EMBO Molecular Medicine*, *3*(5), 266–278. https://doi.org/10.1002/emmm.201100134

Dhaka, A., Earley, T. J., Watson, J., & Patapoutian, A. (2008). Visualizing Cold Spots: TRPM8-Expressing Sensory Neurons and Their Projections. *Journal of Neuroscience*, *28*(3), 566–575. https://doi.org/10.1523/JNEUROSCI.3976-07.2008

Dhaka, A., Murray, A. N., Mathur, J., Earley, T. J., Petrus, M. J., & Patapoutian, A. (2007). TRPM8 Is Required for Cold Sensation in Mice. *Neuron*, *54*(3), 371–378. https://doi.org/10.1016/j.neuron.2007.02.024

Diver, M. M., Cheng, Y., & Julius, D. (2019). Structural insights into TRPM8 inhibition and desensitization. *Science (New York, N.Y.)*, *365*(6460), 1434–1440. https://doi.org/10.1126/science.aax6672

Dixon, R. E., Navedo, M. F., Binder, M. D., & Santana, L. F. (2022). Mechanisms and physiological implications of cooperative gating of clustered ion channels. *Physiological Reviews*, *102*(3), 1159–1210. https://doi.org/10.1152/physrev.00022.2021

Doan, T. L., Pollastri, M., Walters, M. A., & Georg, G. I. (2011). Chapter 23 - The Future of Drug Repositioning: Old Drugs, New Opportunities. In J. E. Macor (Ed.), *Annual Reports in Medicinal Chemistry* (Vol. 46, pp. 385–401). Academic Press. https://doi.org/10.1016/B978-0-12-386009-5.00004-7

Dragoni, I., Guida, E., & McIntyre, P. (2006). The Cold and Menthol Receptor TRPM8 Contains a Functionally Important Double Cysteine Motif*. *Journal of Biological Chemistry*, *281*(49), 37353–37360. https://doi.org/10.1074/jbc.M607227200

Du, J., Zheng, X., Chen, Y., Huang, Z., Cai, S., Jiao, H., Zhu, Z., & Hu, B. (2018). Elevated Transient Receptor Potential Melastatin 8 (TRPM8) Expression Is Correlated with Poor Prognosis in Pancreatic Cancer. *Medical Science Monitor*, *24*, 3720–3725. https://doi.org/10.12659/MSM.909968

Dumont, F. J., & Su, Q. (1995). Mechanism of action of the immunosuppressant rapamycin. *Life Sciences*, *58*(5), 373–395. https://doi.org/10.1016/0024-3205(95)02233-3

Duncan, L. M., Deeds, J., & Hunter, J. (1998). *Down-Regulation of the Novel Gene Melastatin Correlates with Potential for Melanoma Metastasis*. 7.

Dussor, G., & Cao, Y.-Q. (2016). TRPM8 and Migraine. *Headache*, *56*(9), 1406–1417. https://doi.org/10.1111/head.12948

Ellgaard, L., & Helenius, A. (2003). Quality control in the endoplasmic reticulum. *Nature Reviews Molecular Cell Biology*, *4*(3), Article 3. https://doi.org/10.1038/nrm1052

Erlanger, J., & Gasser, H. S. (1937). *Electrical signs of nervous activity* (p. 221). Univ. Penn. Press.

Erler, I., Al-Ansary, D. M. M., Wissenbach, U., Wagner, T. F. J., Flockerzi, V., & Niemeyer, B. A. (2006). Trafficking and Assembly of the Cold-sensitive TRPM8 Channel *. *Journal of Biological Chemistry*, *281*(50), 38396–38404. https://doi.org/10.1074/jbc.M607756200

Everaerts, W., Gees, M., Alpizar, Y. A., Farre, R., Leten, C., Apetrei, A., Dewachter, I., Leuven, F. van, Vennekens, R., Ridder, D. D., Nilius, B., Voets, T., & Talavera, K. (2011). The Capsaicin Receptor TRPV1 Is a Crucial Mediator of the Noxious Effects of Mustard Oil. *Current Biology*, *21*(4), 316–321. https://doi.org/10.1016/j.cub.2011.01.031

Feketa, V. V., Balasubramanian, A., Flores, C. M., Player, M. R., & Marrelli, S. P. (2013). Shivering and tachycardic responses to external cooling in mice are substantially suppressed by TRPV1 activation but not by TRPM8 inhibition. *American Journal of Physiology - Regulatory, Integrative and Comparative Physiology*, *305*(9), R1040–R1050. https://doi.org/10.1152/ajpregu.00296.2013

Fleig, A., & Penner, R. (2004). The TRPM ion channel subfamily: Molecular, biophysical and functional features. *Trends in Pharmacological Sciences*, *25*(12), 633–639. https://doi.org/10.1016/j.tips.2004.10.004

Fruhstorfer, H., Hermanns, M., & Latzke, L. (1986). The effects of thermal stimulation on clinical and experimental itch. *PAIN*, *24*(2), 259. https://doi.org/10.1016/0304-3959(86)90048-5

Gallar, J., Pozo, M. A., Tuckett, R. P., & Belmonte, C. (1993). Response of sensory units with unmyelinated fibres to mechanical, thermal and chemical stimulation of the cat's cornea. *The Journal of Physiology*, *468*(1), 609–622. https://doi.org/10.1113/jphysiol.1993.sp019791

Ghosh, D., Pinto, S., Danglot, L., Vandewauw, I., Segal, A., Van Ranst, N., Benoit, M., Janssens, A., Vennekens, R., Vanden Berghe, P., Galli, T., Vriens, J., & Voets, T. (2016). VAMP7 regulates constitutive membrane incorporation of the cold-activated channel TRPM8. *Nature Communications*, *7*(1), Article 1. https://doi.org/10.1038/ncomms10489

Ghovanloo, M.-R., Effraim, P. R., Tyagi, S., Cheng, X., Yuan, J.-H., Schulman, B. R., Jacobs, D. S., Dib-Hajj, S. D., & Waxman, S. G. (2024). TRPM8 mutations associated with persistent ocular pain after refractive surgery: D665N and V915M. *Biophysical Journal*, *123*(3), 391a. https://doi.org/10.1016/j.bpj.2023.11.2376

Gkika, D., Flourakis, M., Lemonnier, L., & Prevarskaya, N. (2010). PSA reduces prostate cancer cell motility by stimulating TRPM8 activity and plasma membrane expression. *Oncogene*, *29*(32), Article 32. https://doi.org/10.1038/onc.2010.210

Göbel, H., Schmidt, G., & Soyka, D. (1994). Effect of Peppermint and Eucalyptus Oil Preparations on Neurophysiological and Experimental Algesimetric Headache Parameters. *Cephalalgia*, *14*(3), 228–234. https://doi.org/10.1046/j.1468-2982.1994.014003228.x

Gong, J., Liu, J., Ronan, E. A., He, F., Cai, W., Fatima, M., Zhang, W., Lee, H., Li, Z., Kim, G.-H., Pipe, K. P., Duan, B., Liu, J., & Xu, X. Z. S. (2019). A cold-sensing receptor encoded by a glutamate receptor gene. *Cell*, *178*(6), 1375-1386.e11. https://doi.org/10.1016/j.cell.2019.07.034

González, A., Ugarte, G., Restrepo, C., Herrera, G., Piña, R., Gómez-Sánchez, J. A., Pertusa, M., Orio, P., & Madrid, R. (2017). Role of the Excitability Brake Potassium Current IKD in Cold Allodynia Induced by Chronic Peripheral Nerve Injury. *The Journal of Neuroscience: The Official Journal of the Society for Neuroscience*, *37*(12), 3109–3126. https://doi.org/10.1523/JNEUROSCI.3553-16.2017

González-Muñiz, R., Bonache, M. A., Martín-Escura, C., & Gómez-Monterrey, I. (2019). Recent Progress in TRPM8 Modulation: An Update. *International Journal of Molecular Sciences*, *20*(11), 2618. https://doi.org/10.3390/ijms20112618

Graham, F. L., Smiley, J., Russell, W. C., & Nairn, R. (1977). Characteristics of a Human Cell Line Transformed by DNA from Human Adenovirus Type 5. *Journal of General Virology*, *36*(1), 59–72. https://doi.org/10.1099/0022-1317-36-1-59

Green, B. G., & McAuliffe, B. L. (2000). Menthol desensitization of capsaicin irritation: Evidence of a short-term anti-nociceptive effect. *Physiology & Behavior*, *68*(5), 631–639. https://doi.org/10.1016/S0031-9384(99)00221-8

Grynkiewicz, G., Poenie, M., & Tsien, R. Y. (1985). A new generation of Ca2+ indicators with greatly improved fluorescence properties. *Journal of Biological Chemistry*, *260*(6), 3440–3450. https://doi.org/10.1016/S0021-9258(19)83641-4

Gualdani, R., Yuan, J.-H., Effraim, P. R., Di Stefano, G., Truini, A., Cruccu, G., Dib-Hajj, S. D., Gailly, P., & Waxman, S. G. (2021). Trigeminal Neuralgia TRPM8 Mutation. *Neurology: Genetics*, *7*(1), e550. https://doi.org/10.1212/NXG.0000000000000550

Güler, A. D., Lee, H., Iida, T., Shimizu, I., Tominaga, M., & Caterina, M. (2002). Heat-Evoked Activation of the Ion Channel, TRPV4. *The Journal of Neuroscience*, *22*(15), 6408–6414. https://doi.org/10.1523/JNEUROSCI.22-15-06408.2002

Guterres, H., & Im, W. (2023). CHARMM-GUI-Based Induced Fit Docking Workflow to Generate Reliable Protein–Ligand Binding Modes. *Journal of Chemical Information and Modeling*, *63*(15), 4772–4779. https://doi.org/10.1021/acs.jcim.3c00416

Hamill, O. P., Marty, A., Neher, E., Sakmann, B., & Sigworth, F. J. (1981). Improved patch-clamp techniques for high-resolution current recording from cells and cell-free membrane patches. *Pflügers Archiv - European Journal of Physiology*, *391*(2), 85–100. https://doi.org/10.1007/BF00656997

Hardie, R. C., & Minke, B. (1992). The trp gene is essential for a light-activated Ca2+ channel in Drosophila photoreceptors. *Neuron*, *8*(4), 643–651. https://doi.org/10.1016/0896-6273(92)90086-S

Harraz, O. F., & Delpire, E. (2024). Recent insights into channelopathies. *Physiological Reviews*, *104*(1), 23–31. https://doi.org/10.1152/physrev.00022.2023

Heitman, J., Movva, N. R., & Hall, M. N. (1991). Targets for cell cycle arrest by the immunosuppressant rapamycin in yeast. *Science (New York, N.Y.)*, *253*(5022), 905–909. https://doi.org/10.1126/science.1715094

Hensel, H., & Zotterman, Y. (1951). The Effect of Menthol on the Thermoreceptors. *Acta Physiologica Scandinavica*, *24*(1), 27–34. https://doi.org/10.1111/j.1748-1716.1951.tb00824.x

Heppelmann, B., Gallar, J., Trost, B., Schmidt, R. F., & Belmonte, C. (2001). Three-dimensional reconstruction of scleral cold thermoreceptors of the cat eye. *Journal of Comparative Neurology*, *441*(2), 148–154. https://doi.org/10.1002/cne.1403

Hernández-Ortego, P., Torres-Montero, R., de la Peña, E., Viana, F., & Fernández-Trillo, J. (2022). Validation of Six Commercial Antibodies for the Detection of Heterologous and Endogenous TRPM8 Ion Channel Expression. *International Journal of Molecular Sciences*, *23*(24), Article 24. https://doi.org/10.3390/ijms232416164

Hilton, J. K., Salehpour, T., Sisco, N. J., Rath, P., & Van Horn, W. D. (2018). Phosphoinositide-interacting regulator of TRP (PIRT) has opposing effects on human and mouse TRPM8 ion channels. *The Journal of Biological Chemistry*, *293*(24), 9423–9434. https://doi.org/10.1074/jbc.RA118.003563

Hirata, H., & Meng, I. D. (2010). Cold-Sensitive Corneal Afferents Respond to a Variety of Ocular Stimuli Central to Tear Production: Implications for Dry Eye Disease. *Investigative Ophthalmology & Visual Science*, *51*(8), 3969–3976. https://doi.org/10.1167/iovs.09-4744

Horne, D. B., Biswas, K., Brown, J., Bartberger, M. D., Clarine, J., Davis, C. D., Gore, V. K., Harried, S., Horner, M., Kaller, M. R., Lehto, S. G., Liu, Q., Ma, V. V., Monenschein, H., Nguyen, T. T., Yuan, C. C., Youngblood, B. D., Zhang, M., Zhong, W., … Gavva, N. R. (2018). Discovery of TRPM8 Antagonist (S)-6-(((3-Fluoro-4-(trifluoromethoxy)phenyl)(3-fluoropyridin-2-yl)methyl)carbamoyl)nicotinic Acid (AMG 333), a Clinical Candidate for the Treatment of Migraine. *Journal of Medicinal Chemistry*, *61*(18), 8186–8201. https://doi.org/10.1021/acs.jmedchem.8b00518

Izquierdo, C., Martín-Martínez, M., Gómez-Monterrey, I., & González-Muñiz, R. (2021). TRPM8 Channels: Advances in Structural Studies and Pharmacological Modulation. *International Journal of Molecular Sciences*, *22*(16), Article 16. https://doi.org/10.3390/ijms22168502

Janssens, A., Gees, M., Toth, B. I., Ghosh, D., Mulier, M., Vennekens, R., Vriens, J., Talavera, K., & Voets, T. (2016). Definition of two agonist types at the mammalian cold-activated channel TRPM8. *eLife*, *5*, e17240. https://doi.org/10.7554/eLife.17240

Jordt, S.-E., Bautista, D. M., Chuang, H., McKemy, D. D., Zygmunt, P. M., Högestätt, E. D., Meng, I. D., & Julius, D. (2004). Mustard oils and cannabinoids excite sensory nerve fibres through the TRP channel ANKTM1. *Nature*, *427*(6971), Article 6971. https://doi.org/10.1038/nature02282

Jourdan, J., Bureau, R., Rochais, C., & Dallemagne, P. (2020). Drug repositioning: A brief overview. *The Journal of Pharmacy and Pharmacology*, *72*(9), 1145–1151. https://doi.org/10.1111/jphp.13273

Kamatou, G. P. P., Vermaak, I., Viljoen, A. M., & Lawrence, B. M. (2013). Menthol: A simple monoterpene with remarkable biological properties. *Phytochemistry*, *96*, 15–25. https://doi.org/10.1016/j.phytochem.2013.08.005

Kandel, E. R. (Ed.). (2013). *Principles of neural science* (5th ed). McGraw-Hill.

Kang, D., Choe, C., & Kim, D. (2005). Thermosensitivity of the two-pore domain K+ channels TREK-2 and TRAAK. *The Journal of Physiology*, *564*(1), 103–116. https://doi.org/10.1113/jphysiol.2004.081059

Kang, K., Panzano, V. C., Chang, E. C., Ni, L., Dainis, A. M., Jenkins, A. M., Regna, K., Muskavitch, M. A. T., & Garrity, P. A. (2012). Modulation of TRPA1 thermal sensitivity enables sensory discrimination in Drosophila. *Nature*, *481*(7379), 76–80. https://doi.org/10.1038/nature10715

Karashima, Y., Talavera, K., Everaerts, W., Janssens, A., Kwan, K. Y., Vennekens, R., Nilius, B., & Voets, T. (2009). TRPA1 acts as a cold sensor in vitro and in vivo. *Proceedings of the National Academy of Sciences*, *106*(4), 1273–1278. https://doi.org/10.1073/pnas.0808487106

Kathuria, S. V., Chan, Y. H., Nobrega, R. P., Özen, A., & Matthews, C. R. (2016). Clusters of isoleucine, leucine, and valine side chains define cores of stability in high-energy states of globular proteins: Sequence determinants of structure and stability. *Protein Science : A Publication of the Protein Society*, *25*(3), 662–675. https://doi.org/10.1002/pro.2860

Kayama, Y., Shibata, M., Takizawa, T., Ibata, K., Shimizu, T., Ebine, T., Toriumi, H., Yuzaki, M., & Suzuki, N. (2018). Functional interactions between transient receptor potential M8 and transient receptor potential V1 in the trigeminal system: Relevance to migraine pathophysiology. *Cephalalgia*, *38*(5), 833–845. https://doi.org/10.1177/0333102417712719

Kearney, M., Shine, R., & Porter, W. P. (2009). The potential for behavioral thermoregulation to buffer “cold-blooded” animals against climate warming. *Proceedings of the National Academy of Sciences*, *106*(10), 3835–3840. https://doi.org/10.1073/pnas.0808913106

Key, F. M., Abdul-Aziz, M. A., Mundry, R., Peter, B. M., Sekar, A., D’Amato, M., Dennis, M. Y., Schmidt, J. M., & Andrés, A. M. (2018). Human local adaptation of the TRPM8 cold receptor along a latitudinal cline. *PLOS Genetics*, *14*(5), e1007298. https://doi.org/10.1371/journal.pgen.1007298

Kiefer, M., Van Sluys, M., & Rocha, C. (2006). Thermoregulatory behaviour in Tropidurus torquatus (Squamata, Tropiduridae) from Brazilian coastal populations: An estimate of passive and active thermoregulation in lizards. *Acta Zoologica*, *88*, 81–87. https://doi.org/10.1111/j.1463-6395.2007.00254.x

Kijpornyongpan, T., Sereemaspun, A., & Chanchao, C. (2014). Dose-Dependent Cytotoxic Effects of Menthol on Human Malignant Melanoma A-375 Cells: Correlation with TRPM8 Transcript Expression. *Asian Pacific Journal of Cancer Prevention*, *15*(4), 1551–1556. https://doi.org/10.7314/APJCP.2014.15.4.1551

Kim, H. R., Kim, J. C., Kang, S. Y., Kim, H. O., Park, C. W., & Chung, B. Y. (2021). Rapamycin Alleviates 2,3,7,8-Tetrachlorodibenzo-p-dioxin-Induced Aggravated Dermatitis in Mice with Imiquimod-Induced Psoriasis-Like Dermatitis by Inducing Autophagy. *International Journal of Molecular Sciences*, *22*(8), 3968. https://doi.org/10.3390/ijms22083968

Knowlton, W. M., Daniels, R. L., Palkar, R., McCoy, D. D., & McKemy, D. D. (2011). Pharmacological Blockade of TRPM8 Ion Channels Alters Cold and Cold Pain Responses in Mice. *PLoS ONE*, *6*(9), e25894. https://doi.org/10.1371/journal.pone.0025894

Knowlton, W. M., Palkar, R., Lippoldt, E. K., McCoy, D. D., Baluch, F., Chen, J., & McKemy, D. D. (2013). A Sensory-Labeled Line for Cold: TRPM8-Expressing Sensory Neurons Define the Cellular Basis for Cold, Cold Pain, and Cooling-Mediated Analgesia. *Journal of Neuroscience*, *33*(7), 2837–2848. https://doi.org/10.1523/JNEUROSCI.1943-12.2013

Krames, E. S. (2014). The Role of the Dorsal Root Ganglion in the Development of Neuropathic Pain. *Pain Medicine*, *15*(10), 1669–1685. https://doi.org/10.1111/pme.12413

Kühn, F. J. P., Winking, M., Kühn, C., Hoffmann, D. C., & Lückhoff, A. (2013). Surface expression and channel function of TRPM8 are cooperatively controlled by transmembrane segments S3 and S4. *Pflügers Archiv - European Journal of Physiology*, *465*(11), 1599–1610. https://doi.org/10.1007/s00424-013-1302-4

Kwan, K. Y., & Corey, D. P. (2009). Burning Cold: Involvement of TRPA1 in Noxious Cold Sensation. *Journal of General Physiology*, *133*(3), 251–256. https://doi.org/10.1085/jgp.200810146

Kwon, Y., Shim, H.-S., Wang, X., & Montell, C. (2008). Control of thermotactic behavior via coupling of a TRP channel to a phospholipase C signaling cascade. *Nature Neuroscience*, *11*(8), 871–873. https://doi.org/10.1038/nn.2170

Laing, R. J., & Dhaka, A. (2016). ThermoTRPs and Pain. *The Neuroscientist*, *22*(2), 171–187. https://doi.org/10.1177/1073858414567884

Lashinger, E. S. R., Steiginga, M. S., Hieble, J. P., Leon, L. A., Gardner, S. D., Nagilla, R., Davenport, E. A., Hoffman, B. E., Laping, N. J., & Su, X. (2008). AMTB, a TRPM8 channel blocker: Evidence in rats for activity in overactive bladder and painful bladder syndrome. *American Journal of Physiology-Renal Physiology*, *295*(3), F803–F810. https://doi.org/10.1152/ajprenal.90269.2008

Lev, S., & Minke, B. (2010). CONSTITUTIVE ACTIVITY OF TRP CHANNELS: METHODS FOR MEASURING THE ACTIVITY AND ITS OUTCOME. *Methods in Enzymology*, *484*, 591–612. https://doi.org/10.1016/B978-0-12-381298-8.00029-0

Lev, S., Zeevi, D. A., Frumkin, A., Offen-Glasner, V., Bach, G., & Minke, B. (2010). Constitutive Activity of the Human TRPML2 Channel Induces Cell Degeneration. *The Journal of Biological Chemistry*, *285*(4), 2771–2782. https://doi.org/10.1074/jbc.M109.046508

Li, H. (2017). TRP Channel Classification. In Y. Wang (Ed.), *Transient Receptor Potential Canonical Channels and Brain Diseases* (Vol. 976, pp. 1–8). Springer Netherlands. https://doi.org/10.1007/978-94-024-1088-4_1

Li, J., Kim, S. G., & Blenis, J. (2014). Rapamycin: One drug, many effects. *Cell Metabolism*, *19*(3), 373–379. https://doi.org/10.1016/j.cmet.2014.01.001

Li, Q., Wang, X., Yang, Z., Wang, B., & Li, S. (2009). Menthol Induces Cell Death via the TRPM8 Channel in the Human Bladder Cancer Cell Line T24. *Oncology*, *77*(6), 335–341. https://doi.org/10.1159/000264627

Linares-Alba, M. A., Gómez-Guajardo, M. B., Fonzar, J. F., Brooks, D. E., García-Sánchez, G. A., & Bernad-Bernad, M. J. (2016). Preformulation Studies of a Liposomal Formulation Containing Sirolimus for the Treatment of Dry Eye Disease. *Journal of Ocular Pharmacology and Therapeutics*, *32*(1), 11–22. https://doi.org/10.1089/jop.2015.0032

Liskiewicz, D., Zhang, Q., Barthem, C. S., Jastroch, M., Liskiewicz, A., Khajavi, N., Grandl, G., Coupland, C., Kleinert, M., Garcia-Caceres, C., Novikoff, A., Maity, G., Boehm, U., Tschöp, M. H., & Müller, T. D. (2023). Neuronal loss of TRPM8 leads to obesity and glucose intolerance in male mice. *Molecular Metabolism*, *72*, 101714. https://doi.org/10.1016/j.molmet.2023.101714

Liu, B., Fan, L., Balakrishna, S., Sui, A., Morris, J. B., & Jordt, S.-E. (2013). TRPM8 is the Principal Mediator of Menthol-induced Analgesia of Acute and Inflammatory Pain. *Pain*, *154*(10), 2169–2177. https://doi.org/10.1016/j.pain.2013.06.043

Liu, B., & Qin, F. (2005). Functional Control of Cold- and Menthol-Sensitive TRPM8 Ion Channels by Phosphatidylinositol 4,5-Bisphosphate. *The Journal of Neuroscience*, *25*(7), 1674–1681. https://doi.org/10.1523/JNEUROSCI.3632-04.2005

Liu, L., Yudin, Y., Nagwekar, J., Kang, C., Shirokova, N., & Rohacs, T. (2019). *G* $_{\alpha q}$ Sensitizes TRPM8 to Inhibition by PI(4,5)P $_2$ Depletion upon Receptor Activation. *The Journal of Neuroscience*, *39*(31), 6067–6080. https://doi.org/10.1523/JNEUROSCI.2304-18.2019

Liu, Y., Mikrani, R., He, Y., Faran Ashraf Baig, M. M., Abbas, M., Naveed, M., Tang, M., Zhang, Q., Li, C., & Zhou, X. (2020a). TRPM8 channels: A review of distribution and clinical role. *European Journal of Pharmacology*, *882*, 173312. https://doi.org/10.1016/j.ejphar.2020.173312

Liu, Y., Mikrani, R., He, Y., Faran Ashraf Baig, M. M., Abbas, M., Naveed, M., Tang, M., Zhang, Q., Li, C., & Zhou, X. (2020b). TRPM8 channels: A review of distribution and clinical role. *European Journal of Pharmacology*, *882*, 173312. https://doi.org/10.1016/j.ejphar.2020.173312

Liu, Z., Wu, H., Wei, Z., Wang, X., Shen, P., Wang, S., Wang, A., Chen, W., & Lu, Y. (2016). TRPM8: A potential target for cancer treatment. *Journal of Cancer Research and Clinical Oncology*, *142*(9), 1871–1881. https://doi.org/10.1007/s00432-015-2112-1

Lumpkin, E. A., & Bautista, D. M. (2005). Feeling the pressure in mammalian somatosensation. *Current Opinion in Neurobiology*, *15*(4), 382–388. https://doi.org/10.1016/j.conb.2005.06.005

Lumpkin, E. A., & Caterina, M. J. (2007). Mechanisms of sensory transduction in the skin. *Nature*, *445*(7130), 858–865. https://doi.org/10.1038/nature05662

Ma, S., G, G., Ak, V.-E., Jf, D., & H, H. (2008). Menthol derivative WS-12 selectively activates transient receptor potential melastatin-8 (TRPM8) ion channels. *Pakistan Journal of Pharmaceutical Sciences*, *21*(4), 370–378.

Madrid, R., Donovan-Rodríguez, T., Meseguer, V., Acosta, M. C., Belmonte, C., & Viana, F. (2006). Contribution of TRPM8 Channels to Cold Transduction in Primary Sensory Neurons and Peripheral Nerve Terminals. *The Journal of Neuroscience*, *26*(48), 12512–12525. https://doi.org/10.1523/JNEUROSCI.3752-06.2006

Madrid, R., Peña, E. de la, Donovan-Rodriguez, T., Belmonte, C., & Viana, F. (2009). Variable Threshold of Trigeminal Cold-Thermosensitive Neurons Is Determined by a Balance between TRPM8 and Kv1 Potassium Channels. *Journal of Neuroscience*, *29*(10), 3120–3131. https://doi.org/10.1523/JNEUROSCI.4778-08.2009

Mahieu, F., Janssens, A., Gees, M., Talavera, K., Nilius, B., & Voets, T. (2010). Modulation of the cold-activated cation channel TRPM8 by surface charge screening. *The Journal of Physiology*, *588*(Pt 2), 315–324. https://doi.org/10.1113/jphysiol.2009.183582

Mahieu, F., Owsianik, G., Verbert, L., Janssens, A., Smedt, H. D., Nilius, B., & Voets, T. (2007). TRPM8-independent Menthol-induced Ca2+ Release from Endoplasmic Reticulum and Golgi *. *Journal of Biological Chemistry*, *282*(5), 3325–3336. https://doi.org/10.1074/jbc.M605213200

Maingret, F., Lauritzen, I., Patel, A. J., Heurteaux, C., Reyes, R., Lesage, F., Lazdunski, M., & Honoré, E. (2000). TREK-1 is a heat-activated background K+ channel. *The EMBO Journal*, *19*(11), 2483–2491. https://doi.org/10.1093/emboj/19.11.2483

Malin, S. A., Davis, B. M., & Molliver, D. C. (2007). Production of dissociated sensory neuron cultures and considerations for their use in studying neuronal function and plasticity. *Nature Protocols*, *2*(1), 152–160. https://doi.org/10.1038/nprot.2006.461

Mälkiä, A., Madrid, R., Meseguer, V., De La Peña, E., Valero, M., Belmonte, C., & Viana, F. (2007). Bidirectional shifts of TRPM8 channel gating by temperature and chemical agents modulate the cold sensitivity of mammalian thermoreceptors: Pharmacological modulation of cold receptor TRPM8. *The Journal of Physiology*, *581*(1), 155–174. https://doi.org/10.1113/jphysiol.2006.123059

Malkia, A., Pertusa, M., Fernández-Ballester, G., Ferrer-Montiel, A., & Viana, F. (2009). Differential Role of the Menthol-Binding Residue Y745 in the Antagonism of Thermally Gated TRPM8 Channels. *Molecular Pain*, *5*, 1744-8069-5–62. https://doi.org/10.1186/1744-8069-5-62

Manolache, A., Selescu, T., Maier, G. L., Mentel, M., Ionescu, A. E., Neacsu, C., Babes, A., & Szedlacsek, S. E. (2020). Regulation of TRPM8 channel activity by Src-mediated tyrosine phosphorylation. *Journal of Cellular Physiology*, *235*(6), 5192–5203. https://doi.org/10.1002/jcp.29397

Manzano, G. M., Giuliano, L. M. P., & Nóbrega, J. A. M. (2008). A brief historical note on the classification of nerve fibers. *Arquivos de Neuro-Psiquiatria*, *66*(1), 117–119. https://doi.org/10.1590/S0004-282X2008000100033

Matos-Cruz, V., Schneider, E. R., Mastrotto, M., Merriman, D. K., Bagriantsev, S. N., & Gracheva, E. O. (2017). Molecular prerequisites for diminished cold sensitivity in ground squirrels and hamsters. *Cell Reports*, *21*(12), 3329–3337. https://doi.org/10.1016/j.celrep.2017.11.083

McCoy, D. D., Zhou, L., Nguyen, A.-K., Watts, A. G., Donovan, C. M., & McKemy, D. D. (2013). Enhanced insulin clearance in mice lacking TRPM8 channels. *American Journal of Physiology-Endocrinology and Metabolism*, *305*(1), E78–E88. https://doi.org/10.1152/ajpendo.00542.2012

McKemy, D. D. (2007). TRPM8: The Cold and Menthol Receptor. In W. B. Liedtke & S. Heller (Eds.), *TRP Ion Channel Function in Sensory Transduction and Cellular Signaling Cascades*. CRC Press/Taylor & Francis. http://www.ncbi.nlm.nih.gov/books/NBK5238/

McKemy, D. D., Neuhausser, W. M., & Julius, D. (2002). Identification of a cold receptor reveals a general role for TRP channels in thermosensation. *Nature*, *416*(6876), 52–58. https://doi.org/10.1038/nature719

Melzack, R., & Wall, P. D. (1965). Pain Mechanisms: A New Theory. *Science*, *150*(3699), 971–979. https://doi.org/10.1126/science.150.3699.971

Meseguer, V., Karashima, Y., Talavera, K., D'Hoedt, D., Donovan-Rodríguez, T., Viana, F., Nilius, B., & Voets, T. (2008). Transient receptor potential channels in sensory neurons are targets of the antimycotic agent clotrimazole. *The Journal of Neuroscience: The Official Journal of the Society for Neuroscience*, *28*(3), 576–586. https://doi.org/10.1523/JNEUROSCI.4772-07.2008

Mishra, S. K., Tisel, S. M., Orestes, P., Bhangoo, S. K., & Hoon, M. A. (2011). TRPV1-lineage neurons are required for thermal sensation. *The EMBO Journal*, *30*(3), 582–593. https://doi.org/10.1038/emboj.2010.325

Missiaen, L., Van Acker, K., Van Baelen, K., Raeymaekers, L., Wuytack, F., Parys, J. B., De Smedt, H., Vanoevelen, J., Dode, L., Rizzuto, R., & Callewaert, G. (2004). Calcium release from the Golgi apparatus and the endoplasmic reticulum in HeLa cells stably expressing targeted aequorin to these compartments. *Cell Calcium*, *36*(6), 479–487. https://doi.org/10.1016/j.ceca.2004.04.007

Mochizuki, T., Wu, G., Hayashi, T., Xenophontos, S. L., Veldhuisen, B., Saris, J. J., Reynolds, D. M., Cai, Y., Gabow, P. A., Pierides, A., Kimberling, W. J., Breuning, M. H., Deltas, C. C., Peters, D. J. M., & Somlo, S. (1996). PKD2, a Gene for Polycystic Kidney Disease That Encodes an Integral Membrane Protein. *Science*, *272*(5266), 1339–1342. https://doi.org/10.1126/science.272.5266.1339

Mohandass, A., Krishnan, V., Gribkova, E. D., Asuthkar, S., Baskaran, P., Nersesyan, Y., Hussain, Z., Wise, L. M., George, R. E., Stokes, N., Alexander, B. M., Cohen, A. M., Pavlov, E. V., Llano, D. A., Zhu, M. X., Thyagarajan, B., & Zakharian, E. (2020). TRPM8 as the rapid testosterone signaling receptor: Implications in the regulation of dimorphic sexual and social behaviors. *The FASEB Journal*, *34*(8), 10887–10906. https://doi.org/10.1096/fj.202000794R

Montell, C., Birnbaumer, L., Flockerzi, V., Bindels, R. J., Bruford, E. A., Caterina, M. J., Clapham, D. E., Harteneck, C., Heller, S., Julius, D., Kojima, I., Mori, Y., Penner, R., Prawitt, D., Scharenberg, A. M., Schultz, G., Shimizu, N., & Zhu, M. X. (2002). A Unified Nomenclature for the Superfamily of TRP Cation Channels. *Molecular Cell*, *9*(2), 229–231. https://doi.org/10.1016/S1097-2765(02)00448-3

Montell, C., & Rubin, G. M. (1989). Molecular characterization of the drosophila trp locus: A putative integral membrane protein required for phototransduction. *Neuron*, *2*(4), 1313–1323. https://doi.org/10.1016/0896-6273(89)90069-X

Moore, E. D. W., Becker, P. L., Fogarty, K. E., Williams, D. A., & Fay, F. S. (1990). Ca2+ imaging in single living cells: Theoretical and practical issues. *Cell Calcium*, *11*(2), 157–179. https://doi.org/10.1016/0143-4160(90)90068-6

Moparthi, L., Kichko, T. I., Eberhardt, M., Högestätt, E. D., Kjellbom, P., Johanson, U., Reeh, P. W., Leffler, A., Filipovic, M. R., & Zygmunt, P. M. (2016). Human TRPA1 is a heat sensor displaying intrinsic U-shaped thermosensitivity. *Scientific Reports*, *6*(1), 28763. https://doi.org/10.1038/srep28763

Moqrich, A., Hwang, S. W., Earley, T. J., Petrus, M. J., Murray, A. N., Spencer, K. S. R., Andahazy, M., Story, G. M., & Patapoutian, A. (2005). Impaired thermosensation in mice lacking TRPV3, a heat and camphor sensor in the skin. *Science (New York, N.Y.)*, *307*(5714), 1468–1472. https://doi.org/10.1126/science.1108609

Moran, M. M., & Szallasi, A. (2018). Targeting nociceptive transient receptor potential channels to treat chronic pain: Current state of the field. *British Journal of Pharmacology*, *175*(12), 2185–2203. https://doi.org/10.1111/bph.14044

Morenilla-Palao, C., Luis, E., Fernández-Peña, C., Quintero, E., Weaver, J. L., Bayliss, D. A., & Viana, F. (2014). Ion Channel Profile of TRPM8 Cold Receptors Reveals a Role of TASK-3 Potassium Channels in Thermosensation. *Cell Reports*, *8*(5), 1571–1582. https://doi.org/10.1016/j.celrep.2014.08.003

Morenilla-Palao, C., Pertusa, M., Meseguer, V., Cabedo, H., & Viana, F. (2009). Lipid Raft Segregation Modulates TRPM8 Channel Activity *. *Journal of Biological Chemistry*, *284*(14), 9215–9224. https://doi.org/10.1074/jbc.M807228200

Nagata, K., Duggan, A., Kumar, G., & García-Añoveros, J. (2005). Nociceptor and Hair Cell Transducer Properties of TRPA1, a Channel for Pain and Hearing. *The Journal of Neuroscience*, *25*(16), 4052–4061. https://doi.org/10.1523/JNEUROSCI.0013-05.2005

Nakanishi, O., Fujimori, Y., Aizawa, N., Hayashi, T., Matsuzawa, A., Kobayashi, J., Hirasawa, H., Mutai, Y., Tanada, F., & Igawa, Y. (2020). KPR-5714, a Novel Transient Receptor Potential Melastatin 8 Antagonist, Improves Overactive Bladder via Inhibition of Bladder Afferent Hyperactivity in Rats. *Journal of Pharmacology and Experimental Therapeutics*, *373*(2), 239–247. https://doi.org/10.1124/jpet.119.263616

Neher, E., & Sakmann, B. (1976). Single-channel currents recorded from membrane of denervated frog muscle fibres. *Nature*, *260*(5554), 799–802. https://doi.org/10.1038/260799a0

Neher, E., Sakmann, B., & Steinbach, J. H. (1978). The extracellular patch clamp: A method for resolving currents through individual open channels in biological membranes. *Pflugers Archiv: European Journal of Physiology*, *375*(2), 219–228. https://doi.org/10.1007/BF00584247

Nilius, B., & Owsianik, G. (2011). The transient receptor potential family of ion channels. *Genome Biology*, *12*(3), 218. https://doi.org/10.1186/gb-2011-12-3-218

Oh, S. T., Yang, K. J., Kim, Y. H., Bae, J. M., Park, H. J., Kim, J. W., & Park, Y. M. (2018). Increased immunoreactivity for TRPM8 in cutaneous squamous cell carcinoma. *Journal of Cutaneous Pathology*, *45*(12), 970–972. https://doi.org/10.1111/cup.13358

Ohmi, M., Shishido, Y., Inoue, T., Ando, K., Fujiuchi, A., Yamada, A., Watanabe, S., & Kawamura, K. (2014). Identification of a novel 2-pyridyl-benzensulfonamide derivative, RQ-00203078, as a selective and orally active TRPM8 antagonist. *Bioorganic & Medicinal Chemistry Letters*, *24*(23), 5364–5368. https://doi.org/10.1016/j.bmcl.2014.10.074

Ordás, P., Hernández-Ortego, P., Vara, H., Fernández-Peña, C., Reimúndez, A., Morenilla-Palao, C., Guadaño-Ferraz, A., Gomis, A., Hoon, M., Viana, F., & Señarís, R. (2021). Expression of the cold thermoreceptor TRPM8 in rodent brain thermoregulatory circuits. *Journal of Comparative Neurology*, *529*(1), 234–256. https://doi.org/10.1002/cne.24694

Oz, M., El Nebrisi, E. G., Yang, K.-H. S., Howarth, F. C., & Al Kury, L. T. (2017). Cellular and Molecular Targets of Menthol Actions. *Frontiers in Pharmacology*, *8*. https://www.frontiersin.org/articles/10.3389/fphar.2017.00472

Pagano, E., Romano, B., Cicia, D., Iannotti, F. A., Venneri, T., Lucariello, G., Nanì, M. F., Cattaneo, F., De Cicco, P., D'Armiento, M., De Luca, M., Lionetti, R., Lama, S., Stiuso, P., Zoppoli, P., Falco, G., Marchianò, S., Fiorucci, S., Capasso, R., … Izzo, A. A. (2023). TRPM8 indicates poor prognosis in colorectal cancer patients and its pharmacological targeting reduces tumour growth in mice by inhibiting Wnt/β-catenin signalling. *British Journal of Pharmacology*, *180*(2), 235–251. https://doi.org/10.1111/bph.15960

Palchevskyi, S., Czarnocki-Cieciura, M., Vistoli, G., Gervasoni, S., Nowak, E., Beccari, A. R., Nowotny, M., & Talarico, C. (2022). *Structure of human TRPM8 channel* [Preprint]. Molecular Biology. https://doi.org/10.1101/2022.10.19.512915

Palkar, R., Ongun, S., Catich, E., Li, N., Borad, N., Sarkisian, A., & McKemy, D. D. (2018). Cooling Relief of Acute and Chronic Itch Requires TRPM8 Channels and Neurons. *The Journal of Investigative Dermatology*, *138*(6), 1391–1399. https://doi.org/10.1016/j.jid.2017.12.025

Paricio-Montesinos, R., Schwaller, F., Udhayachandran, A., Rau, F., Walcher, J., Evangelista, R., Vriens, J., Voets, T., Poulet, J. F. A., & Lewin, G. R. (2020). The Sensory Coding of Warm Perception. *Neuron*, *106*(5), 830-841.e3. https://doi.org/10.1016/j.neuron.2020.02.035

Parra, A., Madrid, R., Echevarria, D., del Olmo, S., Morenilla-Palao, C., Acosta, M. C., Gallar, J., Dhaka, A., Viana, F., & Belmonte, C. (2010). Ocular surface wetness is regulated by TRPM8-dependent cold thermoreceptors of the cornea. *Nature Medicine*, *16*(12), 1396–1399. https://doi.org/10.1038/nm.2264

Peier, A. M., Moqrich, A., Hergarden, A. C., Reeve, A. J., Andersson, D. A., Story, G. M., Earley, T. J., Dragoni, I., McIntyre, P., Bevan, S., & Patapoutian, A. (2002). A TRP Channel that Senses Cold Stimuli and Menthol. *Cell*, *108*(5), 705–715. https://doi.org/10.1016/S0092-8674(02)00652-9

Pertusa, M., González, A., Hardy, P., Madrid, R., & Viana, F. (2014). Bidirectional Modulation of Thermal and Chemical Sensitivity of TRPM8 Channels by the Initial Region of the N-terminal Domain. *The Journal of Biological Chemistry*, *289*(32), 21828–21843. https://doi.org/10.1074/jbc.M114.565994

Pertusa, M., Madrid, R., Morenilla-Palao, C., Belmonte, C., & Viana, F. (2012). N-Glycosylation of TRPM8 Ion Channels Modulates Temperature Sensitivity of Cold Thermoreceptor Neurons. *The Journal of Biological Chemistry*, *287*(22), 18218–18229. https://doi.org/10.1074/jbc.M111.312645

Pertusa, M., Rivera, B., González, A., Ugarte, G., & Madrid, R. (2018). Critical role of the pore domain in the cold response of TRPM8 channels identified by ortholog functional comparison. *Journal of Biological Chemistry*, *293*(32), 12454–12471. https://doi.org/10.1074/jbc.RA118.002256

Pertusa, M., Solorza, J., & Madrid, R. (2023). Molecular determinants of TRPM8 function: Key clues for a cool modulation. *Frontiers in Pharmacology*, *14*. https://www.frontiersin.org/articles/10.3389/fphar.2023.1213337

Phelps, C. B., & Gaudet, R. (2007). The Role of the N Terminus and Transmembrane Domain of TRPM8 in Channel Localization and Tetramerization. *Journal of Biological Chemistry*, *282*(50), 36474–36480. https://doi.org/10.1074/jbc.M707205200

Piña, R., Ugarte, G., Campos, M., Íñigo-Portugués, A., Olivares, E., Orio, P., Belmonte, C., Bacigalupo, J., & Madrid, R. (2019). Role of TRPM8 Channels in Altered Cold Sensitivity of Corneal Primary Sensory Neurons Induced by Axonal Damage. *The Journal of Neuroscience*, *39*(41), 8177–8192. https://doi.org/10.1523/JNEUROSCI.0654-19.2019

Plaza-Cayón, A., González-Muñiz, R., & Martín-Martínez, M. (2022). Mutations of TRPM8 channels: Unraveling the molecular basis of activation by cold and ligands. *Medicinal Research Reviews*, *42*(6), 2168–2203. https://doi.org/10.1002/med.21920

Premkumar, L. S., Raisinghani, M., Pingle, S. C., Long, C., & Pimentel, F. (2005). Downregulation of Transient Receptor Potential Melastatin 8 by Protein Kinase C-Mediated Dephosphorylation. *The Journal of Neuroscience*, *25*(49), 11322–11329. https://doi.org/10.1523/JNEUROSCI.3006-05.2005

Prince, P. B., Rapoport, A. M., Sheftell, F. D., Tepper, S. J., & Bigal, M. E. (2004). The Effect of Weather on Headache. *Headache: The Journal of Head and Face Pain*, *44*(6), 596–602. https://doi.org/10.1111/j.1526-4610.2004.446008.x

Proudfoot, C. J., Garry, E. M., Cottrell, D. F., Rosie, R., Anderson, H., Robertson, D. C., Fleetwood-Walker, S. M., & Mitchell, R. (2006). Analgesia Mediated by the TRPM8 Cold Receptor in Chronic Neuropathic Pain. *Current Biology*, *16*(16), 1591–1605. https://doi.org/10.1016/j.cub.2006.07.061

Purves, D. (Ed.). (2004). *Neuroscience* (3rd ed). Sinauer Associates, Publishers.

Quallo, T., Vastani, N., Horridge, E., Gentry, C., Parra, A., Moss, S., Viana, F., Belmonte, C., Andersson, D. A., & Bevan, S. (2015). TRPM8 is a neuronal osmosensor that regulates eye blinking in mice. *Nature Communications*, *6*(1), Article 1. https://doi.org/10.1038/ncomms8150

Ramachandran, R., Hyun, E., Zhao, L., Lapointe, T. K., Chapman, K., Hirota, C. L., Ghosh, S., McKemy, D. D., Vergnolle, N., Beck, P. L., Altier, C., & Hollenberg, M. D. (2013). TRPM8 activation attenuates inflammatory responses in mouse models of colitis. *Proceedings of the National Academy of Sciences*, *110*(18), 7476–7481. https://doi.org/10.1073/pnas.1217431110

Ramsey, I. S., Delling, M., & Clapham, D. E. (2006). AN INTRODUCTION TO TRP CHANNELS. *Annual Review of Physiology*, *68*(1), 619–647. https://doi.org/10.1146/annurev.physiol.68.040204.100431

Reid, G., Babes, A., & Pluteanu, F. (2002). A cold- and menthol-activated current in rat dorsal root ganglion neurones: Properties and role in cold transduction. *The Journal of Physiology*, *545*(2), 595–614. https://doi.org/10.1113/jphysiol.2002.024331

Reimúndez, A., Fernández-Peña, C., García, G., Fernández, R., Ordás, P., Gallego, R., Pardo-Vazquez, J. L., Arce, V., Viana, F., & Señarís, R. (2018). Deletion of the cold thermoreceptor TRPM8 increases heat loss and food intake leading to reduced body temperature and obesity in mice. *Journal of Neuroscience*. https://doi.org/10.1523/JNEUROSCI.3002-17.2018

Reimúndez, A., Fernández-Peña, C., Ordás, P., Hernández-Ortego, P., Gallego, R., Morenilla-Palao, C., Navarro, J., Martín-Cora, F., Pardo-Vázquez, J. L., Schwarz, L. A., Arce, V., Viana, F., & Señarís, R. (2023). The cold-sensing ion channel TRPM8 regulates central and peripheral clockwork and the circadian oscillations of body temperature. *Acta Physiologica*, *237*(3), e13896. https://doi.org/10.1111/apha.13896

Rivera, B., Moreno, C., Lavanderos, B., Hwang, J. Y., Fernández-Trillo, J., Park, K.-S., Orio, P., Viana, F., Madrid, R., & Pertusa, M. (2021). Constitutive Phosphorylation as a Key Regulator of TRPM8 Channel Function. *The Journal of Neuroscience: The Official Journal of the Society for Neuroscience*, *41*(41), 8475–8493. https://doi.org/10.1523/JNEUROSCI.0345-21.2021

Robbins, A., Kurose, M., Winterson, B. J., & Meng, I. D. (2012). Menthol Activation of Corneal Cool Cells Induces TRPM8-Mediated Lacrimation but Not Nociceptive Responses in Rodents. *Investigative Ophthalmology & Visual Science*, *53*(11), 7034–7042. https://doi.org/10.1167/iovs.12-10025

Rohacs, T. (2016). Phosphoinositide signaling in somatosensory neurons. *Advances in Biological Regulation*, *61*, 2–16. https://doi.org/10.1016/j.jbior.2015.11.012

Rohács, T., Lopes, C. M. B., Michailidis, I., & Logothetis, D. E. (2005). PI(4,5)P2 regulates the activation and desensitization of TRPM8 channels through the TRP domain. *Nature Neuroscience*, *8*(5), Article 5. https://doi.org/10.1038/nn1451

Roza, C., Belmonte, C., & Viana, F. (2006). Cold sensitivity in axotomized fibers of experimental neuromas in mice. *Pain*, *120*(1), 24–35. https://doi.org/10.1016/j.pain.2005.10.006

Sabatini, D. M. (2017). Twenty-five years of mTOR: Uncovering the link from nutrients to growth. *Proceedings of the National Academy of Sciences*, *114*(45), 11818–11825. https://doi.org/10.1073/pnas.1716173114

Sabnis, A. S., Shadid, M., Yost, G. S., & Reilly, C. A. (2008). Human Lung Epithelial Cells Express a Functional Cold-Sensing TRPM8 Variant. *American Journal of Respiratory Cell and Molecular Biology*, *39*(4), 466–474. https://doi.org/10.1165/rcmb.2007-0440OC

Samanta, A., Hughes, T. E. T., & Moiseenkova-Bell, V. Y. (2018). Transient Receptor Potential (TRP) Channels. *Sub-Cellular Biochemistry*, *87*, 141–165. https://doi.org/10.1007/978-981-10-7757-9_6

Sauls, J. (1999). Efficacy of Cold for Pain: Fact or Fallacy? *Worldviews on Evidence-Based Nursing Presents the Archives of Online Journal of Knowledge Synthesis for Nursing*, *E6*(1), 103–111. https://doi.org/10.1111/j.1524-475X.1999.00103.x

Schäfer, K., Braun, H. A., & Isenberg, C. (1986). Effect of menthol on cold receptor activity. Analysis of receptor processes. *The Journal of General Physiology*, *88*(6), 757–776. https://doi.org/10.1085/jgp.88.6.757

Sehgal, S. N., Baker, H., & Vézina, C. (1975). RAPAMYCIN (AY-22, 989), A NEW ANTIFUNGAL ANTIBIOTIC II. FERMENTATION, ISOLATION AND CHARACTERIZATION. *The Journal of Antibiotics*, *28*(10), 727–732. https://doi.org/10.7164/antibiotics.28.727

Selescu, T., Ciobanu, A. C., Dobre, C., Reid, G., & Babes, A. (2013). Camphor Activates and Sensitizes Transient Receptor Potential Melastatin 8 (TRPM8) to Cooling and Icilin. *Chemical Senses*, *38*(7), 563–575. https://doi.org/10.1093/chemse/bjt027

Señarís, R., Ordás, P., Reimúndez, A., & Viana, F. (2018). Mammalian cold TRP channels: Impact on thermoregulation and energy homeostasis. *Pflügers Archiv - European Journal of Physiology*, *470*(5), 761–777. https://doi.org/10.1007/s00424-018-2145-9

Shah, M., Edman, M. C., Reddy Janga, S., Yarber, F., Meng, Z., Klinngam, W., Bushman, J., Ma, T., Liu, S., Louie, S., Mehta, A., Ding, C., MacKay, J. A., & Hamm-Alvarez, S. F. (2017). Rapamycin Eye Drops Suppress Lacrimal Gland Inflammation In a Murine Model of Sjögren's Syndrome. *Investigative Ophthalmology & Visual Science*, *58*(1), 372–385. https://doi.org/10.1167/iovs.16-19159

Shankar Kikkeri, N., & Nagalli, S. (2023). Migraine With Aura. In *StatPearls*. StatPearls Publishing. http://www.ncbi.nlm.nih.gov/books/NBK554611/

Sherrington, C. S. (1906). *The integrative action of the nervous system* (pp. xvi, 411). Yale University Press. https://doi.org/10.1037/13798-000

Singh, A., Hildebrand, M., Garcia, E., & Snutch, T. (2010). The transient receptor potential channel antagonist SKF96365 is a potent blocker of low-voltage-activated T-type calcium channels. *British Journal of Pharmacology*, *160*(6), 1464–1475. https://doi.org/10.1111/j.1476-5381.2010.00786.x

Smith, G. D., Gunthorpe, M. J., Kelsell, R. E., Hayes, P. D., Reilly, P., Facer, P., Wright, J. E., Jerman, J. C., Walhin, J.-P., Ooi, L., Egerton, J., Charles, K. J., Smart, D., Randall, A. D., Anand, P., & Davis, J. B. (2002). TRPV3 is a temperature-sensitive vanilloid receptor-like protein. *Nature*, *418*(6894), Article 6894. https://doi.org/10.1038/nature00894

Spekker, E., Körtési, T., & Vécsei, L. (2023). TRP Channels: Recent Development in Translational Research and Potential Therapeutic Targets in Migraine. *International Journal of Molecular Sciences*, *24*(1), Article 1. https://doi.org/10.3390/ijms24010700

Sridhar, M. S. (2018). Anatomy of cornea and ocular surface. *Indian Journal of Ophthalmology*, *66*(2), 190–194. https://doi.org/10.4103/ijo.IJO_646_17

Ständer, S., Augustin, M., Roggenkamp, D., Blome, C., Heitkemper, T., Worthmann, A. c., & Neufang, G. (2017). Novel TRPM8 agonist cooling compound against chronic itch: Results from a randomized, double-blind, controlled, pilot study in dry skin. *Journal of the European Academy of Dermatology and Venereology*, *31*(6), 1064–1068. https://doi.org/10.1111/jdv.14041

Stanley, P., Moremen, K. W., Lewis, N. E., Taniguchi, N., & Aebi, M. (2022). N-Glycans. In A. Varki, R. D. Cummings, J. D. Esko, P. Stanley, G. W. Hart, M. Aebi, D. Mohnen, T. Kinoshita, N. H. Packer, J. H. Prestegard, R. L. Schnaar, & P. H. Seeberger (Eds.), *Essentials of Glycobiology* (4th ed.). Cold Spring Harbor Laboratory Press. http://www.ncbi.nlm.nih.gov/books/NBK579964/

Stein, R. J., Santos, S., Nagatomi, J., Hayashi, Y., Minnery, B. S., Xavier, M., Patel, A. S., Nelson, J. B., Futrell, W. J., Yoshimura, N., Chancellor, M. B., & De miguel, F. (2004). COOL (TRPM8) AND HOT (TRPV1) RECEPTORS IN THE BLADDER AND MALE GENITAL TRACT. *The Journal of Urology*, *172*(3), 1175–1178. https://doi.org/10.1097/01.ju.0000134880.55119.cf

Stewart, A. P., Egressy, K., Lim, A., & Edwardson, J. M. (2010). AFM imaging reveals the tetrameric structure of the TRPM8 channel. *Biochemical and Biophysical Research Communications*, *394*(2), 383–386. https://doi.org/10.1016/j.bbrc.2010.03.027

Stillwell, W. (2016). Membrane Transport. *An Introduction to Biological Membranes*, 423–451. https://doi.org/10.1016/B978-0-444-63772-7.00019-1

Story, G. M., Peier, A. M., Reeve, A. J., Eid, S. R., Mosbacher, J., Hricik, T. R., Earley, T. J., Hergarden, A. C., Andersson, D. A., Hwang, S. W., McIntyre, P., Jegla, T., Bevan, S., & Patapoutian, A. (2003). ANKTM1, a TRP-like Channel Expressed in Nociceptive Neurons, Is Activated by Cold Temperatures. *Cell*, *112*(6), 819–829. https://doi.org/10.1016/S0092-8674(03)00158-2

Suh, B.-C., & Hille, B. (2008). PIP2 is a necessary cofactor for ion channel function: How and why? *Annual Review of Biophysics*, *37*, 175–195. https://doi.org/10.1146/annurev.biophys.37.032807.125859

Sui, Y., Li, S., Zhao, Y., Liu, Q., Qiao, Y., Feng, L., & Li, S. (2020). Identification of a natural compound, sesamin, as a novel TRPM8 antagonist with inhibitory effects on prostate adenocarcinoma. *Fitoterapia*, *145*, 104631. https://doi.org/10.1016/j.fitote.2020.104631

Sun, M. (2000). Mucolipidosis type IV is caused by mutations in a gene encoding a novel transient receptor potential channel. *Human Molecular Genetics*, *9*(17), 2471–2478. https://doi.org/10.1093/hmg/9.17.2471

Taberner, F. J., López-Córdoba, A., Fernández-Ballester, G., Korchev, Y., & Ferrer-Montiel, A. (2014). The Region Adjacent to the C-end of the Inner Gate in Transient Receptor Potential Melastatin

8 (TRPM8) Channels Plays a Central Role in Allosteric Channel Activation. *The Journal of Biological Chemistry*, *289*(41), 28579–28594. https://doi.org/10.1074/jbc.M114.577478

Tajino, K., Matsumura, K., Kosada, K., Shibakusa, T., Inoue, K., Fushiki, T., Hosokawa, H., & Kobayashi, S. (2007). Application of menthol to the skin of whole trunk in mice induces autonomic and behavioral heat-gain responses. *American Journal of Physiology-Regulatory, Integrative and Comparative Physiology*, *293*(5), R2128–R2135. https://doi.org/10.1152/ajpregu.00377.2007

Talavera, K., Startek, J. B., Alvarez-Collazo, J., Boonen, B., Alpizar, Y. A., Sanchez, A., Naert, R., & Nilius, B. (2020). Mammalian Transient Receptor Potential TRPA1 Channels: From Structure to Disease. *Physiological Reviews*, *100*(2), 725–803. https://doi.org/10.1152/physrev.00005.2019

Talavera, K., Yasumatsu, K., Voets, T., Droogmans, G., Shigemura, N., Ninomiya, Y., Margolskee, R. F., & Nilius, B. (2005). Heat activation of TRPM5 underlies thermal sensitivity of sweet taste. *Nature*, *438*(7070), 1022–1025. https://doi.org/10.1038/nature04248

Tan, C.-H., & McNaughton, P. A. (2016). The TRPM2 ion channel is required for sensitivity to warmth. *Nature*, *536*(7617), Article 7617. https://doi.org/10.1038/nature19074

Tanaka, B. S., Nguyen, P. T., Zhou, E. Y., Yang, Y., Yarov-Yarovoy, V., Dib-Hajj, S. D., & Waxman, S. G. (2017). Gain-of-function mutation of a voltage-gated sodium channel NaV1.7 associated with peripheral pain and impaired limb development. *The Journal of Biological Chemistry*, *292*(22), 9262–9272. https://doi.org/10.1074/jbc.M117.778779

Tang, Z., Kim, A., Masuch, T., Park, K., Weng, H., Wetzel, C., & Dong, X. (2013). Pirt Functions as an Endogenous Regulator of TRPM8. *Nature Communications*, *4*, 2179. https://doi.org/10.1038/ncomms3179

Terry, L. E., Arige, V., Neumann, J., Wahl, A. M., Knebel, T. R., Chaffer, J. W., Malik, S., Liston, A., Humblet-Baron, S., Bultynck, G., & Yule, D. I. (2022). Missense mutations in inositol 1,4,5-trisphosphate receptor type 3 result in leaky Ca2+ channels and activation of store-operated Ca2+ entry. *iScience*, *25*(12). https://doi.org/10.1016/j.isci.2022.105523

Thebault, S., Lemonnier, L., Bidaux, G., Flourakis, M., Bavencoffe, A., Gordienko, D., Roudbaraki, M., Delcourt, P., Panchin, Y., Shuba, Y., Skryma, R., & Prevarskaya, N. (2005). Novel Role of Cold/Menthol-sensitive Transient Receptor Potential Melastatine Family Member 8 (TRPM8) in the Activation of Store-operated Channels in LNCaP Human Prostate Cancer Epithelial Cells*.

Journal of Biological Chemistry, *280*(47), 39423–39435. https://doi.org/10.1074/jbc.M503544200

Togashi, K., Hara, Y., Tominaga, T., Higashi, T., Konishi, Y., Mori, Y., & Tominaga, M. (2006). TRPM2 activation by cyclic ADP-ribose at body temperature is involved in insulin secretion. *The EMBO Journal*, *25*(9), 1804–1815. https://doi.org/10.1038/sj.emboj.7601083

Toro, C. A., Eger, S., Veliz, L., Sotelo-Hitschfeld, P., Cabezas, D., Castro, M. A., Zimmermann, K., & Brauchi, S. (2015). Agonist-Dependent Modulation of Cell Surface Expression of the Cold Receptor TRPM8. *The Journal of Neuroscience*, *35*(2), 571–582. https://doi.org/10.1523/JNEUROSCI.3820-13.2015

Tsavaler, L., Shapero, M. H., Morkowski, S., & Laus, R. (2001). Trp-p8, a Novel Prostate-specific Gene, Is Up-Regulated in Prostate Cancer and Other Malignancies and Shares High Homology with Transient Receptor Potential Calcium Channel Proteins. *Cancer Research*, *61*(9), 3760–3769.

Tsuruda, P. R., Julius, D., & Minor, D. L. (2006). Coiled Coils Direct Assembly of a Cold-Activated TRP Channel. *Neuron*, *51*(2), 201–212. https://doi.org/10.1016/j.neuron.2006.06.023

Vandewauw, I., De Clercq, K., Mulier, M., Held, K., Pinto, S., Van Ranst, N., Segal, A., Voet, T., Vennekens, R., Zimmermann, K., Vriens, J., & Voets, T. (2018). A TRP channel trio mediates acute noxious heat sensing. *Nature*, *555*(7698), Article 7698. https://doi.org/10.1038/nature26137

Vangeel, L., & Voets, T. (2019a). Transient Receptor Potential Channels and Calcium Signaling. *Cold Spring Harbor Perspectives in Biology*, *11*(6), a035048. https://doi.org/10.1101/cshperspect.a035048

Vangeel, L., & Voets, T. (2019b). Transient Receptor Potential Channels and Calcium Signaling. *Cold Spring Harbor Perspectives in Biology*, *11*(6), a035048. https://doi.org/10.1101/cshperspect.a035048

Viana, F. (2016). TRPA1 channels: Molecular sentinels of cellular stress and tissue damage. *The Journal of Physiology*, *594*(15), 4151–4169. https://doi.org/10.1113/JP270935

Viana, F., de la Peña, E., & Belmonte, C. (2002). Specificity of cold thermotransduction is determined by differential ionic channel expression. *Nature Neuroscience*, *5*(3), Article 3. https://doi.org/10.1038/nn809

Villar-Martinez, M. D., & Goadsby, P. J. (2022). Pathophysiology and Therapy of Associated Features of Migraine. *Cells*, *11*(17), Article 17. https://doi.org/10.3390/cells11172767

Voets, T. (2012). Quantifying and Modeling the Temperature-Dependent Gating of TRP Channels. In B. Nilius, S. G. Amara, T. Gudermann, R. Jahn, R. Lill, S. Offermanns, & O. H. Petersen (Eds.), *Reviews of Physiology, Biochemistry and Pharmacology 162* (pp. 91–119). Springer Berlin Heidelberg. https://doi.org/10.1007/112_2011_5

Voets, T., Droogmans, G., Wissenbach, U., Janssens, A., Flockerzi, V., & Nilius, B. (2004). The principle of temperature-dependent gating in cold- and heat-sensitive TRP channels. *Nature*, *430*(7001), Article 7001. https://doi.org/10.1038/nature02732

Voets, T., Owsianik, G., Janssens, A., Talavera, K., & Nilius, B. (2007a). TRPM8 voltage sensor mutants reveal a mechanism for integrating thermal and chemical stimuli. *Nature Chemical Biology*, *3*(3), 174–182. https://doi.org/10.1038/nchembio862

Voets, T., Owsianik, G., Janssens, A., Talavera, K., & Nilius, B. (2007b). TRPM8 voltage sensor mutants reveal a mechanism for integrating thermal and chemical stimuli. *Nature Chemical Biology*, *3*(3), 174–182. https://doi.org/10.1038/nchembio862

Vriens, J., Owsianik, G., Hofmann, T., Philipp, S. E., Stab, J., Chen, X., Benoit, M., Xue, F., Janssens, A., Kerselaers, S., Oberwinkler, J., Vennekens, R., Gudermann, T., Nilius, B., & Voets, T. (2011). TRPM3 Is a Nociceptor Channel Involved in the Detection of Noxious Heat. *Neuron*, *70*(3), 482–494. https://doi.org/10.1016/j.neuron.2011.02.051

Wang, S., Zhang, D., Hu, J., Jia, Q., Xu, W., Su, D., Song, H., Xu, Z., Cui, J., Zhou, M., Yang, J., & Xiao, J. (2017). A clinical and mechanistic study of topical borneol-induced analgesia. *EMBO Molecular Medicine*, *9*(6), 802–815. https://doi.org/10.15252/emmm.201607300

Wang, Y. (Ed.). (2017). *Transient Receptor Potential Canonical Channels and Brain Diseases* (Vol. 976). Springer Netherlands. https://doi.org/10.1007/978-94-024-1088-4

Wei, E. T. (2015). *Di-Isopropyl-Phosphinoyl-Alkane (dapa) Compounds as Topical Agents for the Treatment of Sensory Discomfort*. https://patentscope.wipo.int/search/en/detail.jsf?docId=WO2015059432

Wei, E. T. (2017). *Dialkyl-phosphinoyl-alkane (Dapa) compounds and compositions for treatment of lower gastrointestinal tract disorders* (United States Patent US20170189428A1). https://patents.google.com/patent/US20170189428A1/en

Weil, A., Moore, S. E., Waite, N. J., Randall, A., & Gunthorpe, M. J. (2005). Conservation of Functional and Pharmacological Properties in the Distantly Related Temperature Sensors TRPV1 and TRPM8. *Molecular Pharmacology*, *68*(2), 518–527. https://doi.org/10.1124/mol.105.012146

Wilkinson, J. E., Burmeister, L., Brooks, S. V., Chan, C.-C., Friedline, S., Harrison, D. E., Hejtmancik, J. F., Nadon, N., Strong, R., Wood, L. K., Woodward, M. A., & Miller, R. A. (2012). Rapamycin slows aging in mice. *Aging Cell*, *11*(4), 675–682. https://doi.org/10.1111/j.1474-9726.2012.00832.x

Winter, Z., Gruschwitz, P., Eger, S., Touska, F., & Zimmermann, K. (2017). Cold Temperature Encoding by Cutaneous TRPA1 and TRPM8-Carrying Fibers in the Mouse. *Frontiers in Molecular Neuroscience*, *10*, 209. https://doi.org/10.3389/fnmol.2017.00209

Xing, H., Chen, M., Ling, J., Tan, W., & Gu, J. G. (2007). TRPM8 mechanism of cold allodynia after chronic nerve injury. *The Journal of Neuroscience: The Official Journal of the Society for Neuroscience*, *27*(50), 13680–13690. https://doi.org/10.1523/JNEUROSCI.2203-07.2007

Xu, H., Ramsey, I. S., Kotecha, S. A., Moran, M. M., Chong, J. A., Lawson, D., Ge, P., Lilly, J., Silos-Santiago, I., Xie, Y., DiStefano, P. S., Curtis, R., & Clapham, D. E. (2002). TRPV3 is a calcium-permeable temperature-sensitive cation channel. *Nature*, *418*(6894), Article 6894. https://doi.org/10.1038/nature00882

Xu, L., Han, Y., Chen, X., Aierken, A., Wen, H., Zheng, W., Wang, H., Lu, X., Zhao, Z., Ma, C., Liang, P., Yang, W., Yang, S., & Yang, F. (2020). Molecular mechanisms underlying menthol binding and activation of TRPM8 ion channel. *Nature Communications*, *11*(1), Article 1. https://doi.org/10.1038/s41467-020-17582-x

Xue, S., Nicoud, M. R., Cui, J., & Jovin, D. J. A. (1994). High concentration of calcium ions in Golgi apparatus. *Cell Research*, *4*(1), Article 1. https://doi.org/10.1038/cr.1994.10

Yang, J. M., Li, F., Liu, Q., Rüedi, M., Wei, E. T., Lentsman, M., Lee, H. S., Choi, W., Kim, S. J., & Yoon, K. C. (2017a). A novel TRPM8 agonist relieves dry eye discomfort. *BMC Ophthalmology*, *17*(1), 101. https://doi.org/10.1186/s12886-017-0495-2

Yang, J. M., Li, F., Liu, Q., Rüedi, M., Wei, E. T., Lentsman, M., Lee, H. S., Choi, W., Kim, S. J., & Yoon, K. C. (2017b). A novel TRPM8 agonist relieves dry eye discomfort. *BMC Ophthalmology*, *17*(1), 101. https://doi.org/10.1186/s12886-017-0495-2

Yang, J. M., Wei, E. T., Kim, S. J., & Yoon, K. C. (2018). TRPM8 Channels and Dry Eye. *Pharmaceuticals*, *11*(4), Article 4. https://doi.org/10.3390/ph11040125

Yang, J., Roy, A., & Zhang, Y. (2013). Protein–ligand binding site recognition using complementary binding-specific substructure comparison and sequence profile alignment. *Bioinformatics*, *29*(20), 2588–2595. https://doi.org/10.1093/bioinformatics/btt447

Yang, S., Lu, X., Wang, Y., Xu, L., Chen, X., Yang, F., & Lai, R. (2020). A paradigm of thermal adaptation in penguins and elephants by tuning cold activation in TRPM8. *Proceedings of the National Academy of Sciences of the United States of America*, *117*(15), 8633–8638. https://doi.org/10.1073/pnas.1922714117

Yapa, K. T. D. S., Deuis, J., Peters, A. A., Kenny, P. A., Roberts-Thomson, S. J., Vetter, I., & Monteith, G. R. (2018). Assessment of the TRPM8 inhibitor AMTB in breast cancer cells and its identification as an inhibitor of voltage gated sodium channels. *Life Sciences*, *198*, 128–135. https://doi.org/10.1016/j.lfs.2018.02.030

Yin, Y., Wu, M., Zubcevic, L., Borschel, W. F., Lander, G. C., & Lee, S.-Y. (2018). Structure of the cold- and menthol-sensing ion channel TRPM8. *Science*, *359*(6372), 237–241. https://doi.org/10.1126/science.aan4325

Yin, Y., Zhang, F., Feng, S., Butay, K. J., Borgnia, M. J., Im, W., & Lee, S.-Y. (2022). Activation mechanism of the mouse cold-sensing TRPM8 channel by cooling agonist and PIP_2. *Science*, *378*(6616), eadd1268. https://doi.org/10.1126/science.add1268

Yoon, J., Ben-Ami, H. C., Hong, Y. S., Park, S., Strong, L. L. R., Bowman, J., Geng, C., Baek, K., Minke, B., & Pak, W. L. (2000). Novel Mechanism of Massive Photoreceptor Degeneration Caused by Mutations in the trp Gene of Drosophila. *Journal of Neuroscience*, *20*(2), 649–659. https://doi.org/10.1523/JNEUROSCI.20-02-00649.2000

Zakharian, E., Cao, C., & Rohacs, T. (2010). Gating of Transient Receptor Potential Melastatin 8 (TRPM8) Channels Activated by Cold and Chemical Agonists in Planar Lipid Bilayers. *Journal of Neuroscience*, *30*(37), 12526–12534. https://doi.org/10.1523/JNEUROSCI.3189-10.2010

Zhang, X. (2019). Direct Gαq Gating Is the Sole Mechanism for TRPM8 Inhibition Caused by Bradykinin Receptor Activation. *Cell Reports*, *27*(12), 3672-3683.e4. https://doi.org/10.1016/j.celrep.2019.05.080

Zhang, X., Mak, S., Li, L., Parra, A., Denlinger, B., Belmonte, C., & McNaughton, P. A. (2012). Direct inhibition of the cold-activated TRPM8 ion channel by Gαq. *Nature Cell Biology*, *14*(8), 851–858. https://doi.org/10.1038/ncb2529

Zhao, C., Xie, Y., Xu, L., Ye, F., Xu, X., Yang, W., Yang, F., & Guo, J. (2022). Structures of a mammalian TRPM8 in closed state. *Nature Communications*, *13*(1), Article 1. https://doi.org/10.1038/s41467-022-30919-y

Zhao, J., Cao, Y., & Zhang, L. (2020). Exploring the computational methods for protein-ligand binding site prediction. *Computational and Structural Biotechnology Journal*, *18*, 417–426. https://doi.org/10.1016/j.csbj.2020.02.008

Zimmermann, K., Hein, A., Hager, U., Kaczmarek, J. S., Turnquist, B. P., Clapham, D. E., & Reeh, P. W. (2009). Phenotyping sensory nerve endings in vitro in the mouse. *Nature Protocols*, *4*(2), 174–196. https://doi.org/10.1038/nprot.2008.223

Zimmermann, K., Leffler, A., Babes, A., Cendan, C. M., Carr, R. W., Kobayashi, J., Nau, C., Wood, J. N., & Reeh, P. W. (2007). Sensory neuron sodium channel Nav1.8 is essential for pain at low temperatures. *Nature*, *447*(7146), Article 7146. https://doi.org/10.1038/nature05880

Zimmermann, K., Lennerz, J. K., Hein, A., Link, A. S., Kaczmarek, J. S., Delling, M., Uysal, S., Pfeifer, J. D., Riccio, A., & Clapham, D. E. (2011). Transient receptor potential cation channel, subfamily C, member 5 (TRPC5) is a cold-transducer in the peripheral nervous system. *Proceedings of the National Academy of Sciences of the United States of America*, *108*(44), 18114–18119. https://doi.org/10.1073/pnas.1115387108

Zurborg, S., Yurgionas, B., Jira, J. A., Caspani, O., & Heppenstall, P. A. (2007). Direct activation of the ion channel TRPA1 by Ca2+. *Nature Neuroscience*, *10*(3), Article 3. https://doi.org/10.1038/nn1843

9. Annex:

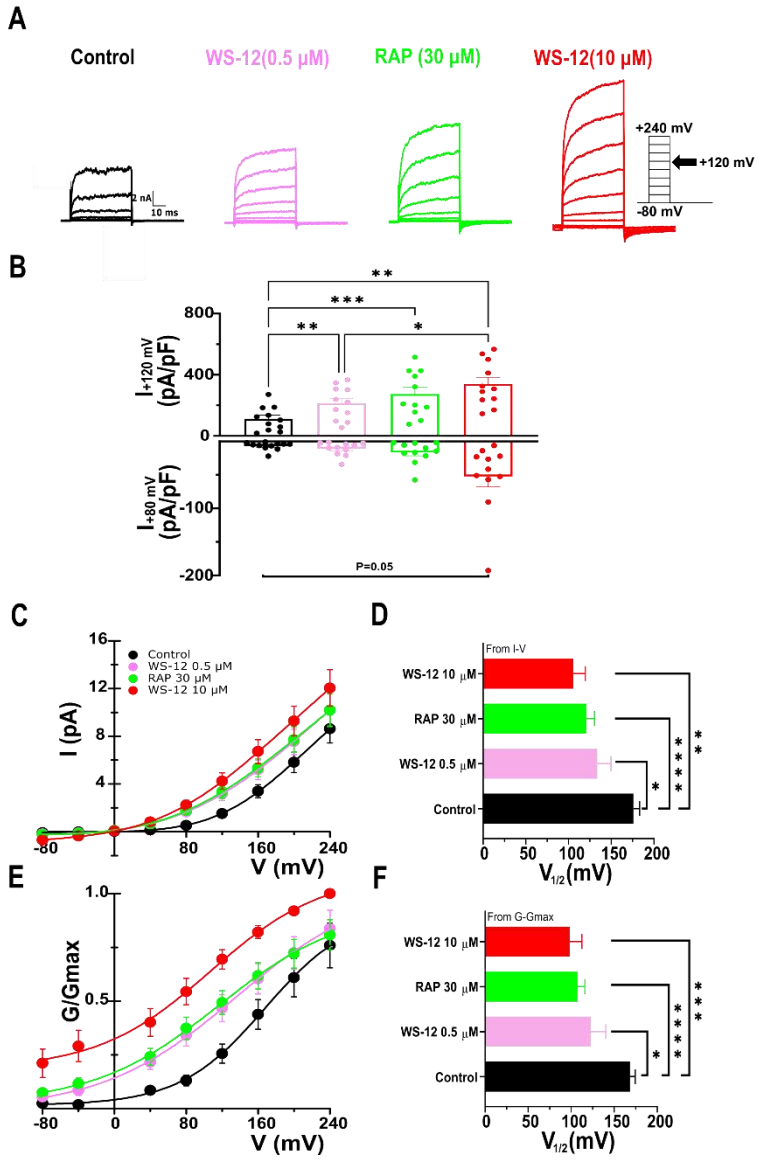

Figure 63. Biophysical characterization of WS-12 effects at low and high concentration on WT TRPM8 gating. A, Representative whole-Cell wild type TRPM8 currents in response to the given voltage steps protocol (from -80 to +240 mV during 50ms, ΔV= 40 mV see material and methods) in control conditions and in the presence of RAP (30 µM), WS-12 (0.5 and 10 µM) at 24 ˚C room temperature. **B,** Bar histogram summarizing the mean ± SEM currents densities at +120 (outward current density) and -80 mV (inward current density) of the different stimuli presented in A, following the color code. Statistical differences were evaluated by one-way Anova followed Bonferroni´s post-hoc test. **C**, Average (n=11) steady-state I-V curves extracted from individual cells after application of protocol the lines represent the fitting to linearized Boltzmann equation (see methods). **D,** Mean (n=11) $V_{1/2}$ value calculated from fitting the individual I-V curve to linearized Boltzmann equation. **E,** Average (n=11) voltage dependence activation curve in control condition and in the presence of different agonists, conductance was calculated as the steady state current divided by the driving force (Driving force = V_{Test}-E_{rev}) and normalized to the estimated maximal conductance (Gmax) which is the G value at +240 mV in the presence of 10 µM WS-12. **F,** Mean (n=11) $V_{1/2}$ value calculated from fitting the individual G/Gmax-V curve Boltzmann equation. The statistical differences were analyzed by one way ANOVA, followed by Bonferroni's post-hoc test.

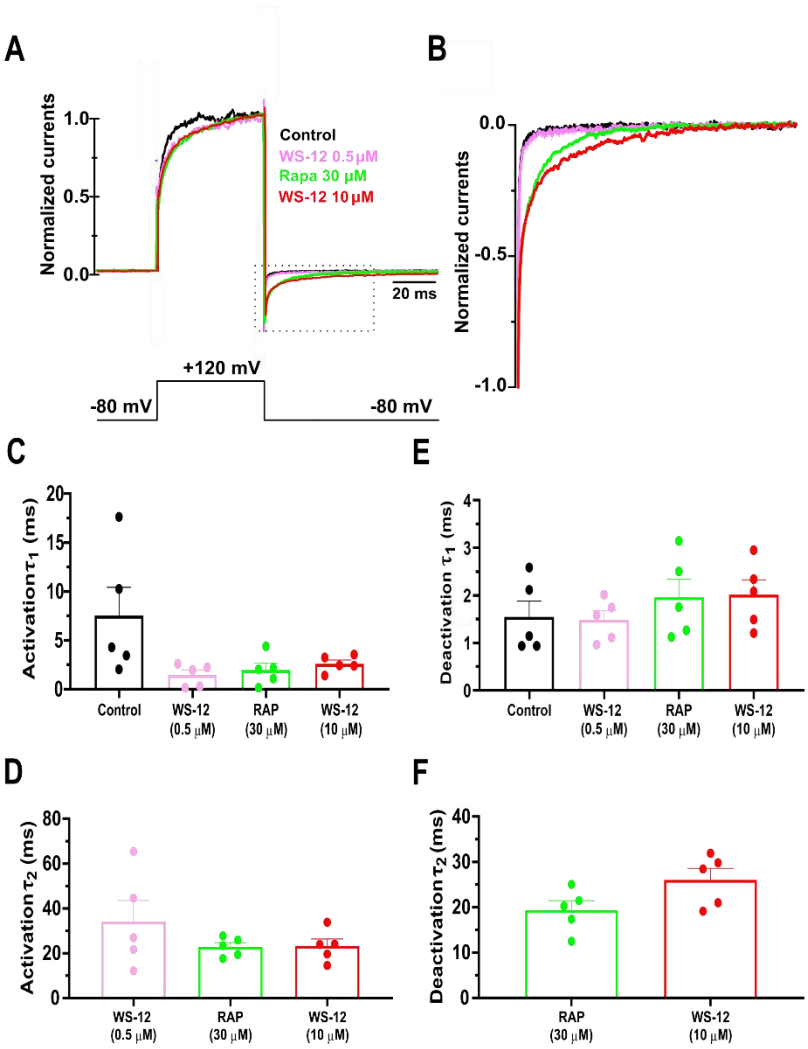

Figure 64. Characterization of the WS-12 effect at low and high concentration on TRPM8 activation and deactivation kinetics. A, Normalized average ± SEM of TRPM8 currents during a voltage step from -80 to +120 mV in control condition and in the presence of different agonists normalized to their steady-state amplitude after baseline subtraction. **B,** Average ± SEM TRPM8 deactivation kinetics at -80 mV extracted from tail current after a voltage step to + 120 mV (box dotted line in A), in both control and in the presence of different agonists. The current was normalized to the maximum value and baseline was subtracted. **C,** Bar histogram showing Mean ± SEM of the faster component first time constant (τ_1) during activation phase from voltage step -80 mV up to +120 mV, extracted from fitting single traces in control condition to a mono-exponential (time constant τ) and agonists traces to a bi-exponential equations (time constant τ_1). **D,** Bar histogram showing Mean ± SEM of Slow component or second time constant (τ_2) during activation phase after a voltage step -80 mV up to +120 mV. **E,** Bar histogram showing Mean ± SEM fast component or first time constant (τ_1) during deactivation phase at -80 mV. **F,** Bar histogram showing Mean ± SEM Slow component or second time constant (τ_2) during deactivation phase at -80 mV. Note that for the activation phase in the control condition the traces following voltage step -80 mV up to +120 mV were fitted to a mono-exponential equation resulting a single time constate (τ) used for comparison with different conditions, while the presence of agonists the activation traces were fitted with a bi-exponential from the baseline up to 100% of current amplitude resulting two activation phase time constants : the fast component or first time constant (τ_1) of the first activation phase, and a slow component time constant (τ_2) of the second activation phase, and deactivation phase the control and WS-12 (0.5 µM) traces were fitted to a mono-exponential equation resulting one time constant used for comparison (τ), whereas in the presence of RAP(30 µM) or WS-12 (10 µM) deactivation traces were fitted to bi-exponential equation resulting two time constants the fast components (τ_1) and the slow component(τ_2) (See materials and methods). Statistical differences were evaluated using ANOVA one way followed by Bonferroni post-hoc test.

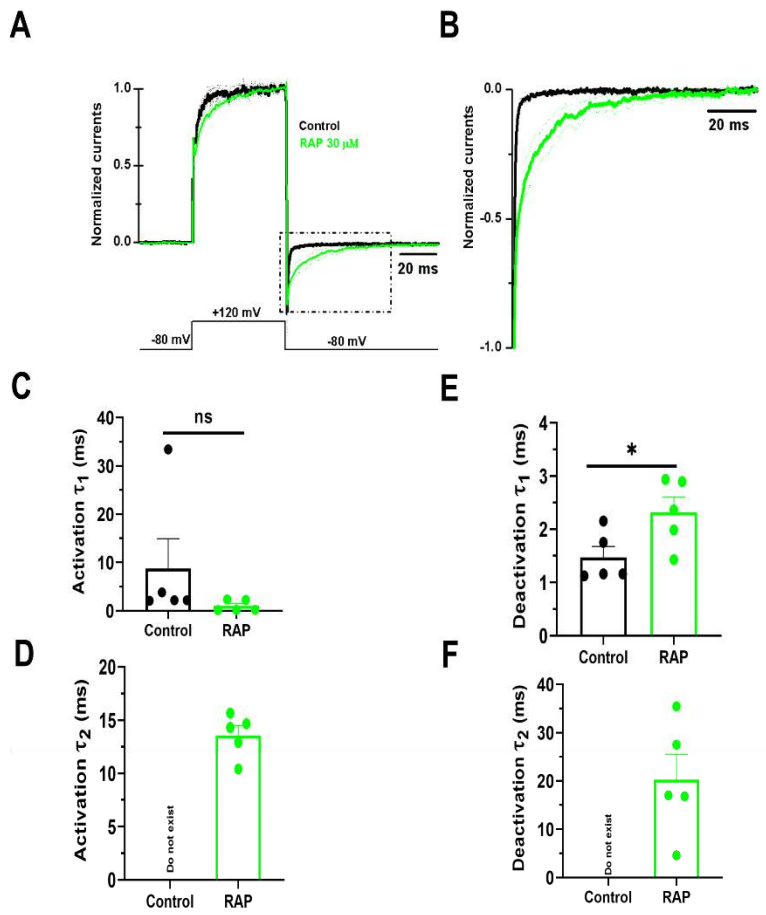

Figure 65. Characterization of the mutation Y745H effect on TRPM8 activation and deactivation kinetics. A, Normalized average ± SEM of Y745H TRPM8 currents during a voltage step from -80 to +120 mV in control condition and in the presence of TRPM8 agonists RAP normalized to its steady-state amplitude after baseline subtraction. **B,** Average ± SEM TRPM8 deactivation kinetics at -80 mV extracted from tail current after a voltage step to + 120 mV (box dotted line in A), in both control and in the presence of RAP. The current was normalized to the maximum value and baseline was subtracted. **C,** Bar histogram showing Mean ± SEM of the fast component or first time constant (τ_1) during activation phase from voltage step -80 mV up to +120 mV, extracted from fitting single traces in control condition to a mono-exponential (time constant τ) and RAP trace to a bi-exponential equations (time constant τ_1). **D,** Bar histogram showing Mean ± SEM of slow component or second time constant (τ_2) during activation phase after a voltage step -80 mV up to +120 mV. **E,** Bar histogram showing Mean ± SEM fast component or first time constant (τ_1) during deactivation phase at -80 mV. **F,** Bar histogram showing Mean ± SEM Slow component or second time constant (τ_2) during deactivation phase at -80 mV. Note that for the activation phase in the control condition the traces following voltage step -80 mV up to +120 mV were fitted to a mono-exponential equation resulting a single time constante (τ) used for comparison. While in the presence of agonists the activation traces were fitted with a biexponential from the baseline up to 100% of current amplitude resulting two activation time constants : the fast component or first time constant (τ_1) of the first activation phase, and a slow component time constante (τ_2) of the second activation phase. During deactivation phase the control trace was fitted to a mono-exponential equation resulting one time constant used for comparison (τ), whereas in the presence of RAP(30 µM) deactivation traces were fitted to bi-exponential equation resulting two time constants the fast components (τ_1) and the slow component(τ_2) (See materials and methods). Statistical differences were evaluated using student T-test.

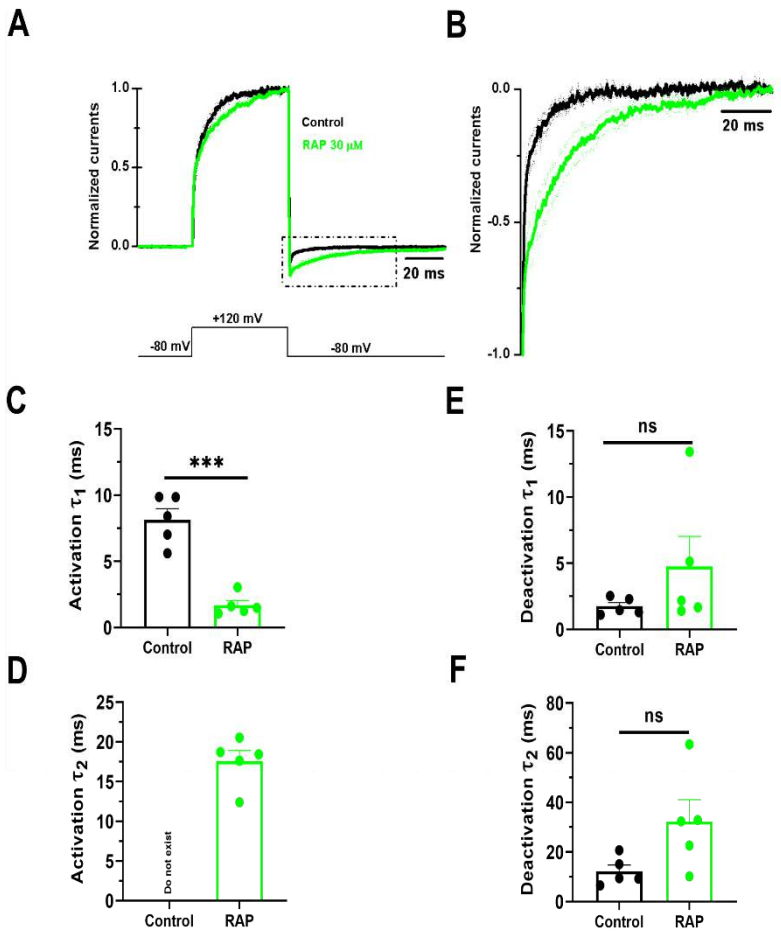

Figure 66. Characterization of the mutation I846D effect on TRPM8 activation and deactivation kinetics. **A,** Normalized average ± SEM of I846D TRPM8 currents during a voltage step from -80 to +120 mV in control condition and in the presence of RAP 30 µM normalized to their steady-state amplitude after baseline subtraction. **B,** Average ± SEM TRPM8 deactivation kinetics at -80 mV extracted from tail current after a voltage step to + 120 mV (box dotted line in A), in both control and in the presence of different agonists. The current was normalized to the maximum value and baseline was subtracted. **C,** Bar histogram showing Mean ± SEM of the fast component or first time constant (τ_1) during activation phase from voltage step -80 mV up to +120 mV, extracted from fitting single traces in control condition to a mono-exponential (time constant τ) and RAP traces to a bi-exponential equations (fast time constant τ_1). **D,** Bar histogram showing Mean ± SEM of slow component or second time constant (τ_2) during activation phase after a voltage step -80 mV up to +120 mV in the presence of RAP. **E,** Bar histogram showing Mean ± SEM fast component or first time constant (τ_1) during deactivation phase at -80 mV. **F,** Bar histogram showing Mean ± SEM slow component or second time constant (τ_2) during deactivation phase at -80 mV. Note that for the activation phase in the control condition the traces following voltage step -80 mV up to +120 mV were fitted to a mono-exponential equation resulting a single time constant (τ) used for comparison. While in the presence of RAP the activation trace was fitted with a biexponential from the baseline up to 100% of current amplitude resulting two activation time constants : the fast component or first time constant (τ_1) of the first activation phase, and a slow component time constant (τ_2) of the second activation phase. During deactivation phase in both control and RAP(30 µM) traces were fitted to a Bi-exponential equation resulting two-time constants used for comparison: fast component (τ_1) and slow component (τ_2), Statistical differences were evaluated using student T-test.

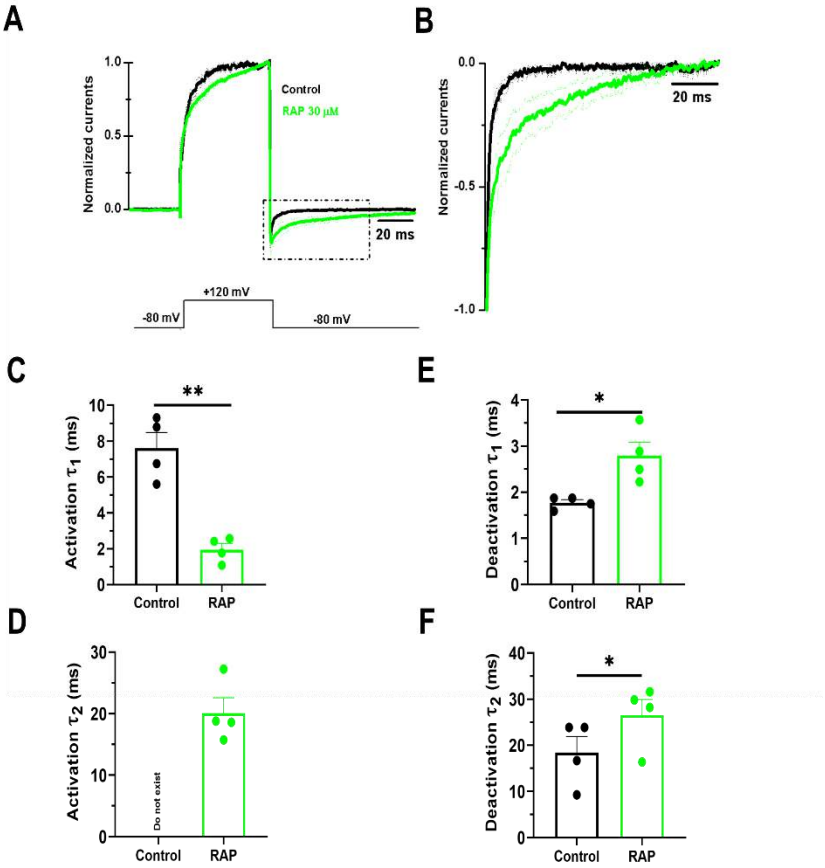

Figure 67. Characterization of the mutation I846T effect on TRPM8 activation and deactivation kinetics. **A,** Normalized average ± SEM of I846T TRPM8 currents during a voltage step from -80 to +120 mV in control condition and in the presence of RAP 30 µM normalized to their steady-state amplitude after baseline subtraction. **B,** Average ± SEM TRPM8 deactivation kinetics at -80 mV extracted from tail current after a voltage step to + 120 mV (box dotted line in A), in both control and in the presence of different agonists. The current was normalized to the maximum value and baseline was subtracted. **C,** Bar histogram showing Mean ± SEM of the fast component or first time constant (τ_1) during activation phase from voltage step -80 mV up to +120 mV, extracted from fitting single traces in control condition to a mono-exponential (time constant τ) and RAP traces to a bi-exponential equations (fast time constant τ_1). **D,** Bar histogram showing Mean ± SEM of slow component or second time constant (τ_2) during activation phase after a voltage step -80 mV up to +120 mV in the presence of RAP. **E,** Bar histogram showing Mean ± SEM fast component or first time constant (τ_1) during deactivation phase at -80 mV. **F,** Bar histogram showing Mean ± SEM slow component or second time constant (τ_2) during deactivation phase at -80 mV. Note that for the activation phase in the control condition the traces following voltage step -80 mV up to +120 mV were fitted to a mono-exponential equation resulting a single time constant (τ) used for comparison. While in the presence of RAP the activation trace was fitted with a biexponential from the baseline up to 100% of current amplitude resulting two activation time constants : the fast component or first time constant (τ_1) of the first activation phase, and a slow component time constant (τ_2) of the second activation phase. During deactivation phase in both control and RAP(30 µM) traces were fitted to a Bi-exponential equation resulting two-time constants used for comparison: fast component (τ_1) and slow component (τ_2), Statistical differences were evaluated using student T-test.

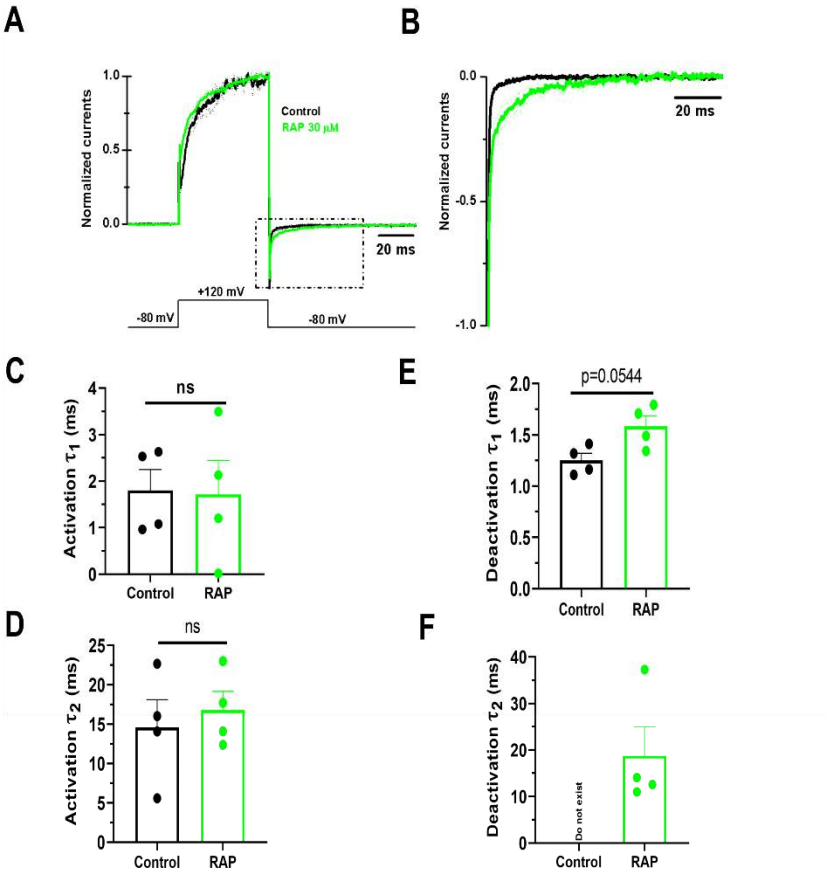

Figure 68. Characterization of the mutation I846V effect on TRPM8 activation and deactivation kinetics. A, Normalized average ± SEM of I846V TRPM8 currents during a voltage step from -80 to +120 mV in control condition and in the presence of RAP, normalized to their steady-state amplitude after baseline subtraction. **B,** Average ± SEM TRPM8 deactivation kinetics at -80 mV extracted from tail current after a voltage step to + 120 mV (box dotted line in A), in both control and in the presence of RAP. The current was normalized to the maximum value and baseline was subtracted. **C,** Bar histogram showing Mean ± SEM of the fast component or first time constant (τ_1) during activation phase from voltage step -80 mV up to +120 mV, extracted from fitting single traces in control condition to a bi-exponential (time constant τ_1) and RAP traces to a bi-exponential equations (time constant τ_1). **D,** Bar histogram showing Mean ± SEM of slow component or second time constant (τ_2) during activation phase after a voltage step -80 mV up to +120 mV. **E,** Bar histogram showing Mean ± SEM fast component or first time constant (τ_1) during deactivation phase at -80 mV. **F,** Bar histogram showing Mean ± SEM slow component or second time constant (τ_2) during deactivation phase at -80 mV. Note that for the activation phase in the control condition the traces following voltage step -80 mV up to +120 mV were fitted to a bi-exponential equation resulting a two time constants: fast component (τ_1) and slow component (τ_2) used for comparison. similarly, in the presence of RAP the activation traces were fitted with a biexponential from the baseline up to 100% of current amplitude resulting two activation time constants : the fast component or first time constant (τ_1) of the first activation phase, and a slow component time constant (τ_2) of the second activation phase. During deactivation phase the control and traces were fitted to a mono-exponential equation resulting one time constant used for comparison (τ), whereas in the presence of RAP(30 µM) deactivation traces were fitted to bi-exponential equation resulting two-time constants the fast components (τ_1) and the slow component(τ_2). Statistical differences were evaluated using student T-test.